

Robert Stobie Spectrograph – Near Infrared (RSS-NIR) Redbook



Mid-Term Review Design Document
May 2009



Table of Contents

1.	EXECUTIVE SUMMARY	1
2.	INTRODUCTION	2
3.	SPECIFICATIONS AND REQUIREMENTS.....	4
3.1	Science Requirements	4
3.1.1	Highest Redshift Forming Galaxies ($z > 7$)	8
3.1.2	High Redshift ($2.5 < z < 5.5$)	8
3.1.3	Moderate Redshift Galaxies ($z \sim 0.5-2$).....	8
3.1.4	Nearby Galaxies ($z < 0.5$)	8
3.1.5	The Milky Way	8
3.1.6	Solar System	9
3.1.7	Miscellaneous	9
3.2	Flow Down of Science Requirements into Tech Requirements.....	11
3.2.1	Spectral Range	12
3.2.2	Spectral Resolution.....	14
3.2.3	Slit Masks	15
3.2.4	Acquisition and Guiding	15
3.2.5	Instrument Sensitivity.....	15
3.3	Competing Instruments	17
3.4	Preliminary Specifications.....	22
3.4.1	Science – Engineering Trade Matrix	23
3.4.2	System Overview	27
4.	PRELIMINARY DESIGN ACTIVITIES	28
4.1.	Feasibility and Design Trades.....	28
4.2.	Maturing the Overall Mechanical Design.....	29
4.3.	Specific PDR Design Issues	29
5.	PRELIMINARY DESIGN	30
5.1.	Optics	30
5.1.1.	Optical Design Description	30
5.1.2	Optical Error Budget and Analysis.....	36
5.1.3.	Detailed Optical Performance.....	37
5.1.4.	Fabry-Perot Selection.....	41
5.1.5.	Fabry-Perot Order Blocking Filter Selection	42
5.1.6	Grating Selection	45
5.1.7.	Polarimetry	46
5.1.8	Calibration System.....	48
5.1.9.	Risk and Risk Mitigation	51
5.1.10.	Test and Integration Plan	51
5.2.	Mechanical Design	54
5.2.1	General Description	54
5.2.2	Dichroic and Doublet.....	56
5.2.3	Fold Mirror	58
5.2.4.	Optical Storage Assembly	59
5.2.5.	Filter Cassette Exchange	62
5.2.6	Grating Rotation Stage.....	63
5.2.7.	Polarizing Beamsplitter Mechanism.....	65
5.2.8.	Camera and Focus Assembly	66
5.2.9.	Dewar	68

5.2.10	Articulation System	75
5.2.11	Pre-dewar Enclosure.....	76
5.2.12	Thermal System Design	78
5.3.	Thermal Stray Light Analysis	80
5.3.1.	Ambient Temperature Components.....	80
5.3.2.	Initial Pre-Dewar Estimates	87
5.3.3.	Gold Coating of the Multi-slit Masks and Long Slit Baffles	88
5.4.	Detector	90
5.4.1.	Selection and Operating Parameters.....	90
5.4.2.	Detector Operating Temperature.....	92
5.4.3.	Integration and Test Plan	96
5.4.4.	Cryogenic Long Wavelength Blocking Filters	100
5.5.	Electrical/Electronics Design.....	102
5.5.1.	Detector Controller	103
5.5.2.	Motion Control.....	109
5.5.3.	Environmental Control.....	113
5.5.4.	Housekeeping	117
5.5.5.	Communications	118
5.5.6.	Power Distribution	120
5.6.	Control System Software	123
5.6.1.	Architecture.....	123
5.6.2.	Implementation.....	128
5.6.3.	Thermal Control	129
5.6.4.	Motion Control.....	129
5.6.5.	Data Flow.....	129
5.7	Operating Modes	130
5.7.1	Imaging	131
5.7.2	Longslit Spectroscopy	131
5.7.3	Multi-Object Spectroscopy	132
5.7.4	Fabry-Perot Imaging	132
5.7.5	Polarimetry.....	133
5.7.6	Simultaneous Visible-NIR Operation	138
5.8.	SALT Facility Interface Control	139
5.8.1.	ADC Optical Performance.....	139
5.8.2.	Moving Baffle Gold Coating.	139
5.8.3.	Calibration Source Change.	139
5.8.4.	ADC Stray Light.	140
5.8.5.	Data Path from SALT Facility to Cape Town.....	140
5.8.6.	Data Archiving capability at SALT.	140
5.8.7.	Labview Version Update and Compatibility.	140
5.8.8.	Critical Power Distribution.	140
6.	MANAGEMENT	140
6.1.	Structure and Organization.....	140
6.1.1.	Principal Investigator (PI).....	141
6.1.2.	Project Scientist (PS).....	141
6.1.3.	Co-Investigators (Co-I).....	142
6.1.4.	Project Manager (PM).....	142
6.1.5.	Systems Engineer (SE).....	142
6.1.6.	Quality Assurance and Safety Manager (QAS)	143

6.1.7. Lead Mechanical Engineer.....	143
6.1.8. Optical Designer	143
6.1.9. Dewar Design Consultant	143
6.1.10. Detector Development	143
6.2. Project Management	143
6.3. Risk Assessment and Management	144
6.3.1. Technology	144
6.3.2. Safety	147
6.3.3. Cost	147
6.3.4. Schedule.....	147
6.4. Quality	148
6.4.1. Quality Assurance.....	148
6.4.2. Configuration Management.....	148
6.4.3. Safety	149
6.4.4. Design Control	149
6.5. Systems Engineering.....	149
6.6. Work Breakdown Structure.....	150
6.7. Schedule	151
6.8. Deliverables	154
6.9. Milestones and Reviews.....	154
6.10. Funding, Spending, and Budget	154
6.10.1. Budget Detail	156
6.10.2. Material Costs	158
6.10.3. Capital Equipment.....	160
6.10.4. Travel Plans	160
7. REFERENCES	162
8. DEFINITIONS, NOMENCLATURE, ACRONYMS AND ASSUMPTIONS	164
8.1. Assumptions	164
8.2. Nomenclature, Acronyms, Definitions and Aliases.....	165
9. APPENDICES.....	172
9.1. 11 x 17 Diagrams.....	172

1. EXECUTIVE SUMMARY

This document summarizes the state of the Robert Stobie Spectrograph – Near Infrared (RSS-NIR) design as of the Mid-Term Review, May 2009. The RSS-NIR will be a semi-warm, near infrared spectrograph to complement the RSS-Visible on the Southern African Large Telescope or SALT. It is a major upgrade to the RSS that was anticipated during the RSS-VIS development. Using a 2K x 2K Hawaii 2RG focal plane array, the NIR will extend the wavelength range of the RSS from 0.85 to 1.7 μm providing a resolution of up to 14,000 (0.5 arcsec slit). The RSS-NIR will specialize in high-throughput, medium resolution multi-object spectroscopy, spectropolarimetry, and Fabry-Perot imaging. The design includes 5 Volume Phase Holographic gratings, 12 filters (Fabry-Perot order blocking filters and broad and narrow-band imaging filters), a Fabry-Perot etalon, a polarizing beamsplitter, and 3 cryogenic long wavelength blocking filters.

The PDR review panel performed a thorough assessment of the RSS-NIR on 17-18 July 2008. They provided constructive feedback to improve the design and development. The RSS-NIR team has used the advice to drive the activities over the last 9 months. A summary of issues addressed include:

- Development of a complete set of science objectives to take full advantage of the NIR. These were flowed down to the functional performance requirements.
- Improvement of the optical design to provide a faster camera with an improved pixel-size matching and larger field of view. This increased the speed of the camera from F/2.025 to F/1.42 and required the addition of one optical element. The resulting design changed the plate scale from 108 microns per arcsecond (6.0 pixels/arcsec) to 76 microns per arcsecond (4.2 pixels/sec) to better match the science requirements and median seeing. This new design, when traced through the entire optical system excluding the telescope over the full bandpass without refocus, produces 90% ensquared energy in 2 x 2 pixels (0.5 arcsec x 0.5 arcsec) with the exception of the very edge of the -y direction which achieves 80% EE in 2 pixels and 90% in 3 pixels.
- Improvement of a detailed optical error budget and analysis on the NIR optical elements to determine fabrication tolerances, alignment and assembly tolerances and options for camera focus. The results of this analysis were iterated with the science flow-down requirements through the instrument performance predictions and mechanical and opto-mechanical design.
- Performance of a series of design feasibilities and trades. These included analysis to develop a filter cassette exchange scheme and design, gold coat the slits, improve the control system architecture and software, cool the slit, and cool the collimator.
- Maturation of the mechanical design to a preliminary design status. This included developing mechanical tolerances; mechanisms to insert the etalon, filters, polarizing beamsplitter and gratings; drive systems for the Optics Storage Assembly, grating rotation, and articulation; structural and optical mounts for the dichroic, doublet, and fold mirrors; preliminary designs for the camera, Dewar, and pre-dewar enclosure; and structural support to address flexure with the camera/Dewar assembly.
- A number of specific design features were added as well:
 - Increased the number of Fabry-Perot Ordering Blocking Filters from 7 to 12.
 - Provided a tilt of 2° to the Fabry-Perot Ordering Blocking Filters in order to reduce potential ghost-images in imaging and spectroscopic modes.
 - Changed the pre-dewar enclosure design to fully enclose the camera/Dewar assembly.
 - Provided active tip/tilt capability to the fold mirror.
 - Improved the flexural stiffness of the grating rotation stage through the addition of a mounting bearing above and below the grating center-of-gravity.

The RSS-NIR project team is excited and motivated to develop one of the first semi-warm near infrared spectrographs to provide a unique capability to a 8-11-meter class telescope. The team feels all design issues have been addressed with viable solutions and the final detailed design will meet or exceed all requirements.

2. INTRODUCTION

The RSS-NIR project started with a Conceptual Design Review before the SALT Science Working Group, held in May 2006 in Cape Town, South Africa. The instrument passed the review. It was considered a valuable addition to the SALT facility and a strong complement to the existing RSS-Visible instrument. SALT granted an initial sum of \$145,000 to proceed to a Preliminary Design Review. This provided a small pool of resources to advance the design from its initial concept. A PDR was held in July 2008 before an independent panel of reviewers composed of astronomers experienced in instrument development. Among other recommendations, a follow up review was suggested before placing orders for long lead procurements. At that time, formal funding commitments were not yet in place. Since then, the project has received \$3.3M from the Wisconsin Alumni Research Foundation and just under \$2.0M from the National Science Foundation through the MRI program. The SALT consortium has committed to providing an additional \$155k with another \$925k formally requested. The funding has created enough support and security to build up the project team to a critical level to include the science, engineering, and technical support appropriate to a project of this magnitude. The total funding, assuming the additional SALT funds, is now just under \$6.5M, which is enough to fully fund the project as scoped including a 15% contingency fund.

The RSS-NIR is being developed as a complementary instrument to the existing RSS-VIS instrument for the SALT Facility. SALT is a fixed-elevation, segmented-mirror-array telescope 11-meters in diameter. It is the largest single-aperture telescope in the world and is similar in design to the Hobby-Eberly Telescope. The combined RSS will be unique among instrumentation for large telescopes due to its ability to provide simultaneous visible and near infrared observations. The RSS-NIR will provide high throughput, low to medium resolution multi-object spectroscopy, narrow-band imaging and spectropolarimetry over a wavelength of 0.85 to 1.7 μm . The design includes an articulated camera, Volume Phase Holographic gratings, a polarizing beamsplitter and a single etalon Fabry-Perot system. It will image a full 8 arcminutes FOV across the linear dimension of the 2K x 2K Hawaii 2RG detector. Given the fixed focal-length of the RSS collimator, this results in a reimaged plate-scale of 76.0 microns/arcsec, which corresponds to 0.24 arcsec/pixel or 4.2 pixels/arcsec. See **Figure 2-1**.

RSS-NIR is being developed at the University of Wisconsin through the joint effort of the Department of Astronomy, Space Astronomy Lab, and the Space Science and Engineering Center. The Principal Investigator, Professor Andrew Sheinis, and the Project Scientist, Dr. Marsha Wolf, are located in the Department of Astronomy. Co-Investigators include Professor Ken Nordsieck, Professor Matt Bershad, Professor Jay Gallagher, and Professor Amy Barger all at the UW department of Astronomy. The project is collaborating with staff at a few other institutions. As on the RSS-VIS, Co-I Professor Theodore Williams, Rutgers University, will lead the selection and testing of the Fabry-Perot etalon. Other key members include Professor Harland Epps (optical design) from UC-Santa Cruz/Lick Observatory and Dr. Stephen Smee (Dewar design) from John Hopkins University. The Project Manager is Mark Mulligan, the Quality Assurance & Safety Manager is Tom Demke, and the Systems Engineer is Don Thielman. The Lead Mechanical Engineer is Michael Smith.

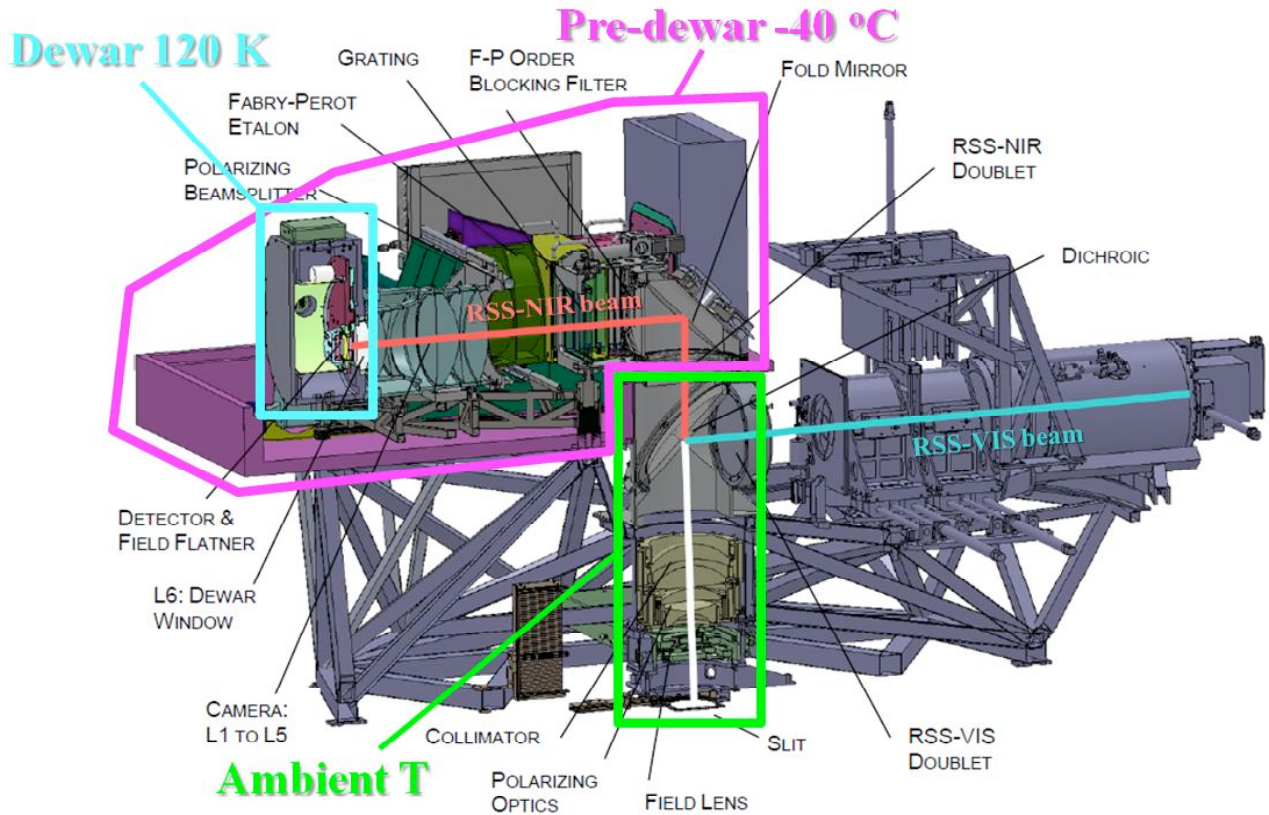


Figure 2-1. RSS-NIR Cross-section with optical path shown. Light from the prime focus of the SALT telescope passes through the slit, field lens, polarizing optics and then the RSS collimator. From there, the dichroic splits it between the RSS-VIS (on right) and RSS-NIR (on left). As the light enters the pre-dewar enclosure of the RSS-NIR, it passes through a collimator doublet. The pre-dewar provides a cold (-30 to -40 °C), dry environment at atmospheric pressure. From the doublet, the light redirect via fold mirror to pass through gratings, order blocking filters, Fabry-Perot etalon, and/or polarizing beamsplitter. The dispersed light is collected by an all-spherical, 7-element refracting camera. Five elements are in the pre-dewar, the 6th forms the window to the Dewar and the field flattener and detector (Hawaii 2RG) are in the Dewar. The Dewar contains a series of low-pass filters.

3. SPECIFICATIONS AND REQUIREMENTS

3.1 Science Requirements

Many of the breakthroughs and advances in astrophysics are enabled by advances in instrumentation. New discoveries or understanding always follow the opening of new observational parameter space. Although infrared observations have been conducted for quite some time, particularly for imaging, efficient near infrared (NIR) spectrographs on 10-meter class telescopes with multiplexing capability are only now beginning to come to fruition. With such instruments large surveys of faint high redshift objects can be conducted. The NIR regime can be used to probe objects that would not otherwise be accessible in optical wavelengths. Hidden objects embedded in obscuring dust can be studied, new NIR spectral features and diagnostics may be observed and defined, and redshifted spectral features that are normally used for galaxy diagnostics in optical bands can be observed in much more distant objects. We outline a few key areas of research below. The detailed science case for RSS-NIR can be found in a separate document (SALT-3501AS0001).

Young stars. Although star formation rates estimated from light integrated over entire galaxies are used as a cosmological diagnostic for galaxy evolution throughout the universe, the details of actual star formation are not very well understood. One problem is that stars form inside molecular clouds that are dense and typically have optical extinctions on the order of 10^3 's of magnitudes. NIR spectrographs can peer through the dust to study details of the young stellar objects and their lingering disks. In order to probe the circumstellar geometry of the most massive young stellar objects, we must use diagnostics at NIR wavelengths, as the more massive young stellar objects remain optically obscured throughout their entire pre-main sequence lives. Multi-object capability is important for studying forming and young star clusters still embedded in molecular clouds.

Low mass stars. The stellar initial mass function (IMF) is very important for understanding global star formation and for properly doing stellar population synthesis of galaxies. Much of what is currently known about star formation is on the high mass end. The low end of the IMF is virtually unknown because these stars are very faint and red. NIR spectrographs on 10-m class telescopes will be able to characterize the low end of the stellar IMF.

Brown dwarfs. Brown dwarfs fall in between stars and planets in mass and atmospheric properties. Studying their formation will help us to understand the bigger picture of the formation of both stars and planets. One interesting aspect is that no brown dwarf companions have been found to low mass stars, while other low mass stars and planets do exist in such pairs. This suggests that we do not understand something about the formation of brown dwarf mass objects. Brown dwarfs harbor more complex atmospheres than stars or planets. Their spectra peak in the NIR and contain a number of molecular band and atomic absorption features. Weather causes variability, so wide simultaneous spectral coverage at a resolution of $R \geq 5000$ will be important in their study. Their low intrinsic luminosities necessitate instruments on large telescopes.

Cool stars. Red supergiants and red giants are the most luminous stars in, respectively, star forming or old passive galaxies. In highly reddened starburst galaxies, the NIR light from red supergiants is sometimes the only direct information available on the stellar populations. Models for their spectra are thus important, even though they are also particularly difficult to construct due to their rich molecular line spectra and extended atmospheres. However, if the models are successful in reproducing empirical spectra, they can be used instead of observed spectral libraries in future analyses of galaxies. At NIR wavelengths (1–2.5 μm), the most prominent molecular features in these stars are those of CO and CN,

which have sensitivity to surface gravity and effective temperature (Lancon et al. 2007). Adding to the library of observed spectra of these stars will help to improve stellar population synthesis models.

Supernova explosion physics. One important aspect of supernovae (SNe) that is not yet well understood is their asymmetry, which may impact their observed brightness (in the case of SNe Ia) as well as the deposition of kinetic energy and enriched material into their environment. Observational probes of SN asymmetries have been challenging: the most effective way of probing the asymmetries in SNe is with spectropolarimetry, and this has been pursued only recently with the advent of spectropolarimeters on 10-meter class telescopes. In SNe, a net continuum polarization of the integrated light results from an asymmetry of the photosphere, while polarization in the P-Cygni lines results from asymmetries in the overlying ejecta. By measuring the variation of line polarization with wavelength, we can observe asymmetries as a function of velocity (in SNe, this is equivalent to radius) so that line polarization gives us information about chemical and density inhomogeneities within the ejecta, which can then be compared with the results of explosion codes. Different lines show different polarization, indicating that the thermonuclear processing of the explosion is inhomogeneous. RSS-NIR will be the first instrument capable of SNe spectropolarimetry in the NIR, bringing in a range of unobserved lines that are important for constraining explosion physics models. Especially interesting in SN Ia are the [Fe II] lines at 1.26 and 1.65 μm . Combining information from these lines with those of Si and Ca simultaneously observed in the visible will trace elements produced in the full range of the thermonuclear explosion chain for the first time. Following each SN regularly throughout its light curve will show how this evolves as the envelope becomes optically thin. A statistical study of a number of SNe will then determine whether SNe can be divided into further subclasses based on structure.

Galactic center objects. Although the center of our galaxy is much nearer than neighboring galaxies, little is known about the stellar populations because of the high extinction in this region. Studying the history of star formation at the galactic center may help to understand secular evolution in individual galaxies and the behavior of active galactic nuclei. Detailed data on the stellar dynamics, age, and iron abundances of a large sample of stars at the nucleus would answer questions about how the nucleus of our galaxy was formed – quickly at the formation of the galaxy or built up by gas accretion over time – and if it is dynamically similar or distinct from the bulge. NIR spectra of multiple objects simultaneously near the nucleus will drastically increase our understanding of the formation and evolution of Milky Way.

Stellar populations in nearby starburst galaxies. Starburst galaxies host large numbers of star clusters. NIR spectroscopy breaks a strong degeneracy between age and extinction in the NIR colors of the red supergiant-dominated phase of stellar evolution in these clusters. The use of extended spectra allows the constraint of both the ages and the shape of the extinction law near in homogeneously dusty massive star clusters. IR-bright star clusters in M82 have been found to be the product of recent episodes of star formation in the galaxy (Gallagher et al. 2008). Although NIR derived ages from these spectra sometimes disagree with optically derived ages because they sample different populations, they add important elements to the age distribution of massive clusters in dusty starbursts. Joint optical and NIR spectroscopic studies will provide strong constraints on the uncertain physics of massive stars on which the accuracy of population synthesis models rest.

Interaction-triggered starbursts. There are spectral features in the $\lambda = 1.45 - 1.67 \mu\text{m}$ NIR wavelength region that are indicative of thermal shocks from supernova remnants ([Fe II], 1.644 μm) and recombination processes in young HII regions (Br 12-4 [1.641 μm], Br 13-4 [1.611 μm], and Br 14-4 [1.588 μm]). By determining the spatial distributions of these emission lines and using the timescales associated with each process, past interaction-induced star formation episodes in nearby galaxies can be deduced (de Grijs et al. 2004). Adding to this information the ages, masses, and spatial distribution of

young massive star clusters will tell quite detailed histories of past interactions and star formation episodes in nearby galaxies.

Surveys of galaxies at $z > 1$. Spectral features typically used to date stellar populations in passively evolving red galaxies are shifted out of the optical band at $z > 1$. Referring to **Figure 3-1**, at $z = 1.5$ absorption features used to characterize early-type galaxies, the 4000 Å break, Mg I (5183 Å), H α , H β , and H γ , will all be shifted into the NIR bandpass. In galaxies containing dust, the reddening can be estimated from the H α /H β Balmer decrement at $z \sim 0.5$ using simultaneous RSS-VIS and RSS-NIR spectra, and at $z > 1$ using just RSS-NIR.

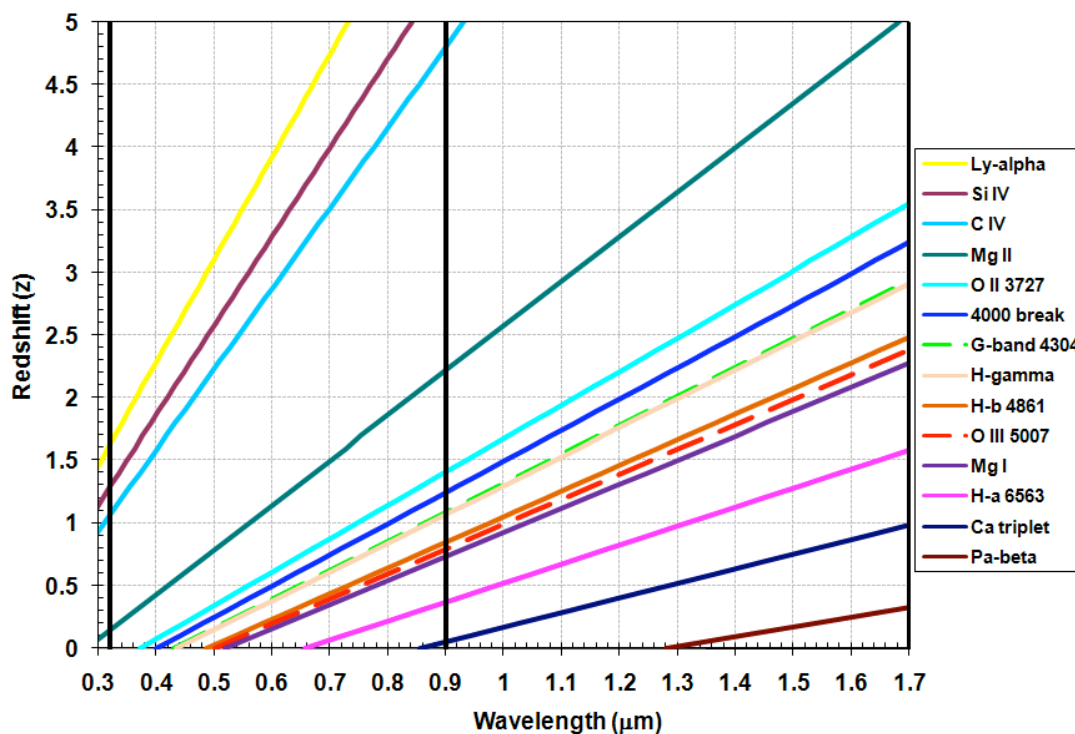


Figure 3-1. Redshifted spectral features.

Disentangling age and metallicity in galaxies. Much progress has been made in estimating the ages of galaxies by fitting continually improving stellar population synthesis models to their spectra. However, even when the entire optical spectrum of a galaxy is used the age-metallicity degeneracy is still prevalent in model fits to the data. This is particularly true for low S/N spectra typical of individual galaxies in large surveys, in which line indices for determining metallicity are unreliable due to the noisy data. Often the metallicity has to be assumed to determine an age or a number of discrete ages of the stellar populations in a galaxy. Nevertheless, this is one case where wide spectral coverage does help. It has been shown that extending the galaxy spectrum into the NIR helps to disentangle this degeneracy (Wolf 2005). When age and metallicity are both estimated from fits to optical galaxy spectra with $S/N \leq 10$, the lowest metallicities included in the model grid are often chosen as the best fit from minimizing χ^2 , since the low metallicity model spectra tend to have smaller absorption lines. However, when NIR spectra are added to the fit, more realistic estimates of metallicity result. UV-vis-NIR galaxy surveys will provide spectra that will allow reliable analyses of individual galaxies in the surveys.

“First Light” surveys. The new frontier in extragalactic astronomy and cosmology lies at $z > 7$, when the universe emerged from a period known as the “cosmic dark age.” This epoch is marked by the formation of the first (Pop III) stars in proto-galactic units, i.e., “First Light.” The observational approach to finding these objects is challenging because the key diagnostic, $\text{Ly}\alpha$, is shifted beyond $1 \mu\text{m}$ (the end of the optical window) at $z > 7$. Adding NIR capability enables searches for $\text{Ly}\alpha$ emitters up to $z \sim 12$. Such searches utilizing a NIR Fabry-Perot system, with simultaneous visible Fabry-Perot observations to eliminate interlopers will be very powerful.

Active Galactic Nuclei in the NIR. The NIR range covered by RSS-NIR is home to several permitted active galactic nuclei (AGN) emission lines of H and He with fluxes \sim few percent to 10% of that of $\text{H}\alpha$; e.g., $\text{Pa}\beta$ at $\lambda = 1.28 \mu\text{m}$ and He I at $\lambda = 1.08 \mu\text{m}$ (Glickman, Helfand, & White 2006). These are accessible by RSS-NIR to modest redshifts ($z = 0.25$ for $\text{Pa}\beta$, $z = 0.48$ for He I). Several forbidden coronal lines are also present in this part of the spectrum, including [S VIII] at $\lambda = 0.99 \mu\text{m}$, [Fe XIII] at $\lambda = 1.07 \mu\text{m}$, [S IX] at $\lambda = 1.25 \mu\text{m}$, and [Si X] at $\lambda = 1.43 \mu\text{m}$. While these are typically fainter than the prominent near-IR permitted lines, they have been detected in many nearby active galaxies with 3-4-meter class telescopes (Ramos Almeida, Perez Garcia, & Acosta-Pulido 2009; Portilla, Rodriguez-Ardila, & Tejeiro 2008), indicating their potential broad utility with an 11-meter telescope. These coronal lines come from species with such large ionization potentials (100 to several hundred eV) that they are unambiguous indicators of the presence of AGN and sample the hard ionizing spectrum of the central engine. They may provide an additional means of estimating black hole mass that is robust against the presence of a strong starburst (due to the high ionization potentials), as was recently found using space-based data for mid-infrared lines from [Ne V] and [O IV] (Dasyra et al. 2008).

Quasar absorption line studies of high- z galaxies. Quasar absorption line spectroscopy in the near-IR would be an efficient technique for detecting H I gas and associated metals in the disks and extended gaseous halos of high- z galaxies. Since the absorption technique is unbiased by luminosity, the NIR observations would supplement the existing high- z photometric and spectroscopic samples that are biased towards the higher end of the galaxy luminosity function. Among the various classes of quasar absorbers, the strong Mg II systems are often found within close impact parameters ($d \leq 75 \text{ kpc}$) of $L > 0.1 L^*$ galaxies (Steidel & Sargent 1992). Numerous spectroscopic absorption line surveys in the optical have offered a full census of this absorber population over the redshift interval $0.4 < z < 2.4$. At $z > 2.4$, the MgII doublet lines are redshifted into the NIR ($\lambda > 0.9 \mu\text{m}$). The $z > 2.4$ regime corresponds to the epoch where galaxies seem to have gone through significant morphological and chemical evolution, as revealed by the large population of Lyman-break galaxies, sub-mm galaxies (Smail et al. 1997) and galaxies with peculiar morphologies or irregular luminosity profiles (Elmegreen et al. 2005). At $z \sim 1$ Nestor et al. (2007) have detected a number of *very* strong MgII absorbers (rest equivalent width $\sim 4 \text{ \AA}$) with kinematically broad ($\Delta v \sim 400 \text{ km/s}$) line profiles. Follow-up imaging observations from the ground have shown that these absorption systems are mostly associated with galaxy pairs that are in the process of interacting and merging, thus contributing to the large velocity spreads. Through NIR observations of luminous quasars at $z > 3$, it will be possible to detect similar absorption systems at higher redshifts ($z > 2.4$) and thus select galaxy pairs and interacting systems. The NIR sample would allow us to also observationally constrain the redshift number density evolution of such systems.

Quasar absorption line studies of the IGM. Near-IR spectroscopy of $z > 5$ quasars can be used to study the distribution of metals associated with the IGM close to the epoch of reionization. Several groups (Ryan-Weber et al. 2006, Becker et al. 2008) have succeeded in detecting CIV doublet absorption lines in the IGM at those early epochs through moderate resolution spectroscopy in the NIR using ISSAC/VLT and NIRSPEC/Keck. Such observations enabled the estimation of the mass density of metals in the IGM.

The apparent lack of evolution in the mass density of metals over $1.4 < z < 5.4$, corresponding to a significant fraction of the history of the universe, is an unresolved mystery. The results are however limited by a small sample size. Detection of metals at higher- z ($z \sim 5.5$) over a sufficiently large number of sight lines (~ 50) would set a constraint on the nature of sources (star-forming galaxies vs. pop III stars) that were responsible for the enrichment of IGM with metals at those early epochs and also measure any differential variation that might exist in their distribution.

Specific science interests of the SALT consortium are listed in the following sections.

3.1.1 Highest Redshift Forming Galaxies ($z > 7$)

- Very high redshift Ly- α emitters (Barger, Bershady, *UW*)

3.1.2 High Redshift ($2.5 < z < 5.5$)

- QSO absorption line studies of interacting galaxies and the IGM (Narayanan, Savage, *UW*)

3.1.3 Moderate Redshift Galaxies ($z \sim 0.5-2$)

- Redshifted galaxies, AGN, QSO hosts – stars and gas (Sheinis & Wolf, *UW*)
- Very faint high- z galaxies (Gawiser, *Rutgers*)
- Faint galaxies at $z > 0.5$ (Menanteau, *Rutgers*)
- High z galaxy kinematics (Kannappan, *UNC*)
- Faint $z > 1$ galaxies (Aragon-Salamanca, *Nottingham – UK*)
- Low/high redshift galaxies, AGN (Exgal Group, *Gottingen*)
- Feedback in galaxies from AGN or star formation, galaxy evolution (Tremonti, *UW*)
- Star forming galaxies: SFRs, nebular abundances (Bershady, *UW*)
- Star-forming galaxies, HII regions, planetary nebulae, mergers (Kniazev, *SAAO*)
- Galaxies in clusters, starbursting galaxies (Crawford, *SAAO*)
- Faint galaxies in clusters (Hughes, *Rutgers*)
- Stellar populations of galaxies (Wolf, *UW*)

3.1.4 Nearby Galaxies ($z < 0.5$)

- Quasars and host galaxies – stars and gas (Sheinis & Wolf, *UW*)
- Nearby galaxies and their components (Sparke, *UW*; Bershady, *UW*)
- M82 (Gallagher, *UW*)
- Stellar populations in LMC and SMC (Gallagher, *UW*)
- E+A galaxies as a phase in galaxy evolution: obscured AGN, star formation (Wolf & Hooper, *UW*)
- AGN diagnostic lines in the NIR (Hooper, *UW*)
- Strongly star-forming galaxies, interacting galaxies, AGN (Vaisanen, *SAAO*)
- Low/high redshift galaxies, AGN (Exgal Group, *Gottingen*)
- Galaxy clusters out to $z \sim 0.6$ (Vaisanen, *SAAO*)

3.1.5 The Milky Way

3.1.5.1 Star Formation

- Ionized gas and shocks in nearby star forming regions (Churchwell, *UW*)
- Low end of the stellar initial mass function, IMF (Churchwell, *UW*)
- Star formation emission lines (Gallagher, Bershady, *UW*)

3.1.5.2 Stars

- Emission line stars (Shara, *AMNH*)
- Young massive stars (Vink, *Armagh Observatory – UK*)
- Circumstellar regions of young massive stars (Nordsieck, *UW*)
- Cool stars; dust obscured sources; stellar populations in Fornax and the bulge; AGB stars (Gallagher, *UW*)
- LMXRB, (Buckley, *SAAO*; Kaluzny, *CAMK Poland*)
- Binary brown dwarfs (Kaluzny, *CAMK Poland*)
- Magnetic CVs (Potter, Buckley, *SAAO*)

3.1.5.3 Supernova

- Asymmetries of supernovae with spectropolarimetry (Nordsieck, *UW*)
- Faint, late-time emission of supernovae (all types) & galactic/extragalactic nebula (Fesen, *Dartmouth*)
- Features in galactic supernova remnants (Hughes, *Rutgers*)

3.1.6 Solar System

- Asteroids, Kuiper Belt Objects (Gulbis, *SAAO*)

3.1.7 Miscellaneous

- Exoplanet transits (Buckley, *SAAO*)
- Gamma ray bursts (Buckley, *SAAO*)

The main science programs planned by the University of Wisconsin and their instrument requirements are summarized in **Table 3-1**.

Table 3-1. Instrument requirements of main science drivers from UW.

Project	Description	z	RSS Mode	R	Long λ (μm)	Sensitivity Limit ($\text{erg s}^{-1} \text{cm}^{-2}$)	Simultaneous Observations
Ultra-high Redshift Universe: Discovering First Light	Discover when and how rapidly the first galaxies formed. When is reionization complete?	$z \leq 10$	Fabry-Perot	2500	1.35	$1.00\text{E-}18$ $1 M_{\text{sun}} \text{yr}^{-1}$	visible FP tuned to redshifted [OII]3727 if NIR line is $\text{H}\alpha$
		$z = 12\text{-}13$	Fabry-Perot	2500	1.65	few $M_{\text{sun}} \text{yr}^{-1}$	
Star-Formation in the "Desert:" When Galaxies Were Young	Map star-formation rate and dynamical masses using [OII]3727 in the $1.4 < z < 2.6$ regime when most of the mass-assembly for massive galaxies is believed to have taken place.	$1.4 < z < 2.6$	MOS	> 4000	1.35	$\geq 1 M_{\text{sun}} \text{yr}^{-1}$	visible MOS to cull interlopers and acquire multiple lines for metallicity estimates and ISM diagnostics

RSS-NIR Redbook
 Mid-Term Review Design Document
 May 2009

Project	Description	z	RSS Mode	R	Long λ (μm)	Sensitivity Limit ($\text{erg s}^{-1} \text{cm}^{-2}$)	Simultaneous Observations
	well-beyond peak in co-moving SFR and AGN activity	$z < 3.4$	MOS	> 4000	1.65		
Baryon Processing in a Mature Universe	Precision mapping of down-turn in co-moving SFR and chemical enrichment from $0 < z < 1$ as function of dynamical mass using $H\alpha$ and strong-line nebular diagnostics ($[\text{NII}]/H\alpha$, $[\text{OIII}]/H\beta$)	$z < 1$	MOS	> 4000	1.35		Simultaneous optical-NIR MOS at $R > 4000$ out to $1.35 \mu\text{m}$; split $[\text{OII}]3727$ doublet and cull interlopers; acquire multiple lines for metallicity estimates and ISM diagnostics.
	kinematics of narrow-lined ($\sigma < 70$ km/s) systems at the low-mass end		MOS	7000, 14000 (0.5" slit)	1.35		
		$z < 1.5$	MOS		1.65		
Massive Star-Formation at $z = 0$	Constrain theories of massive star-formation that link production of elements and luminosity, to the energetics of feedback mechanisms and chemical enrichment which drive the evolution of baryons in galactic systems. $H\alpha/\text{Pa}\beta$ flux ratios in obscured, star-forming regions and linear spectropolarimetry of circumstellar regions in obscured sources are the primary measurements.	$z = 0$	longslit spectro-polarimetry	> 4000	1.35		Simultaneous optical-NIR MOS at $R > 4000$ out to $1.35 \mu\text{m}$ to sample $H\alpha$ and $\text{Pa}\beta$ ($1.28 \mu\text{m}$)
	$\text{Pa}\beta$ out to $z=0.3$, roughly the Sloan volume	$z < 0.3$			1.65		

Project	Description	z	RSS Mode	R	Long λ (μm)	Sensitivity Limit ($\text{erg s}^{-1} \text{cm}^{-2}$)	Simultaneous Observations
Supernovae Explosion Physics	Measuring the variation of line polarization with wavelength to observe asymmetries as a function of velocity so that line polarization gives information about chemical and density inhomogeneities within the ejecta, which can then be compared with the results of explosion codes	z = 0	longslit spectropolarimetry	> 500	1.65	S/N = 1000 (0.1% polarization)	<p>Maximum spectral coverage is required in one observation since these are time variable objects.</p> <p>Simultaneous VIS spectropolarimetry to get additional time-variable lines.</p> <p>Imaging polarimetry of the SN fields to remove foreground Galactic interstellar polarization.</p>

3.2 Flow Down of Science Requirements into Tech Requirements

From the beginning, the optical RSS on SALT has envisioned an additional NIR arm. This extension of the instrument, RSS-NIR, will be the first NIR instrument on SALT, expanding the capabilities of the telescope into an entirely new regime. With the exception of X-shooter on the VLT, the combined RSS will be unique among instrumentation for 8-11 meter class telescopes in its ability to simultaneously record data in the UV-visible and NIR. It is currently the only 8-11 meter class instrument planned to deliver Fabry-Perot imaging or spectropolarimetry at first light. It will open a new window for the discovery and study of the most distant and earliest galaxies in the universe. The RSS-NIR upgrade will include a number of operational modes over the $\lambda = 0.9$ to 1.7 μm wavelength range: imaging, very high throughput low to medium resolution spectroscopy, narrow-band Fabry-Perot imaging, and spectropolarimetry. All modes will exploit the instrument's large 8 arcmin field of view. The design incorporates an articulated camera, volume phase holographic (VPH) gratings, and a single-etalon Fabry-Perot system. This instrument leverages the considerable effort and expense undertaken by UW researchers and others for the visible system, while preserving all of the visible capability. The design philosophy for RSS-NIR was to duplicate the capabilities of the visible side where possible, with any necessary adaptations for operation in the NIR. **Table 3-2** lists the main RSS-NIR instrument parameters.

Table 3-2. RSS-NIR instrument parameters.

Optical	
Telescope Aperture	11 meters
Telescope focal ratio	f/4.18
Collimator Focal Length	302 mm
Camera Focal Length	220 mm
Image space F/#	1.4289
Efl	15718.39 mm
Plate scale	76.205 $\mu\text{m}/\text{arcsec}$
Plate scale	4.233 pixels per arcsec (18 μm pixels)
Image Quality	Pixel limited in all modes , 2 pixels =0.5 arcsec
Field of View	8 arcmin dia (imaging), 8 x 8 arcmin (spectroscopic)
Spectroscopy	
Wavelength Coverage	0.9 – 1.7 μm , $\Delta\lambda = 0.8 \mu\text{m}$
Gratings	4 articulated VPHGs, 1 conventional low R grating
Spectral Resolution	800, 2000-7000 (1arcsec slit)
Free Spectral Range (FSR) in one grating setting	FSR ~ 0.13 μm @ R ~ 2000 FSR ~ 0.11 μm @ R ~ 4000 FSR ~ 0.09 μm @ R ~ 7000 R~800 conventional grating to cover entire range, FSR = 0.8 μm
Pixel Scale	0.24
Field of View	8 x 8 arcmin
Multiplex	laser-cut MOS masks, up to 40 slits per mask
Throughput	45%, not including telescope
Detector	2048 x 2048 Teledyne Hawaii 2RG and ASIC, 18 μm pixels, long-wavelength cutoff @1.7 μm
Fabry-Perot Imaging	
Spectral Resolution	2500
Field of View	8 arcmin dia
Etaion Finesse	50
Order Blocking Filters	R ~ 50, 12 filters covering discrete atmospheric windows in J and H bands
Spectropolarimetry	
Polarization Measurements	linear, circular, all stokes
Instrument Modes	imaging, spectroscopy
Field of View	4 x 8 arcmin
Imaging	
Field of View	8 arcmin dia
Broadband Filters	Y, J, H

3.2.1 Spectral Range

Because RSS-NIR is being added to an existing facility-class optical spectrograph with which it shares a common slit plane and collimator elements, coupled with the fact that at prime focus there is the neither the space nor weight envelope sufficient to add a stand-alone NIR instrument, a fully cryogenic

instrument design that would allow operation through the K-band was never an option. Therefore, we were limited to the semi-warm spectrograph range of $\lambda < 1.8$ mm (like CIRPASS and FMOS). This led to the choice of a detector with a sensitivity cutoff at $\lambda \sim 1.7$ mm to avoid problematic thermal backgrounds at longer wavelengths. Depending on ambient operating temperatures at the telescope and the mode in which the instrument is being used, we expect RSS-NIR to operate out to $\lambda = 1.55$ - 1.7 mm with selectable long wavelength blocking filters.

3.2.1.1 The Dichroic Split Between Arms

Both the wavelength at which the dichroic beamsplitter separates the light for the visible and NIR arms and the steepness of the wavelength split are driven by science arguments. A shallow transition would provide more overlap between spectra from the two arms. However, virtually no science applications within the SALT consortium require much overlap between the visible and NIR arms when spectra are obtained simultaneously. Calibration of each arm will be done separately by observing spectrophotometric standards. On the other hand, spectropolarimetric observations prefer a sharp cut because coating properties of the dichroic vary with polarization and may prevent the measurement of accurate polarizations near the split wavelength.

The Ca IR triplet at $\lambda = 8498, 8542, \text{ and } 8662 \text{ \AA}$ is a spectral feature important to many science programs. One aspect of the decision on exactly where to make the dichroic wavelength split is which system will be most efficient for observing this feature. **Figure 3-2** shows the estimated system throughputs of both the visible and the NIR arms of RSS. These include all optics, coatings, gratings, and detector QEs. The throughput crossover occurs just blueward of the Ca triplet. Operationally, it should not matter which arm is used to observe the feature since the thermal background is not an issue at this wavelength. An important scientific consideration is what other features are likely to be observed at the same time as the Ca IR triplet? This will be considered for the final decision on this exact wavelength. Nominally, the split will be at $\lambda = 0.9$ mm.

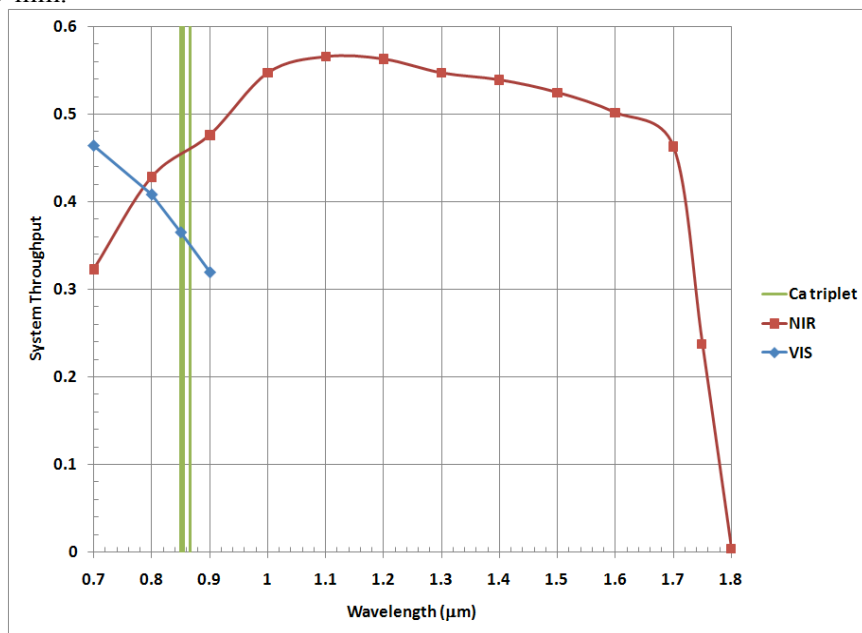


Figure 3-2. System throughputs for the VIS and NIR arms of RSS. The vertical lines mark the Ca IR triplet wavelengths. Throughput crossover occurs just blueward of this feature. The nominal location of our dichroic split is at $\lambda = 0.9 \mu\text{m}$.

3.2.2 Spectral Resolution

3.2.2.1 Grating Spectroscopy

In addition to scientific requirements for measuring spectral features, spectral resolution has restrictions set by the night sky in the NIR. For faint objects at low spectral resolution, unresolved sky emission lines place the limit on the object magnitude that can be reached, independent of the telescope size or the instrument used. However, at higher spectral resolution the night sky lines are resolved and spectral features of astronomical objects can be observed down to the sky continuum between these lines. **Figure 3-3** shows an expanded scale sky spectrum (observed on Mauna Kea) smoothed to resolutions of $R \sim 7000$ (red) and $R \sim 2000$ (blue). At $R < 4000$ the majority of night sky lines are blended and observations cannot reach the true sky continuum between these lines over most of the range. Our analysis shows that over the RSS-NIR spectral range of $\lambda = 0.9 - 1.7 \text{ mm}$, at $R=2000$, 33% of the spectrum is free of sky emission lines; at $R=4000$, 47% is free; and at $R=7000$, 54% is free. Observations of faint objects should be made at $R \geq 4000$ to achieve the true sky continuum limit within specific atmospheric windows between sky emission lines.

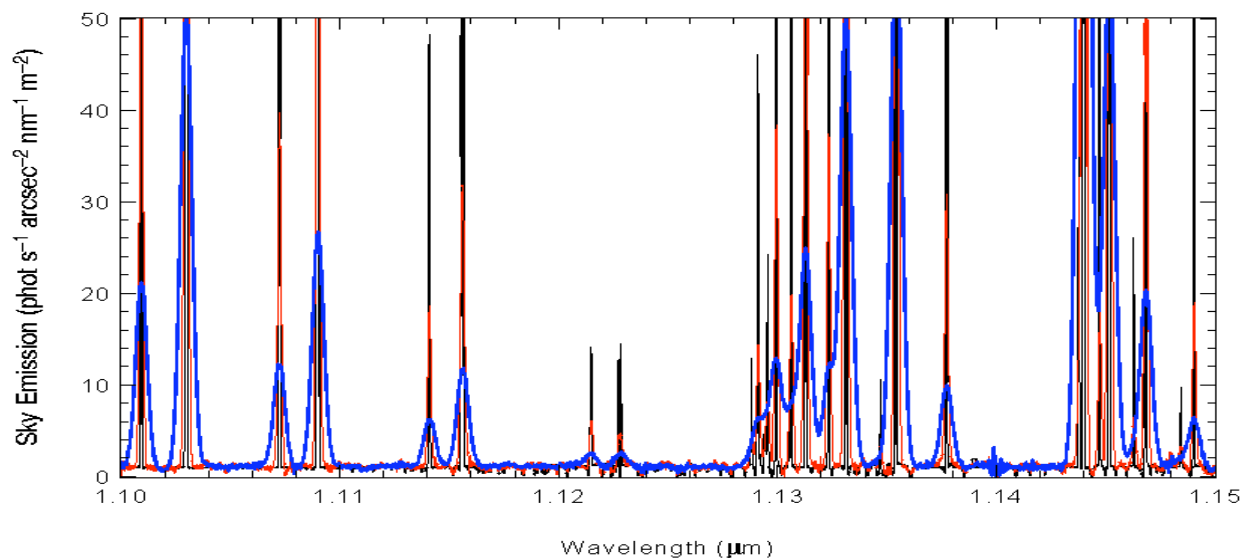


Figure 3-3. Night sky spectrum at different spectral resolutions. Underlying black is the original Mauna Kea spectrum at $R \sim 33750$, red is smoothed to $R \sim 7000$, and blue is $R \sim 2000$.

3.2.2.2 Fabry-Perot Imaging

The night sky emission lines similarly affect Fabry-Perot observations. Only objects with emission lines (intrinsic or redshifted) falling within atmospheric windows between sky emission lines can be observed without sky contamination. These atmospheric windows determine the set of order blocking filters required for the Fabry-Perot mode. One of our strongest science drivers for this operational mode requires an etalon spectral resolution of $R \sim 2500$ (see **Table 3-1**). For an etalon Finesse of 50, this leads to order blocking filters with $R \sim 50$, or an average spectral width of 0.027 nm (see Section 5.1.5 for a description of the Fabry-Perot order blocking filter selection).

3.2.2.3 Spectropolarimetry

Unlike spectroscopy, many spectropolarimetric programs will favor a lower dispersion, with higher spectral coverage. There are two reasons, one that many programs want very high S/N, and are going to a large telescope to get more photons: these objects are not at the sky limit, so high dispersion is not required to get around the sky lines. The other is that a wide spectral coverage is required to separate different polarimetric effects by wavelength dependence, like electron scattering and dust. In order to cover the entire NIR spectral range, a grating with $R \sim 800$ will be required. This would likely have to be a conventional transmission grating or grism, as the volume phase holographic gratings do not perform well in this low dispersion regime.

3.2.3 Slit Masks

RSS uses custom laser-cut multi-object slit masks. This system was developed for RSS-VIS and will also be utilized for the NIR arm. Common masks are used during simultaneous operation of both arms. The slit masks are fabricated from a carbon fiber composite material. RSS-NIR will require low emissivity gold-coated masks. We are currently running tests on laser-cutting pre-coated substrates of the same material. This process will be developed further as the results of these tests are analyzed. (See section 5.3.3)

3.2.4 Acquisition and Guiding

RSS-NIR will be used in imaging mode to acquire science fields. We envision the setup procedure for spectroscopy to include the following steps: 1) take an image of the science field and note the location of the desired target, 2) slide the slit mask in and take an image (or use a flat field image of the slit mask if it exists), 3) move the telescope tracker to place the science object at the desired location on the slit, 4) take another image to verify its placement on the slit, 5), tweak the object placement if necessary, 6) insert the grating and rotate, 7) articulate the camera to the proper angle, 8) begin guiding, 9) begin the science exposure.

A slit-viewing camera is available for guiding during long slit spectroscopic observations. The longslits are made of a reflective material and tilted at a 12° angle to allow SALTICAM to image the focal plane. The reflective area of the slit is approximately $2'$ in the dispersion direction by the length of the slit in the cross-dispersion direction.

A guide probe system is available for guiding during multi-object observations where a slit mask placed perpendicular to the beam path is used. Both of these systems were designed for the existing arm of the instrument, RSS-VIS.

3.2.5 Instrument Sensitivity

We have designed RSS-NIR to optimize high throughput, which has led our choices to: volume phase holographic gratings (VPHGs) for an increase in efficiency over conventional gratings, all transmissive optics with efficient AR coatings (we are investigating hardened solgel), and a HAWAII 2RG detector for which arrays have demonstrated quantum efficiency > 0.8 over our entire operating wavelength range. Preliminary throughput predictions of RSS-NIR are shown in **Figure 3-4**.

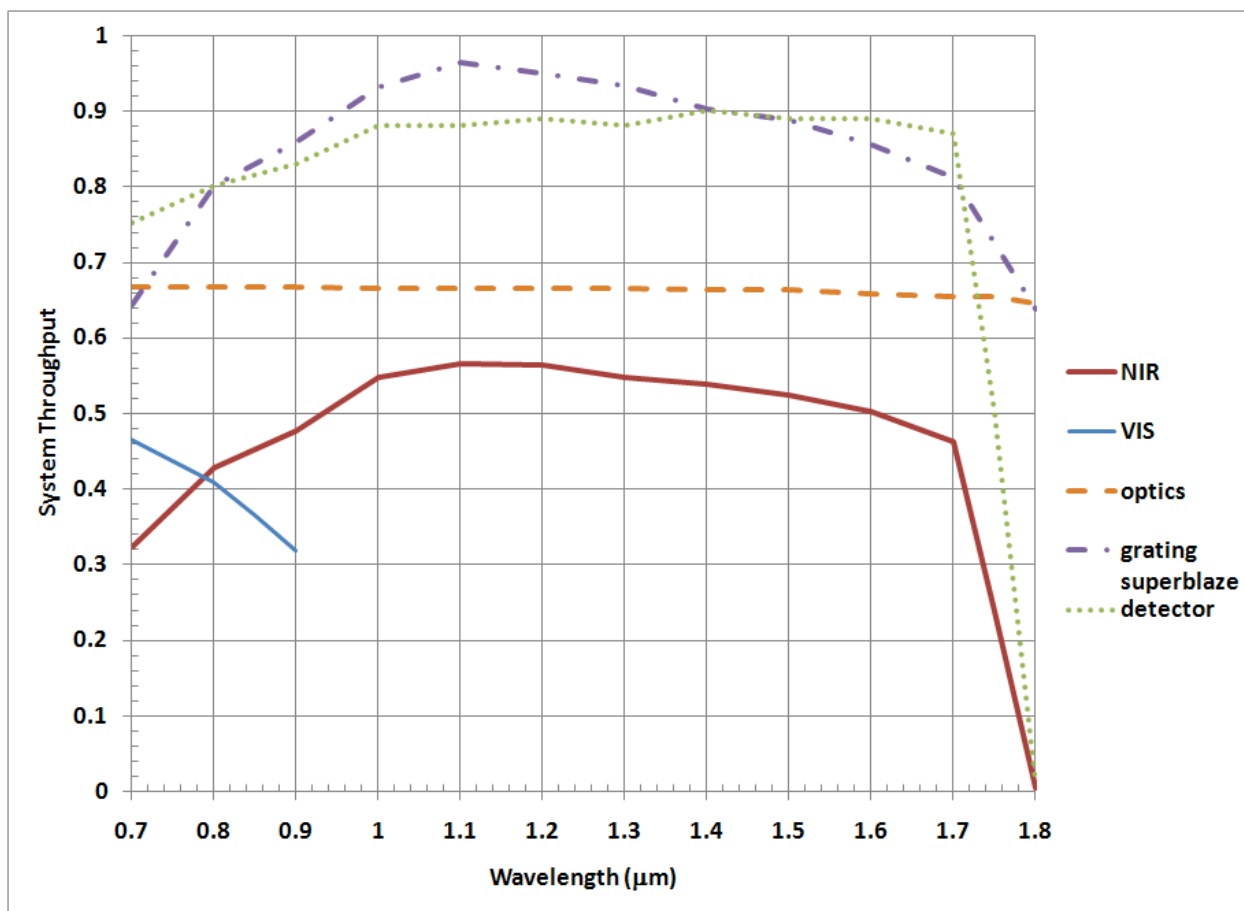


Figure 3-4. Predicted throughput of RSS-NIR components, excluding telescope losses.

We have developed a sky-limited performance model for RSS-NIR that uses actual material transmissions of all optics, predicted volume phase holographic grating efficiencies (using the Kolgelnik approximation), and a detector quantum efficiency spectrum for a Hawaii 2RG-1.7mm array from Teledyne (Beletic et al. 2008). The instrument thermal backgrounds used in this model were determined from actual ray traces in a detailed thermal stray light analysis, which has been integral to the design of this instrument (Section 5.3, RSS-NIR Thermal Stray Light Analysis document SALT-3501AA0002). We have assumed 5 “dirty” telescope mirrors with $R_{\text{primary}} = 0.89$ and each of the 4 spherical aberration corrector (SAC) mirrors at $R_{\text{SAC}} = 0.96$. Resulting performance predictions for RSS-NIR are given in **Table 3-3** and shown as a function of wavelength in **Figure 3-5** and **Figure 3-6**. These are limiting magnitudes to reach $S/N = 10$ per spectral resolution element in a 1 hour exposure for 1 arcsec^2 .

Two different cases are shown. In **Figure 3-5** the top plots shows the flux density of the backgrounds reaching the detector for $R=7000$ and an ambient temperature of $T_{\text{amb}} = 0 \text{ }^\circ\text{C}$ as a function of wavelength. This represents a cold winter night, with the median SALT winter temperature at $+3 \text{ }^\circ\text{C}$. The black spectrum is the sky (using a Maunaea Kea sky observation), the cyan line is a fit to the sky continuum, and the symbols are the instrument backgrounds. The different symbols represent different amounts of slit cooling below the ambient observatory temperature: none (red squares), $dT_{\text{slit}} = -20 \text{ }^\circ\text{C}$ (blue triangles), and $dT_{\text{slit}} = -30 \text{ }^\circ\text{C}$ (green circles). These plots are instructive to see at what wavelength the instrument thermal background due to self emission begins to dominate the sky background. The bottom plot shows the limiting Vega magnitude as a function of wavelength. **Figure 3-7** shows the same plots for $T_{\text{amb}} = +20$

°C, the maximum typical summer temperature, with the summer median at $T_{amb} = +13$ °C. **Table 3-3** also gives limiting magnitudes for $R=4000$ under the same conditions. The minimum spectral resolution that we discuss here is $R = 4000$, because below that resolution the observed spectrum becomes dominated by night sky emission lines that are no longer resolved. Sky-limited observations of faint objects cannot typically be done at $R < 4000$. Objects that are much brighter than the sky could be observed at lower spectral resolution, however, for them these limits due to backgrounds will not be an issue.

Table 3-3. *RSS-NIR limiting magnitude performance predictions for $S/N = 10$ per spectral resolution element in 1 hour for 1 arcsec^2 .*

Spectral Resolution (R)	Ambient Temperature (°C)	Slit Cooling below Ambient (°C)	Limiting J mag Vega (AB)	Limiting H mag Vega (AB) to $1.7 \mu\text{m}$
4000	0	0	21.1 (22.0)	20.1 (21.5)
4000	0	-20	21.1 (22.0)	20.1 (21.5)
4000	0	-30	21.1 (22.0)	20.1 (21.5)
7000	0	0	20.7 (21.6)	19.6 (21.0)
7000	0	-20	20.7 (21.6)	19.6 (21.0)
7000	0	-30	20.7 (21.6)	19.6 (21.0)
4000	20	0	21.2 (22.1)	19.8 (21.2)
4000	20	-20	21.2 (22.1)	20.0 (21.4)
4000	20	-30	21.2 (22.1)	20.0 (21.4)
7000	20	0	20.7 (21.6)	19.2 (20.6)
7000	20	-20	20.7 (21.6)	19.5 (20.9)
7000	20	-30	20.7 (21.6)	19.5 (20.9)

3.3 Competing Instruments

RSS-NIR fills an obvious gap in SALT instrumentation since it will be the first NIR instrument on the telescope. It is also important to compare the unique capabilities of RSS to instrumentation on large telescopes worldwide. **Table 3-4** lists the spectroscopic capabilities of NIR instruments on 4-11 meter class telescopes worldwide. Any extra instrument modes are noted in the last column. Of all NIR instruments on 4-11 meter class telescopes, RSS and X-shooter are the only two that can simultaneously cover the UV-VIS-NIR wavelength range. X-shooter does this routinely at the optimal design spectral resolutions. While RSS can observe at any of its instrument resolutions simultaneously in the VIS-NIR, it could only achieve contiguous coverage at low resolution, $R \sim 800$. However, for X-shooter, detector real estate for spectral coverage comes at the price of observing only single objects. RSS has a wide field multi-object mode utilizing custom laser-cut masks with up to 40 slits per mask. Furthermore, the tunable VPHGs (in both wavelength region and spectral resolution) in each arm, in conjunction with multi-object slit masks, allow great flexibility in observations. For example, the gratings on each side could be tuned to observe both $H\alpha$ and $H\beta$ in a galaxy cluster at $z=0.5$ (refer to **Figure 3-1** for redshifted spectral features), or to simultaneously observe the star formation indicators $H\alpha$ and $[O II]$, or to observe the Ca IR triplet at $R > 4000$ to get between the sky lines in the NIR arm and simultaneously observe typical optical features over a wider spectral range at lower resolution in the VIS arm. There are many projects that will not require the entire contiguous spectral coverage, but where two discrete regions in the UV-VIS and the NIR would be highly desired.

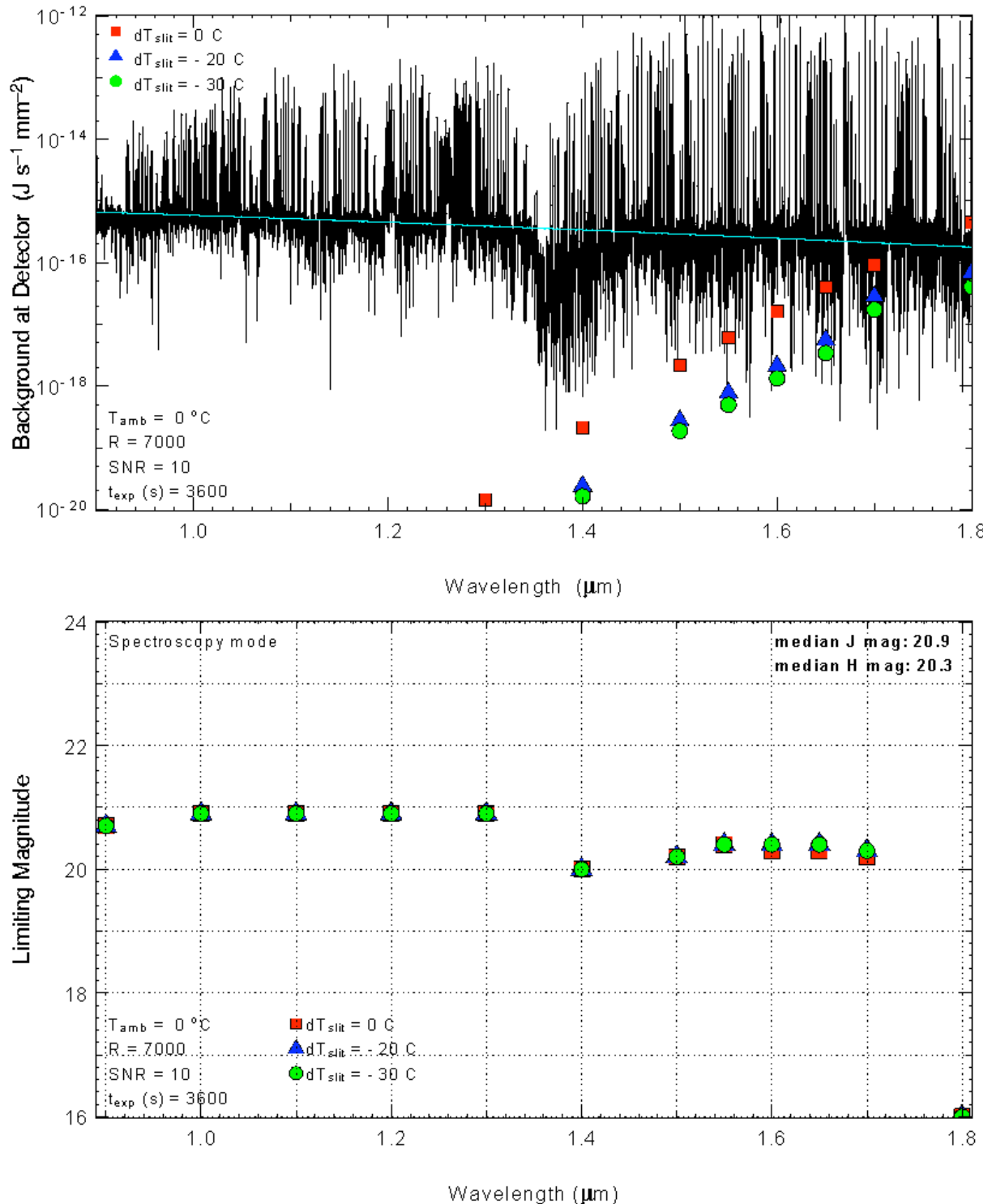


Figure 3-5. RSS-NIR performance predictions. The top plot shows the background flux density at the detector for $R=7000$ and $T_{\text{amb}} = 0^\circ\text{C}$. The black spectrum is the sky, and the symbols are the instrument background for no slit cooling (red squares), $dT_{\text{slit}} = -20^\circ\text{C}$ (blue triangles), and $dT_{\text{slit}} = -30^\circ\text{C}$ (green circles). The bottom plot shows the limiting Vega magnitudes to reach $\text{S/N}=10$ per spectral resolution element in a 1 hour exposure for 1 arcsec^2 as a function of wavelength.

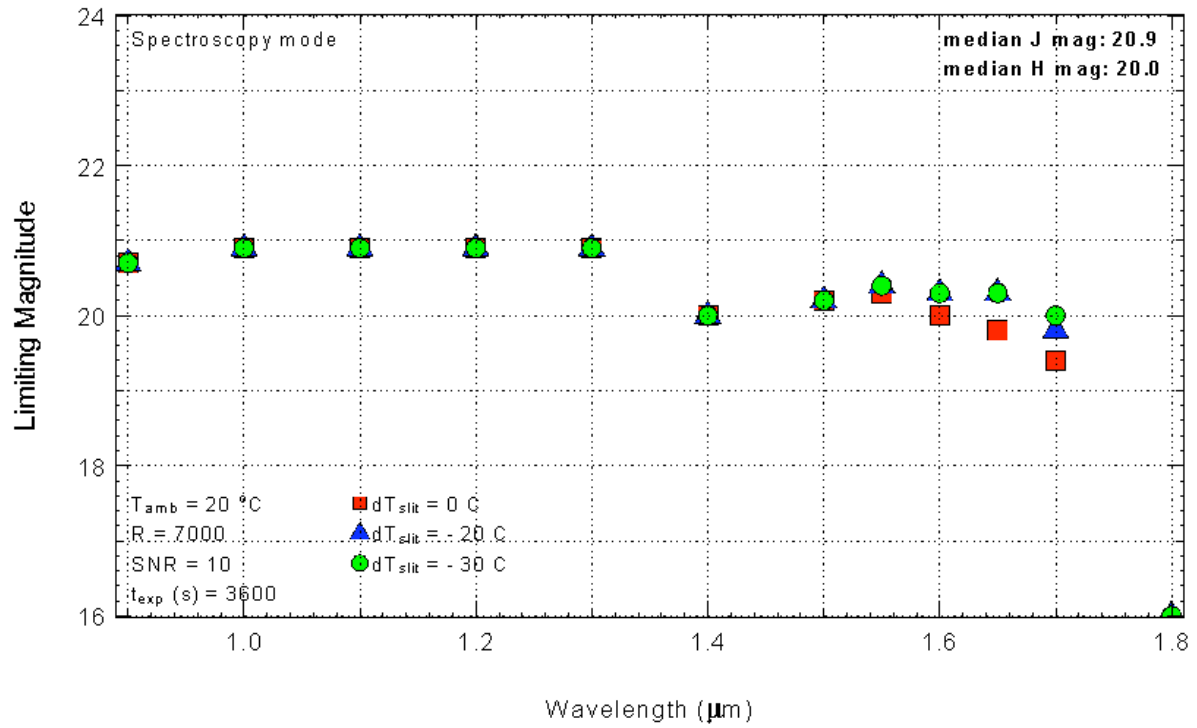
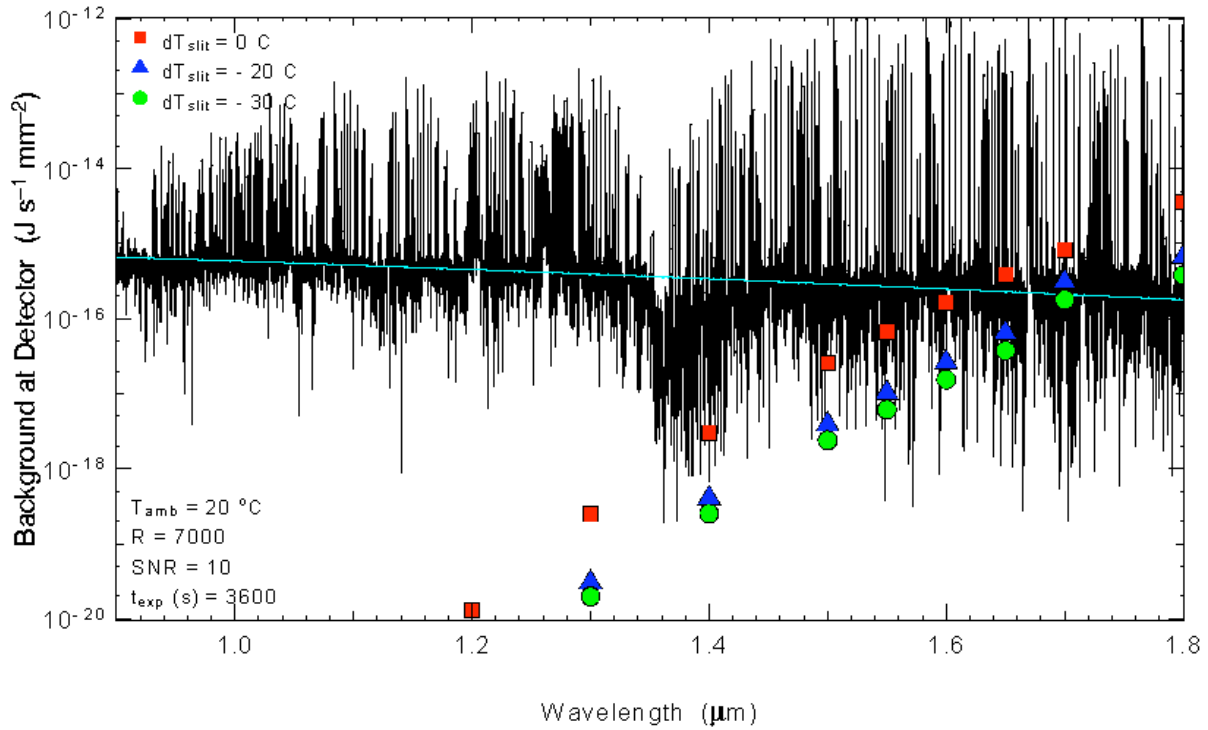


Figure 3-6. RSS-NIR performance predictions. Same as **Figure 3-5** but for $T_{\text{amb}} = +20 \text{ }^\circ\text{C}$.

RSS-NIR Redbook
Mid-Term Review Design Document
May 2009

We define an instrument comparison metric here that attempts to quantify the amount of information collected in a single instrument observation (Bershady et al. 2004). We plot the product of the telescope size and instrument field of view, $A\Omega$ ($m^2 \text{ arcsec}^2$), against the spectral power, defined as the product of spectral resolution ($\lambda/\Delta\lambda$), number of spectral resolution elements in one setup ($N_{\Delta\lambda}$), and the number of objects observed in the setup (N_{obj}). This comparison for the instruments listed in **Table 3-4** is shown in **Figure 3-7**. Solid lines connect points representing a continuous range of R, while dotted lines indicate two separate R's available in the instrument.

Table 3-4. Comparison of NIR instruments on 4-10 meter class telescopes worldwide.

Telescope	Instr.	Field of View	λ range (μm)	R ($\lambda/\Delta\lambda$)	# Objects	Pixel size (")	FSR in one setting (μm)	Limiting magnitudes Vega	Extra modes
SALT	RSS-NIR RSS	8'x8' 8'x8'	0.9 - 1.7 0.32 - 0.9	1000- 7000	40	0.22	$\Delta\lambda \sim 0.09 - 0.2$ 0.32 - 1.7 @ low R	H=19.8 (19.2), S/N=10, t = 1 hr, R=4000 (7000)	Fabry- Perot, Spectro- polarimetry
Gemini	NIFS ‡	3"x3"	0.95 - 2.4	5000- 6000	single IFU	0.04	z, J, H, or K	H=18.3, S/N=5, t = 1 hr	
	Flamingos -2	2'x6'	0.95 - 2.5	1200,3 000	MOS masks	0.18	0.9-1.8, 1.25- 2.5 J, H, or K		Fabry- Perot†
Keck	MOSFIRE	6'x3'	0.97 - 2.45	3270	45	0.18	1.48-1.81, 1.97-2.42	H=20.1, S/N=10, t = 1000 s, R=3270	
	OSIRIS ‡	2.2"x 3.2"	1.0 - 2.4	3900	391 fibers	0.02- 0.1	$\Delta\lambda \sim 0.06 - 0.4$	H=21.1,** S/N=10, t = 1 hr	
Subaru	MOIRCS ‡	4'x7'	0.9 - 2.5	500, 1500- 1600	40	0.117	0.9 - 2.5	H=18.4,** S/N=10, 1 hr, R=1600	
	FMOS	30'	0.9 - 1.8	500, 2200	400 fibers		0.9 - 1.8 @ R=500, 4 settings at R=2200	H=20.9, S/N=5, t = 1 hr	
VLT	X-shooter	12" slit	0.3 - 1.9	5000	1	0.14- 0.31	0.3 - 1.9	H=18.6, S/N = 10, t = 1 hr, R=5000	IFU*, Spectro- polarimetry *
GTC	EMIR	6'x4'	0.9 - 2.5	4000	45	0.2	0.9 - 2.5	H=21.1, S/N = 5, t = 4 hr, R=4000	
LBT	Lucifer	4'x3'	0.9 - 2.5	500- 5000, 1000- 10000	MOS masks	0.25, 0.12	$\Delta\lambda = 0.46,$ 0.22		IFU*
Magellan	FIRE	7" slit, 1' slit	0.8 - 2.5	6000, 900- 2500	1	0.18	0.89 - 2.51	J=20.0, S/N=10, t = 2.3 hr, R=6000	
MMT	ARIES	107"	1 - 5	2000, 30000	MOS	0.1	J,H, and K J-H, H-K	J=20.7 (18.5) S/N = 10, t = 1hr, R=2000 (30000)	

‡, instrument in operation, † planned upgrade, * possible upgrade option, ** our estimate

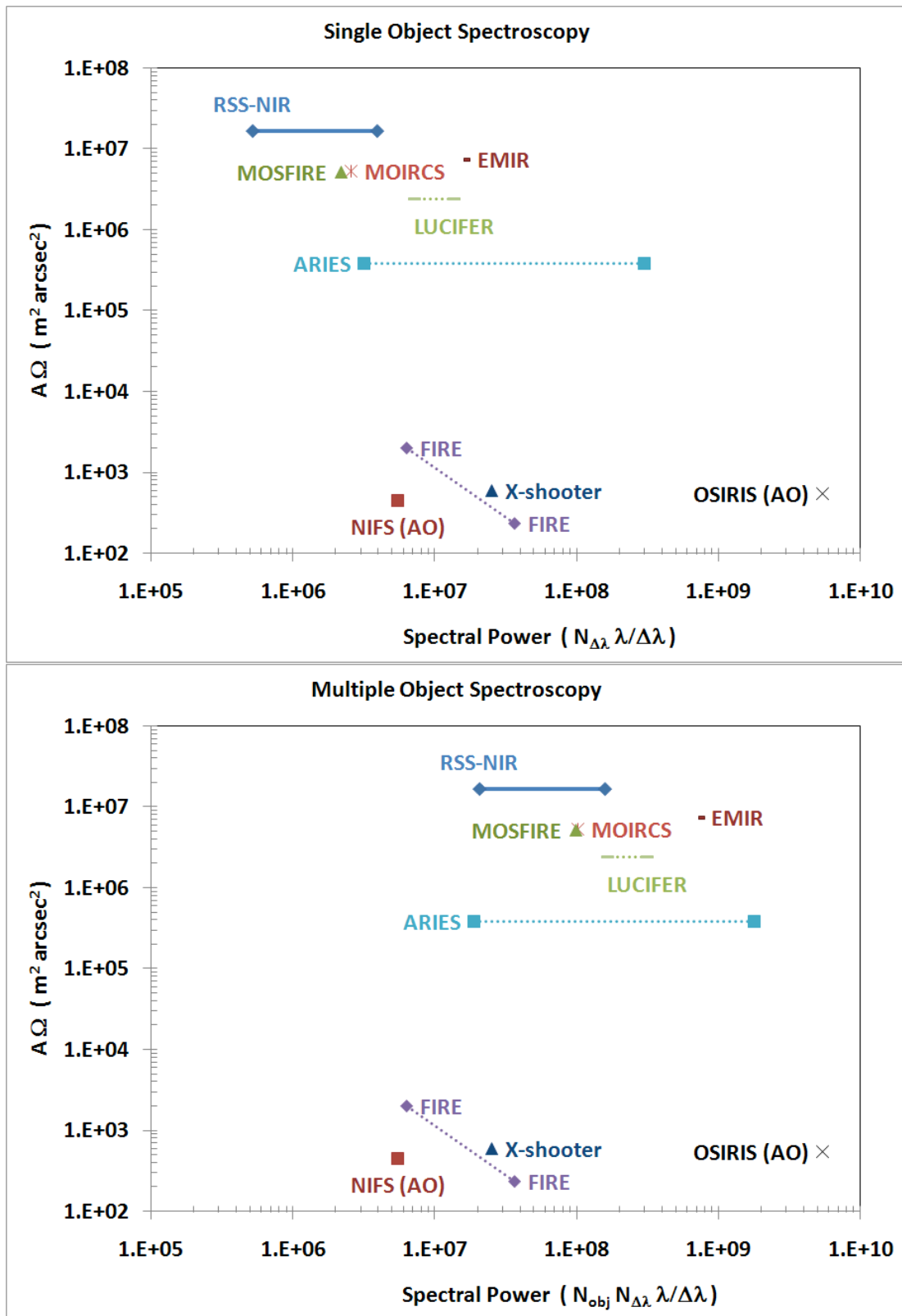


Figure 3-7. Instrument comparison of $A\Omega$ and spectral power.

We also adopt a performance metric from the X-shooter team, the “power” of a spectrograph. This metric is defined as $P = R (l_2/l_1) / t$, where R is the spectral resolution ($\lambda/\Delta\lambda$), l_2 is the longest wavelength of the free spectral range (FSR) of one setting, l_1 is the shortest wavelength of the FSR, and t is the time in sec to reach $S/N=10 \text{ \AA}^{-1}$ for a $H_{AB}=19.5$ object. Values are given in **Table 3-5** for the instruments for which we have enough information to scale the predicted observations. The AO instruments have been excluded. The last two columns give the power for a single object and for multi-object spectroscopy (MOS). At $R\sim 4000$ RSS-NIR for observing a single object has a $P = 6.6$, while X-shooter is at $P = 6.9$ at $R\sim 5000$. If we consider the MOS mode of RSS-NIR where 40 objects can be multiplexed, the power goes up to $P = 263$.

Table 3-5. Comparison of spectrograph power.

Telescope	Instrument	Resolution	Time (s)	P (single)	P (MOS)
SALT	RSS-NIR	4000	652.17	6.58	263.21
	RSS-NIR	7000	1125.45	6.74	269.67
Keck	MOSFIRE	3270	127.52	31.36	1411.25
Subaru	MOIRCS	1600	21493.27	0.21	8.27
VLT	X-shooter	5000	4586.19	6.90	6.90
GTC	EMIR	4000	951.66	11.68	525.40
Magellan	FIRE	6000	6698.35	2.53	2.53
MMT	ARIES	2000	7219.09	0.58	3.48
	ARIES	30000	1846.29	23.14	138.83

3.4 Preliminary Specifications

Table 3-2 outlined the basic instrument parameters needed for RSS-NIR to satisfy its science requirements. In this section we present a number of science-engineering tradeoffs that have been considered to this point in the design. Then we overview the entire instrument system and summarize additional operating parameters.

3.4.1 Science – Engineering Trade Matrix

The table below summarizes instrument engineering decisions that would affect capabilities and thus the science programs that could be conducted. Time percentages for different long wavelength cutoffs are % of hours between 18° astronomical twilight throughout a year, based on historical SALT temperature data.

Table 3-6. Science – Engineering Trade Matrix.

Engineering Decision	Option	Capability Change / Complexity Implications	Science Affected	Engineering Impact	Cost Estimate
Pre-dewar cooling	none	λ_{cutoff} limit at 1.35 μm ; Compromises probability of overall instrument success	Lose: Galaxy diagnostics at $z > 1$; Thermal shocks from supernova remnants ([Fe II], 1.644 μm) and recombination processes in young HII regions (Br 12-4 [1.641 μm], Br 13-4 [1.611 μm], and Br 14-4 [1.588 μm]); Ly α at $z > 10$	Straightforward: This would reduce requirements in the design.	Reduce baseline budget by \$280k
	cool to -40 °C	Components in pre-dewar will not thermally limit operation	Allows observations out to $\lambda \sim 1.55\text{-}1.67 \mu\text{m}$; Ly α to $z \sim 13$	Manageable: This is the current baseline requirement. Many components operational to this temperature.	None – in the baseline budget.
	cool below -40 °C	Minimal performance increase, unless entire instrument is cooled and longer wavelength detector used	None, given our 1.7 μm detector cutoff wavelength	Difficult: Electronics and motors will be difficult to find, it is a rare exception that an off-the-shelf item is rated this low. Larger load on the chilling system.	Increase baseline by \$75-125k (materials and labor)

RSS-NIR Redbook
 Mid-Term Review Design Document
 May 2009

Engineering Decision	Option	Capability Change / Complexity Implications	Science Affected	Engineering Impact	Cost Estimate
Slit cooling (assuming gold slits)	none	λ_{cutoff} for R=7000 (4000): 1.65 μm 7% (29%) of time, 1.6 μm 47% (74%) of time, 1.55 μm 86% (100%) of time	Compromises many diagnostic lines in $\lambda = 1.6\text{-}1.67 \mu\text{m}$ region	None	None
	cool to $dT_{\text{slit}} = 30 \text{ }^\circ\text{C}$ below T_{amb}	λ_{cutoff} for R=7000 (4000): 1.7 μm 41% (69%) of time, 1.65 μm 90% (99%) of time, 1.6 μm 100% (100%) of time	More likely to be able to observe Fe II 1.644 μm line and Br lines at $\lambda > 1.6 \mu\text{m}$	Challenging: This has been assessed and viable options have been developed. This will require some bench testing to verify and test a design scheme.	Increase baseline by \$150-200k
	cool more than $dT_{\text{slit}} = -30 \text{ }^\circ\text{C}$	Only incremental long λ performance increase, unless collimator is also cooled	Not much gained	Difficult: Removing enough energy and mitigating condensation become very difficult beyond 30 $^\circ\text{C}$ below ambient.	Increase baseline by \$175-250k
Collimator cooling	none	Does not affect performance unless the slit is cooled to $dT_{\text{slit}} > 30 \text{ }^\circ\text{C}$ below T_{ambient}	Not necessary for main science cases	None	None
	cool	Could go to longer wavelength detector; More stringent specs on long wavelength cutoff filters; Compromises probability of overall instrument success	Observe higher redshift objects, Pa- α line, better data on asteroids & KBOs at longer wavelengths	Challenging with risks: collimator is significantly spaced limited by original design that compensates alignment over a larger temperature range and the spaceframe. May require remounting the optics to take advantage of radial space for cooling. Exposes optics and coatings to significant risk.	Increase baseline by \$275-375k

RSS-NIR Redbook
 Mid-Term Review Design Document
 May 2009

Engineering Decision	Option	Capability Change / Complexity Implications	Science Affected	Engineering Impact	Cost Estimate
Number of gratings	increase from 5	Would decrease gaps in contiguous spectral coverage between gratings at a given R for $R > 4000$; Could extend to $R > 7000$ or $800 < R < 4000$ Would decrease number of available FP filters	Improve chances of observing particular redshifted lines at a specific R; Would increase contiguous spectral coverage for stellar populations in galaxies; Decreases spectral windows for FP observations (filters)	None to challenging: If the number of filters is reduced to provide space, there is no impact. If not, this is very challenging if not difficult. RSS-NIR is pushing the SALT envelope now.	~None: if gratings are swapped for filters. Adding a grating: ~\$25k (w/ redesign, holder, grating...)
Exchangeable gratings	while pre-dewar is cold	Increases timing flexibility of observations at $R > 7000$ or $800 > R > 4000$ to days rather than months	Quicker observations of bright objects at intermediate or very high R	Challenging: Requires new scheme and design to isolate and remove grating cassette. Can be done, but significant engineering time required.	Increase baseline by: \$75-125k
	only when pre-dewar is warm	Forces above observations to campaign mode	Have to observe $R > 7000$ in campaign mode	None: in baseline plan	None
Number of FP filters	increase from 12	Would allow FP observations in more atmospheric windows; Would mean fewer gratings in pre-dewar	More flexible observations of redshifted objects: high z Ly α emitter search	Challenging: RSS-NIR is pushing the SALT envelope now. No space available.	Increase baseline by: ~\$25k per filter
Number of exchangeable FP filters	increase from 3	Would decrease required frequency of filter exchanges	More flexible observations of redshifted objects; Otherwise delayed by ~days-weeks for filter exchanges	Manageable: Can be done, up to 6. Impacts: 1) heavier cassette for handler. 2) Potentially needless thermal cycles on filters that do not need to be removed	Negligible: Redesign of preliminary design, ~\$5k

RSS-NIR Redbook
 Mid-Term Review Design Document
 May 2009

Engineering Decision	Option	Capability Change / Complexity Implications	Science Affected	Engineering Impact	Cost Estimate
Gold coating long slits	none	λ_{cutoff} limit at 1.5 μm	Lose: Galaxy diagnostics at $z \sim 1-2$; Thermal shocks from supernova remnants ([Fe II], 1.644 μm) and recombination processes in young HII regions (Br 12-4 [1.641 μm], Br 13-4 [1.611 μm], and Br 14-4 [1.588 μm]); Ly α at $z > 11$	Straightforward: Simply need to coat slits.	\$150-300 slit
Gold coating MOS masks	none	λ_{cutoff} limit at 1.5 μm ; Decreases complexity, time, cost of making masks	same as above	Manageable: Working on a processes to gold coat. Will add lead-time to order and receive masks at facility.	Operational increase: \$150-300/mask
ADC	Remove for NIR observations	Would improve NIR performance	Problem for simultaneous UV-NIR observations	None	SALT Facility
Dichroic split λ		Determines whether Ca IR triplet is on VIS or NIR arm	None Nominally at 0.9 μm		
Exchangeable Dichroic	Manual process during the day	Would allow more than one split wavelength, fold mirror for only VIS observations, straight through for only NIR observations	Spectropolarimetry may have issues with a dichroic beamsplitter – would be forced into campaign mode with manual change	Challenging: Requires a redesign of the dichroic and VIS & NIR doublets mounts to streamline access and alignment. Very tight and difficult working conditions.	Increase baseline by: ~\$30k + cost of additional optics
	Remote process during observing	Would allow more than one split wavelength, fold mirror for only VIS observations, straight through for only NIR observations	More flexible timing for spectropolarimetric observations if dichroic is a problem	Difficult: The tight space may make this impossible. Significant engineering required for concept, preliminary, detail design. Additional fabrication and testing.	Increase baseline by: ~\$175-250k

3.4.2 System Overview

Very high efficiency VPH transmission gratings are available. This allows a compact, efficient, all transmissive system. Visible VPH gratings are installed and commissioned in the RSS-visible beam. Because the gratings will be used at angles of up to 100 degrees (between collimator and camera), the spectrometer can produce a higher dispersion than a conventional reflection-grating spectrometer with a moderate beam diameter. This allows the spectrometer to be as compact as possible.

The scientific and technical requirements of RSS-NIR have led to the following baseline system design.

1. Instrument modes
 - a. Imaging
 - b. Spectroscopy
 - i. Long slit
 - ii. MOS
 - c. Fabry-Perot narrow band imaging
 - d. Polarimetry
 - i. This mode can be added to any other modes
2. A fixed dichroic beamsplitter separates the visible and NIR arms of RSS. The nominal wavelength at which the split happens is 0.9 μm .
3. RSS-NIR is laid out in sections operating at 3 different temperatures.
 - a. Ambient temperature components include:
 - i. Slit plane (slit cooling will be engineered as an upgrade)
 - ii. Waveplates for polarimetry
 - iii. Collimator
 - iv. Dichroic beamsplitter
 - v. Separate final collimator doublet for each arm to optimize image quality
 - b. Pre-dewar operating at -40 °C encloses:
 - i. Second element in NIR collimator doublet serves as the window to the pre-dewar. The air space between the doublet elements and on the outside of the first element will be purged with dry air to prevent condensation.
 - ii. Fold mirror
 - iii. 5 remotely deployable spectroscopic gratings:
 1. 4 VPHGs providing $R \sim 4000-7000$ (1" slit)
 2. 1 conventional grating or grism providing $R \sim 800$
 - iv. 1 remotely deployable Fabry-Perot etalon ($R \sim 2500$)
 - v. 12 remotely deployable Fabry-Perot order blocking filters
 - vi. 1 remotely deployable polarizing beamsplitter for polarimetry
 - vii. Camera optics – first 5 of 7 at pre-dewar temperature
 - c. Cryogenic vacuum Dewar operating at 120 K. Completely contained inside the pre-dewar. Cooled with a closed cycle cooling system. Dewar contains:
 - i. Last 2 camera optics
 - ii. Camera lens #6, IFPL51Y, is the window from the pre-dewar into the Dewar
 - iii. 5 position filter wheel: open, blocked, 3 long wavelength cutoff filters
 - iv. Detector array: 2048x2048 HAWAII2-RG, 1.7 μm wavelength cutoff
 - v. SIDECAR ASIC electronics
 - vi. Temperature control system
4. Camera and gratings are each remotely articulated to set spectral resolution and central wavelength. Grating angles up to 50 degrees can be accommodated. Maximum resolution is 7000 with 1" slit, 14000 with 0.5" slit (minimum slit width at Nyquist sampling).

5. Camera focus is remotely controlled using a group of lenses in the pre-dewar, outside the cryogenic Dewar. Focus mechanism is similar to that designed for the visible beam.
6. Camera optics will be held within metal cells by an elastomer, similar to the visible beam.
7. Fold mirror is actuated to allow nodding along the slit by 10's of arcsec during long spectroscopic exposures. A second tip/tilt stage on the fold mirror allows open loop flexure compensation.
8. Any of the 12 Fabry-Perot filters can be exchanged during the day while keeping the pre-dewar cold via an air lock system that allows the removal and replacement of a 3 filter cassette. This also allows for the insertion of guest, or campaign filters to be inserted during normal daytime operation.
9. Custom multi-object slit masks are laser-cut with a system designed for the RSS visible instrument.
10. Slit masks will have a low emissivity gold coating, allowing sky-limited spectroscopy out to 1.55 – 1.67 mm, depending on the ambient temperature and the spectral resolution of the observations.
11. No slit cooling will be provided initially. A feasibility study has been done and viable solutions identified. This may be added as a later upgrade to allow sky-limited spectroscopy to be possible during more of the year and to extend out to 1.7 mm.
12. The NIR camera and doublet will have a small amount of passive optical compensation for focus with temperature as these optics will be held essentially isothermally within the Dewar and pre-dewar.
13. Three cryogenic IR blocking filters will reside in the Dewar to allow for a selectable maximum long wavelength spectral cutoff for sky-limited observations. The cutoff wavelength will be based on the ambient temperature and spectral resolution of the observations.
14. Assembly and integration will occur offsite in at the SAAO facilities in Cape Town. The visible instrument will be shipped fully assembled to Cape Town for this procedure.

4. PRELIMINARY DESIGN ACTIVITIES

Since the PDR, the project team has executed a number of feasibility and design trades, matured the overall mechanical design, and addressed specific design issues raised at the PDR.

4.1. Feasibility and Design Trades

- Gold coated slits: while gold coating the long slits is a straightforward process, a means to gold coat the multi-object slits is in the process of being optimized.
- Filter cassette exchanges: several schemes to swap filter cassettes were considered and traded-off one another. An “internal air-lock” design has been matured.
- Control system hardware and software: the impact of switching to a new control system hardware architecture versus using the same as RSS-VIS has been considered along with upgrading to LabView 8.6.
- Thermal design considerations: a number of thermal issues were re-analyzed as the design matured, including: utilizing the doublet as a “thermal pane” for the pre-dewar (thermal and stress analysis), updating the pre-dewar enclosure analysis, and reexamining the cooling line runs.
- Cooling the collimator: an initial assessment was conducted to weigh different options for cooling the collimator. This included extending the pre-dewar down to the collimator or remounting the collimator optic to function at one, fixed temperature and then utilize the freed up space for

cooling. These options were not pursued further as the ASAP modeling indicated the collimator thermal noise was not the limiting factor.

- Cooling the slit: several schemes were evaluated for cooling the slit and were narrowed down to three viable choices using TECs, forced air convective cooling, or conductively cooling. While conceptually viable, no option was matured into a preliminary design as the increased scope and cost were not warranted by the science team. These options are not presented here, but will be discussed in the MTR.

4.2. Maturing the Overall Mechanical Design

The design efforts were focused on maturing the design of the following subsystems and assemblies:

- Optics Storage Assembly design and drive mechanism;
- Filter cassette and holder design and insertion mechanism;
- Grating cassette, holder, and rotation stage design and insertion mechanism;
- Fabry-Perot etalon insertion mechanism;
- Polarizing beamsplitter holder and insertion mechanism;
- Dichroic, doublet, and fold mirror structural and alignment mounts;
- Camera housing and optical focus design;
- Dewar design;
- Pre-dewar enclosure design and construction scheme;
- Filter cassette exchange scheme and accommodation within the pre-dewar enclosure;
- Camera/Dewar assembly articulation; and
- Establishing mechanical tolerances flowed down from an optical tolerance analysis, which drove the mechanism and mount designs.

4.3. Specific PDR Design Issues

Additional design details were addressed in response to specific design issues raised at the PDR.

- Increased the number of Fabry-Perot Ordering Blocking Filters from 7 to 12.
- Provided a tilt of 2° to the Fabry-Perot Ordering Blocking Filters.
- Changed the pre-dewar enclosure design to fully enclose the camera/Dewar assembly and switched to a static seal between the top and bottom.
- Provided tip/tilt ability to the fold mirror.
- Provided a lightweight, independent, and stiff truss structure to support the camera/Dewar assembly articulation to address flexure issues experienced by the RSS-VIS.
- Improved the flexural stiffness of the grating rotation stage through the addition of a mounting bearing above and below the grating center-of-gravity.

5. PRELIMINARY DESIGN

5.1. Optics

5.1.1. Optical Design Description

The Robert Stobie Spectrograph-Visible side (RSS-VIS), originally called the Prime Focus Imaging Spectrograph (PFIS) was designed by Professor Ken Nordsieck. It is described in detail in Document Number SALT-3120AE0001, Revision 2.21 (10 March, 2003). The concept makes use of an all-refracting collimator, which is designed to accommodate the full 8 arcminute field of view (FOV) and the full (0.32 to 1.70)-micron spectral range by including a dichroically-split dual-beam configuration whose final achromatic-doublet lens group(s) are individually tuned for the "visible" (0.32 to 0.90)-micron and near-IR (0.85 to 1.70)-micron spectral ranges, respectively. The (non-cryogenic) near-IR arm was originally anticipated as a follow-on addition to the RSS-VIS mainframe. A [CaF₂/Schott K7] preliminary near-IR doublet was included in the collimator optical design as a proof of concept. However the required near-IR camera was left undefined.

Professor Harland Epps of Lick Observatory performed an initial optical design study for the RSS CoDR and PDR reviews. This design study provided the preliminary optical design alternatives for a near-IR camera, which were suitable for use with RSS-VIS.

After the PDR review panel performed a thorough assessment of the RSS-NIR on 17-18 July 2008. They provided constructive feedback to improve the design and development. In particular they requested the following changes to the optical prescription be implemented: Modification of the optical design to provide a faster camera with an improved pixel-size matching and larger field of view. This increased the speed of the camera from F/2.025 to F/1.42 and required the addition of one optical element. The resulting design changed the plate scale from 108 microns per arcsecond (6.0 pixels/sec) to 76 microns per arcsecond (4.2 pixels/sec) to better match the science requirements and median seeing. Epps was again contracted to provide a new preliminary design for MTR, given these new parameters.

The design requirements for the optical design were as follows:

1. RSS-VIS will be illuminated at $f/4.1756$ by the 11.0-m SALT telescope and field corrector whose combined optical prescription is given in the document, SALT-3300AS0001, 13 June, 2002. The telescope scale is 222.68 microns/arcsec upon a flat focal surface.
2. The RSS-VIS near-IR reimaged scale was initially 108.0 microns/arcsec and changed to 76.0 microns/arcsecond after PDR. The detector will be a flat (2048 by 2048 by 18-micron) Hawaii-2RG array such that the inscribed circle would correspond to an 8.0-arcmin field diameter at the telescope. The optical design must accommodate this field size for imaging and for spectroscopy, with only the spectroscopic mode illuminating the detector outside the 8 arcmin circular FOV. The reimaged scale corresponded originally to 0.167 arcsec/pixel or 6.0 pixels/arcsec and was changed to 0.234 arcsec/pixel or 4.2 pixels/arcsec after PDR.
3. RSS-VIS near-IR must operate over a (0.85 to 1.70)-micron chromatic range, which is limited on the long wavelength end by expected thermal noise in the (intentionally) non-cryogenic design. It must accommodate all spectral sub-intervals covered by its anticipated VPH gratings and/or direct imaging passbands without refocus. Typically, these would include the customary z-, Y-, and J-band(s) and part of the H-band as examples.

4. The optical design should be linear and all-refracting. In order to maximize photon efficiency in the coatings, the optical design should make use of low-index materials where practical, such as CaF₂, BaF₂, and IR Fused Quartz (such as Heraeus Infrasil 301), which have been proven for use in near-infrared applications. The lens elements should be all-spherical if possible for ease of manufacture. The number of lens elements should be minimized. The optics should be sized so as to cause less than 5.0% vignetting over the full field in any mode of operation.
5. The collimator focal length is assumed to be some 622.7 mm. The telescope's f/4.1756 geometry yields a beam diameter of some 149.1 mm.
6. The effective entrance pupil to the camera should be located at least 260.0 mm ahead of the camera's first lens vertex so as to provide adequate space in the collimated beam for gratings and/or VPH gratings which will be used in spectroscopic mode.
7. All lens elements should be free-standing with no lens surfaces in contact. Attention should be paid to eliminating ghost images and ghost pupils, particularly those formed by back-reflection off of the detector array. Geometric distortion at the reimaged focal plane should be held to less than 1.0% at full field, with 0.5% or less as a goal.
8. Some optical element within the camera must serve as a vacuum Dewar window. It should be thick enough to sustain the vacuum with minimum danger. This element will be mounted such that it will be maintained at the camera's ambient temperature while all following optics will be at T= 100 +/- 20 deg K. Provision must be made for one filter wheel within the cryogenic volume.
9. The detector array must be shielded such that no radiation with wavelengths longer than 1.70 microns can reach it, either by direct irradiation or by scattering. It should be mentioned that during this study, all of the optical designing, the optimization and the real-time and subsequent image analyses for the camera and collimator doublet were calculated with Epp's proprietary code, OARSA. The analysis of the full system and the scaled lens drawings and the spot diagram evaluations were done with the commercially available code, ZEMAX which provides a convenient and completely independent cross-check of the quantitative results.

5.1.1.1. Materials Selection

The design of large high-performance optics for the traditional (1.0 to 2.4)-micron chromatic range is strongly curtailed by the limited selection of suitable optical materials, see for example: Epps and Elston 2002. However, limiting the long-wavelength cut-off for the design to 1.6 microns makes it practical to consider a number of standard optical glasses, which would otherwise have been excluded due to strong absorption beyond 1.8 microns.

The Ohara catalog was reviewed in order to select available optical glasses, which exhibit an internal transmission of 0.994 or greater at a wavelength of 1.40 microns, for a 10.0-mm thickness. Those optical glasses are in Table 1 (2 pages) of the Epps design study (located in the MTR document website) wherein the wavelength-dependent dispersive power(s) [derivative of index with wavelength divided by (index - 1.0)] are given for each glass. The glasses are listed in order of increasing dispersive power at the 1.0-micron wavelength.

Traditional infrared materials from the aforementioned SPIE reference are also included, such as BaF₂, CaF₂, LiF, IR Fused Quartz (called FQTZ), etc. It can be seen that the uniquely small dispersive power of Barium Fluoride (BaF₂) makes it extremely attractive as the provider of substantial positive power in a fast, high-performance camera, in spite of its well known hygroscopic tendency (some 100 times worse than CaF₂) and its extreme softness (which makes it difficult to polish and to coat).

For convenience of intercomparison, the data are all given at "room temperature" ($T = +25.0$ C for the optical glasses; $T = +20.0$ C for the traditional infrared materials). The preliminary optical designs reported here were also done at room-temperature as the detailed temperature distribution through the camera had not been specified at the outset of the optical design process. Generic refractive indices were used for the various optical materials. The corrections to proper temperature(s) will all be at the level of typical "melt-sheet", corrections, which can be done when the selected design is updated prior to construction.

One notes also that the camera designs presented make no distinction between "air" and "vacuum." This approximation is safe as refractive index corrections at that small level can also be made at construction-design time or even ignored entirely as they always result only in a very small wavelength-independent focus shift, even in optical systems which are much faster optically than the camera needed for the RSS-VIS near-IR arm.

5.1.1.2. 7-Element All-Spherical Camera Design Description

The camera for the RSS-NIR beam (Epps Run No. 021209AA) consists of a 7-element, all-spherical air-spaced optical system that is essentially a pair of loosely grouped triplets. The front triplet consists of a bi-convex CaF₂ lens element followed by a negative meniscus S-LAH60 lens element and a closely spaced positive meniscus lens element made of CaF₂. The rear triplet consists a negative meniscus of fused quartz, a bi-convex BaF₂ lens, and a thick positive meniscus of S-FPL51Y, which will serve as the Dewar window and a 5 mm thick low-pass filter. Lastly a bi-concave field flattener made of S-NPH is placed before the detector.

RSS-NIR Redbook
Mid-Term Review Design Document
May 2009

This camera shows excellent monochromatic imaging performance and broad-passband chromatic correction over the entire usable instrument band (0.85-1.7um). The system prescription is given in **Table 5-1**. The units are in mm and one notes also that surface radii are shown instead of the more customary curvatures. The Schott- or Sellmeier-formula dispersion coefficients to be used with this camera design are given in Table 3 of the Epps Design Report. Representative values of refractive indices calculated from those coefficients are also given in Table 3 of the Epps Design Report at several wavelengths.

Table 5-1. The optical design prescription for the RSS-NIR Camera and doublet Run # 021209AA.

CAMERA Run 021209AA					
Name	Radius (mm)	Thickness (mm)	Material	Clear Aperture (radius, mm)	comments
DOUBLET 1	Infinity	10	F_QUARTZ	188.8294	BICONICX
DOUBLET 1	323.282	4.428		188.7767	
DOUBLET 2	350.6908	59.01226	CAF2_NIR	189.7401	
DOUBLET 2	-529.2243	245		190.5735	
PUPIL	Infinity	260		162.133	
L1	279.5755	63	CAF2/I	178.7126	
L1	-214.9752	4		176.2395	
L2	-218.1591	7	S-LAH60	173.5313	
L2	-737.5395	3		175.5894	
L3	175.0607	58.212	CAF2/I	175.4766	
L3	3259.794	121.2945		163.4667	
L4	-146.7166	6.5998	FQTZ/I	112.9415	
L4	-293.2433	3.745245		112.4096	
L5	176.0615	35	BAF2/I	108.1874	
L5	-276.207	3		100.1857	
L6	113.5358	37.8486	I-FPL51Y	87.66453	
L6	332.5673	8.964778		63.58056	
filter	Infinity	5	NBK7&120	55.10134	
filter	Infinity	8		51.61968	
L7	-155.5433	3	S-NPH1	44.35554	
L7	140.3536	9.906		37.31841	
detector	Infinity			37.31841	

A scaled drawing of this camera is shown in **Figure 5-1**. Parallel ray bundles of light radiate from the entrance pupil on the left, moving toward the right. Those which will form an image at full-field can be seen as they appear on the first lens surface. The rays pass through the lens elements and converge to focus at the flat detector array on the right. The lens apertures shown are minimum clear apertures. In practice, the lens elements will be made larger in diameter so as to allow sufficient material for mounting purposes, for beveling and for convenience of optical figuring and coating.

The state of the design is that of Pre-Construction, in that optical performance has been shown to be feasible with the number of elements and the chosen materials. All major optical parameters have been evaluated at laboratory or room-temperature and nominal index of refraction. No attempt has been made yet to fit the element radii to test plates or to optimize for a particular glass melt or to evaluate the system

at operating temperatures. These are tasks that are required for CDR, but are beyond the scope of an MTR.

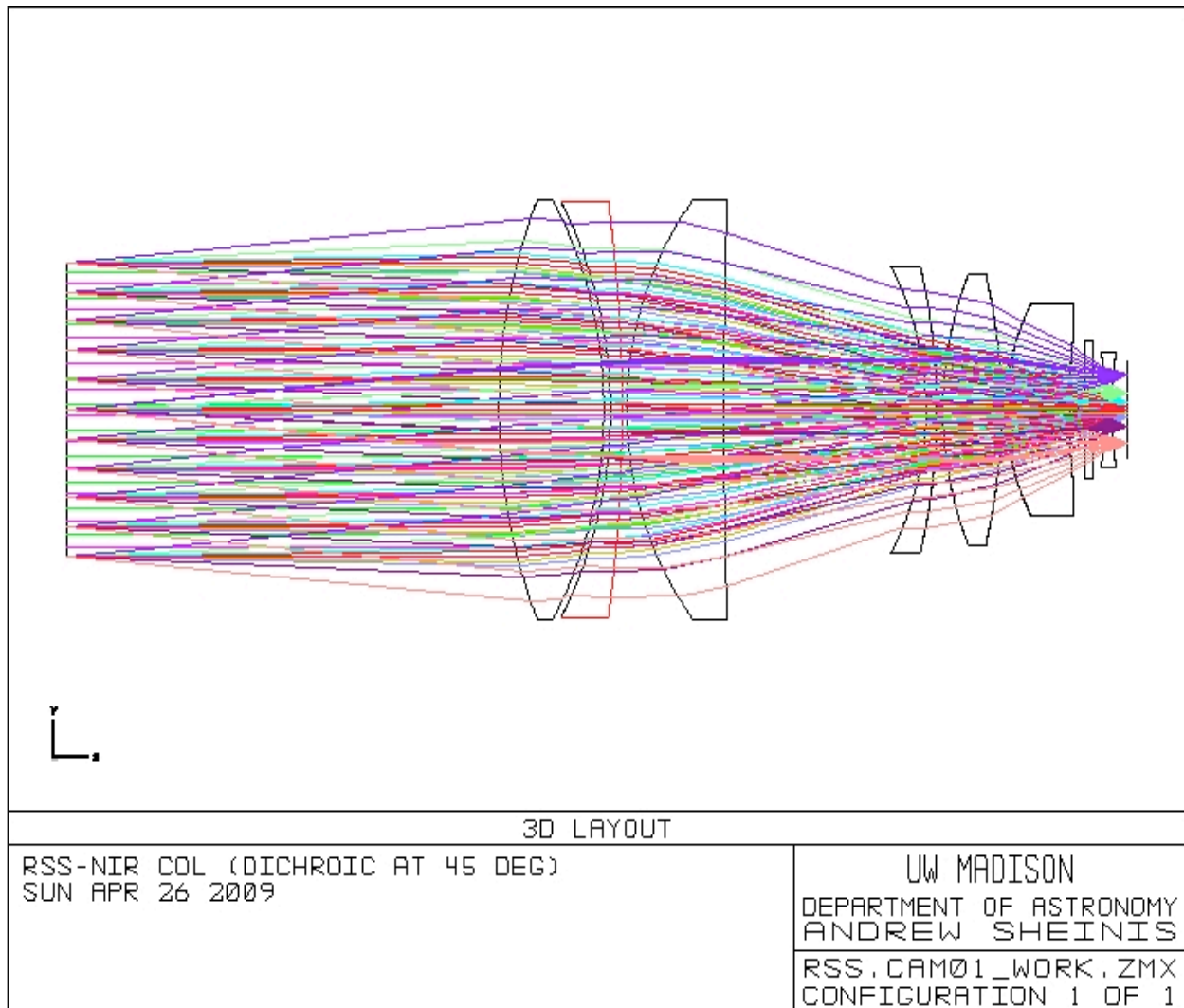


Figure 5-1. RSS-NIR Camera Layout, showing the 149.1 mm diameter external pupil (260 mm from vertex of surface #1). The camera for the RSS-NIR beam consists of a 7-element, all-spherical air-spaced optical system that is essentially a pair of loosely grouped triplets. The front triplet consists of a bi-convex CaF2 lens element followed by a negative meniscus S-LAH60 lens element and a closely spaced positive meniscus lens element made of CaF2. The rear triplet consists a negative meniscus of fused quartz, a bi-convex BaF2 lens, and a thick positive meniscus of S-FPL51Y, which will serve as the Dewar window and a 5 mm thick low-pass filter. Lastly a bi-concave field flattener made of S-NPH is placed before the detector.

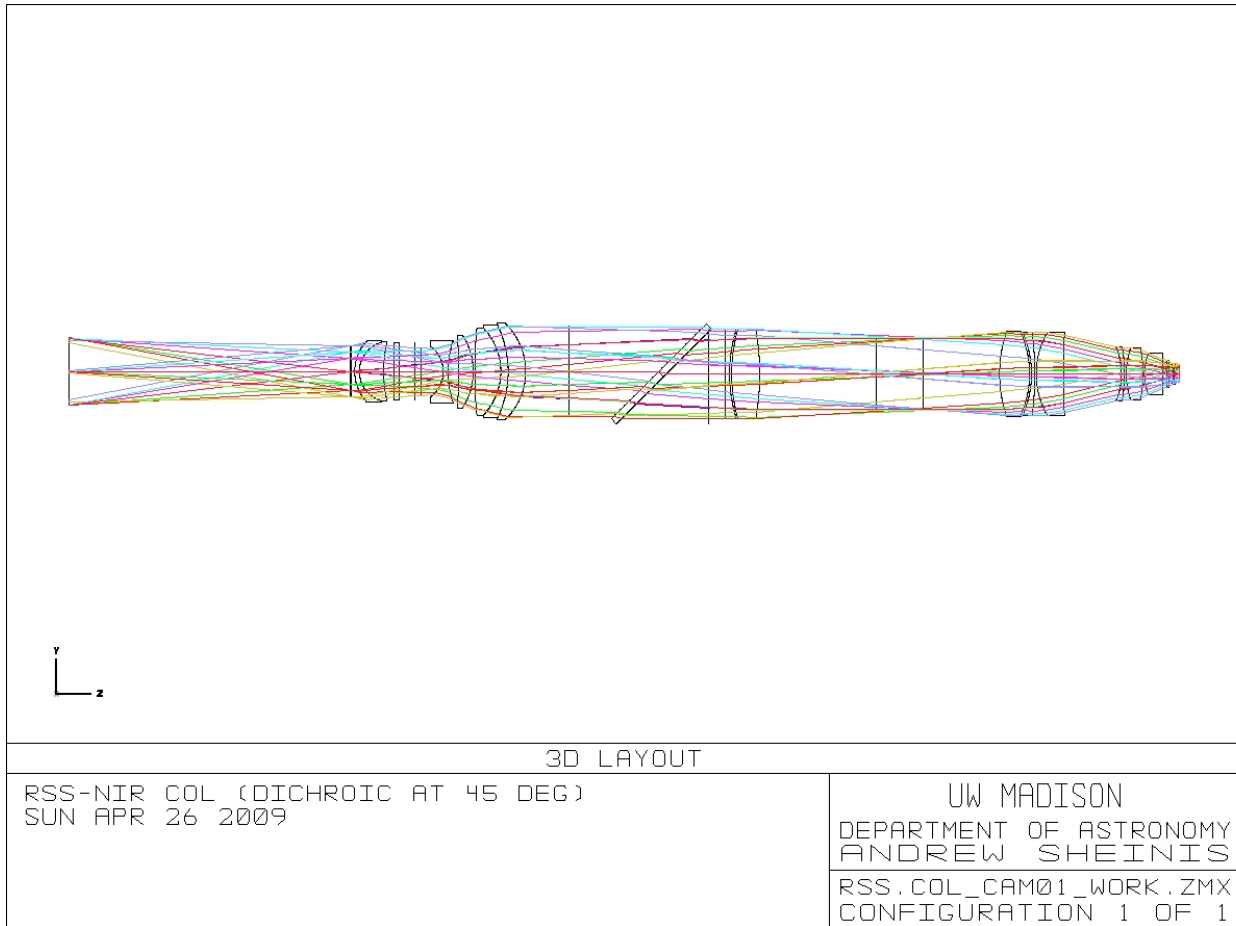


Figure 5-2. *RSS-NIR system layout.*

5.1.1.3. Collimator Doublet Design

The collimator NIR doublet has been re-optimized by Epps with the existing as-built optical collimator dimensions. The prescription uses a fused quartz plano-concave lens air-spaced to a biconvex CaF2 lens. A 15-mm thick dichroic is tipped at 45° and inserted into the mildly diverging beam before the doublet. The Plano front surface of the doublet is designed to have an appropriate cylindrical radius in order to compensate for the astigmatism induced by the dichroic beamsplitter.

Image analysis was performed over 4 passbands, which include an I-band (0.85 to 0.95)mi, a standard Y-band (0.975 to 1.12)mi, a standard J-band (1.15 to 1.35)mi, and a short H-band (1.46 to 1.70)mi. In all cases the system produced polychromatic images, which placed 92% or more of the energy into a (2 x 2)-pixel Nyquist box. Note, it is generally agreed that if a system puts 80% or more of the energy into a Nyquist box, it is pixel-sampling-limited. Thus, this system is now fully pixel-sampling-limited as traced through the full camera and collimator.

5.1.2 Optical Error Budget and Analysis

A preliminary image quality error budget was performed with the Zemax lens design program, using its Monte-Carlo tolerance analysis feature. For the analysis, we assume that optical manufacturing errors will be measured after the individual components are completed. We will re-optimize the spacings after these numbers are generated and if necessary reserve the radii or thickness (or both) of a single last element to compensate of the aggregate manufacturing errors. This will likely be the first element L1, which with the exception of the BaF2 element has the most system power and has the largest effect on image quality.

Assembly tilt and displacement errors were analyzed for the complete system in several operational modes. The polychromatic RMS spot radius of the nominal system is 11 microns (0.14 arcseconds) averaged over all field points and wavelengths. The preliminary image quality error budget allows for an RMS image radius of 18 microns (0.23 arcseconds) after assembly of the camera and collimator. This is 38% of the image size (~1/2 of the variance) to be due to assembly and alignment errors. An initial analysis determined that the tilt and displacement of lenses L1 and L2 were the most sensitive followed by their axial spacing.

After consultation with the mechanical design team it was decided to put tight tolerances on the tilt, decenter and axial spacing of L1,L2 and L3, as these would be all held to a single lathe-turned barrel. This is particularly appropriate in light of the desire to use L4 and L5 as the focusing group, which would imply a looser tolerance for these elements. Tolerances adopted L1, L2 and L3 were then based on what is “reasonable” for a “tight machine-shop tolerance”. These were chosen to be 0.0375 mm in decenter, and axial spacing and a tip/tilt of .0375 degrees. Placing these tolerances back in the analysis with looser tolerances on the other degrees of freedom (0.2 mm axial spacing and 0.1 mm tip/tilt and decenter) showed that the tilt and decenter for the two elements of the doublet as well as the elements of the triplet, were the next most sensitive elements with similar sensitivities.

In consultation with the mechanical design team, it was determined that it is easier to tighten the tolerances on the triplet, and field lens/detector group rather than the doublet. Tolerances adopted for L4, L5, L6, and L7 were then based on what is “reasonable” for a “machine-shop tolerance”. These were chosen to be 0.05 mm in decenter, and 0.1 mm in axial spacing and .05 degrees in tip/tilt. Detector tolerances were slightly tighter with 0.1 mm decenter, 0.0375 mm axial displacement and 0.0375 degree tip/tilt. Placing these tolerances back in the analysis again with looser tolerances on doublet (0.1mm decenter, 0.2 mm axial displacement and 0.1 degree tip/tilt) with standard matching tolerances on all the remaining degrees of freedom (0.2 mm axial spacing and 0.1 mm tip/tilt and decenter) produced the final result shown in table 5.1.2.1. For these adopted alignment and assembly errors, the system produced RMS spot radii below 18 microns for 68% (1 standard deviation) of the Monte-Carlo runs and below 29 microns for 100% of the Monte-Carlo runs.

Table 5-2. *Alignment and assembly tolerances for RSS-NIR camera and collimator doublet.*

Lens #	Decenter mm	Tip/Tilt degrees	Axial Displacement mm
D1	0.1	0.1	0.2
D2	0.1	0.1	0.2
L1	0.0375	0.0375	0.05
L2	0.0375	0.0375	0.05
L3	0.0375	0.0375	0.05
L4	0.05	0.05	0.1
L5	0.05	0.05	0.1
L6	0.05	0.05	0.1
L7	0.05	0.05	0.05
D	0.1	0.0375	0.0375

5.1.3. Detailed Optical Performance

When illuminated in a perfectly converging light beam at $f/4.1765$ from a simulated telescope this 7-element all-spherical camera coupled to the existing collimator with the re-optimized IR doublet shows residual aberrations with an RMS image diameter ranging from 19-29 microns averaged over all field angles and wavelengths within the (0.85 to 1.70)-micron passband without refocus, with 7.4 microns of maximum RMS lateral color. Maximum 3rd-order barrel distortion is some 0.39% at the edge of the full field (the corners of the detector). Thus the image quality is more than sufficient to be seeing limited given the alignment and assembly tolerances produced in section 5.1.2 above.

Polychromatic image analyses for the camera are given in **Figure 5-3**, which includes RMS image diameters in pixel units over the full spectral range without refocus. A (150 by 156)-mm entrance pupil at an entrance-pupil distance of 260.0 mm was used for the calculations and the cameras were illuminated in perfectly parallel light.

The RMS image radii are shown on each Figure in microns. The 36-micron (2-pixel) Nyquist-sampling boxes are 0.5 arcsec on a side. While some lateral color is apparent in the vertical direction, almost all of the energy is contained within 0.5 arcsec such that the camera is strongly sampling limited. The worst-case polychromatic RMS image diameter at full field is only 0.380 arcsec (1.6 pixels) for the full system.

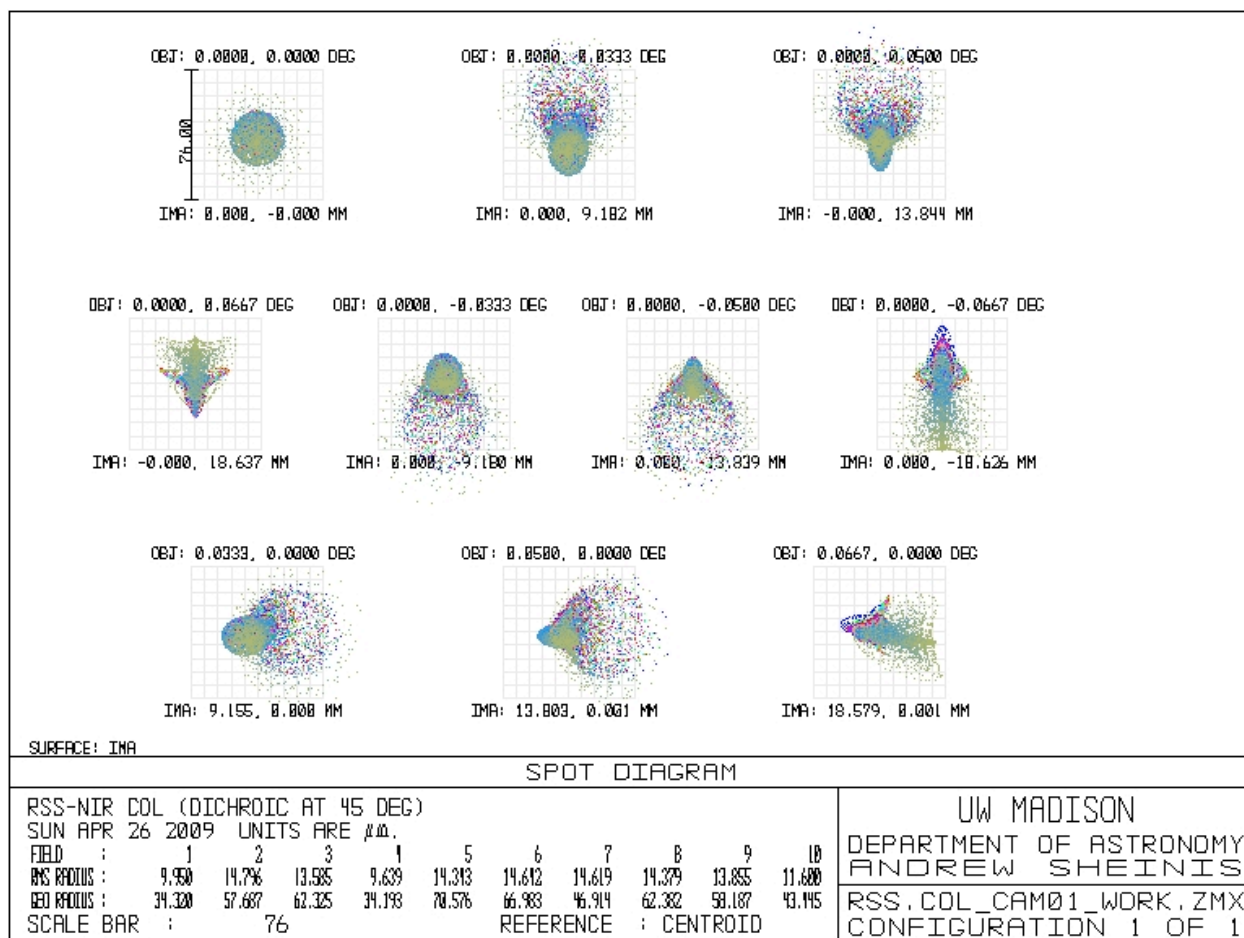


Figure 5-3. System polychromatic spot diagrams, traced through the full 0.85-1.7 μm wavelength range without refocus, from slit plane to detector. Each box is 1.0 arcseconds.

Polychromatic ensquared energy analysis is shown in **Figure 5-4**. It shows that when the full spectrograph (exclusive of the telescope) is raytraced over the over the full passband of the instrument it exhibits an ensquared energy of 90% within a 2x2-pixel Nyquist box (0.5 arcseconds on a side) for all except the outer-most field point in the -Y direction, which has a 90% ensquared energy in 3x3-pixel square and 80% in 2x2 pixels. When traced at monochromatic wavelengths the image quality is certainly better. Therefore sampling-limited and/or slit-width limited optical performance can be expected from the camera in spectroscopic mode, over the full spectral range and the full field of view.

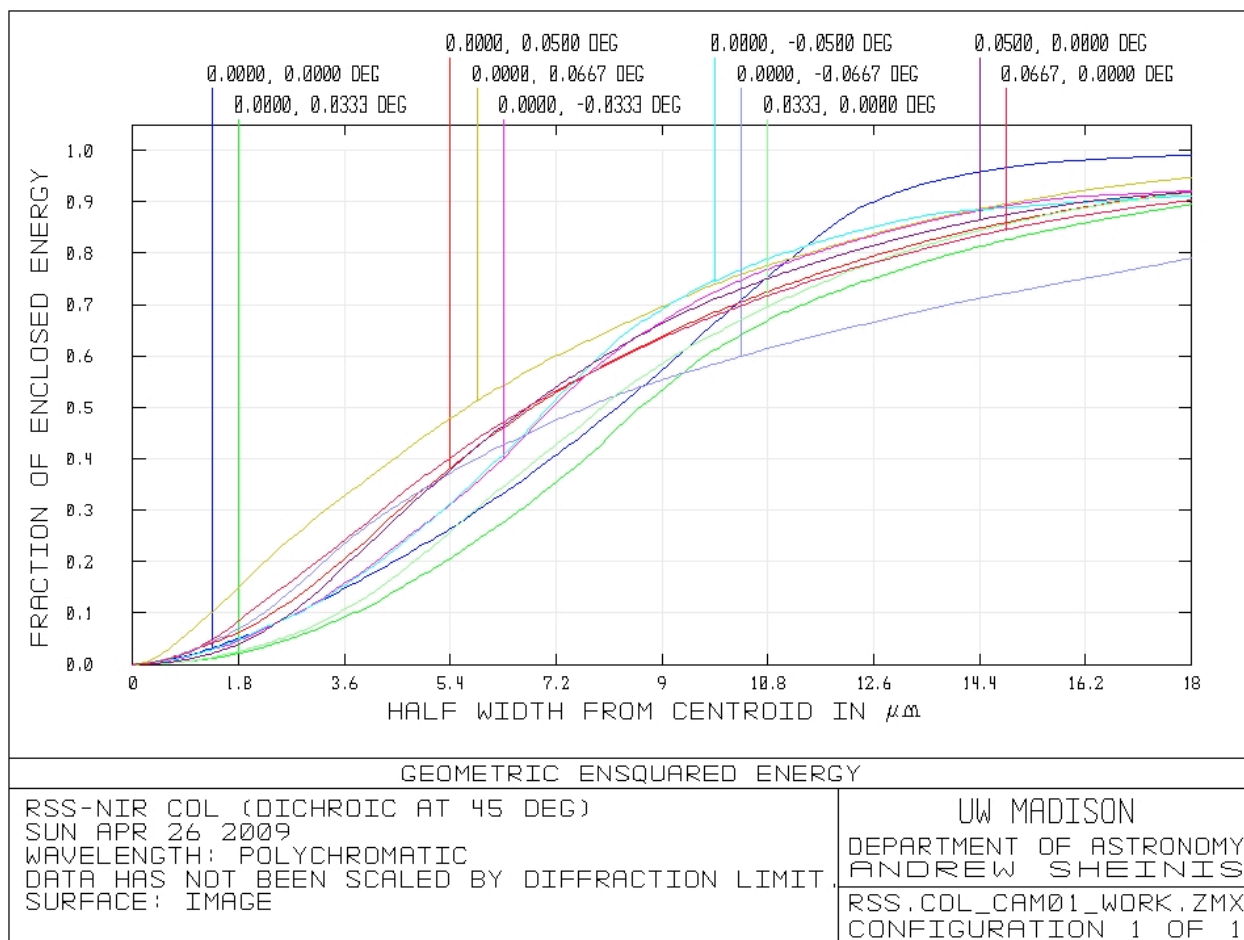


Figure 5-4. Polychromatic ensquared energy analysis shows that when the full spectrograph (exclusive of the telescope) is raytraced over the over the full passband of the instrument it exhibits an ensquared energy of 90% within a 2x2-pixel Nyquist box (0.5 arcseconds on a side) for all except the outer-most field point in the -Y direction, which has a 90% ensquared energy in 3x3-pixel square and 80% in 2x2 pixels. Therefore sampling-limited and/or slit-width limited optical performance can be expected from the camera in spectroscopic mode, over the full spectral range and the full field of view.

5.1.3.1. Optical Focusing Options Evaluation

A design study was undertaken to determine possible camera re-focusing schemes in the event that the NIR beam would require refocusing on the slit before or during an observation. Prior experience with other spectrographs suggests that small motions of the [field flattener and detector] taken as a single unit is often the preferred option. In general, as one considers possible motions of other lenses that are located farther away from the focus, the interplay of geometric and chromatic aberrations leads quickly to image quality decay as the desired focus motion is generated. Thus one is able to recover a "best focus" condition but the resulting image quality becomes unacceptable for appreciable perturbations. With that preconception in mind, several options were explored as follows:

1. A Perturbation Near the Telescope Focus.

The K_short (1.46, 1.52, 1.58, 1.54, 1.70)-micron passband was chosen for analysis as it is the least well-corrected band. Imaging performance was evaluated over the standard set of 10 field angles in the current RSS-NIR Zemax prescription.

The distance between the slit and first element of the collimator, X_5 in the Zemax model, was increased by + 2.0-mm value. This caused the RMS image diameters to take on (120 to 142)-micron sizes. Reoptimizing the spacing of the surface ahead of the field flattener by 0.200 mm produced images that were *better* than the nominal system and the ensquared energy plot was better also. However some - 0.022 mm of that correction corresponds to the improvement one gets by refocusing the unperturbed system for the K_short passband (as distinct from adopting a single focus for all passbands). Thus, only - 0.178 mm of this correction, which is the part that is compensating the perturbed system, should be evaluated for image restoration. That restored the images and the ensquared energy plot to a condition that was almost indistinguishable from the unperturbed state.

Next compensation the X_5 perturbation by moving the detector only was attempted. This showed that a - 0.265 mm change in the detector-only position provided a quasi-acceptable "best focus" but the character of the images was different from the non-perturbed state and the ensquared energy plot was not quite as favorable as in the unperturbed state.

Next test was to move the vacuum Dewar as a unit. A change in the position of the Dewar of - 0.320 mm produced images that are comparable to those in the unperturbed system and the ensquared energy is comparable as well.

A similar ray trace, wherein the BaF2 lens (alone) was moved to compensate the X_5 perturbation, failed to produce acceptable image quality. Motions of the 4 larger lenses, which are farther from focus, were not deemed appropriate options for evaluation as they would be mechanically awkward to move.

Lastly the two optical elements directly upstream of the Dewar window (L4 and L5) were moved as a group. The results of this optimization are shown in **Figure 5-5**. A change of 0.907 mm produced images that are comparable to those in the unperturbed system and the ensquared energy is comparable as well.

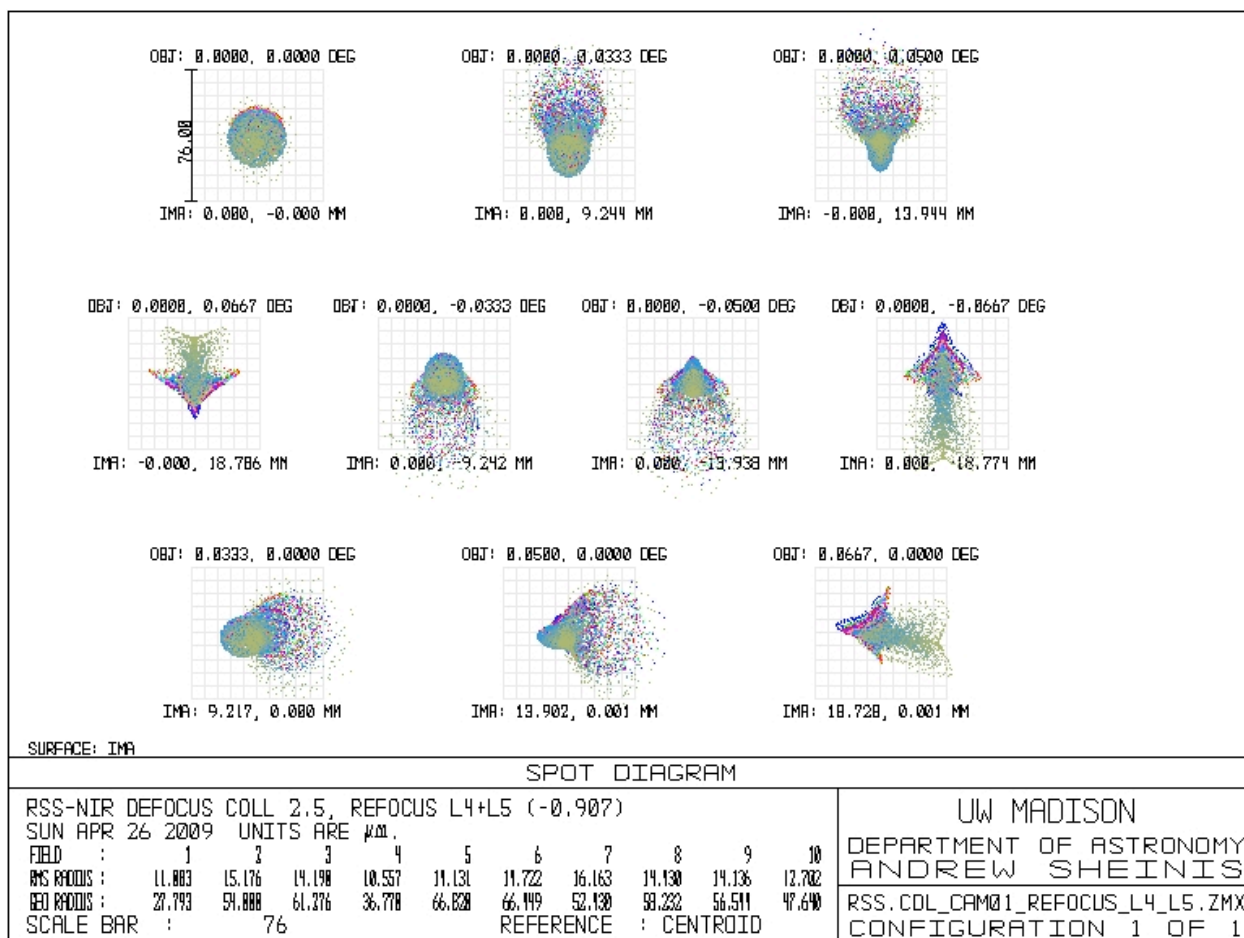


Figure 5-5. System spot diagrams after refocus with the L4-L5 group.
 Slit defocus = 0.25 mm, L4-L5 refocus = 0.907 mm.

The conclusion is that the [field flattener and detector] unit motion; the vacuum Dewar unit motion; or the L4 – L5 group motion produced acceptable image restoration for this type of system perturbation, while motion of the detector alone, or the BaF2 lens alone did not. The required amplitude of [field flattener and detector] motion is only about 64% as large as the vacuum Dewar motion and the later would be mechanically more difficult to achieve in practice. We note that an existing mechanical design from the visible camera can be used to articulate the L4-L5 group for refocus. All things being equal, the L4-L5 option was chosen for this mechanical reason and taking in to account the considerable additional risk of placing another stage inside the cryogenic Dewar.

5.1.4. Fabry-Perot Selection

The RSS-NIR spectrograph will use Fabry-Perot (FP) technology to provide full-field spectroscopic imaging. The FP acts as a filter with spectroscopic resolution that can be tuned to any desired wavelength within the RSS-NIR operating range. A series of images are taken, stepping the wavelength of each image, to sample a spectral line of interest. This data cube is then analyzed to provide maps of line strength, line width, and velocity at every position in the image. The system has very high throughput, in excess of 60%, and provides an extremely efficient way to measure kinematic and/or spectral information over an extended object or cluster of objects.

The FP mode will employ a single 150 mm clear aperture etalon, cooled and located in the collimated beam, in conjunction with an order-selecting filter. The transmitted wavelength is selected by adjusting the separation of the etalon plates. The spacing and parallelism of the etalon are measured with capacitive sensors optically attached to the plates, and piezoelectric actuators controller by a servo system to set and maintain the desired spacing. The preliminary etalon design will have a gap of 33 μm , plate reflectivity of 95%, and surfaces flat to $\lambda/150$ or better. This will produce a spectral resolution ($\lambda/\delta\lambda$) of 2500 and a separation between adjacent orders of 24 nm at wavelength 1.25 μm . We would use filters of bandwidth 17 nm (at wavelength 1.25 μm) to select the desired order of the etalon and reject parasitic light from adjacent orders to less than 2%.

We have used 150 mm etalons in the visible beam side of RSS, so the proposed system is based upon an extension of our previous experience. We plan on using etalons and controllers from ICOS, Ltd., the supplier of the visible beam system (and with whom we have an extensive and successful previous experience).

5.1.5. Fabry-Perot Order Blocking Filter Selection

Unlike the visible side, the RSS-NIR Fabry-Perot will not require enough order blocking filters to cover the entire spectral range. This is because there are only discrete atmospheric windows between sky lines in which observations can be made. Two kinds of observations are envisioned for the Fabry-Perot instrument: 1) observations of specific lines at $z\sim 0$ in the ISM, nebulae, and star forming regions; and 2) searches for redshifted emission line galaxies. **Table 5-3** lists lines of interest that have been identified by SALT consortium astronomers, as well as the types astronomical objects in which they occur. The goal in selecting spectral locations of FP blocking filters is to choose the regions that are relatively free of night sky emission lines, but also to include important lines of interest at $z=0$, even if they lie close to a night sky line.

Table 5-3. *Lines of interest and the types of objects in which they occur.*

Wavelength (μm)	Element	Location		Wavelength (μm)	Element	Location
0.9069	[S III]	SF		1.26	[Fe II]	ISM, SN
0.91882	H-a, z=0.4	z search		1.28	Pa-b	ISM, SF
0.93175	[O II], z=1.5	z search		1.3126	H-a, z=1	z search
0.9532	[S III]	SF		1.3376	Ly-a, z=10	z search
0.9722	H-b, z=1	z search		1.43	[Si X]	nebula, AGN
0.9728	Ly-a, z=7	z search		1.4583	H-b, z=2	z search
0.9827	[C I]	nebula		1.4908	[O II], z=3	z search
0.9853	[C I]	nebula		1.5	Mg I	nebula
0.99	[S VIII]	AGN		1.5021	[O III], z=2	z search
1.0014	[O III], z=1	z search		1.5808	Ly-a, z=12	z search
1.0287	[S II]	SF		1.588	Br 14-4	H II regions
1.0321	[S II]	ISM, SF		1.611	Br 13-4	H II regions
1.0395	[N I]	SF		1.63	CO(6,3)	supergiants
1.0401	[N I]	SF		1.64075	H-a, z=1.5	z search
1.07	[Fe XIII]	AGN		1.641	Br 12-4	H II regions
1.08	He I	ISM, nebula		1.644	[Fe II]	ISM, SN
1.1181	[O II], z=2	z search		1.65231	[O III], z=2.3	z search
1.12	O I	nebula		1.65274	H-b, z=2.4	z search
1.25	[S IX]	AGN		1.68	Br 11	H II regions

Figure 5-6 shows a plot of the NIR night sky spectrum with preliminary locations of a set of 12 FP order blocking filters. The black spectrum is the night sky from Maunaea Kea that has been used throughout all our analyses. The cyan line near the bottom marks a factor of 2 above the sky continuum. Any spectral regions with a width of 5 etalon line widths (so that 5 etalon settings could occur) that contain no sky lines above the cyan line are marked by small red dashes. (The y-axis level of these dashes is offset with wavelength for clarity to see individual marks.) These are line-free regions of the spectrum. The blue spectrum near the top is the atmospheric transmission, which has to be considered as well when selecting observing windows. The vertical green lines mark the locations of the spectral lines in **Table 5-3**. The thick horizontal magenta lines mark possible filter locations. Because the free spectral range of the etalon changes with wavelength, so do the widths of the filters.

This is only a preliminary set of filters to demonstrate our selection process, as more analysis is forthcoming. Future plans include convolving the sky spectrum with an etalon line shape to analyze the effects of the large wings of the etalon transmission profile in the presence of strong sky emission lines, and making a better determination of how much sky emission we can tolerate (e.g. what factor above the continuum we need to set to determine “clear” windows).

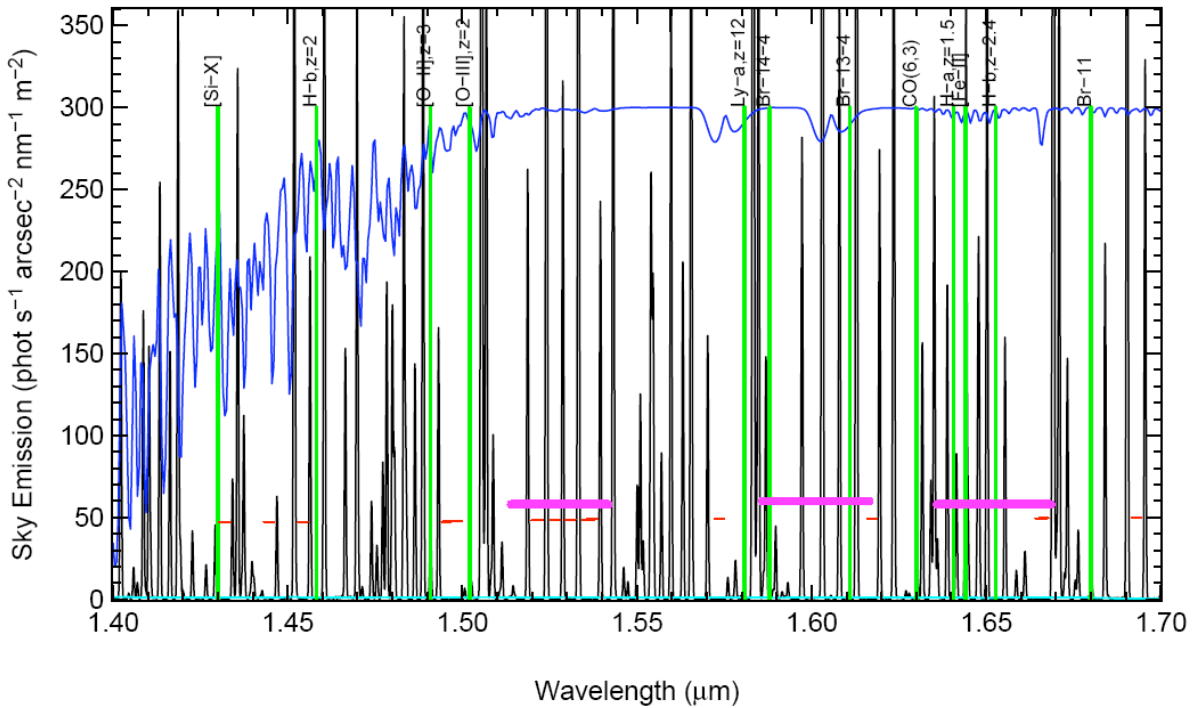
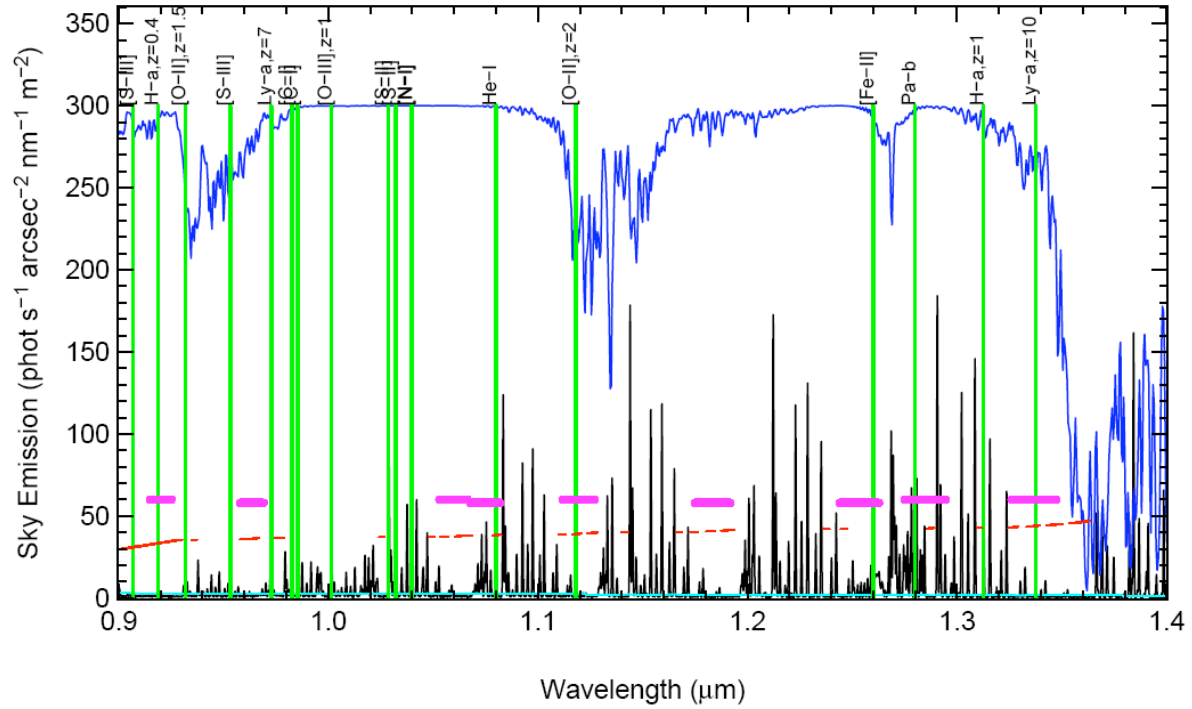


Figure 5-6. Preliminary locations of FP order blocking filters. See text for description.

5.1.6 Grating Selection

Our choice to use volume phase holographic gratings gains on two fronts over conventional gratings. It gives us higher diffraction efficiency, which translates into instrument throughput, and it provides more flexibility in spectral coverage per grating with the ability to angle-tune the gratings via articulation.

The range of spectral resolution for RSS-NIR operation is chosen based on 1) that required by the planned science programs, 2) physical limitations on achievable resolution for the size of the optics and available space for camera articulation to high angles to get high spectral resolution, and 3) limitations set by the night sky and thermal backgrounds.

For sky-limited spectroscopy of faint targets, Section 3.2.2.1 discussed the lower limit set on spectral resolution. This lower limit is $R \sim 4000$ and is the point at which night sky OH emission lines are resolved and $\sim 50\%$ of the $l = 0.9-1.7$ mm band is free of contamination by these lines. Objects that are brighter than the sky, of course, can be observed at lower spectral resolution. The maximum achievable resolution for RSS-NIR is $R = 14000$ for a Nyquist sampled $0.5''$ slit.

Extragalactic science dictates two spectral resolution regimes: $R \sim 4000$ for faint $z \sim 0.5-2$ galaxies, and $R \sim 7000$, $s \sim 15-20$ km/s, to study dynamics and metallicities of galaxies. These two cases are demonstrated from the results of our RSS-NIR science survey of SALT consortium astronomers in **Figure 5-7** by the peaks at $R \sim 4000$ and $R \sim 7000$ for expected MOS observations. Expected single object long slit observations peak at the higher resolution. At these spectral resolutions a number of grating settings will be required to cover the entire instrument wavelength range.

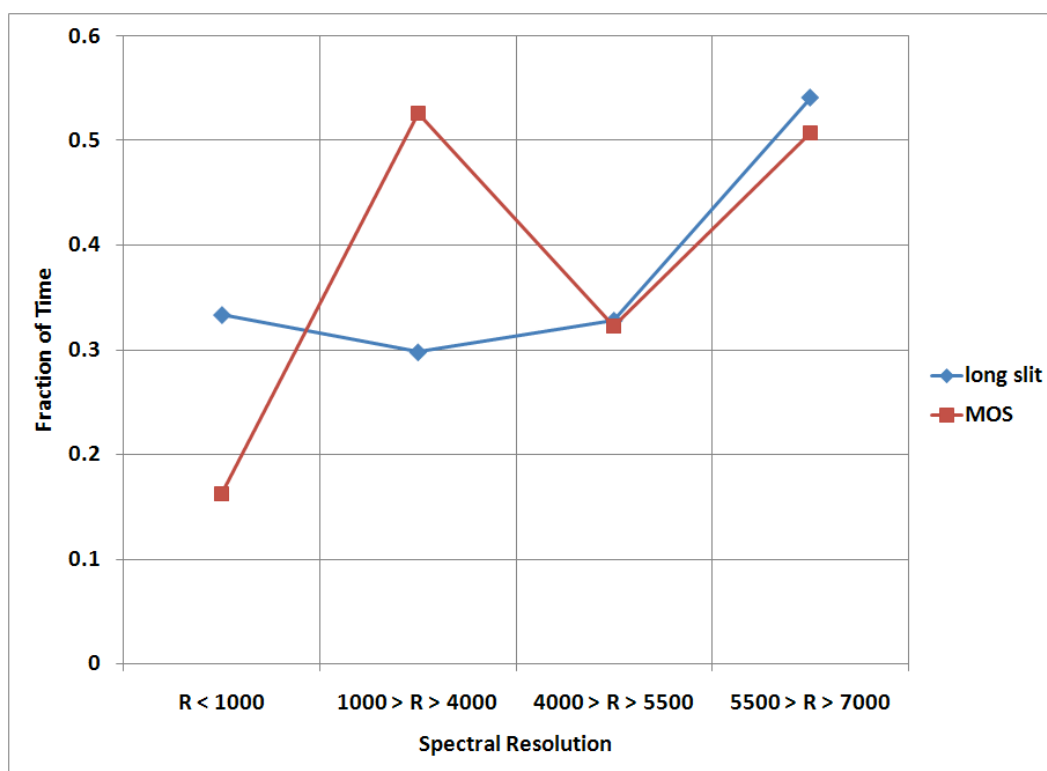


Figure 5-7. Fraction of time SALT consortium astronomers expect to spend observing at different spectral resolutions. These are results from the NIR science survey conducted for RSS-NIR in 2008.

Observations in other instrument modes have very different requirements. Many of the planned spectropolarimetry programs will take place on bright targets, where the night sky is not an issue. Because these objects tend to be quite variable, a wide spectral coverage in each observation is required. These types of observations dictate a spectral resolution of $R \sim 800$, which allows coverage of 0.9-1.7 μm at once. When used simultaneously with the VIS side, one could achieve coverage over the entire 0.32-1.7 μm range.

The RSS-NIR pre-dewar contains 5 grating holders. The space in which extra gratings are held competes with space in which Fabry-Perot blocking filters can be stored. The number of 5 gratings was a compromise between having enough gratings in the suite to meet all science needs and the number of Fabry-Perot filters available at a time (currently 12). **Figure 5-8** shows the predicted performance of our proposed grating suite, assuming a 1" slit. The exact parameters of the VPHGs can be easily optimized with no impact on the instrument design.

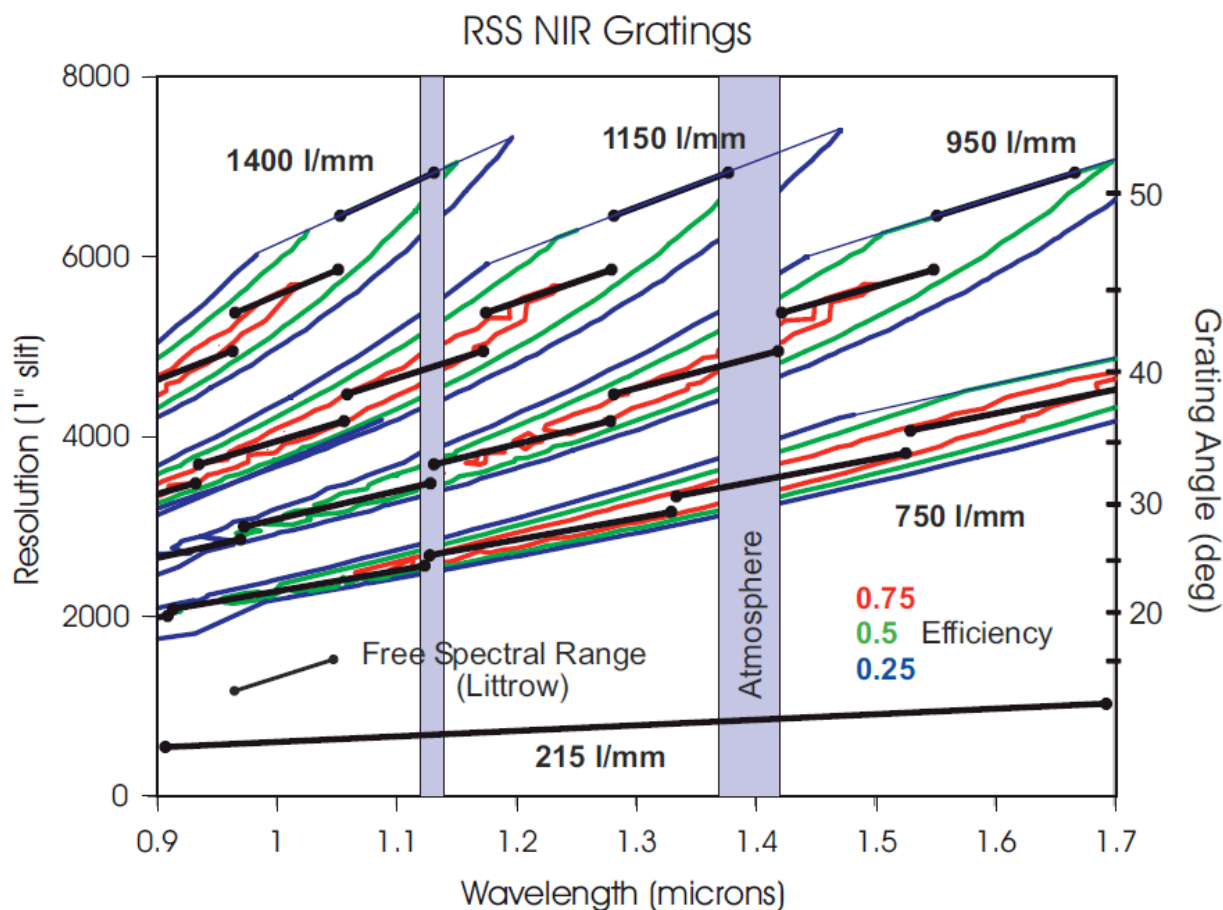


Figure 5-8. RSS-NIR grating suite. The top 4 are VPHGs and the bottom one is a conventional grating or grism.

5.1.7. Polarimetry

The RSS-NIR polarimetric capabilities will be modeled on those of the existing visible beam, which include linear and circular imaging polarimetry, grating multi-object spectropolarimetry, and Fabry-Perot

spectropolarimetry. The visible-beam polarimetric optics is described in Nordsieck, et al. (2003). The visible beam spectropolarimetry has been tested on-sky successfully. In this system, a “wide-field” design, rotating waveplates placed after the field lens in the common collimator modulate the polarization, and the orthogonal polarization beams are split by half the telescope field by a large Wollaston beamsplitter in the collimated beam. The rotating waveplate subsystem is already part of the existing RSS optics, and was designed to function simultaneously over the full 320 nm – 1.7 micron RSS dual-beam wavelength range. The NIR side needs to supply only a NIR Wollaston prism for its collimated beam to accomplish polarimetry.

The existing rotating waveplate subsystem consists of two slides, a halfwave plate slide and a quarterwave plate slide, together with plane-parallel windows when not in use (the waveplates are in the diverging beam of the collimator, requiring focus compensation). The halfwave plate alone is used for linear polarimetry, and the combination of the linear- and quarterwave plates are used for circular and all-Stokes polarimetry. Each plate (fabricated by Bernhard Halle, Berlin) consists of a Pancharatnam “superachromatic” stack of six thin pieces of crystal quartz and magnesium fluoride, glued between two fused quartz substrates. The waveplates are rotated by miniature stepper motors, and actively detented at each rotation position, for angular repeatability.

The visible side polarizing beamsplitter (**Figure 5-9**) consists of a 3x3 mosaic of calcite Wollaston prisms, mounted in a slide just before the first element of the camera, so that it articulates with the camera. When the beamsplitter is inserted, the collimated beam is split perpendicular to the grating dispersion direction into two beams with polarization parallel and perpendicular to the articulation axis of the camera, with a separation of four arcminutes. For polarimetric observations, polarimetric slitmasks limit the field of view to 4x8 arcmin, so that half the telescope field of view appears twice, at the top of the detector and at the bottom. In imaging mode, because of the chromatic dependence of the Wollaston splitting, without a filter each star is dispersed perpendicular to the grating dispersion by about 20 arcsec, giving an “imaging spectropolarimetry” mode, whereas with a narrow-band filter (typically the 150 Angstrom interference filters also used for Fabry-Perot order blocking) diffuse objects are split with good imaging. In grating spectropolarimetry, each spectrum appears twice, separated by 4 arcmin, so that MOS spectropolarimetry may be accomplished with a MOS mask limited to the 4x8 arcmin polarimetric field. In Fabry-Perot mode, the Fabry-Perot “rings” appear twice, with each having exactly the same wavelengths, since the polarizing beamsplitter is located after the etalon.

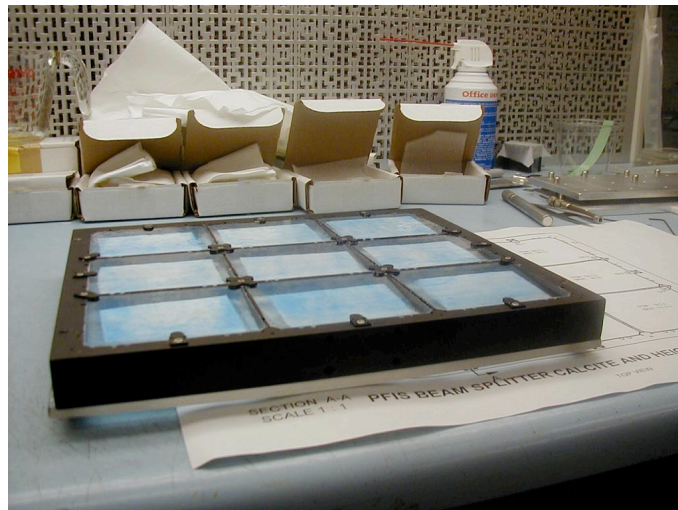


Figure 5-9. RSS-VIS Wollaston Beamsplitter.

For the NIR side, there are two issues to be resolved in accomplishing the same capabilities as the visible side, the detailed construction of the Wollaston beamsplitter, and the specification requirements for the dichroic beamsplitter. For the Wollaston, on the visible side the two prism wedges of each Wollaston mosaic element are lens fluid coupled, both to reduce ghost images at the prism interface and to allow for co-alignment of the mosaic by adjusting the fluid wedges individually until the mosaic lines up. The latter was advantageous because the prism manufacturer, Karl Lambrecht Corp, could not guarantee matching the mosaic wedges to within the imaging specification. For the NIR side, a fluid interface is considered to be risky at the -40 C temperature of the pre-dewar where the beamsplitter is located, so the prism wedges will be air-coupled. The ghosts will be controlled by AR coatings (which are easier in the NIR than in the UV-visible), and Karl Lambrecht has quoted for accomplishing the wedge matching by fabricating enough wedges that selection allows the specification to be met. This is feasible in the NIR since NIR quality calcite is much easier to obtain than UV quality calcite. The possible issue of the dichroic arises because in the past some dual-beam instruments used for spectropolarimetry (Keck LRIS and Lick Kast) have shown instrumental polarimetric calibration stability problems at the 0.1% level, problems, which went away when those instruments were used in single-beam mode. This clearly must be a function of the dichroic polarimetric properties, which can be controlled by specification. The goal will be to reduce the uncalibratable systematic instrument polarization to 0.03%, a factor of three. As a backup, the mechanical design will allow for a replacement of the dichroic by mirror or window, to allow for single beam operation for the highest precision spectropolarimetry on either beam.

5.1.8 Calibration System

SALT has a facility calibration system that consists of a number of spectral line lamps, a broadband flat field lamp, liquid light guides to input the lamp light into the SAC, and a stack of Fresnel lenses and a light-shaping diffuser screen to simulate the actual telescope vignetting pattern imparted on observations of the sky (Buckley et al. 2008). This system was designed for the first generation optical instruments on the telescope to provide calibrations out to a wavelength of $\lambda = 0.9$ mm. The simplest method of calibrating RSS-NIR would be to modify the existing system.

The same material is used for both the Fresnel lenses and the diffuser screen, a UV-transmitting acrylic. For the thickness of all the acrylic elements in the SALT calibration system, a transmission curve is shown in **Figure 5-10**. The strong feature at 1.35-1.45 mm is the water absorption band also seen in the atmosphere, so observations will not typically be made in this region. This leaves an absorption feature at 1.17 mm that dips to ~40% transmission and a transmission cutoff by 1.68 mm as potential problems for the NIR arm. Without slit-cooling sky-limited spectroscopy will typically only go out to 1.65 mm due to thermal backgrounds, so the material cutoff is not an issue for these observations. Given the large effort it would require to redesign the entire calibration system to gain transmission from 1.68 to 1.7 mm, we feel that this performance will be sufficient for calibration of the NIR instrument.

The remaining transmissive elements are the liquid light guides used to inject lamp light into the telescope. The calibration system currently uses a blue and a red light guide from Lumatec. Transmission of these elements is shown in **Figure 5-11**. Another product is available from the same company that transmits well out to 1.7 mm. This Series 2000 light guide would result in just a few % transmission loss at 600 nm over the current red Series 380 light guide.

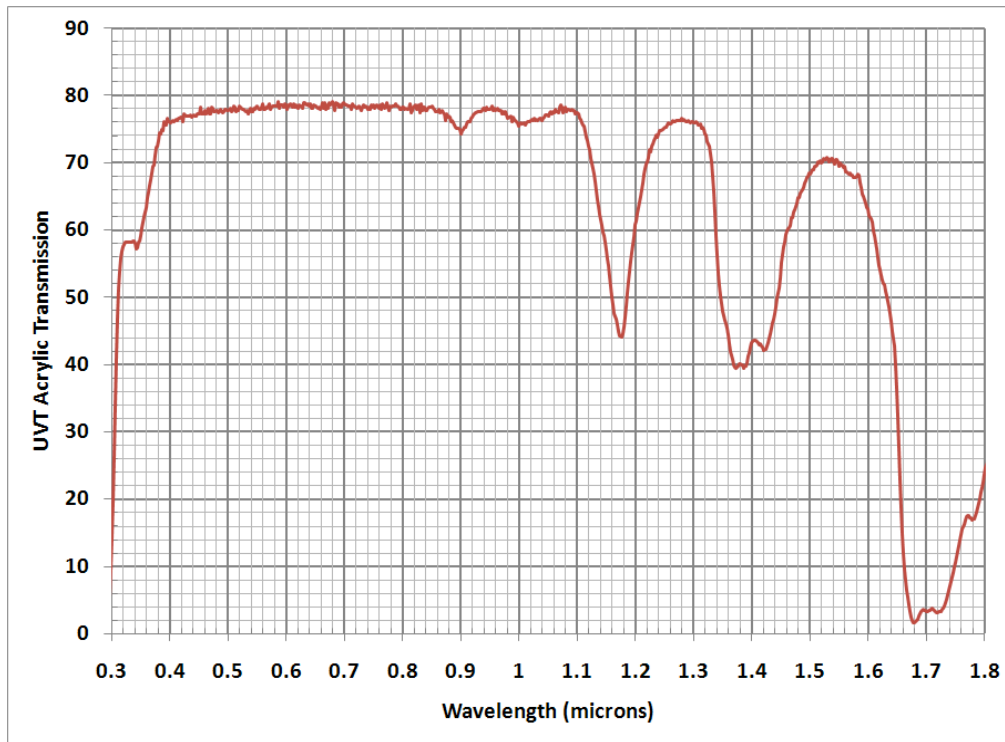


Figure 5-10. Transmission of materials in the SALT facility calibration system.

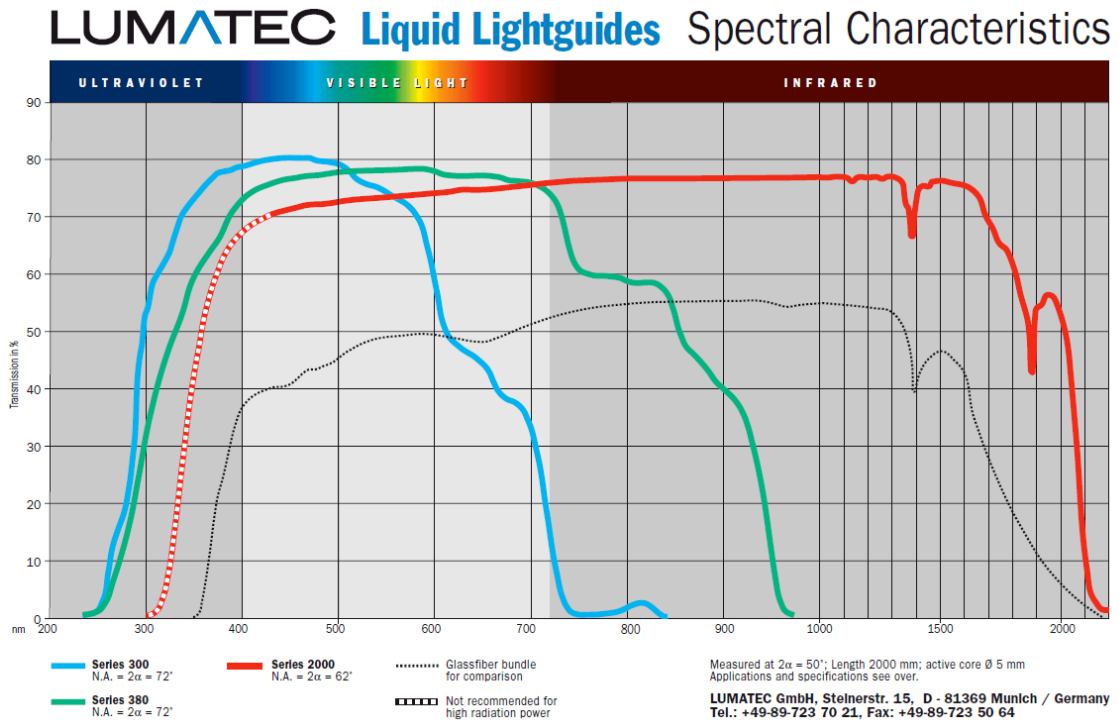


Figure 5-11. Transmission of liquid light guides in the SALT facility calibration system currently uses Series 380 for the “red” lamps. We propose to change it to the Series 2000, which transmits well into the NIR.

The QTH flat field lamp in the current system works well in the NIR. The last item is wavelength calibration. Many NIR instruments use night sky lines for wavelength calibration. We plan to do this, particularly on the long wavelength end, but were concerned that some sky lines at the shortest wavelengths might not be of sufficient strength. Therefore, we plan to include a line lamp that can be used for both the visible and the NIR arms. The current SALT facility calibration system contains penray Ar, Hg, Xe, and Ne lamps. Both Ar and Ne would be useful in the NIR, and are used on some current instruments. Penray lamps that contain both gases are available, so we plan to replace either the Ar or the Ne lamp on the current system with a combined ArNe penray lamp. Lines from these lamps are overplotted on night sky emission lines in **Figure 5-12**. (The neon lines in this plot do not have proper relative strengths.)

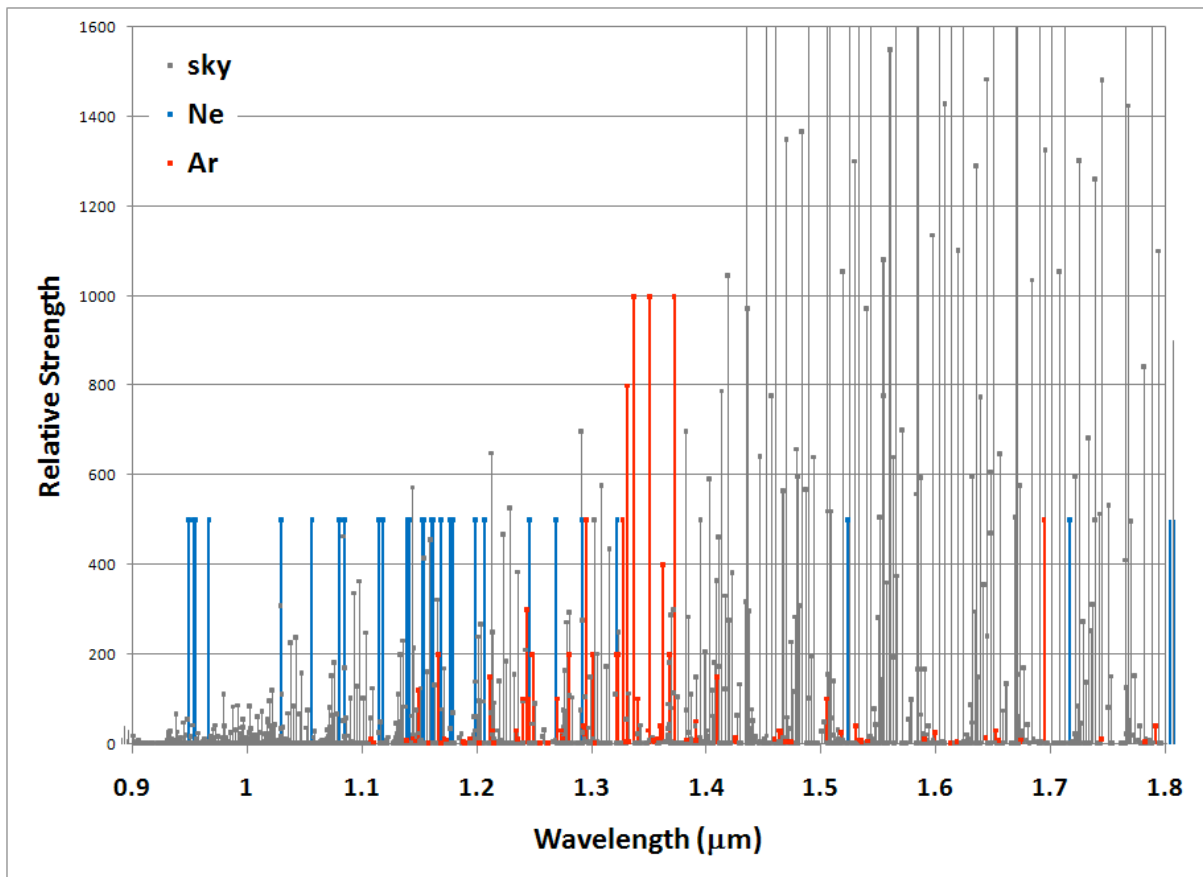


Figure 5-12. NIR spectral lines from the night sky (gray), a neon lamp (blue), and an argon lamp (red). Note that the neon lines are not plotted with correct relative strengths.

To summarize, we plan to modify the existing SALT facility calibration system by 1) replacing the red liquid light guide with one that transmits into the NIR, and 2) replacing either the Ar or the Ne penray lamp with one that combines the two gases for NIR wavelength calibration. We believe that the transmission of the calibration system field shaping optics through $l = 1.68$ mm will be sufficient for calibration of RSS-NIR.

5.1.9. Risk and Risk Mitigation

An informal risk analysis was performed of the RSS-NIR beam for the CoDr by the design team in consultation with other instrumentation experts throughout the field. This risk analysis has been updated and modified as the design has progressed from CoDr to PDR to MTR. Below, is a list of risks to the optics briefly summarized with mitigating design factors. Additional risks and their mitigations are in Section 6.3.

1. **Focusing Mechanism.** Active focusing of the NIR camera will be required in order to compensate for filter thickness changes, etc. Two focusing options were evaluated for optical performance and mechanical complexity. They are: a) an in-the-Dewar detector/field-lens and focusing stage and b) an external focusing stage moving L4 and L5 as a group.

Although the in the-Dewar option was slightly better, both of these options produced pixel-limited optical performance, within the alignment and assembly tolerances. In addition, we explored the option of using existing mechanical designs for both options. Option a) is the focusing stage used in the MOSFIRE system, and option b) is very similar to the focusing stage used in the RSS-VIS system.

All things being equal, it was decided that the stage outside of the cryogenic environment presented fewer operational risks and there this was chosen as the primary option with the in-the-Dewar stage as a back-up position.

- 2) **Cold operation.** A very large environmental chamber exists at UW that will allow for all stages and systems to be run at operational temperature (-40° C) in the lab prior to assembly into the pre-dewar.
- 3) **Cooled Fabry-Perot.** We have acquired a “dummy” Fabry-Perot device to allow for mechanical and electronic testing to occur at operational temperature (-40 °C) and to allow for thermal cycling of the device well in advance of the taking delivery of the actual device. This dummy device contains similar optical and mechanical systems to the actual FP etalon, without the coatings or optical polish. The primary failure mode observed by our graduate student, Corey Wood, when he worked on a cryogenic FP with Pat Hartington at Colorado was a mechanical failure of the piezo-to-glass connection. We will test for this failure mode by thermally cycling the test device many more times than it is likely to see at SALT.

5.1.10. Test and Integration Plan

The primary test and integration plan consists of two-parts, first in Madison and then in Cape Town.

Madison testing is scheduled for 7 months with a 3-month contingency. This will consist of:

- a) Camera + detector optical testing
- b) Doublet null test
- c) Flexure test on tilting bench
- d) Burn-in, cycling of all stages and mechanisms

Final Integration in Cape Town is scheduled for 5 month with a 1-month contingency. This in effect means that the RSS spectrograph will be down and unavailable for observations for up to 6-months. This test and integration procedure will consist of:

- a) End-to-end optical test in the NIR with an NIR test of the collimator with doublet alone if necessary in order to isolate its performance from the camera. This will be an auto-collimated star test.
- b) End-to-end flexure testing of the full up system on the tilting flexure platform.
- c) Further burn-in cycling of all stages and mechanisms.

5.1.10.1. Madison Subsystem Testing Outline

Optical Testing

- 1) Camera testing:
 - a) Star test
 - i) Measure RMS spot size
 - ii) Hot and cold
 - iii) Through filters
 - iv) On axis/off axis,
 - v) Field curvature
 - vi) Distortion
 - vii) BflConfirm design and assembly of camera
 - viii) Confirm image quality
 - b) Interferometric
 - i) Test camera in double pass
 - ii) Compare wavefront quality over aperture to design, hot and cold.
 - iii) UWAST has a phase measuring interferometer at 633nm
 - iv) Can we test camera at 633nm?
 - v) Can we modify interferometer to 850nm?
 - vi) May require outside vendor with NIR interferometer (SAGEM for example)
 - vii) All at room temp and at operational temperature if possible
- 2) Collimator
 - a) Null test Interferometric
- 3) Gratings
 - a) Throughput
 - b) Blaze angle
 - c) Interferometric surface
- 4) Filters
 - a) Interferometric surface
- 5) System throughput.

Mechanical Testing

- 1) Build up and test enclosure
- 2) Flexure test on tilting bench
- 3) Burn-in, cycling
 - a. Automated testing of stage actuation
 - b. Use hall effect or capacitive sensors to measure insertion errors
 - c. Run all stages at least 1000 times

- d. Run hot/cold and varying gravity
- e. Report error statistics after pass.
- 4) Environmental testing: Several facilities exist for -40 °C work
 - a. PSL large environmental chamber
 - b. Smaller facilities in SSEC
 - c. Can do star test, and interferometry at -40 °C
 - d. Burn-in cycling at -40 °C

Camera Testing (see 5.4.3 for details)

- 1) Camera SNR characterization
 - a) Readnoise
 - b) Dark current
 - c) QE

5.1.10.2. Integration Testing in Cape Town

The Cape Town technical facilities of SAAO were chosen for the final system integration and test over the mountaintop observatory due to availability of resources in Cape Town such as machine shops, plating facilities, shipping and receiving times and component and hardware purchases, as well as human resources such as engineers and machinists.

The plan calls for a minimum downtime for the RSS instrument of 16 weeks with a 4-week contingency to assemble the full instrument and duplicate much of the testing performed in Madison. This testing will include all the flexure testing as well as in-situ optical testing at operational temperature and then an extensive “burn-in” time for all mechanisms and stages at the different gravity orientations.

Specific tests include:

- 1) In Situ Optical testing:
 - a) Star test (full spectrograph, slit to detector), in
 - i) Imaging,
 - (1) Measure RMS spot size:
 - (2) On axis/off axis,
 - (3) Bfl
 - ii) MOS
 - (1) Measure RMS spot size:
 - (2) On axis/off axis,
 - (3) distortion
 - iii) Longslit modes (all filters)
 - (1) Measure RMS spot size:
 - (2) On axis/off axis,
 - (3) Bfl
 - b) System throughput
- 2) Flexure test on tilting bench
- 3) Burn-in, cycling
 - a) Automated testing of stage actuation
 - b) Use hall effect or capacitive sensors to measure insertion errors
 - c) Run all stages at least 1000 times
 - d) Run cold and varying gravity
 - e) Report error statistics after pass.

- 4) Data acquisition and camera control for various acquisition modes
- 5) Camera SNR characterization (see 5.4.3 for details)
 - a) Readnoise
 - b) Dark current
 - c) QE

5.2. Mechanical Design

The Mechanical Design has progressed since the PDR and a number of significant evolutions have occurred. All of the mechanical elements now exist as preliminary designs, which are enabling further analysis (flexure, thermal, alignment tolerance). The design of the mechanisms has advanced to the point where actuators and major components have been selected and fed into the electrical and thermal design. We have also gained a higher degree of fidelity in our mass estimate.

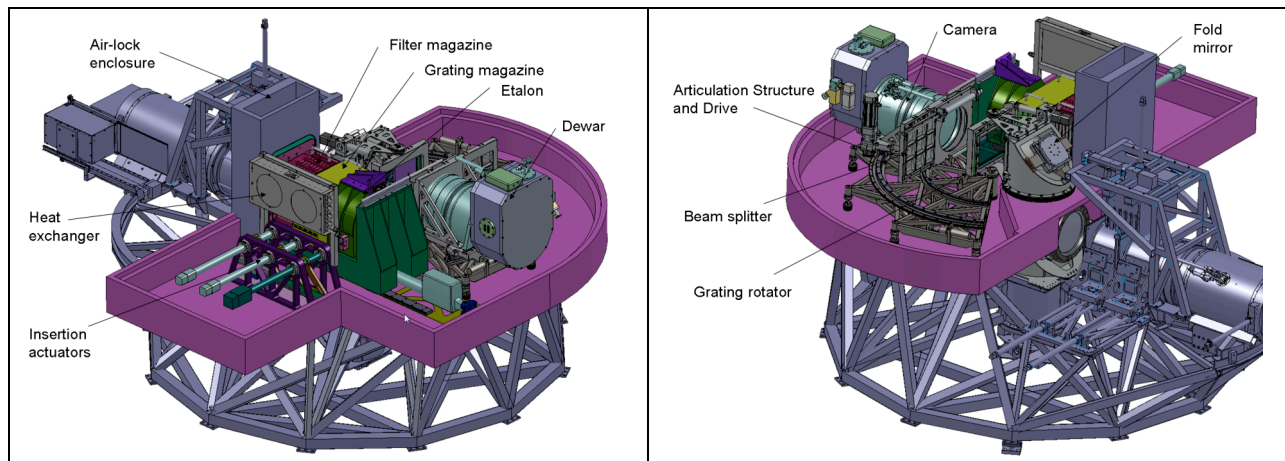


Figure 5-13. *Model Views of the RSS- NIR instrument.*

5.2.1 General Description

The RSS-VIS fold mirror will be replaced with a 15mm thick dichroic. The NIR collimator doublet is immediately above the dichroic and the first element of the doublet forms the pre-dewar window. The volume between the dichroic and the doublet will be at ambient temperature but will be carefully sealed and humidity controlled to avoid frosting on the first surface of the doublet. The second element of the collimator doublet is made of calcium fluoride and requires special consideration due to the thermal gradient across it because of its location near the entrance window to the pre-dewar.

The fold mirror is actuated and is used for both image motion compensation and dithering the beam. There are 12 filters available in a magazine to be inserted into the beam. There is a pupil mask just after the filter position. The grating magazine holds 5 gratings, which can be rotated up to 50°. The etalon and polarimetric beamsplitter can be inserted or removed from the beam.

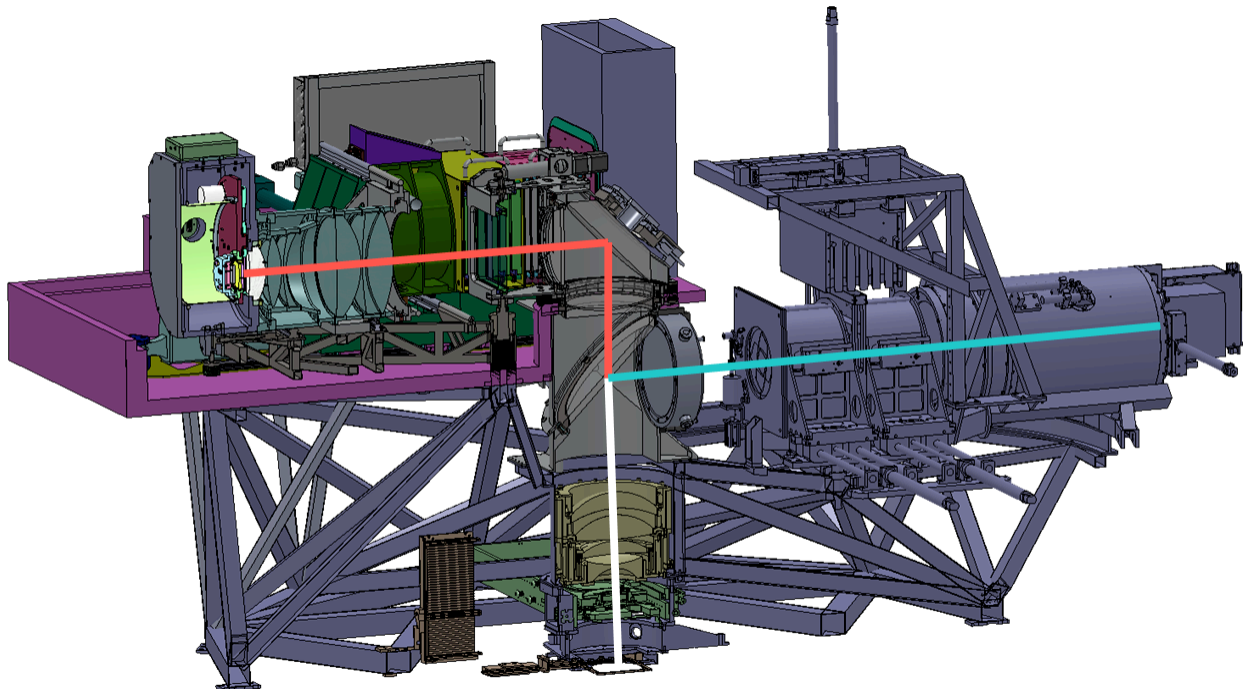


Figure 5-14. Cut view of the RSS-NIR instrument showing the optical path and major components.

The camera and Dewar are mounted onto an articulation mechanism, which can articulate the camera up to 100°. The camera is focused by pistoning two elements within it. The Dewar contains a filter wheel with 3 cold blocking filters, a shutter and a blank position. The field lens and the detector are just behind the filter wheel. The internal components of the Dewar are cooled using a Polycold PCC cryocooler.

Table 5-4. Mass Summary Table

SUBSYSTEMS	kg
Optics Tower Assembly	58
Fabry-Perot Etalon Assembly	20
Polarizing Beamsplitter Assembly	8
Camera Articulation Mount	37
Camera/Dewar Assembly	47
Storage Optics	60
Predewar Assembly	45
Electronics Boxes	54
Wire Harness	12
Cooling Lines	10
Misc (5%)	18
SUBTOTAL	368
GROWTH (10%)	37
TOTAL	405

5.2.2 Dichroic and Doublet

The Optics tower assembly is a three-piece hybrid tubular structure made of invar 36. It provides the support for the dichroic beamsplitter, visible doublet, NIR doublet, fold mirror, filter holder, and grating rotation stage. It is fixed at its base to the existing flanged mounting face of the collimator support structure and extends along the optical Z axis to the underside of the NIR pre-dewar. A lateral stiffener is used to tie directly into the base frame at the NIR articulation axis directly below the pre-dewar insulation. This tubular structure has been designed to have high stiffness, relatively low mass, and fit within existing physical constraints. FEA was used to evaluate design trade-offs in the early conceptual phase of the structural development and to predict the final structural performance once the design had evolved into its present state. The tubular structure fully encloses the volume around the dichroic beamsplitter to facilitate a dry-air purge of potentially cooler surfaces around the pre-dewar window. Mechanical flanges are used at the joints and the joints are configured to facilitate assembly and installation of the mounted optical elements. The flanges will be pinned to ensure repeatability of assembly

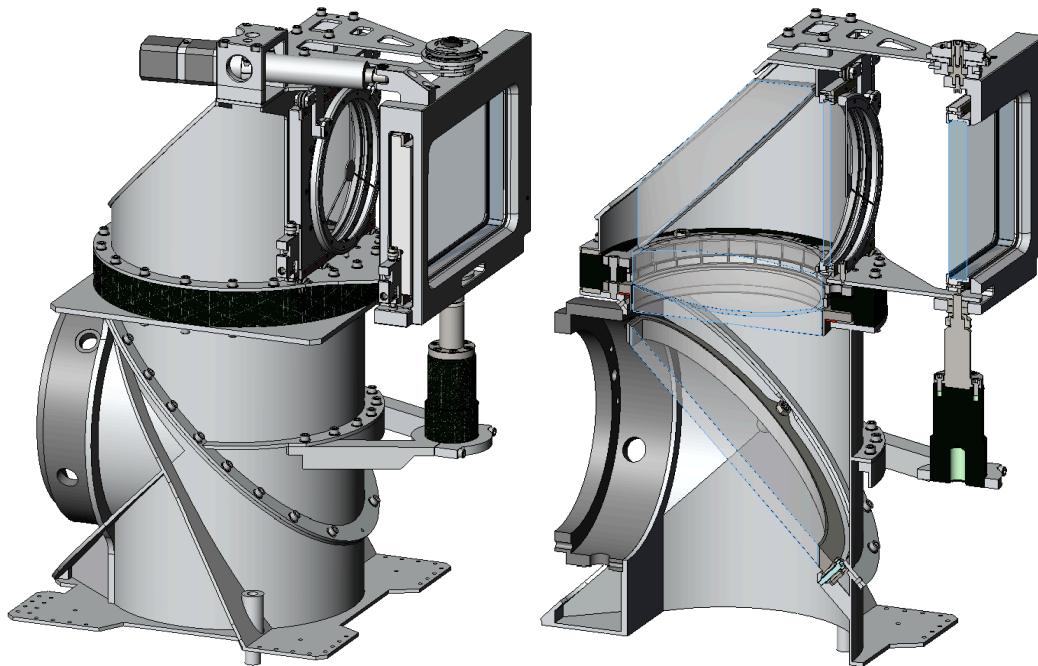


Figure 5-15. *Dichroic, RSS-NIR Doublet, and RSS-VIS Doublet mounting structure*

The first piece of the optics tower is flanged to connect to the existing structure at the collimator. A face flange is provided for mounting the existing visible doublet that will have its mount redesigned to mount to this structure instead of the previous bookend mount. A diagonal flange at forty-five degrees with respect to the optical axis is provided to install and align the dichroic beamsplitter. The dichroic beamsplitter is mounted in an Invar frame semi-kinematic with manual tip, tilt, and Z adjustments. These adjustments are accessible only for installation and alignment of the dichroic beamsplitter. They become covered by the second piece of the tubular structure and the pre-dewar insulation and are inaccessible at that stage of assembly. Therefore, once set and aligned, the dichroic beamsplitter must remain fixed and stable throughout the remaining NIR assembly process. An option for accessing the dichroic adjustment screws is a scheme where adjustments can be made after assembly through holes in the wall of the tube.

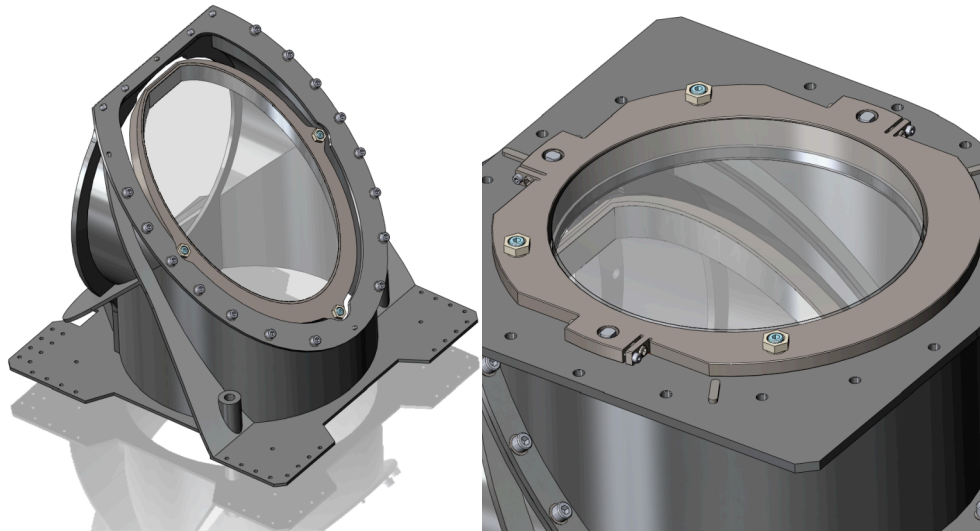


Figure 5-16. *Dichroic mount on left and the RSS-NIR doublet element 1 mount*

The next piece of the structure supports the NIR doublet first element that is mounted in an Invar ring. The Invar ring attaches to the top flange of this structure. It is semi-kinematic with manual X, Y, Z, tip, and tilt adjustments. A silicon gasket is sandwiched between the Invar ring and the top flange to act as a seal and help provide a thermal break between ambient and internal pre-dewar temperatures. An annular G10 section attaches at the top flange outside of the first element. It has been keyed with three radial keyways on its mating surfaces to maintain alignment through thermal cycling. It provides a good mechanical mount and acts as a thermal insulating transition between the ambient and pre-dewar temperatures that insulates the Calcium Fluoride NIR doublet second element. In addition, the G10 supports the doublet second element above the first element with an air gap to help reduce the thermal gradient. The Calcium Fluoride second element is mounted in a 304 stainless steel ring. A set of radial flexures machined into the ring help reduce mechanical stresses in the Calcium Fluoride. The mounted Calcium Fluoride second element is attached to the G10 section semi-kinematic with manual X, Y, Z, tip, and tilt adjustments. The three outside corners on the top flange of the structure are for the mounting of an alignment stand with alignment instruments.

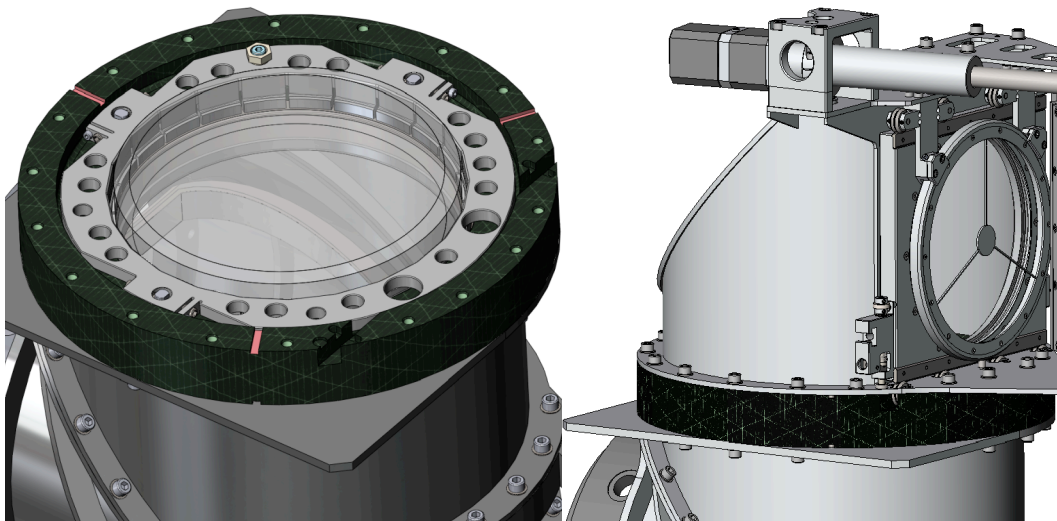


Figure 5-17. *Fold Mirror mount on the optics tower.*

The upper and last component of the optics tower assembly is the fold mirror structure. It has a base flange that connects to the annular G10 section and a diagonal flange at forty-five degrees to the base for attaching the fold mirror assembly. Adjacent to this is an upright structural face flange with a 180mm opening for the folded optical path. The base flange extends outward at the bottom laterally to tie into the truss structure at the camera and grating articulation hub just below the grating rotation stage. This connection will add stability to the upper section of the optics tower provided the camera articulation structure is rigid and stable. If further detailed analysis of the camera articulation structure does not indicate it to be sufficient, then this connection will be made to float in lateral directions and used only to support the mass of the grating rotation stage in the Z direction.

The rollers, which receive the inserted filter, attaches to the upright face flange. A line of four v-rollers are spaced apart and mounted in the base flange extension adjacent and parallel to the face flange. The v-rollers guide the lower v-rail of the filter holder. A latch detent for locking the filter into position is also located in the base flange extension. Directly above the v-rollers on the bottom is a set of four v-rollers mounted in tandem in two flexure assemblies to guide the upper v-rail of the filter holder. Both flexure assemblies are supported on the underside of the eyebrow, which is the structural cap on the top of this section. A pupil mask in its holder is clamped outside and adjacent to the filter.

5.2.3 Fold Mirror

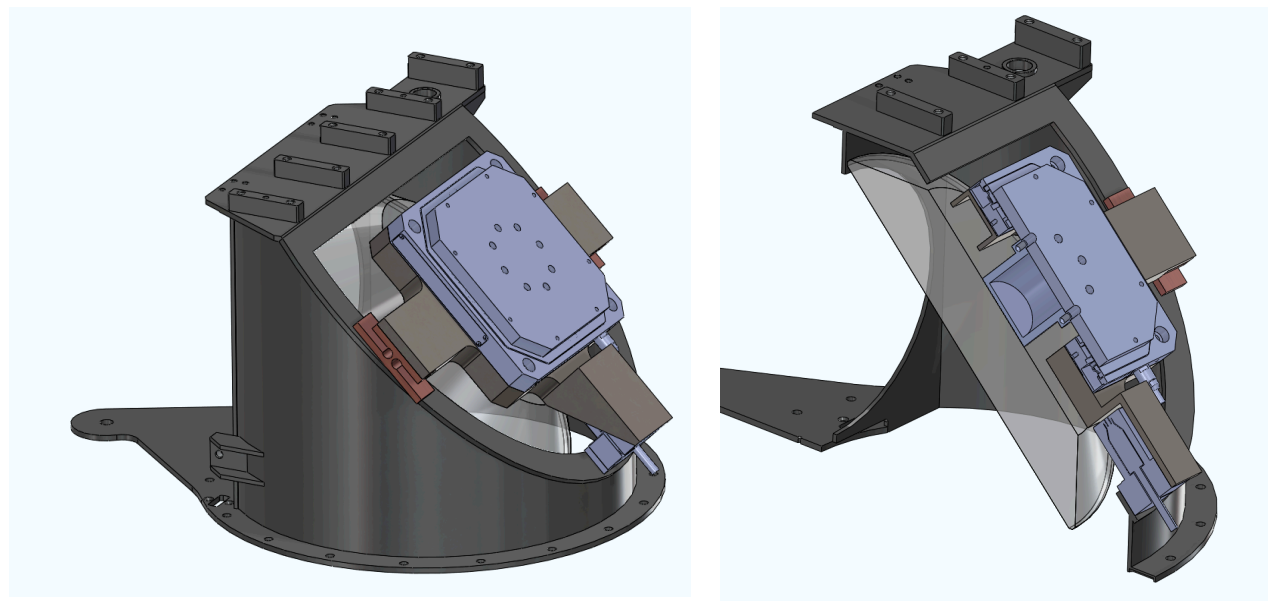


Figure 5-18. *Fold mirror showing two nested actuations, the small motion tip tilt stage directly mounted to the mirror and the large travel tip flexure mechanism*

The fold mirror is an elliptical mirror with a major diameter of 297mm and 38mm thick. It has a basic conical mass relief on the backside. The mirror has an invar puck epoxy bonded to the center of the back side for mounting. An FEA analysis of the mirror shows deflection sag of less than 70nm.

The fold mirror is mounted to an actuated stage to enable motion of the mirror. The first motion is a small tip/tilt motion (0.2urad tip tilt and 200um piston) for flexure compensation. To achieve this the mirror is directly mounted to a PI piezo stage. The stage has internal strain gauge position sensing and will be

controlled open loop from a calibrated look up table. This stage is intended to enable approximately 1pixel (18 μm) image stability.

The tip tilt stage is then mounted to a larger range of motion flexure dithering stage, which allows the mirror to nod up and down. This enables the field to be moved up and down on the detector (perpendicular to dispersion). The single axis tip motion is provided by PI long travel piezo stage coupled through a flexure pivot behind mirror. This stage gives approximately 10mrad of tip allowing dithering of $\sim 1.8\text{mm}$ or 100pixels at the focal plane.

The flexure tip tilt stage is nested within the dither stage and the two systems operate independently.

5.2.4. Optical Storage Assembly

The Optical Storage Assembly (OSA) is a staging area inside the pre-dewar enclosure where the optical filters, gratings and etalon are kept when not in use. This platform is not directly connected to the main optical elements, i.e. NIR doublet, turning mirror and camera and their support elements. The stored optics must 'jump' this physical gap in order to be deployed into the system. The OSA is also in the same plane as the main optical elements keeping the center of gravity of the instrument low and the movement of the components in 2D space. This keeps the enclosed volume of the instrument low and the complexity of the enclosure simpler.

Figure 5-19 shows the OSA and its orientation to the main optical elements. Notice the physical gap separating the two. The OSA consists of 2 filter cassettes, 1 grating cassette and a single Fabry-Perot etalon. The filter exchange cassette holds 3 filters while the fixed filter cassette holds 9. These filters are tilted in their holders 2 degrees to minimize back reflections in the system. The grating cassette holds 5 gratings. These subsystems are on a single stage, which moves to allow either a filter, a grating or the etalon to be deployed into the beam. Once the element is deployed, the stage can move to deploy a different element. The filters are placed in the optical system behind the turning mirror while the gratings are positioned at the pupil plane in a rotating holder. The etalon is placed behind the pupil plane and can only be deployed when the grating rotation holder is normal to the beam. The filter holder only holds filters while the grating holder can accommodate both filters and gratings. While a filter in the grating holder may not be useful in an optical sense, it allows the filters to be shuffled in the two filter cassettes to any position within these cassettes.

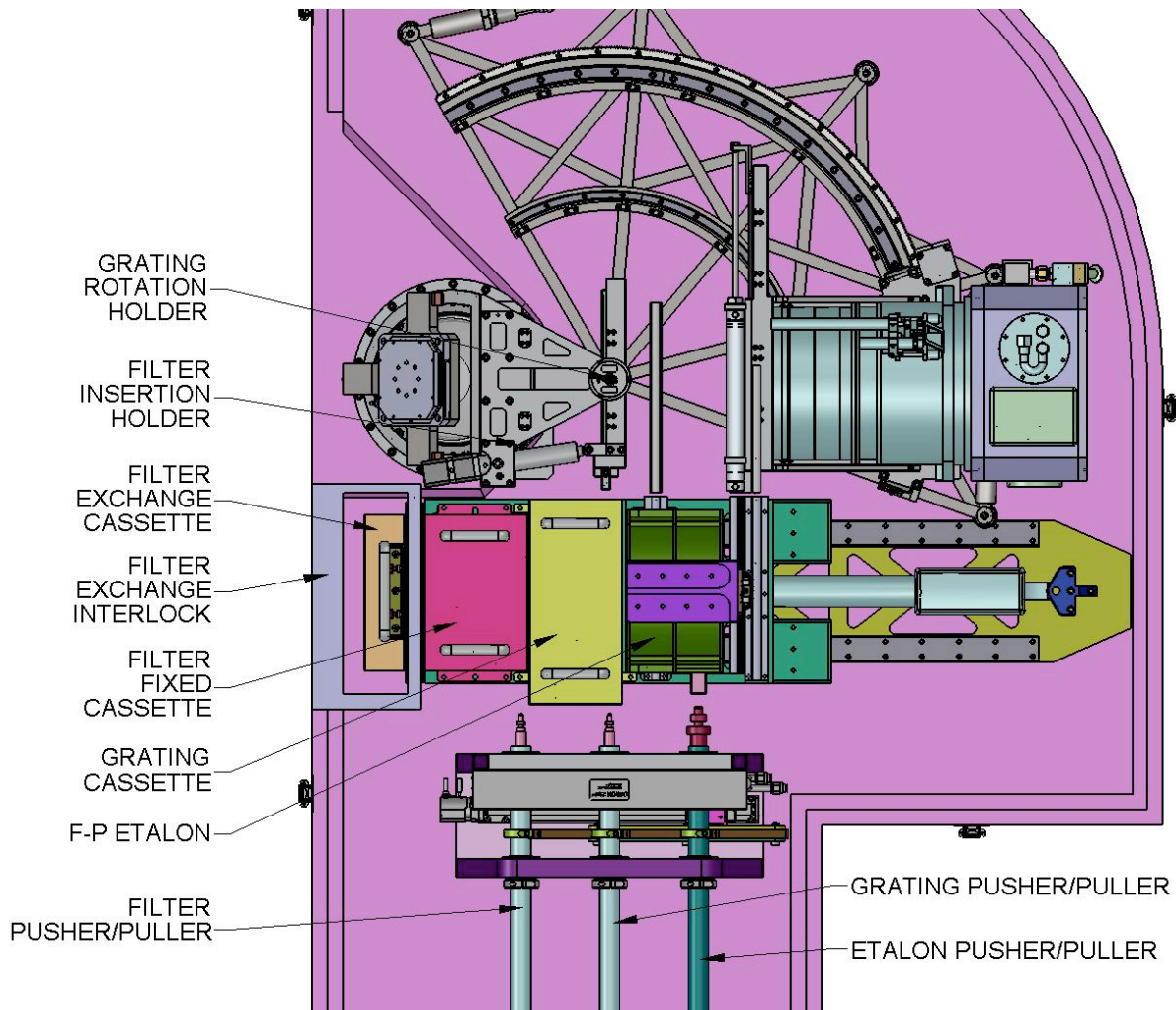


Figure 5-19. *Optical Storage Assembly.*

The filter and grating holders are very similar. The frames have a ‘V’ shape plate both top and bottom. V rollers are mounted in the cassettes and deployment positions to move the filters and gratings between the OSA and the main optics. There is a separate ‘pusher/puller’ for the filters and the gratings, aligned with their respective holders. See **Figure 5-22**. These drives are linear ball screw actuators with encoders. In addition each grating and filter has a latching mechanism, which mechanically locks the filter or grating into the cassette or the deployed position. **Figure 5-20** shows the latching mechanism. It works in concert with the pusher/puller. First the p/p drives into the latch positioning the cam at the end of the p/p against the stop. The p/p is rotated thus capturing the filter or grating and then releasing it from either the cassette or the holder. See **Figure 5-21** to view how the cam action works. Once the filter or grating is released, the p/p moves it either into the holder or back to the cassette. Rotating the cam engages the latch then releases the filter or grating. The p/p is retracted out of the way to end the cycle. Hall effect sensors are placed in the cassette and the 2 holders to verify the 3 states of the latch. The sensors detect the position of the 2 magnets on top of the engagement pin of the latch. Thus, there are no electronic components on the filter or grating frames.

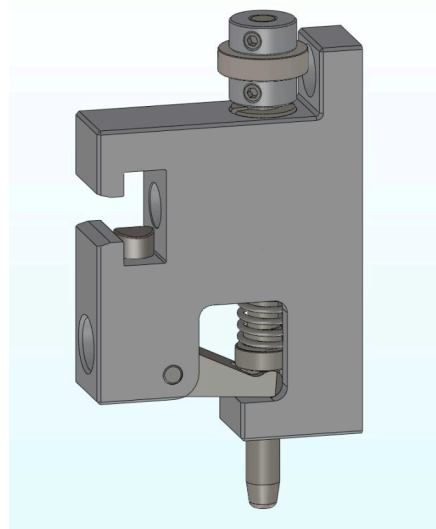


Figure 5-20. Filter & Grating latching mechanism.

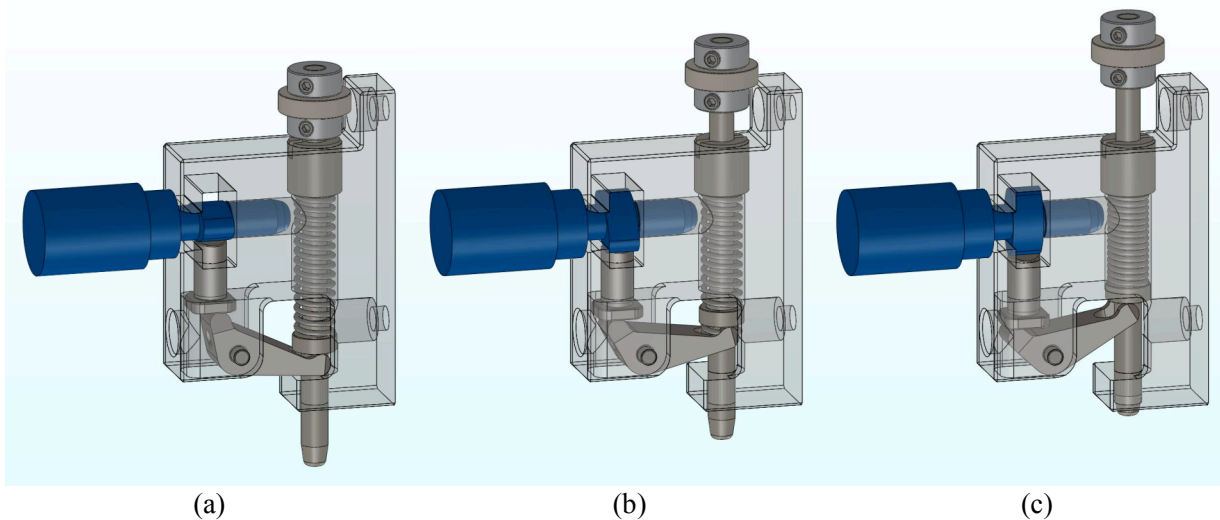


Figure 5-21. The filter and grating latch shown with the (a) latch engaged, (b) latch captured, and (c) latch retracted

Figure 5-22 shows the 3 pusher/pullers for the filter, the grating and the etalon. The etalon has pneumatic instead of mechanical latches, one on the OSA and one that acts when the etalon is deployed in the beam. The etalon pusher/puller capture and engaging works similar to the filters and gratings. Instead of ‘v’ wheels to move it across the gap the etalon uses larger linear roller bearings.

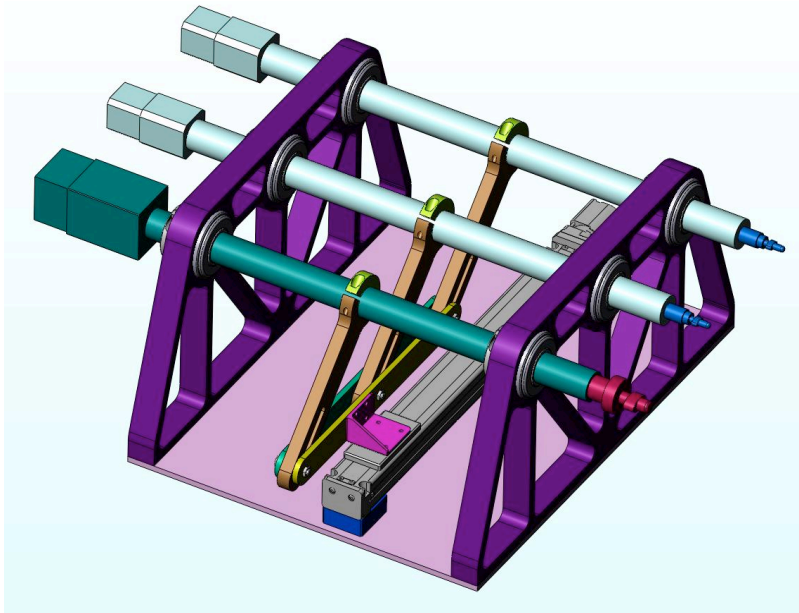


Figure 5-22. *Pushers/Pullers.* A linear stage rotates the actuators to capture, engage, and retract the filter and grating latches.

5.2.5. Filter Cassette Exchange

There are 2 filter cassettes separated by an insulated bulkhead as shown in **Figure 5-23**. The exchange cassette holds 3 filters that can be removed from the system through an air-lock scheme. **Figure 5-24** shows the OSA positioning the exchange filter cassette into the air-lock at the end of travel location. This special insulated and environmentally controlled chamber is attached to the pre-dewar enclosure. This air-lock space has an outside hatch (not shown) for exchanging this cassette with the outside world. Thus 3 filters can be taken out of the system at a time and 3 others can be added. Using the grating holder as a temporary storage space while the filter deck is shuffled around allows one to choose which filters are kept and which ones are removed.

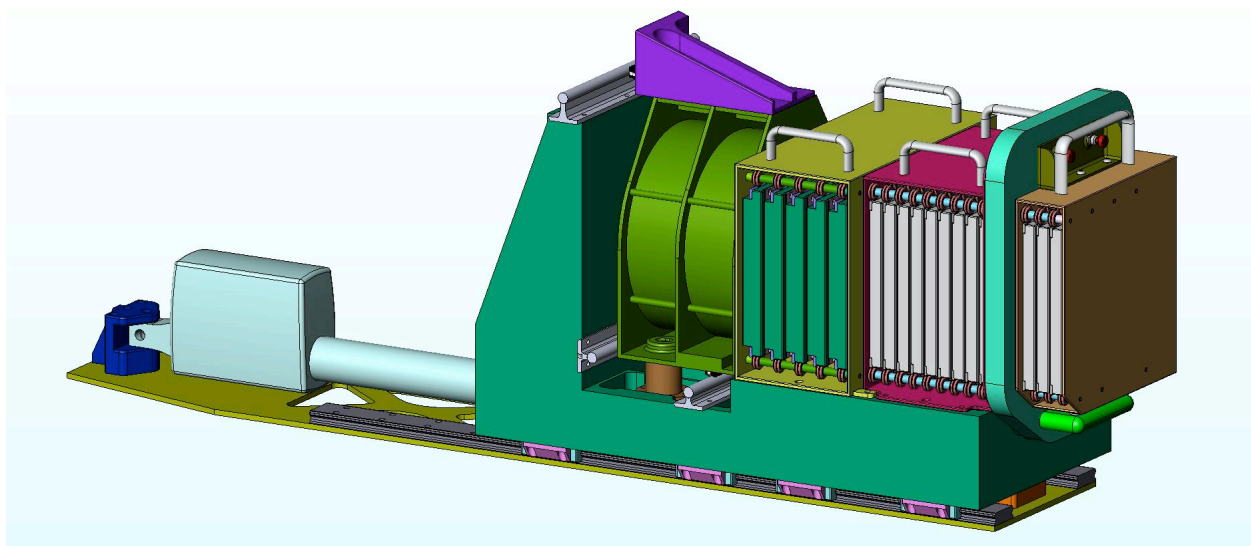


Figure 5-23. *Filter exchange cassette and insulated wall*

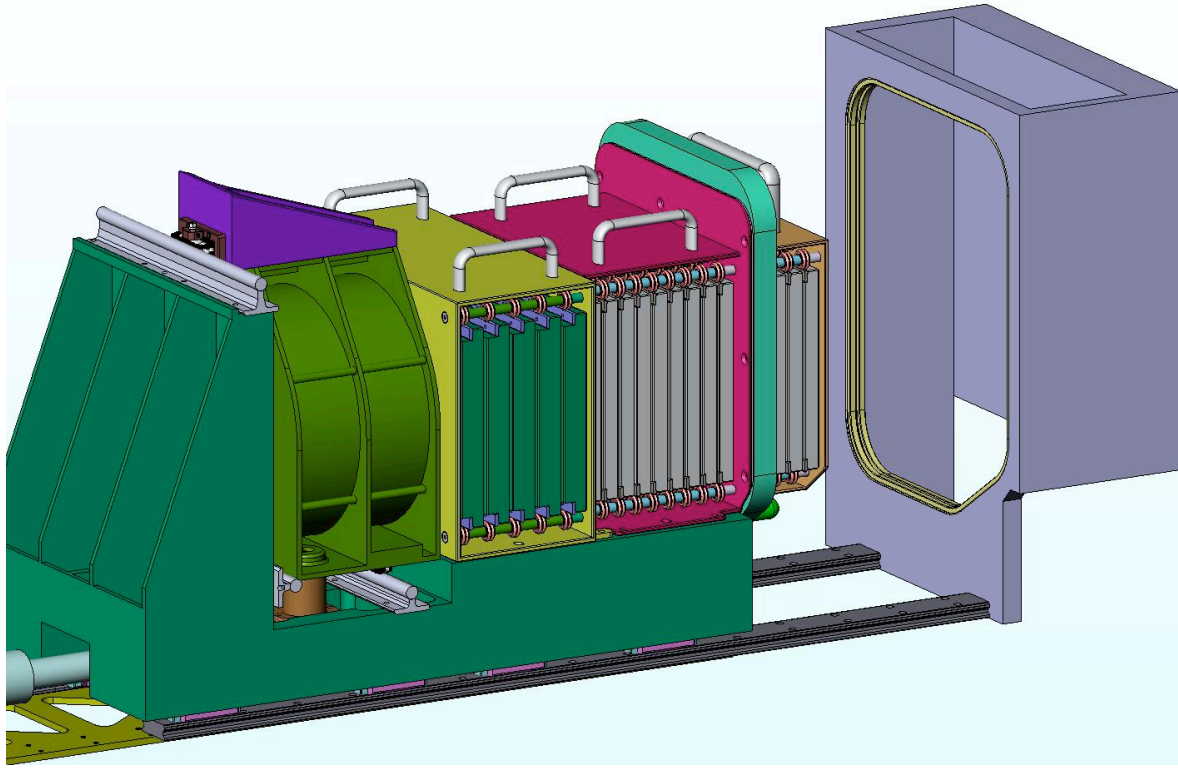


Figure 5-24. *Filter exchange cassette air-lock*

5.2.6 Grating Rotation Stage

The grating rotation stage receives the grating from the magazine and inserts it to the desired angle. The grating rotation axis is coincident with the camera articulation axis. The grating can be rotated from zero to fifty degrees and the rotation must be precise and repeatable within a range of twenty arc seconds. The grating rotation stage is supported laterally both top and bottom by two plates. The lower plate is the extension of the fold mirror structure base flange and the upper plate is fastened to the eyebrow at the top of the fold mirror structure. Support in the Z axis comes from below at the center pin of the camera articulation frame. This support scheme guarantees more rigidity for the grating holder and subsequently less undesirable deflection than a single rotary stage can provide. Rotation of the grating around the optical axis is particularly undesirable and this mounting scheme is designed to maximize stiffness in that direction. Precision instrument ball bearings top and bottom allows low friction rotation of the stage. The complete stage with grating and holder in position is balanced about its rotation axis. This helps to eliminate errors due to the effect of gravity at the various camera positions. A linear electro-mechanical actuator is used to impart rotational motion to the stage. This particular model is rated for cold operation and has a resolution of two arc seconds with the lever arm as configured. Angular encoding is done with a precision absolute encoder connected to the shaft at the top of the rotation stage. This encoder has a resolution of five arc seconds.

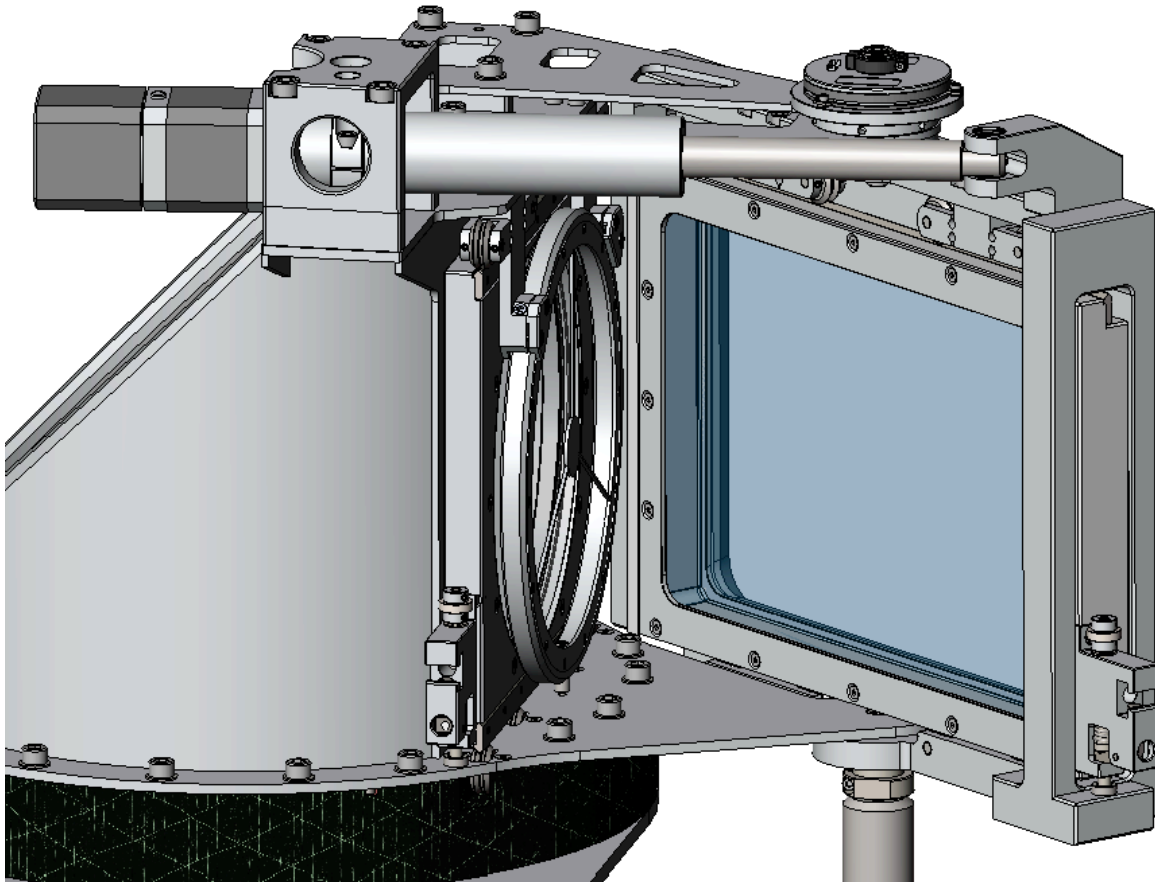


Figure 5-25. *Grating Rotation Stage in a rotated position.*

A line of four V-rollers located in the bottom of the rotation stage provides guidance for the lower rail on the grating holder. The outer two V-rollers are precisely and securely mounted for zero axial play. The inner two V-rollers are mounted slightly below the outer two V-rollers with some small axial clearance on their shaft. In this way, the outer two V-rollers provide location for the grating holder when it is in position while the center V-rollers only help guide the grating holder into position. Another set of four V-rollers is mounted in two tandem flexure assemblies attached to the underside of the rotation stage directly above the lower set. Each of these V-rollers provides a positive force against the grating holder but only an inner V-roller is fitted for zero axial clearance. The other three float some small amount. A latch detent for locking the grating holder in position is located at the bottom near the edge of the rotation stage.

The design of the rotation stage is such that a filter holder may be inserted here as well as a grating holder. This option is desirable for shuffling the order of the filters in the filter cassettes.

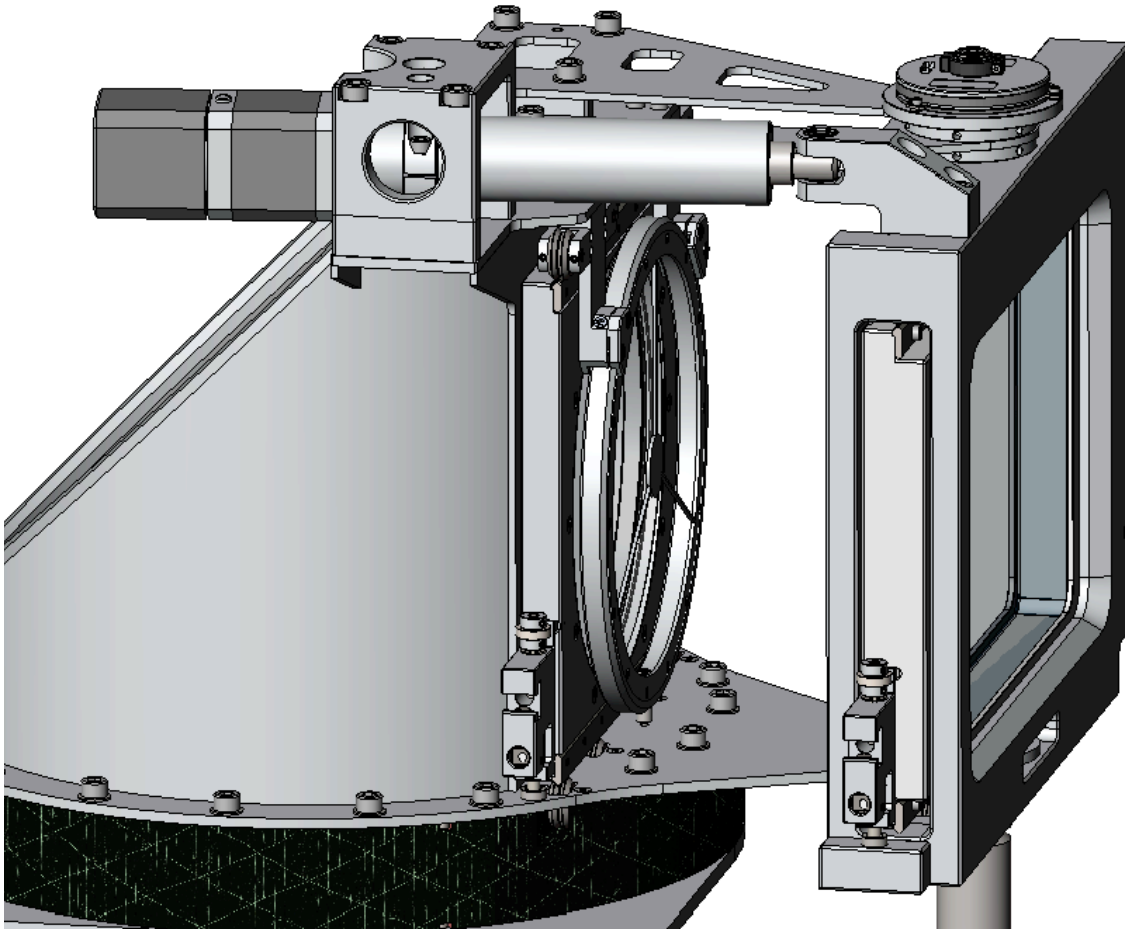


Figure 5-26. *Grating Rotation Stage*

5.2.7. Polarizing Beamsplitter Mechanism

The polarizing beamsplitter resides in front of the camera and behind the etalon (when deployed). The b/s can be moved into the beam at any time. The b/s frame and translation stage are supported by the articulating camera mount and travels with the camera, though not attached to the camera or Dewar. A pneumatic cylinder positions the b/s frame either into the beam or outside it. End of travel sensors detect its position state.

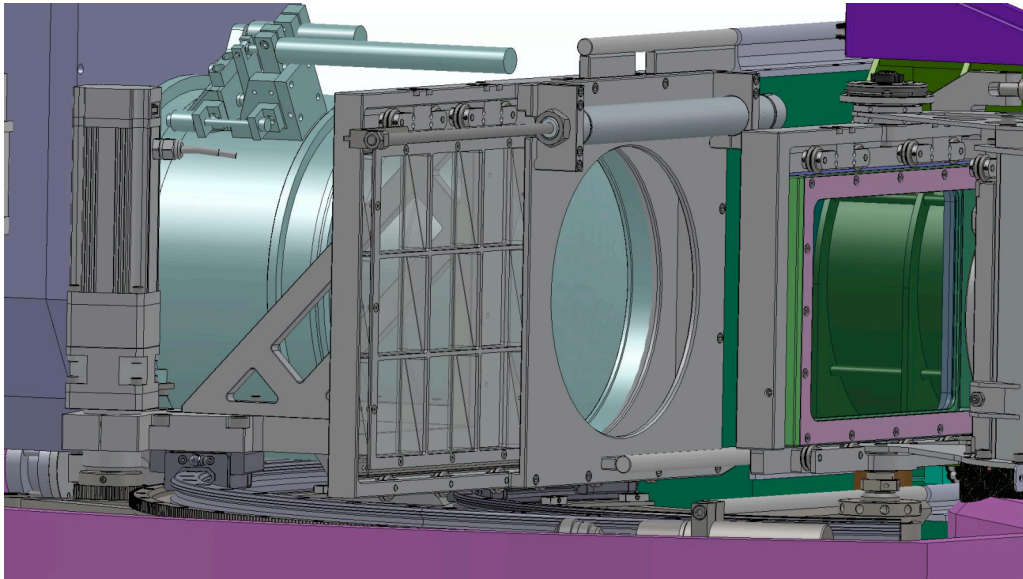


Figure 5-27. Polarizing beamsplitter.

5.2.8. Camera and Focus Assembly

The camera is made up of 7 elements ranging in size from 68mm to 225mm. Elements 1 through 5 reside in the camera barrel with elements 4 and 5 being mounted in the focus mechanism within the barrel. Element 6 is the Dewar window and element 7 is within the Dewar. A basic analysis of the individual element mounting and alignment tolerances was done using ZEMAX. The tolerance analysis shows the first three elements in the camera to have the tightest tolerance, on the order of 25 μ m decenter and 0.025 $^\circ$ in tip tilt. The other tolerances range between 50 μ m decenter and 0.05 $^\circ$ in tip tilt and 100 μ m decenter and 0.1 $^\circ$ in tip tilt. These tolerances are on the tight edge of what can be achieved with standard machining and alignment practices and special attention will be given to the mounting and alignment methods.



Figure 5-28. a. Cut view of camera barrel showing diaphragm flexure mounting of element 4 and 5. **b.** Single element mounted in its cell showing tangential shoulder and ~2mm elastomer gap.

The proposed scheme for mounting the elements within the camera barrel will be to bond them into precisely machined lens cell bezels using an elastomer. The size of the gap between the lens material and the cell will be adjusted for each element so as to athermalize to the aluminum cell.

The lenses will be mounting into the bezel cells on a rotary table. The bezels will have a precisely machined tangential shoulder, which is concentric with the outside of the bezel. The empty bezel will be placed on the rotary table and centered. The lens will then be lowered into the cell and the axial runout or the back surface will be measured optically and small adjustments made to align the lens within the cell. Once the lens is aligned, the lens will be bonded into the cell. Where lenses have matched radius and close spacing, the lenses will be built up in series with polyester shims between the elements in place of the shoulder on the second bezel. The camera barrel lens stack will have axial spacers shims between cells to enable final adjustment of the lens spacings.

Alan Schier used this scheme on the visible camera for RSS as well as on other instruments of comparable size. Analysis done by Schier showed that for similar sized lenses, the maximum stress that the lens sees could be held below 100psi. He also showed that the sag could be limited to $\sim 1\mu\text{m}$ radially and $>20\mu\text{m}$ axially. We are designing to limit the stress in the CaF₂ lenses to < 70 psi in tension and will design in a thermal preload in the CaF₂ lenses. A rigorous analysis of stresses and deflections in all elements will be done as part of the next design phase. We are also planning on testing our mounting methods on aluminum dummy lenses.

The camera is mounted to the articulation mechanism using a ball in a cone at the front and two blade flexures at the Dewar end. The Dewar is flange mounted to the camera. The flange is a shim spacer, which allows for any final adjustment of camera Dewar misalignments. It also allows rotational adjustment to align the detector rows with the spectral lines and the articulation plane.

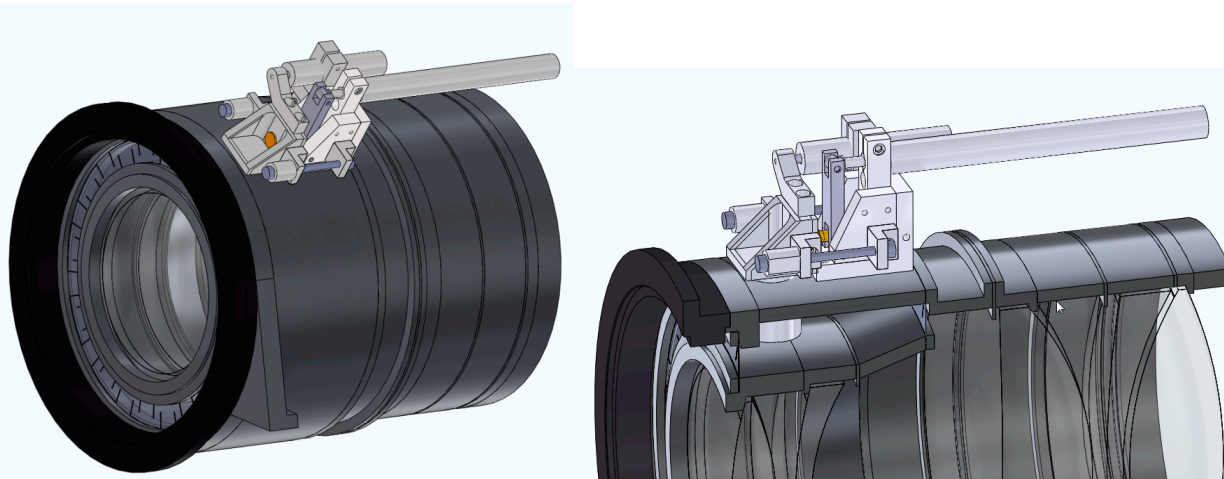


Figure 5-29. *Focus Mechanism, Stepper micrometer driving diaphragm flexured elements using a spring loaded lever.*

Focus adjustment of the camera is achieved by axial movement of elements 4 and 5 as a group. The group has a range of travel of $\pm 1.5\text{mm}$. Elements 4 and 5 are mounted between two diaphragm flexures and driven by a stepper micrometer through a spring loaded lever. An LVDT provides positional feedback. This is the same focus mechanism concept as was successfully used on the visible arm of RSS.

We are in parallel investigating an alternative focus mechanism that would focus the camera by moving element 7 (the field lens) and the detector inside the Dewar. We have been in discussion with the MOSFIRE team about their focus stage and the possibility of adapting it to this instrument. At present it appears that focusing elements 4 and 5 will achieve satisfactory focus compensation but we will continue looking at this option as a contingency.

5.2.9. Dewar

5.2.9.1. Overview

The Dewar for the NIR upgrade to the Robert Stobie Spectrograph mounts at the back end of the re-imaging camera of the near infrared channel, see **Figure 5-30**. It houses a Teledyne Hawaii 2RG array, ASIC cold card, field flattener and filter wheel containing three low-pass filters. A closed-cycle refrigeration system cools these components to cryogenic operating temperature. Light enters the Dewar through the sixth optical element of the camera, which serves as the Dewar window. The window mounts to the front face of the Dewar vacuum vessel, which provides thermal isolation and mechanical support for the cold internal components.

The following sections discuss the preliminary Dewar design. Like any cryogenic optical system, the design details are driven by many factors: opto-mechanical alignment, thermal requirements, flexure, and manufacturability to mention a few. This design represents a compromise of these factors. It utilizes significant heritage from other cryogenic instruments with proven performance. The overarching goal is a simple, elegant, manufacturable design that has a high probability of success.

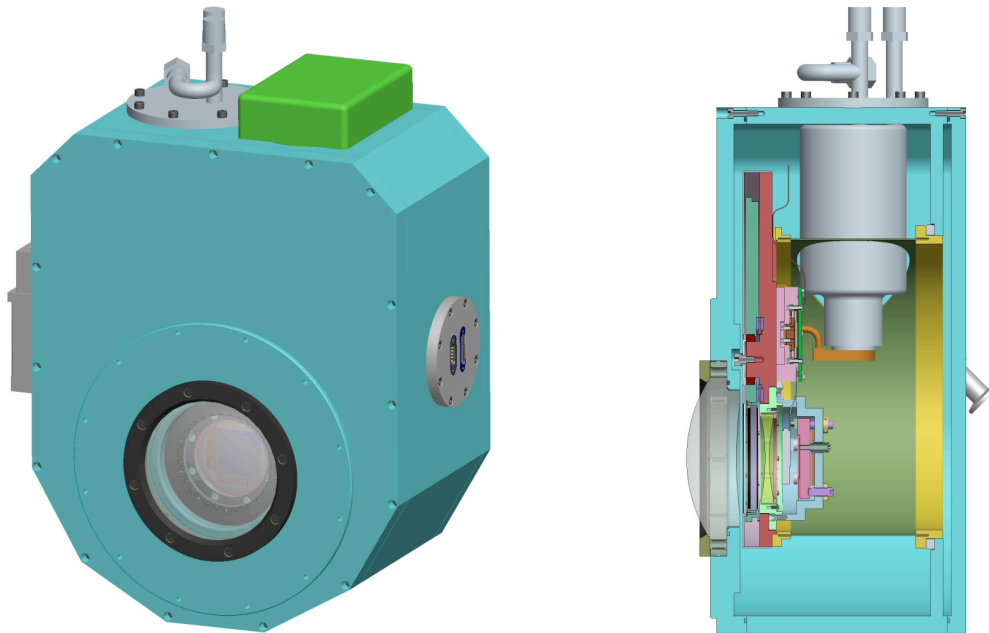


Figure 5-30. *Dewar for the NIR upgrade to the Robert Stobie Spectrograph*

5.2.9.2. Vacuum Vessel

The vacuum vessel serves two purposes. First, it serves the usual roll of thermally isolating the cold internals from the outside ambient; in this case the ambient is approximately 230K as the Dewar is housed

inside the pre-dewar. Second, it is an optical bench since the Dewar contains the last two elements of the camera, L6 and L7.

Three components make up the vacuum vessel: the shell, the front cover, and the rear cover. The front cover houses the window, L6, and interfaces to the camera/Dewar shim. The shell supports the cold optical assembly internally and the faceted outer profile provides the necessary interfaces for the cold head, Jade2 enclosure, vacuum valve and ion pump, as well as electrical penetrations to power the filter wheel and read back telemetry from internal sensors. The rear cover does nothing more than resist atmospheric pressure and provide access to the back of the Cold Optical Assembly (COA). The vessel is constructed of aluminum, is 320 mm wide, 400 mm tall and 200 mm deep. It weighs approximately 15 kg. Using finite element analysis we should be able to optimize the structure and reduce mass through lightweighting. Vacuum sealing interfaces are sealed with viton o-rings. A routine operational vacuum of order 10^{-6} Torr should be achievable with the baselined Kernco 2 l/s ion pump (a thorough analysis needs to be done).

- a) **L6 (Window) Alignment.** L6 is mounted in the vessel front cover of the vessel and is aligned to L5 by dead-reckoning. The front cover contains a precision shoulder to pick up the camera/Dewar shim and precision bore to locate the window, L6. Both are on the front side of the cover and can be machined in the same setup to guarantee concentricity. L6 is mounted to the front cover in a roll-pin flexure cell in a fashion similar to L7 described below, which, by design, eliminates radial play between the cell and lens. Therefore, by accurately controlling the location and size of these reference surfaces, and by minimizing radial clearances, we believe we can center L6 relative to L5 to within $\sim 50 \mu\text{m}$. Achieving the wedge tolerance of $\sim 0.05^\circ$ should not be a problem given the features of this design. Lastly the spacing between L5 and L6 will be adjusted by altering the camera/Dewar shim thickness.

5.2.9.3. Cold Optical Assembly (COA)

The cold optical assembly, shown in Figure 5-34, consists of the detector, field flattener, filter wheel assembly, and radiation shield. It is supported inside the Dewar off the back of the vessel shell by a G10 tube. The G10 tube mechanically aligns the COA relative to L6 and provides conductive thermal isolation between to the ambient environment.

- a) **Filter Wheel.** Figure 5-31 shows isometric and cross-section views of the filter wheel. The five-position wheel has positions for three filters, a stop, and an open position to allow the entire bandpass to be imaged. The geared wheel is driven at its outer diameter by a Phytron VSS-32 stepper motor. Position is controlled by the detent profile below the gear teeth. In operation, the motor drives the wheel to the desired position, current is cut to the motor, and the detent bearing snaps into the wheel detent, accurately clocking the orientation of the wheel. This mode of operation facilitates accurate repeatable positioning of the filters without the use of hold current and the unwanted parasitic heat load. A small magnet at each wheel location is sensed by a Lakeshore cryogenic Hall effect sensor and provides verification that the filter is in the beam. By flipping the polarity of one of the five magnets a unique “home” position can be distinguished.

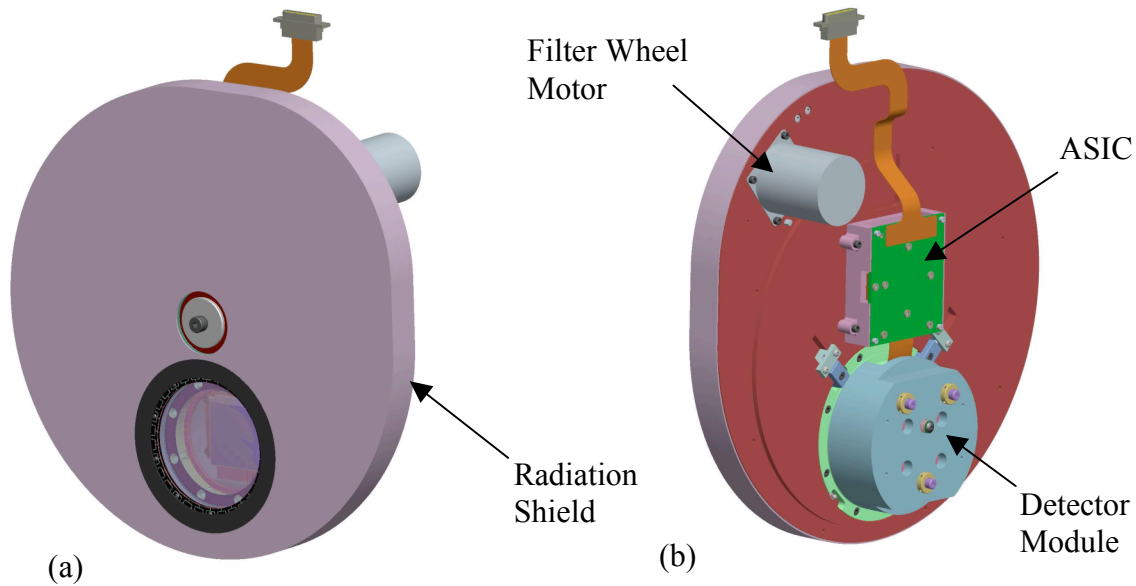


Figure 5-31. (a) Front view, and (b) rear view of the cold optical assembly

The filter wheel will be constructed from 7075-T6 aluminum and will be hard coat anodized with Teflon impregnation. The hard coat anodize with Teflon provides a very durable surface with minimal friction at the gear interface. The motor spur gear is Vespel SP3. The combination of Vespel against Teflon impregnated hard coat anodize has a strong track record of success (WHIRC, IRMOS). A single deep groove radial hybrid ball bearing is used as the rotation axis. The wheel is preloaded on axis against a custom needle roller bearing.

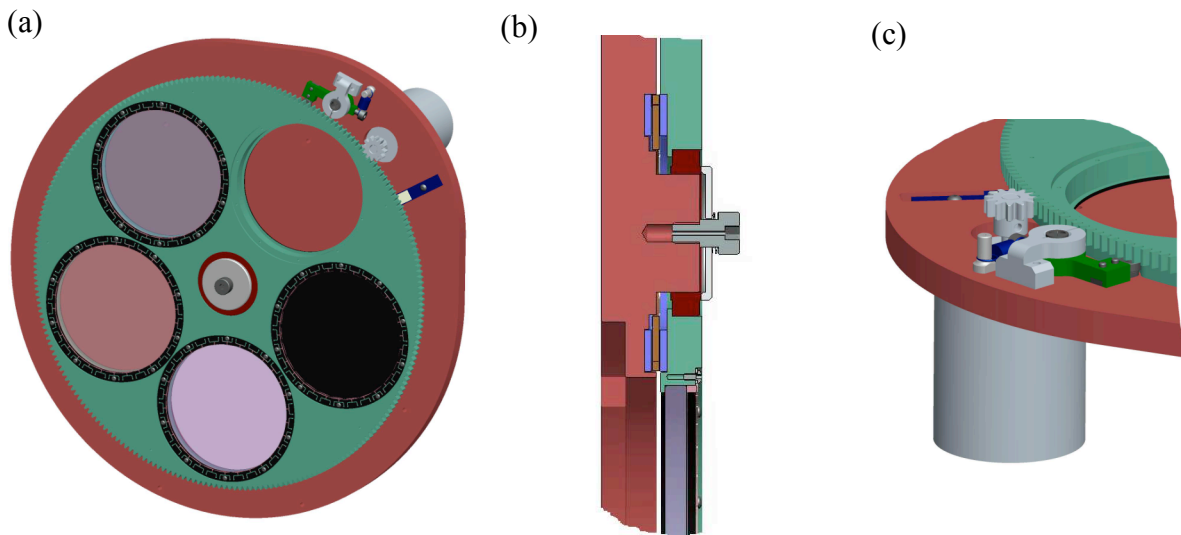


Figure 5-32. (a) Front view of filter wheel, (b) section detail depicting the wheel bearing detail, and (c) detail view of detent arm

Filters are held in recessed bores milled in the wheel. The bore diameter is sized to clear the filter at cryogenic operating temperature to avoid fracture. Axial retention and compliance is achieved with a membrane spring washer and a spacer ring. The spacer ring and spring washer are both made of aluminum (the spring washer being of 7075 alloy). The incident surface of the spring washer, and inside diameter of the spacer and wheel bore will be painted with Aeroglaze Z306 to reduce scattered light. The details presented here borrow largely from the WHIRC filter wheel design, which, to date has performed without failure.

- b) **Detector Module.** The detector and L7 (field flattener) are packaged in a subassembly called the detector module, see **Figure 5-33**. The front half of the module is simply the L7 cell. The back half is the detector mount. When bolted together the detector is naturally protected by the lens in front of it. Packaging the L7 and detector in this way protects the detector and eases alignment of the detector to the rest of the optical system. Since all adjustments are accessible from outside the module, once installed, the detector should not need to be handled.

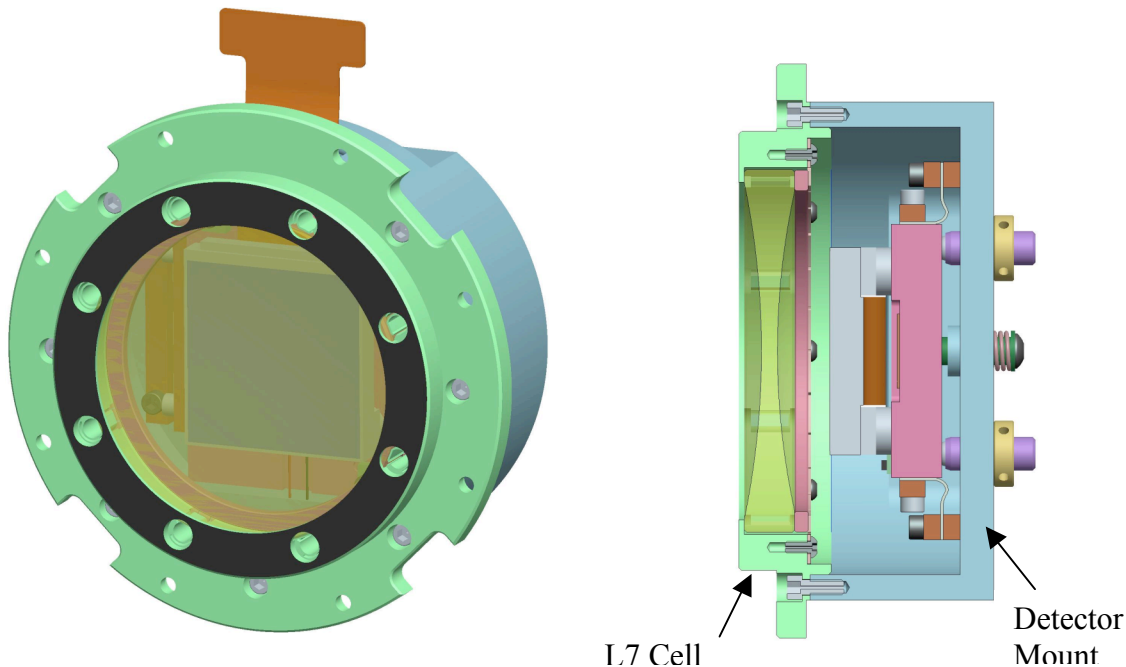


Figure 5-33. *Front view and section view of the detector module*

- c) **Detector Mount.** **Figure 5-34** shows the detector mount. Here the detector mounts to a molybdenum stage; nuts from the backside anchor the detector to the stage. Molybdenum is used so as to match the coefficient of thermal expansion (CTE) of the detector substrate. The stage is kinematically registered on three spherically-tipped fine-threaded adjusters threaded into the back of the detector housing; a spring behind the stage preloads the stage against the tooling balls. The adjusters allow tip, tilt, and piston adjustment of the detector. Indium straps between the moly stage and the housing provide a flexible thermal path to cool the detector.

The kinematic mount is ideal for this application. It isolates the stage from any mechanical loading induced by thermal gradients during cooldown and it naturally accommodates the CTE mismatch between the aluminum housing and the moly stage.

Holes in the back of the detector housing allow access to the detector mount nuts so the detector can be installed after the stage is fully assembled and adjusted.

This detector mount design is nearly identical to that used for the WHIRC and FourStar near infrared imagers.

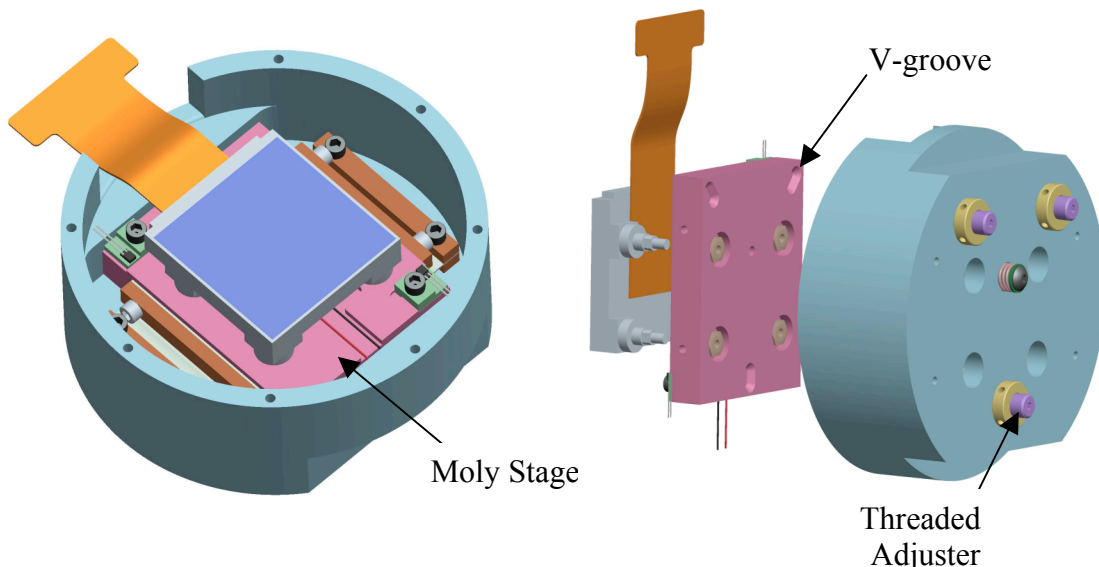


Figure 5-34. *Detector mount design. The detector mounts to a molybdenum stage that is kinematically registered on three threaded adjusters.*

- d) **Detector Adjustment.** Given the $f\#$ of the camera and the exquisite parallelism of the detector surface to its base, the detector tip, tilt, and piston can be adjusted using mechanical metrology of the moly stage without the detector installed. Once installed, any future adjustment of the detector, if needed, can be done without removing the detector since the adjusters are accessible from the back. Rotation of the detector to align the spectra with the rows along the detector is achieved through a rotation adjustment at the Dewar/camera-barrel interface.

- e) **L7 Cell.** **Figure 5-35** shows the L7 roll-pin flexure cell, which borrows from the cell design used successfully for the WHIRC instrument. Here the lens is centered on a radial pattern of flexures machined by wire EDM (electrical discharge machining) into the circumference of the cell. The inherent precision of the wire EDM produces a contact diameter that is centered to the outer diameter of the cell to better than $25\ \mu\text{m}$, typically to $\sim 10\ \mu\text{m}$. The radial compliance of these flexures accommodates the difference in CTE between the glass and metal and keeps the lens centered from ambient to cryogenic temperatures. Axial placement of the lens is defined by the step in the base of the cell and a membrane spring washer is used to apply a compliant axial preload to seat the lens against the step. The cell will be made of 7075-T6 aluminum and the roll-pin and axial seat surfaces will be coated with Teflon impregnated black anodize. For designs like this the clear aperture of the cell and wave spring washer are typically coated with Aeroglaze Z306.

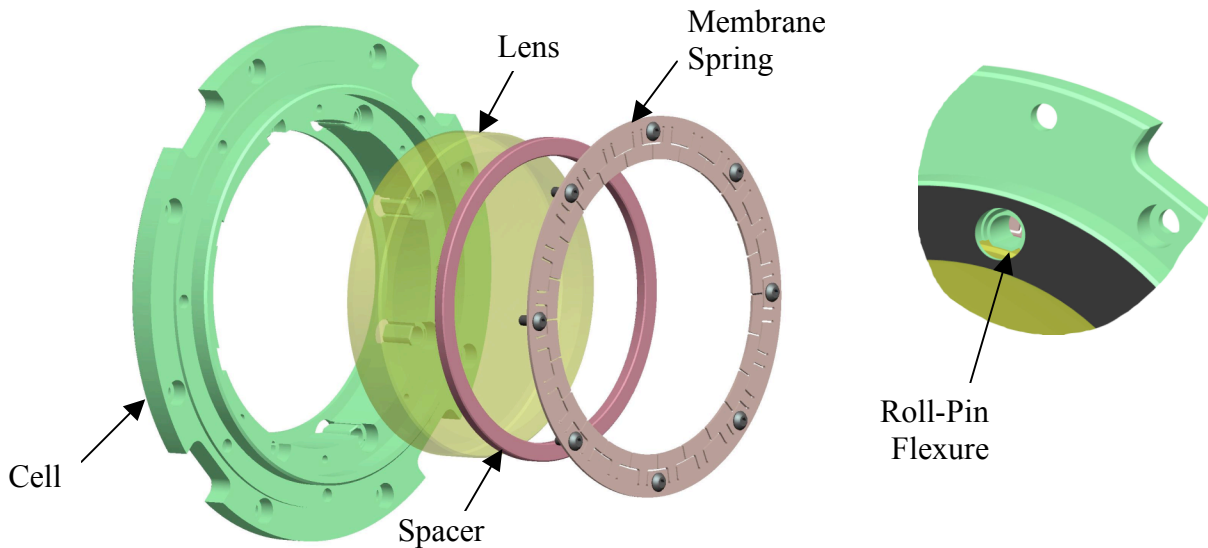


Figure 5-35. L7 cell. The lens is centered by eight roll-pin flexures contacting the outer lens diameter. The membrane spring constrains the lens axially. Compliance in the roll-pin flexures and membrane spring accommodate the differential CTE between the lens and cell. All cell components are aluminum.

- f) **L7 Alignment.** Given the numerous mechanical interfaces that exist through the load path that connects L6 to L7 we do not believe we can place L7 relative to L6 to within the 50 μm decentre tolerance.; we believe that 125 μm is more realistic. Therefore L7 will be centered to L6 via mechanical adjustment. For this purpose an X-Y adjustment mechanism is incorporated into this design, see **Figure 5-36**. The mechanism is used to adjust the position of the detector module, which contains the mount for L7. In this scheme, centration is achieved by adjustment of the module, wedge is controlled by dead-reckoning, and placement along the optical axis is achieved by adjusting the shim thickness between the G10 support tube and the vacuum vessel shell.

5.2.9.4. Thermal Design

Thermal loading on the cold optical assembly is mitigated several ways: first, through the use of G10 to conductively isolate it; second, by virtue of the vacuum space surrounding it, which eliminates convective losses; and third by blanketing, or shielding, it to minimize radiative loading. This approach is standard for most all Dewar designs. The intent here is to minimize the heat load such that the desired detector operating temperature (100 – 120K) can be reached.

In this design, the cold optical assembly is cooled by a closed cycle refrigerator. It is mounted on a G10 tube and is surrounded on the front and perimeter by a radiation shield. The cooling path is a short copper braid strap that connects the cold head to the filter wheel base plate. The filter wheel, detector, and ASIC are all cooled by conductive paths to the filter wheel base plate. The shield is aluminum and will either be polished and gold plated or simply covered with aluminized Kapton. The latter is much cheaper but may not be permitted due to space constraints. A radiation shield inside the G10 tube behind the cold optical assembly will shield the COA against the warm back cover. The interior walls of the vessel will be covered with aluminized Kapton.

A Polycold PCC closed-cycle PT-13 high-performance refrigeration system is the baseline refrigerator for this design. The PT-13 has a cooling capacity of 10 w at 94K (just below the desired operating

temperature range). Based on the preliminary thermal analysis discussed below, the PT-13 should be adequate for this application.

- a) **Preliminary Heat Load Estimate.** A preliminary thermal analysis has been done. Conductive losses were calculated by closed form solution and the radiation loading was determined using finite element analysis. Inputs into the FEA model were conservative as compared to proven values from other analyses.

Table 5-5 below gives the results from this analysis. The total heat dissipation is estimated to be 5.3W, well within the capacity of the PT-13.

Table 5-5. RSS-NIR Dewar Heat Load Estimate

Component	Load (W)
Window	1.6
Chamber	2.3
Parasitics	0.75
G10 Tube	0.63
<i>Total</i>	<i>5.3</i>

- b) **Detector Temperature Control.** The detector temperature is controlled through a PID controller and Kapton film heater bonded to the surface of the moly stage, the detector temperature being controlled to a value just above the running temperature of the COA. Indium thermal straps provide the principal thermal path to the detector. Detector temperature is monitored by two (one primary, one redundant) Lakeshore DT670 diode.

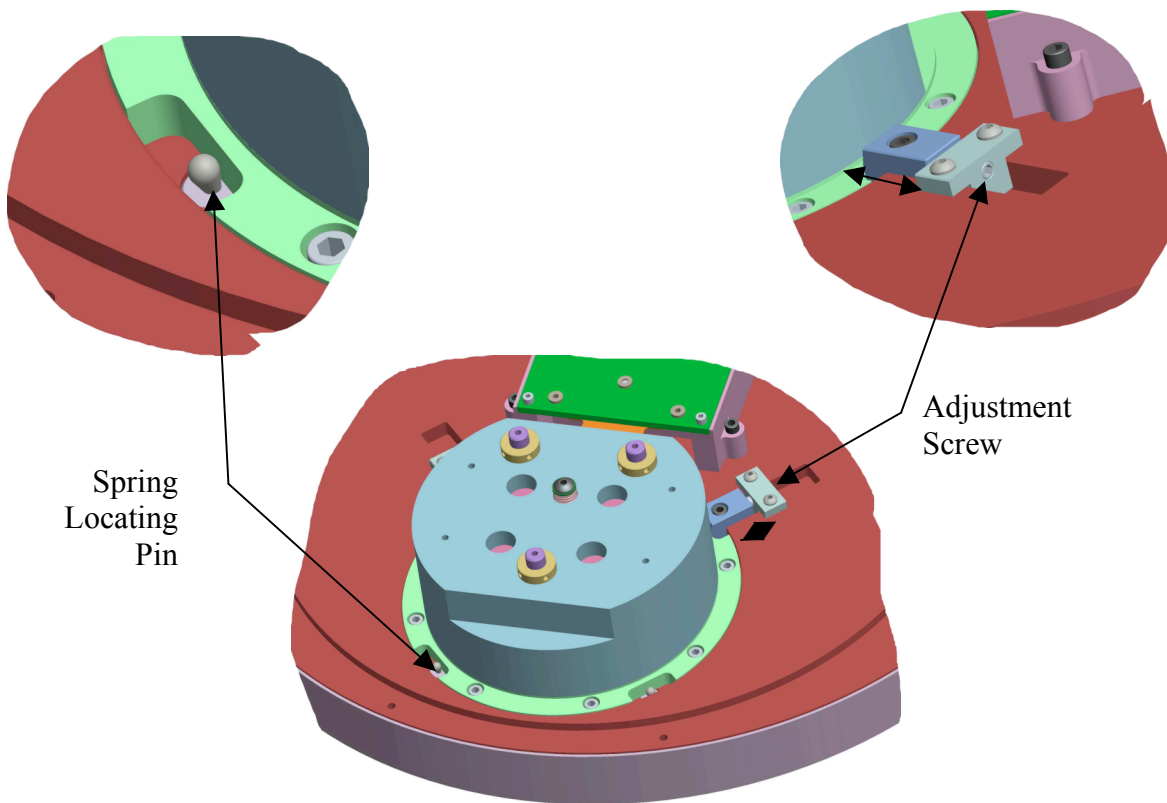


Figure 5-36. *In-plane adjustment of the detector module. L7 and the detector are adjusted as a unit. The spring locating pin preloads the L7 cell against the sliding adjustment block. Rotation of the adjustment screw translates the detector module.*

5.2.9.5. Flexure

At the time of this writing, a flexure analysis has not been done. This will be done prior to the Mid-Term Review and results will be presented. Based on the details of this design and prior analyses of similar Dewars the design presented should be adequate, or close enough to specification that compliance can be reached with minor modification.

5.2.10 Articulation System

The articulation system is the mechanical assembly, which supports and moves the camera, detector, and Dewar. The camera and Dewar assembly is a relatively large and heavy component, which must be able to rotate about an axis coincident with the grating rotation through a range of one hundred degrees. Rotation of the camera and detector around the optical axis is undesirable and the articulation system is designed to provide support against gravitational forces to minimize this effect.

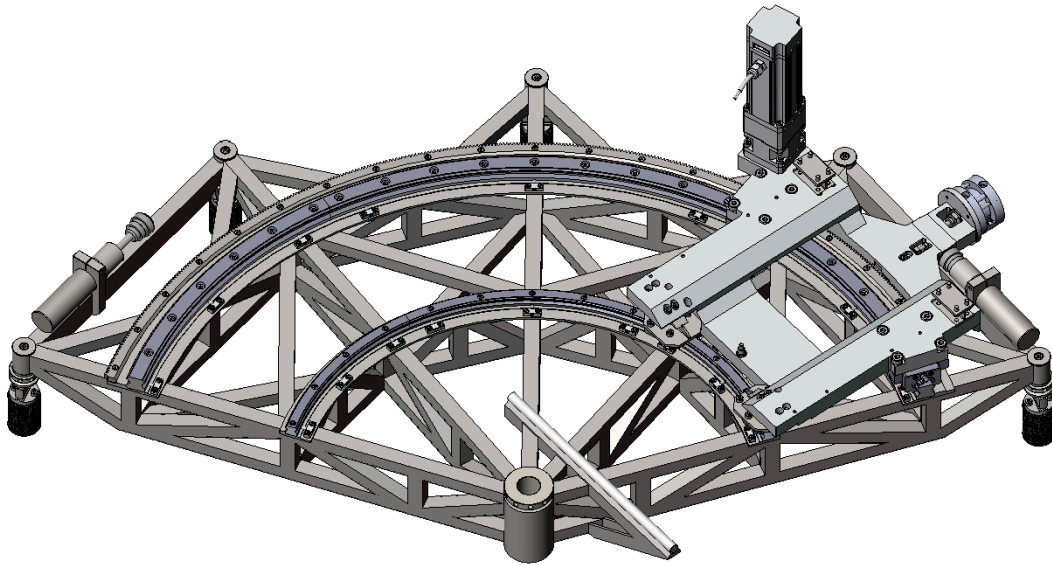


Figure 5-37. *Dewar cradle and articulation support structure*

The main support for this system comes from a light gauge, welded, steel superstructure designed to react forces into the main frame at six node points. A large central hub and five smaller satellite hubs are each located directly above a node point on the main frame. A locking adjuster is provided at each location for setting the height of the space frame. The central adjuster is fixed for lateral displacements and the five satellite adjusters have radial flexures to accommodate displacements due to thermal cycling. G10 spacers are used as standoffs between the superstructure and main frame to provide an insulated load path through the pre-dewar enclosure.

An aluminum saddle is attached to four bearing blocks and guided on two sets of curved rails. The rails are nested and clamped into concentric machined shoulders on the superstructure. The rails define the

center of rotation of the camera and Dewar assembly at the axis through the center hub of the superstructure. The saddle is fixed directly on top of the two larger bearing blocks at the rear and is flexure mounted to the two smaller bearing blocks at the front. These two flexures allow the saddle to change length in a radial direction equal and opposite to that of the steel superstructure. The front of the camera is fixed to the saddle by a pin near the front of the saddle and the back of the camera is attached to the saddle at the rear by flexures. This arrangement provides for thermal compensation of the camera mount.

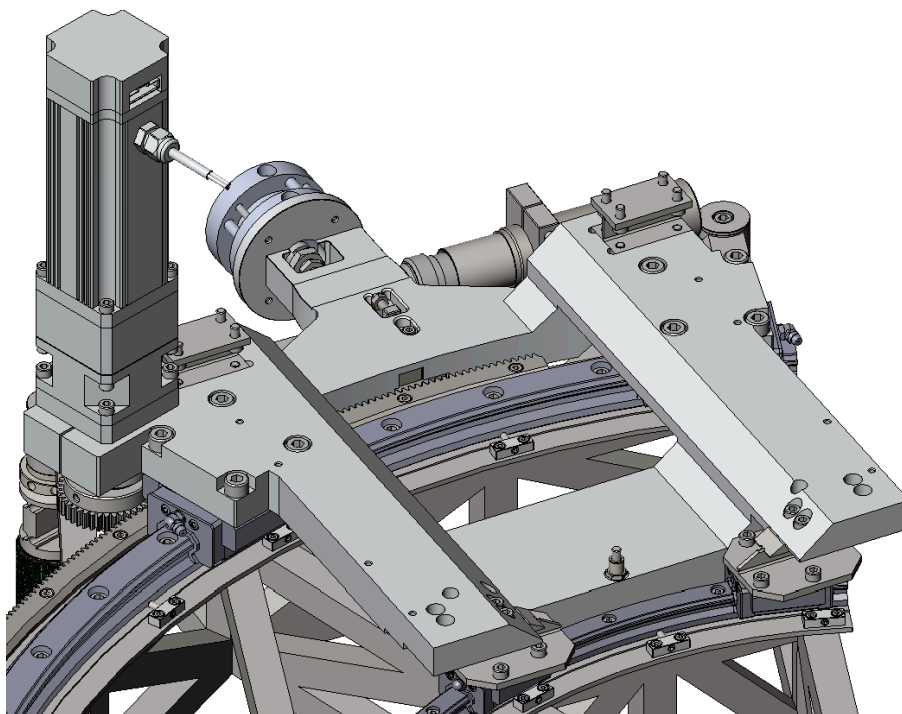


Figure 5-38. *Dewar cradle*

A motor and gear reducer drives the saddle through a pinion and ring gear. The ring gear is manufactured with a standard involute tooth profile and a diametral pitch of 20. This yields an angular spacing of approximately 0.424 degrees per tooth for a ring gear of 1.0795 meter pitch diameter. A spring actuated, pneumatically retracted, slide with gear teeth is used to lock the camera saddle into the ring gear. The slide has an adjustable gib to facilitate removal of side-to-side play. The lock is centrally located at the rear of the saddle between the two large bearing blocks.

A safety shock absorber is positioned at either end of the superstructure to provide a means to dissipate energy in a runaway situation. The shock absorbers also act as end stops to positively limit the saddle travel at set points just beyond the desired 100-degree range. Consideration is being given to implementation of a governor to restrict the maximum speed of the camera and Dewar assembly in the event of a mechanical failure in the drive such as a broken key or drive shaft.

5.2.11 Pre-dewar Enclosure

The majority of the RSS-NIR instrument resides in a pre-dewar enclosure, which maintains an internal temperature of -40 °C. The pre-dewar enclosure performs a number of functions and all of these need to be considered in its design: provide a thermal enclosure which minimizes heat transfer between the

cooled inside and ambient outside of the box, provide a light tight, dust tight and moisture tight seal to the outside, and be sturdy and self supporting under wind loading.

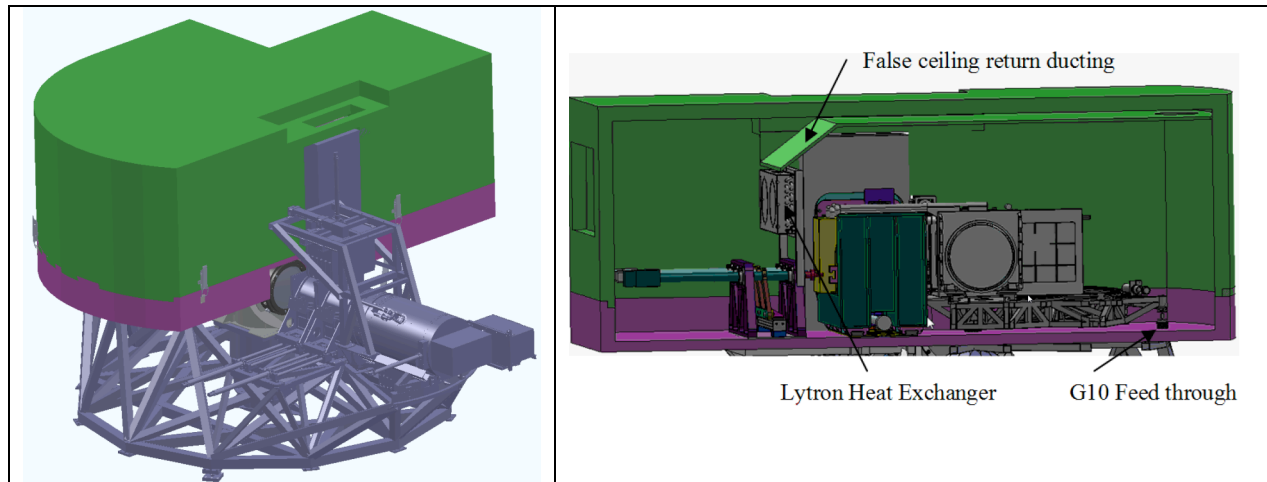


Figure 5-39. *The pre-dewar enclosure mounted on RSS. b. A cross-section of the pre-dewar showing the false-ceiling ducting and heat exchange unit position.*

The pre-dewar enclosure is constructed in two parts, a pre-dewar base which is attached to the RSS structure and a removable pre-dewar top cover. The base (purple) is captured under the articulation frame and has penetration through which the G10 structural feed throughs are installed. These G10 structural feed throughs are the rigid structural attachment points of the instrument. The lower pre-dewar enclosure also contains the bulk head for all the electrical, air and cryogen feed throughs as well as the air lock enclosure box. The pre-dewar top cover (green) is removable and is attached to the base with cam clamps. The top cover has an integral false roof and ducting to improve the flow of cooled air within it.

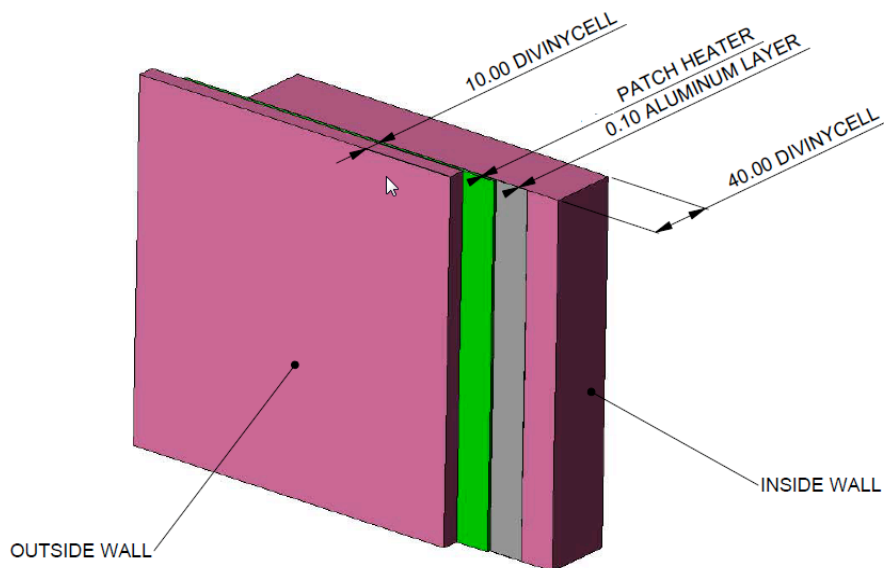


Figure 5-40. *Pre-dewar enclosure multi-layer wall construction.*

The primary material to be used in the construction of the pre-dewar is Divinycel P, which is a thermoplastic sandwich core material that exhibits good mechanical characteristics and offers excellent thermal insulation properties and low water absorption. The enclosure walls will be constructed as follows: The primary insulation layer will be a 40mm of the Divinycell material. On the outside of that will be a well sealed layer of thin aluminum which serves two purposes; it provides a moisture proof barrier and it will provide a thermally conductive layer on which to attach patch heaters and better distribute the heat. The patch heaters are the next layer. They are intended to heat the outer skin of the pre-dewar to within 2°C of ambient so as not to degrade the telescope dome seeing. After the patch heaters is another thinner layer, ~10mm, of Divinycell which improves the uniformity of the skin temperature by smoothing out the patch heater hot spots. The inner and outer walls of the enclosure will need to be coated with a resin or another thin material layer to fully encapsulate the friable Divinycell. Threaded Ultem 1000 inserts will be bonded into the Divinycell material for the attachment of miscellaneous hardware.

5.2.12. Thermal System Design

The overall instrument thermal schematic is shown in **Figure 5-41** below. The primary thermal components are the Dewar, pre-dewar, and electronics enclosure.

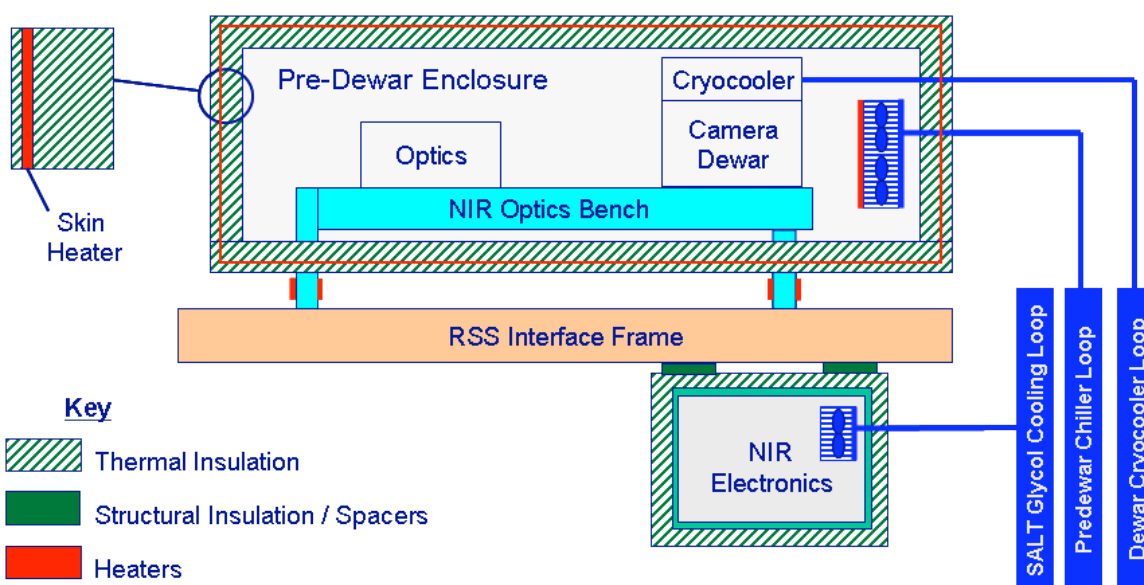


Figure 5-41. Thermal Schematic.

The NIR electronics enclosure will be cooled using a liquid-air heat exchanger coupled to the SALT facility glycol cooling loop.

The camera Dewar has a dedicated cryocooler, which is located in an insulated compartment under the primary mirror. The refrigerant gas travels through the lines at ambient temperature, so no insulation is needed.

The instrument pre-dewar contains most of the instrument optics and the camera Dewar, and is maintained at -40 °C for reduced background IR. The primary requirements for the pre-dewar are as follows:

- Maintain a nominal internal temperature of -40 °C in ambient temperatures ranging from -10 °C to +25 °C, with up to 75 kph steady winds and 90 kph gusts
- Maintain all external surfaces within 2 °C of ambient temperature to prevent condensation and thermal plumes
- The enclosure interior and contents shall be isothermal (+/- 5 °C) and stable (+/- 1 °C, max. rate 0.5 °C/hr)

The pre-dewar is cooled using a heat exchanger connected to a recirculating chiller, which is located in an insulated compartment under the primary mirror. To prevent condensation issues the coolant will travel in vacuum insulated piping. The piping will route through the existing SALT cable wraps, which limits the size of the flex sections to 6.4mm ID, while the straight sections will be larger (12.7 mm ID) rigid piping to minimize pressure losses. The small size of the flex lines limits the fluid flow rate, so the chiller temperature must be 5-10 °C below the pre-dewar temperature. As seen in **Table 5-6**, the total estimated pre-dewar heat load is 560 W, while the chiller capacity is 1000 W at -50 °C.

Table 5-6. Pre-dewar Heat Loads

Source	Heat Load (W)
Enclosure Walls	360
Lens Doublet	10
Support Penetrations	50
Electrical Feedthroughs	10
Instrument Power	20
Heat Exchanger Fans	76
Circulation Fans	100
Coolant Line Losses	24
Total Pre-dewar Chiller Load	560
Chiller Capacity at -50 °C	1000

The heat exchanger fans will provide the primary cooling air circulation inside the pre-dewar, and will be supplemented by additional fans where needed to maintain pre-dewar temperature uniformity. A heater located at the exchanger exit will be used to maintain steady internal pre-dewar temperatures under varying environmental conditions. The pre-dewar will be purged with dry air prior to cooling, and a continuous purge will be applied to maintain positive pressure in the enclosure. The pre-dewar enclosure contains a heated aluminum skin near the outer surface. The heated skin is needed to ensure the outer surface of the enclosure stays within 2 °C of ambient. A small thickness of insulation is needed outside the heated skin to ensure temperature uniformity.

A collimator doublet serves as the window into the pre-dewar enclosure. An air gap between the lenses provides a thermal break, and the lens frames are separated by a G10 spacer. The inner CaF2 lens is fragile so care must be taken to minimize thermal stresses. The mounting flange contains flexures, which are attached to the lens using silicone adhesive. Finite element analysis predicts lens stress within 25% of our target value, providing confidence that the thermal gradients are not too severe and that the stress target can be met with further design iterations. The lens stress under thermal transient conditions will likely limit the allowable instrument warmup and cooldown rates, which will be determined with further analysis. The design will allow the lens temperatures to vary with the ambient conditions so that active environmental control is not required at all times. The transient analysis will also consider the potential effect of ambient temperature fluctuations during instrument operation. To prevent condensation on the outer lens a dry air purge will be used within the optics tower (see section 5.2.2) that extends from the

NIR and VIS doublets to the collimator, while fans will circulate air onto the inner lens to hold it near the pre-dewar temperature.

The filter exchange airlock allows filter changes without warming the entire pre-dewar to ambient temperatures. A small liquid-air heat exchanger with a heater will be used to warm and cool the airlock for filter replacement. A small amount of the chiller loop fluid will be used for cooling, and the airlock will be purged with dry air prior to cooling. During filter warmup and cooldown the airlock will add up to 30 W heat load to the pre-dewar, which is well within the pre-dewar system capacity.

5.3. Thermal Stray Light Analysis

RSS-NIR is a semi-warm instrument, working in a regime where a number of instruments have not been successful. Therefore, from the beginning, detailed thermal stray light analysis has been a high priority for the project, and is integral to the entire design. Our analysis is performed using the Advanced Systems Analysis Program (ASAP) by Breault Research Organization. The optical design of SALT, RSS, and the NIR arm are directly imported into ASAP from Zemax and the mechanical designs of mounts and structures are directly imported from SolidWorks. Every component can be made into a thermal emitter with the proper temperature, emissivity, and scattering characteristics. All rays are traced through the system in a non-sequential Monte Carlo approach. Initially, our model of the NIR arm in ASAP was largely conceptual, but allowed us to roughly determine required operating temperatures of regions of components early in the project. As the mechanical design of the instrument matures, the ASAP model will be used to design baffles, the cold pupil mask, and radiation shields within the cooled areas. Preliminary results of the instrument thermal backgrounds predicted from ASAP have already been incorporated into our instrument performance simulator, described in Section 3.2.5. A brief overview of the thermal analysis is highlighted here. Details can be found in the RSS-NIR Thermal Stray Light Analysis document (SALT-3501AA0002).

RSS-NIR was originally conceived to have three different temperature environments: cryogenic, below ambient, and ambient. A cryogenic Dewar houses the detector, blocking filters, and last 2 camera optics. A pre-dewar, cooled below ambient to approximately -40 °C, contains all components between the cryogenic Dewar and the NIR collimator doublet. These components include the NIR doublet lenses (the first element is the window into the pre-dewar), the fold mirror, order sorting filters for Fabry-Perot mode, the Fabry-Perot etalon, the spectroscopic gratings, the polarizing beamsplitter, the first 7 camera optics, and mounts for all of these components. The final section is not cooled and floats at the ambient temperature. In this section are the dichroic beamsplitter, the collimator optics, the waveplates, the field lens, and the slit mechanism. The components common to both the visible and NIR arms all reside in the ambient temperature section.

5.3.1. Ambient Temperature Components

We began the analysis with the ambient temperature components for two reasons: 1) we expect them to be the largest contributors to the instrument thermal background, and 2) they already exist for the visible side of the instrument, so details of their thermal emission could be analyzed early in our NIR instrument design phases. The slit should be the largest contributor to thermal background since it sits directly in the beam path and it is at ambient temperature.

We also began with analysis of the spectroscopy modes of the instrument since sky-limited spectroscopy of faint targets at high resolution will be the observations most affected by the instrument thermal background preventing us from reaching the sky continuum limit. Initial results are shown in **Figure 5-42**

for a long wavelength cutoff of $\lambda_{\text{cutoff}} = 1.7 \text{ mm}$. The plot shows the thermal background flux reaching the detector from various components at a range of ambient temperatures. Median summer (red) and winter (blue) temperatures at SALT are marked by the solid vertical lines, with the minimum and maximum extremes marked with dotted vertical lines. These values were taken from historical temperatures measured at SALT over the period of Jan 2007 – Feb 2008. Although actual temperatures rarely go below 0°C , the analyses were carried out to much lower temperatures to investigate the possibility of cooling the ambient components. The horizontal lines of different styles represent the night sky continuum levels reaching the detector, using an observed night sky spectrum from Maunaea Kea and assuming an instrument efficiency of 0.3, for different spectral resolutions, $R = 1000, 2000, 4000,$ and 7000 . Note that sky-limited observations of faint targets can only occur at $R \geq 4000$ where the resolution is high enough that the night sky OH emission lines are resolved and more than 50% of the spectrum is free of OH emission lines. Thermal emission from the long slit blank is shown for three different emissivities: 0.95 (black, the black curve), 0.06 (tarnished gold or pristine aluminum, the yellow curve), and 0.02 (pristine gold, the gold curve). We immediately see that if the slit is painted black, it would have to be significantly cooled to reach the sky limit at $\lambda = 1.7 \text{ mm}$. If the slit is gold coated with a mirror-like surface then it would still have to be cooled at least to -10°C to be sky-limited for observations at $R = 7000$ out to $\lambda = 1.7 \text{ mm}$.

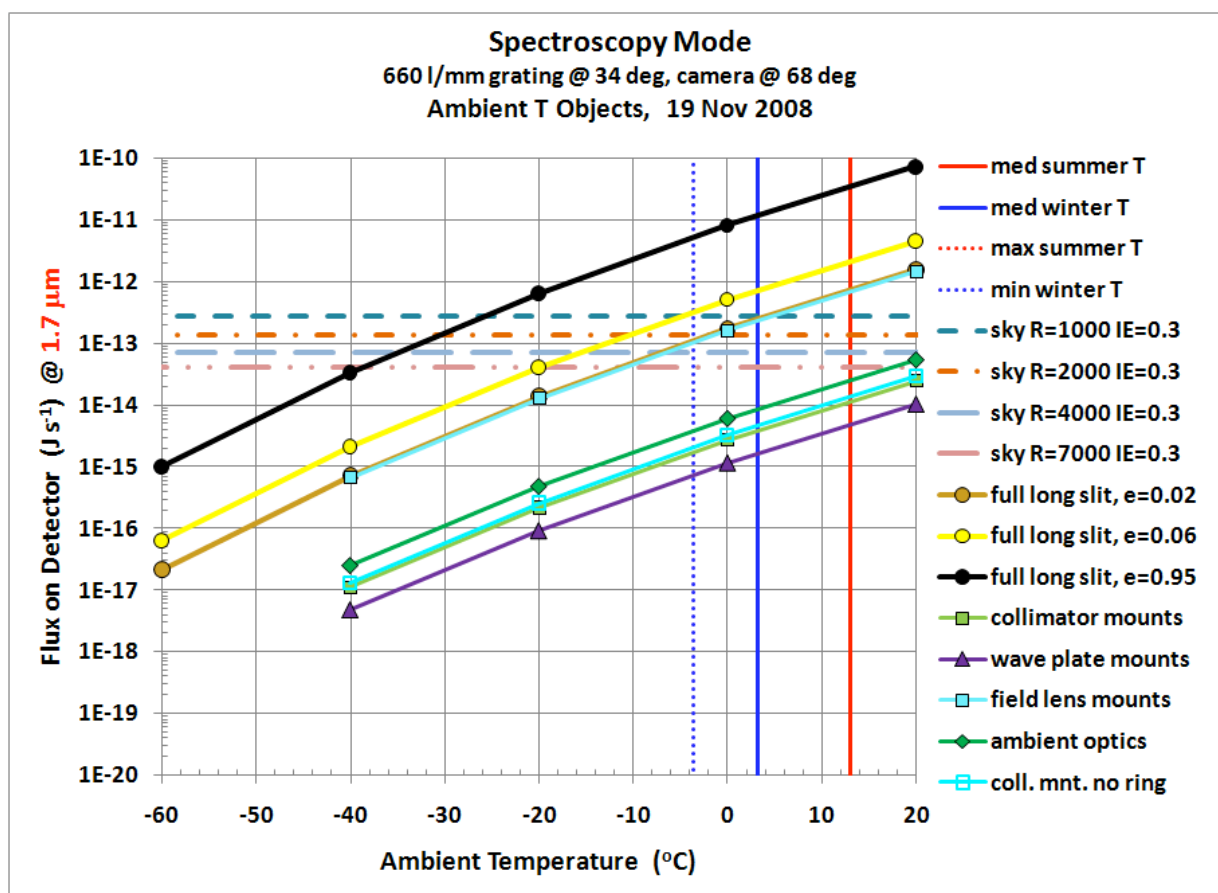


Figure 5-42. Thermal background contributions of the ambient temperature components for a long wavelength cutoff of 1.7 mm .

The background from other ambient temperature components is shown by the remaining curves: the optical elements (dark green diamonds), the collimator mounts (light green squares), the

waveplate/compensator mount (purple triangles), and the field lens mounts (cyan squares). With the exception of the field lens mounts, the other components should not significantly contribute to the instrument thermal background except at the warmest summer temperatures.

The field lens mounts presented an unexpected result. The predicted thermal emission from these components was as high as that from a gold coated slit directly in the beam path. Investigation into the details of the ray traces from these components revealed a situation that would likely never have been caught, had this level of analysis not been carried out. **Figure 5-43** shows the cause of this situation. The bottom retaining ring on the first field lens element is a 5 mm wide ring around a highly powered optical surface. The ring follows the curvature of the surface and thermal emission from it directly couples into the lens and gets refracted into the central beam path through the instrument. The opto-mechanical designer of this mount (Pilot Group in CA) believes that this ring can easily be cut down and a low emissivity gold foil added to the surface facing the lens without causing any structural degradation of the mount. This modification is currently being made while the RSS-VIS optics are undergoing repairs by the Pilot Group. We predict that the modification to this ring will bring the thermal background from the field lens mounts down to the level indicated by cyan curve with open squares (collimator mounts, no ring), making this component negligible.

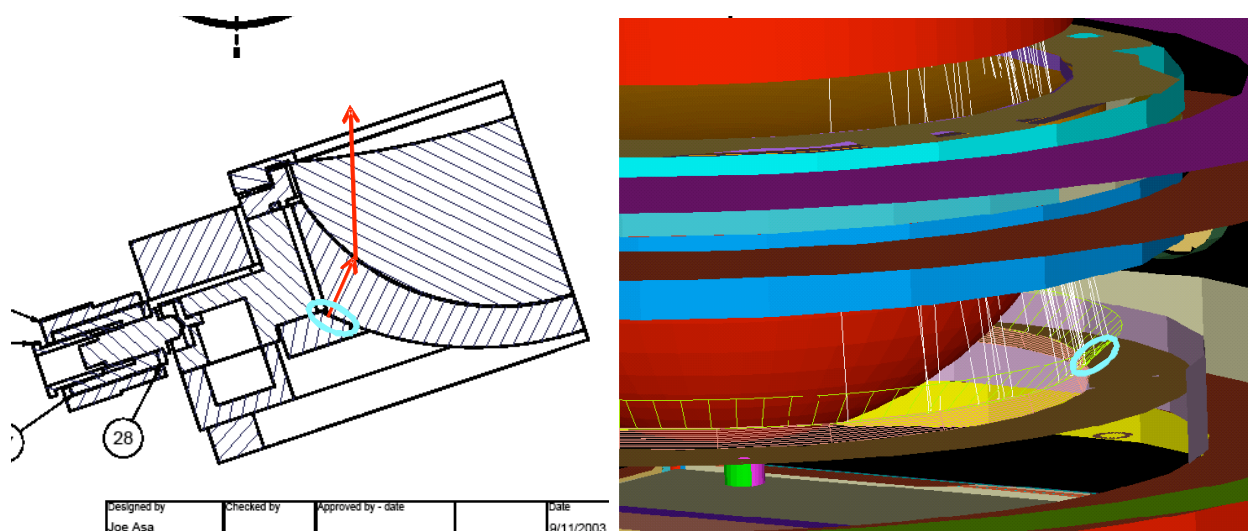


Figure 5-43. Thermal radiation directly coupled into the beam from one surface of the field lens mounts. The retaining ring surface is marked by the ellipse in both views of the lens mount design (left) and the ASAP ray trace (right). The surface of the first element in the field lens has been hidden for clarity. The white lines are rays in ASAP.

Because the warm slit is clearly the limiting factor, as was expected before any analysis, we next turned to an investigation of cooling the slit. **Figure 5-44** shows the predicted total thermal background from the ambient temperature components with the slit cooled to different temperatures below the ambient, T_{amb} , as a function of T_{amb} for $l_{cutoff} = 1.7$ mm. The top orange curve is the same as in **Figure 5-42** with no slit cooling. The remaining curves show the total background with the slit temperature at $dT_{slit} = -20, -30,$ and -40 °C below ambient. The bottom curve shows the total for all components except the slit. With the slit cooled to 20 °C below ambient, sky-limited spectroscopy at $R=7000$ would be possible only for T_{amb} below the winter night time median. With the slit cooled to 30 °C below ambient, the same observations would be possible for $T_{amb} < 6$ °C. Cooling the slit further would only provide incremental improvement.

The same plots are shown in **Figure 5-46** for shorter cutoff wavelengths of $\lambda_{\text{cutoff}} = 1.65, 1.6, 1.55, \text{ and } 1.5$ mm.

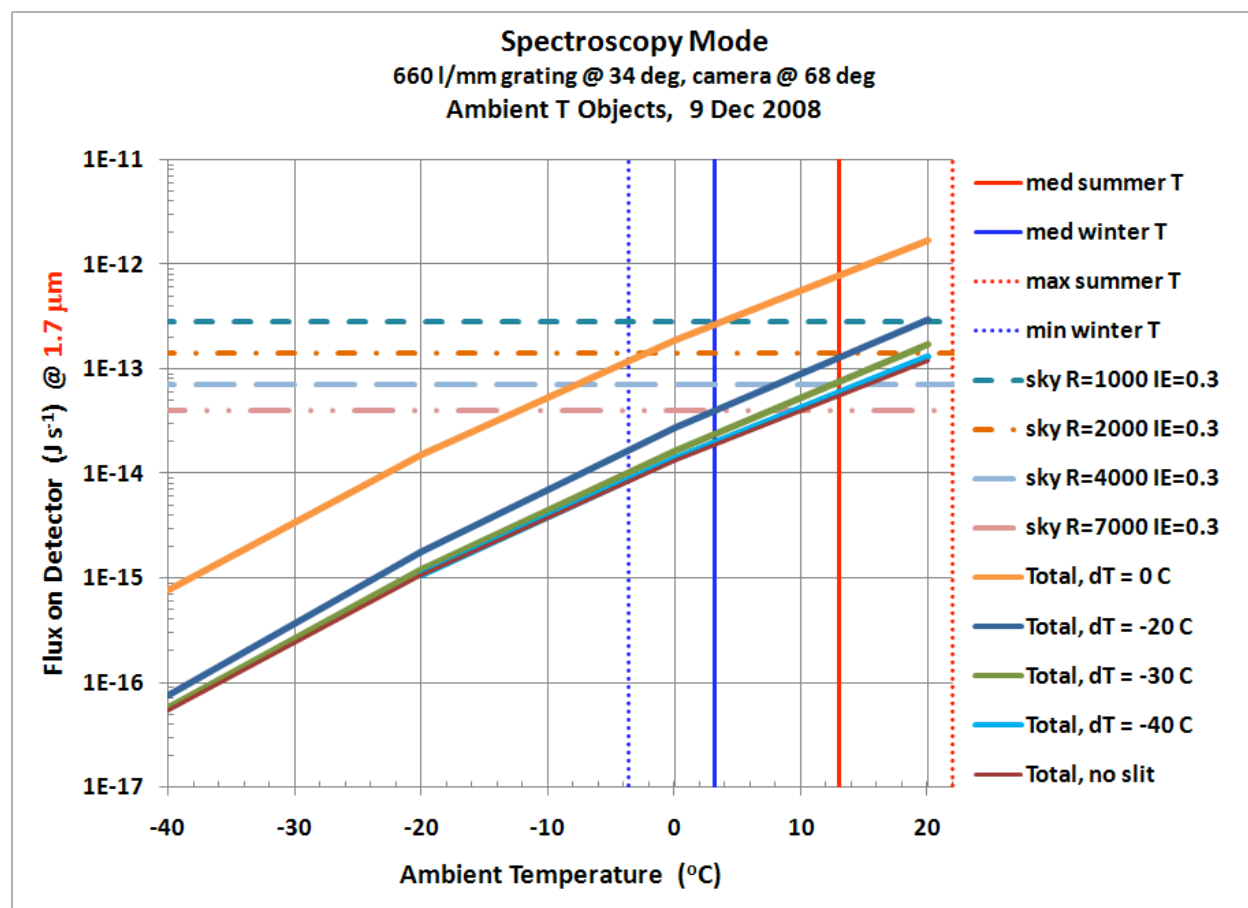


Figure 5-44. Total instrument backgrounds from the long slit assembly and the ambient temperature optics as a function of slit temperature cooled to below ambient, dT_{slit} .

In order to interpret these results in terms of operational time on the telescope, we next include historical SALT weather data. Statistics of night time ambient temperatures measured at SALT are shown in **Figure 5-47**. The top plot shows monthly night time averages over the period of Jan 2007 – Feb 2008. The lower two plots show temperature distributions for the hours between 18^o astronomical twilight over the same time period. Combining these data with our previous instrument background predictions, we can now derive the percentages of astronomical hours during which sky-limited grating spectroscopy could be successfully obtained for our range of spectral resolutions. These percentages are shown in **Figure 5-48** for different long wavelength cutoffs as a function of the amount of slit cooling below the ambient temperature. The top left plot shows that for observations out to $\lambda_{\text{cutoff}} = 1.7$ mm with no slit cooling, sky-limited observations will never be possible, even at the lowest spectral resolution. Cooling the slit to 20 °C below ambient brings the available hours up to 19% of the time for R=7000, 47% for R=4000, and 74% for R=2000. Cooling the slit even more to 30 °C below ambient gives a vast improvement: 41% for R=7000, 69% for R=4000, and 97% for R=2000. Cooling the slit to 40 °C below ambient does not gain much over 30 °C, and is not worth considering.

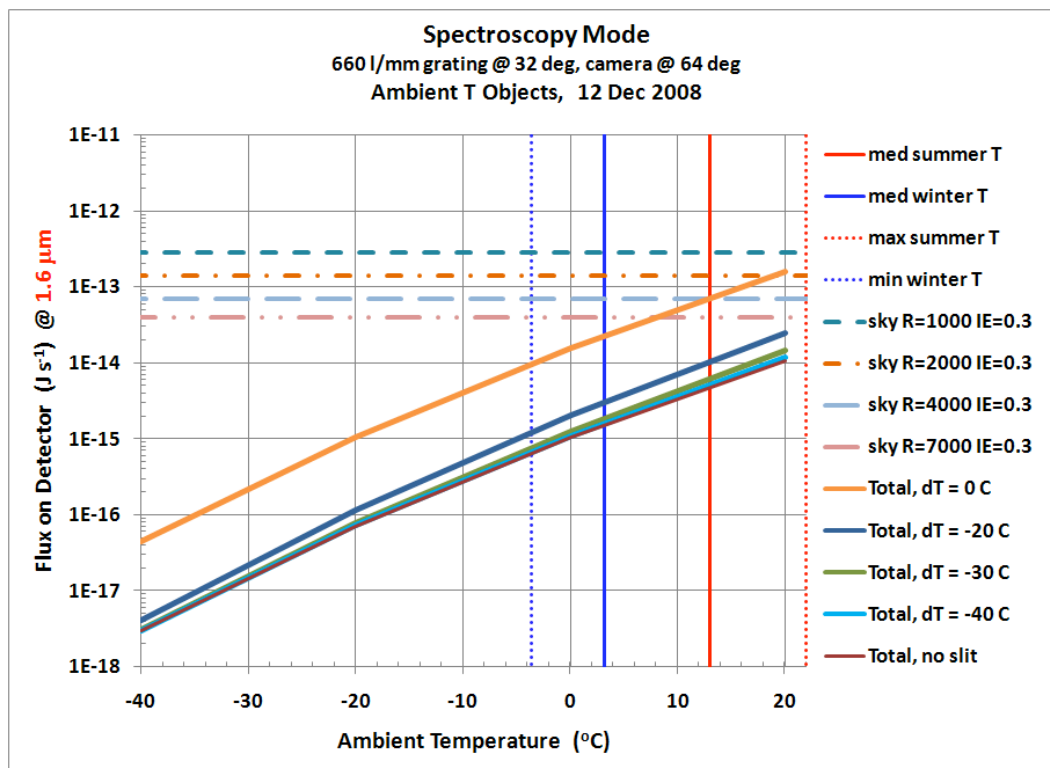
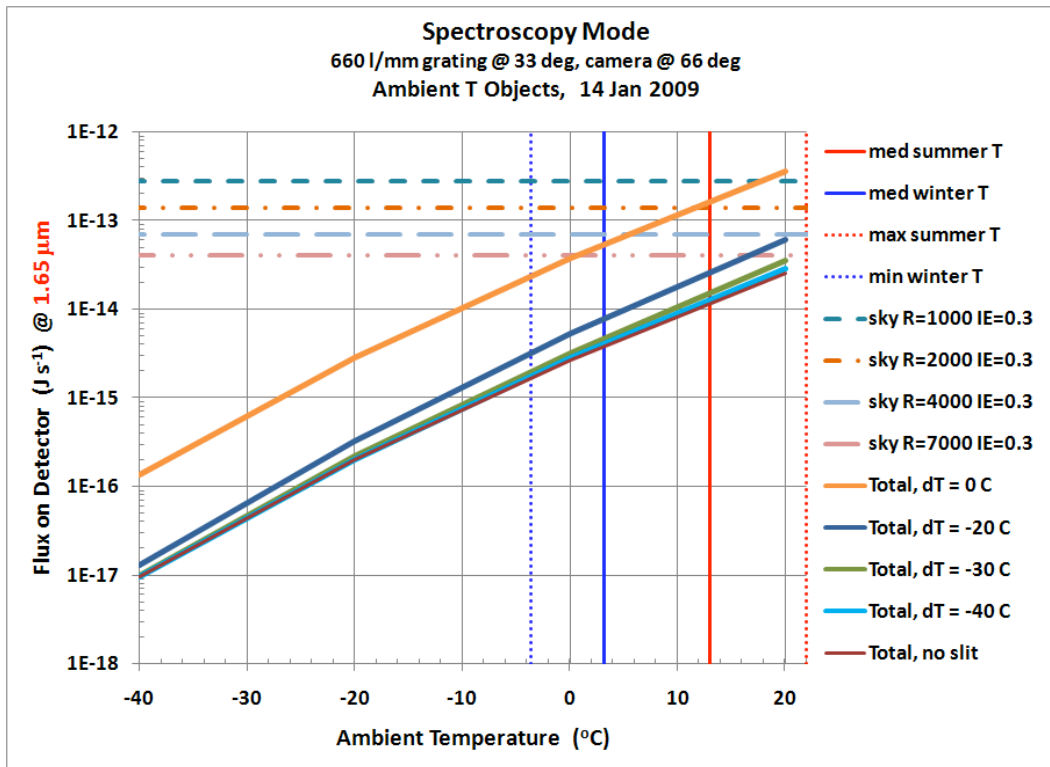


Figure 5-45. Total thermal background from the long tilt and the ambient temperature components for long wavelength cutoffs of 1.65mm (top) and 1.6 mm (bottom)

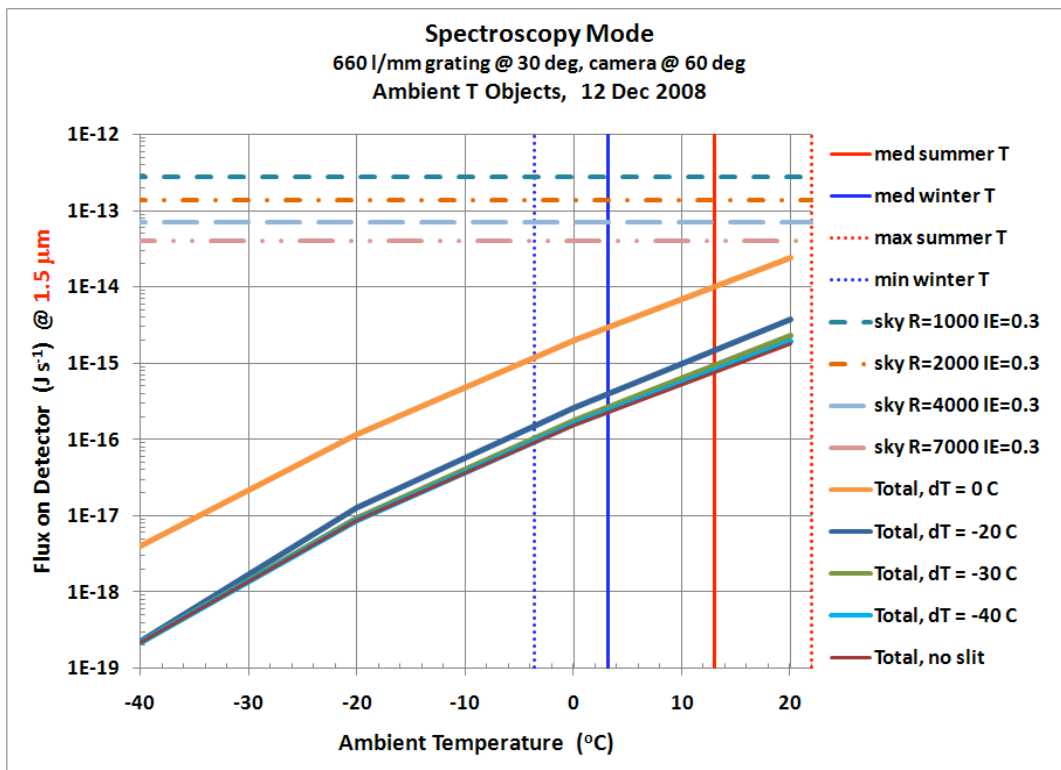
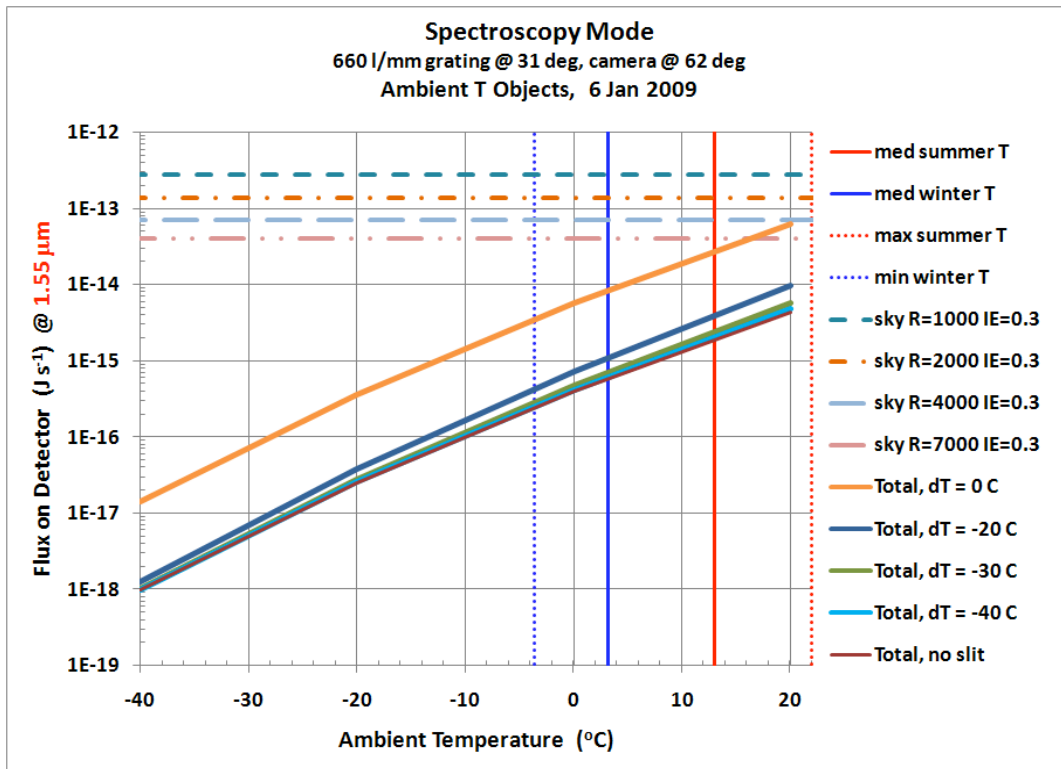


Figure 5-46. Total thermal background from the long tilt and the ambient temperature components for long wavelength cutoffs of 1.55 mm (top) and 1.5 mm (bottom).

RSS-NIR Redbook
Mid-Term Review Design Document
May 2009

An alternative to cooling the slit is to limit observations to a shorter cutoff wavelength. If the slit is not cooled at all, $\lambda_{\text{cutoff}} = 1.6 \text{ mm}$ (lower left plot) would allow sky-limited observations for comparable fractions of the time to the previous case of $dT_{\text{slit}} = -30 \text{ }^\circ\text{C}$ out to $\lambda = 1.7 \text{ mm}$: 47% at $R=7000$, 74% at $R=4000$, and 97% at $R=2000$.

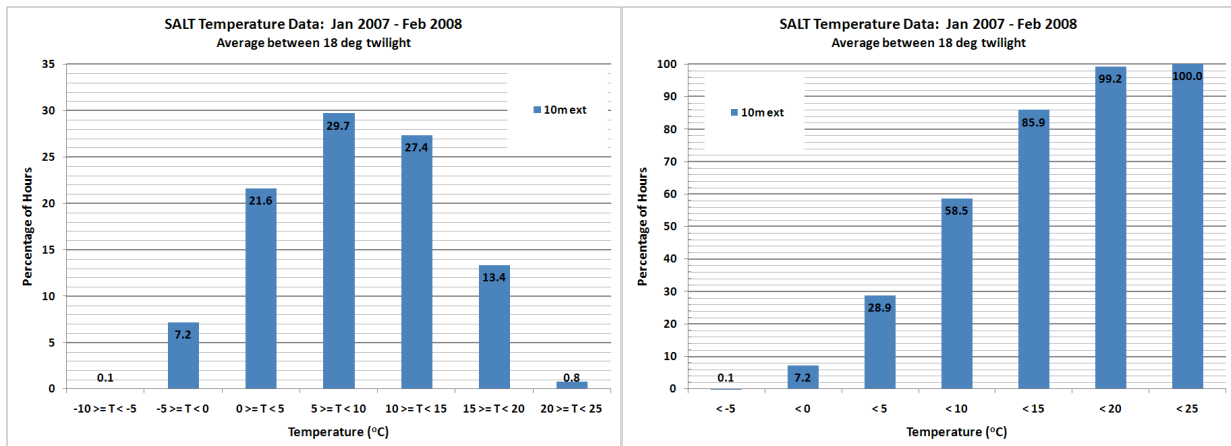
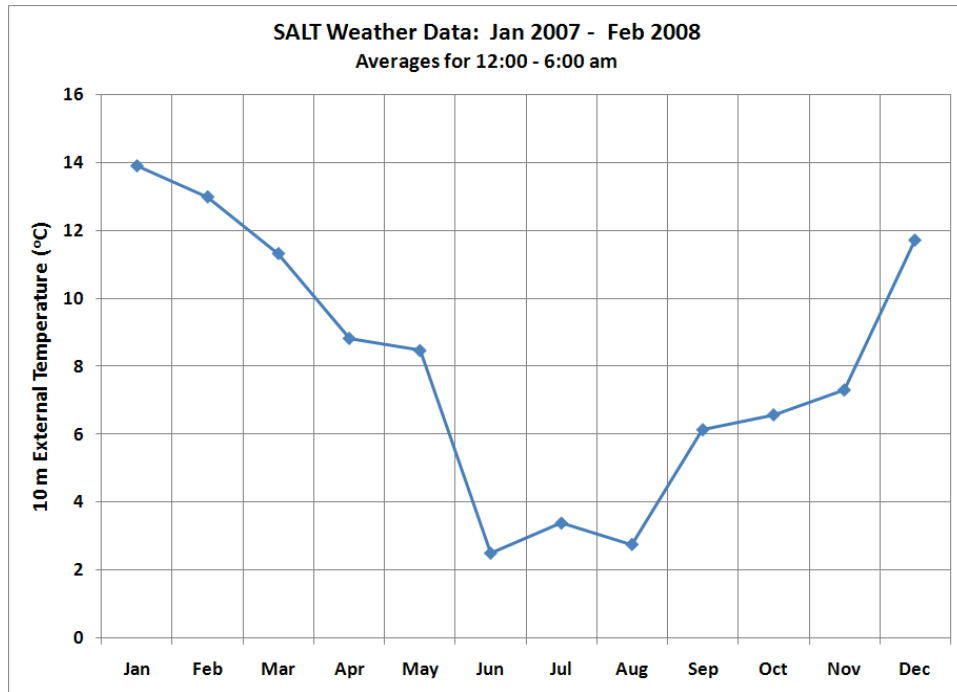


Figure 5-47. Temperature data for the SALT site. These measurements are from the 10-m external weather tower, and match up with SALT payload temperatures to within 5 °C when the dome is open.

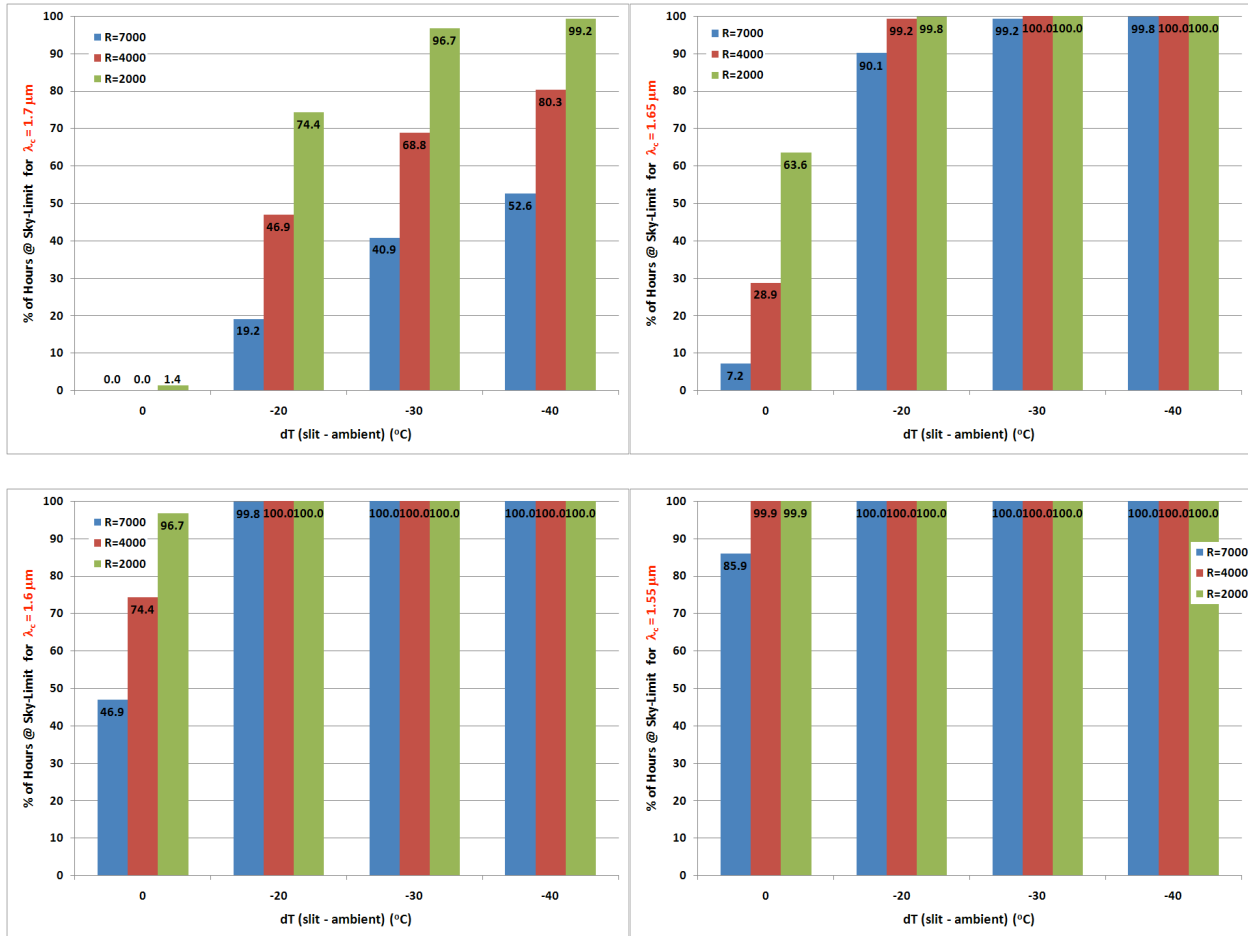


Figure 5-48. Percentage of hours between 18° astronomical twilight available for sky-limited grating spectroscopy at SALT over the period of a year. These results are based on measured site temperatures from Jan 2007 to Feb 2008 and predicted instrument thermal backgrounds. Top left: $l_{\text{cutoff}} = 1.7 \text{ mm}$, top right: $l_{\text{cutoff}} = 1.65 \text{ mm}$, bottom left: $l_{\text{cutoff}} = 1.6 \text{ mm}$, bottom right: $l_{\text{cutoff}} = 1.55 \text{ mm}$. The blue bars are for spectral resolution of $R=7000$, orange are for $R=4000$, and green are for $R=2000$.

5.3.2. Initial Pre-Dewar Estimates

The pre-dewar contains all optics and mounts downstream of the NIR collimator doublet, along with mechanisms for inserting the gratings, etalons, blocking filters, and polarizing beamsplitter into the beam, as shown in **Figure 5-13**. To get an initial estimate of the required operating temperature of the pre-dewar before the mechanical designs were mature, we used a conceptual design of the pre-dewar enclosure and assumed that all components within the enclosure reached the stated pre-dewar temperature. Thermal emission from these components reaching the detector for a cutoff wavelength of $l_{\text{cutoff}} = 1.7 \text{ mm}$ is shown in **Figure 5-49** as a function of pre-dewar temperature. All ambient temperature components shown are assumed to be at a temperature of +20 °C. Based on these estimates, a working operating temperature of -40 °C was chosen for the pre-dewar. This put the total background from the pre-dewar components a factor of ~5 below the lowest ambient temperature component, and ~20 below the sky at $R=7000$. Mil specs for many mechanisms go down to -50 °C, so -40 °C also seemed to be a reasonable level from the operational side.

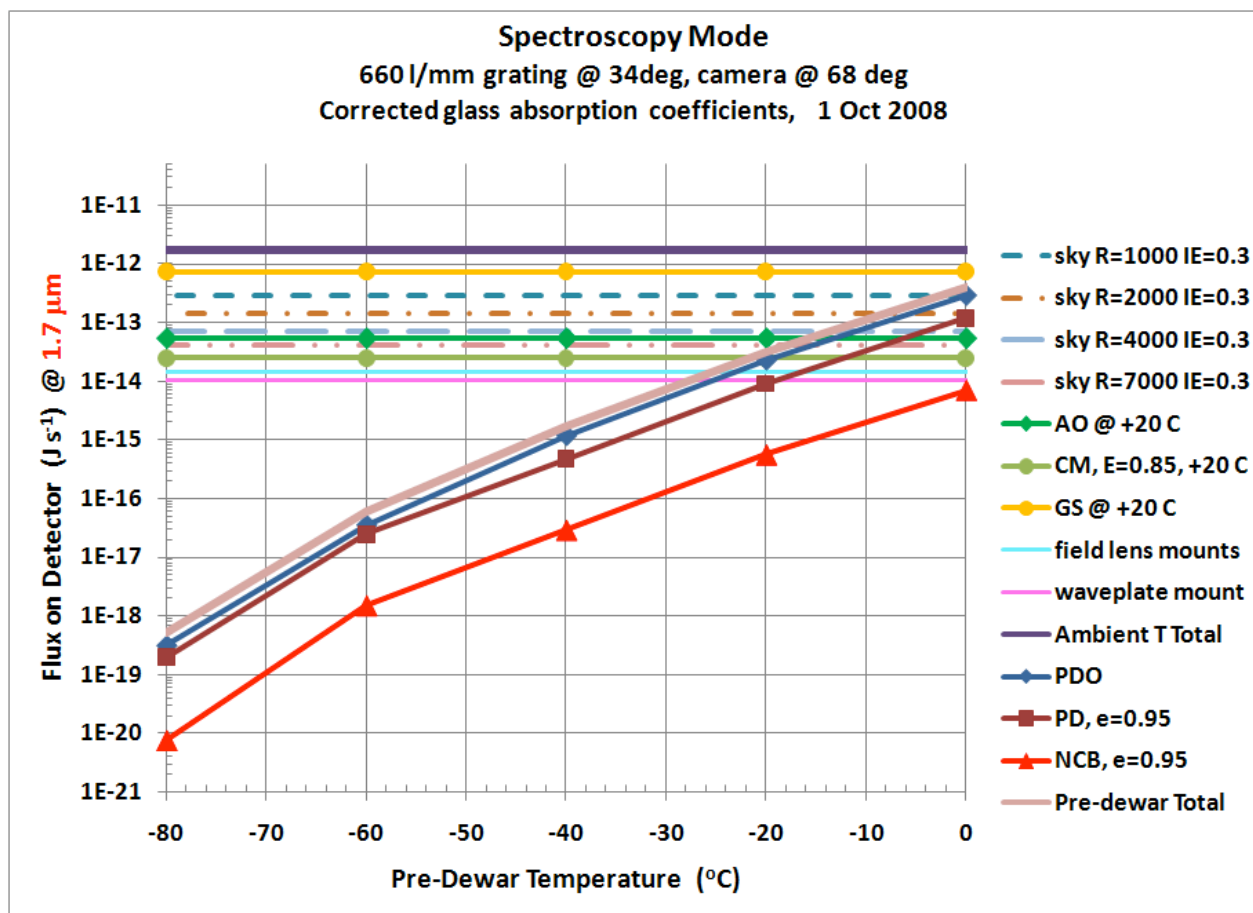


Figure 5-49. Preliminary estimates of pre-dewar operating temperature. This plot shows the thermal emission from instrument components that reaches the detector as a function of the pre-dewar temperature. **PDO** is the optical components in the pre-dewar, **PD** is the pre-dewar enclosure itself, and **NCB** is the NIR camera barrel lens mounts. Ambient temperature components are assumed to be at $T_{amb} = +20^{\circ}C$. **AO** is the ambient optics, **CM** is the collimator mounts, and **GS** is the gold long slit. Sky continuum levels at the detector are shown for a range of spectral resolutions, assuming an instrument efficiency of 0.3.

Future analyses will include detailed pre-dewar components as-designed to determine where baffling and radiation shields should go; the design of a cold pupil mask near the Fabry-Perot blocking filter location; required temperatures inside the cryogenic detector Dewar, including the long wavelength cutoff filter; and stray light analyses of both the NIR and VIS instruments to analyze the effects of a shiny gold back side of the slit masks.

5.3.3. Gold Coating of the Multi-slit Masks and Long Slit Baffles

The current multi-slit masks and the baffles for the long slits (see **Figure 5-50**) were identified as a significant source of thermal stray light that could reach the detector when working in the spectrometer mode. At the current time, both the multi-slit masks and the baffles (masks and baffles) for the long slits are made from a 200 μm thick graphite-epoxy composite that is a natural black color. While this does not cause a problem for the RSS-VIS instrument, the thermal emission of these masks and baffles would significantly contribute to the thermal stray light for the RSS-NIR instrument.

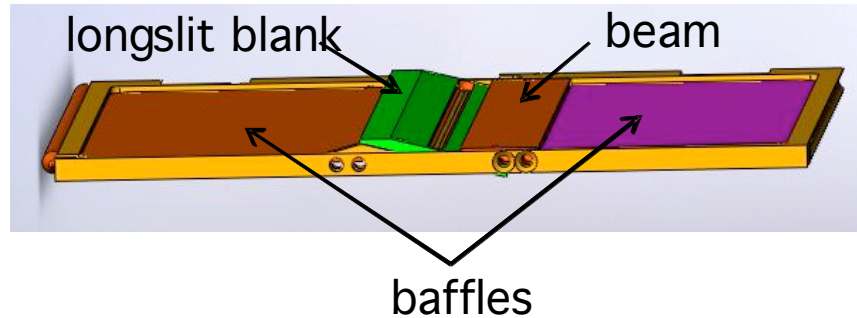


Figure 5-50. Long slit mask assembly, top side. All surfaces are assumed to be gold coated with $e=0.02$ in the analysis.

The RSS-NIR detector has a sharp responsivity cutoff by ≈ 2 microns and even though the detector has responsivity that is significant at wavelengths shorter than 0.8 microns, the flux of the blackbody radiation from the masks and baffles falls off very rapidly at shorter wavelengths, the effective wavelength that we need to attenuate to on the short end is ≈ 1.35 microns.

The thermal stray light from the masks and baffles can be significantly reduced by lowering the emissivity of the masks and baffles in the region over which the detector is responsive. At the current time, the emissivity of the graphite epoxy mask blanks is on the order of 0.80 to 0.95, and by coating them with gold, the emissivity in the wavelengths of interest should be reduced to 0.05 to 0.02, a factor of 16 to 47. Only the back-side of the masks and baffles need to be coated with gold, as that is the only surface that the RSS-NIR instrument directly sees.

The multi-slit mask slits are cut with a micromachining laser at the SALT facility. Because the sides of the slits should not be reflective, as this may cause ghost images, the multi-slit mask blanks will be coated with gold first and then cut with the laser. This eliminates the need for masking off the slits if the masks were cut first and then coated with gold.

The gold needs to be thick enough to be a low emissivity surface in the ~ 1.35 to 2 micron range, but it must also adhere to the masks well, and yet still be thin enough to be cut with the SALT micromachining laser. Since the laser cutting will be done after the gold is deposited and there is debris that is generated by the laser cutting process, the gold surface must either have a durable finish that would allow cleaning or it needs to be protected during the laser cutting and subsequent cleaning process. One of the vendors (Epner) creates a "hard" gold surface that should survive the post-laser cleaning process. Additionally we have identified a number of materials that could be used to protectively coat the gold surface during the laser cutting, and then can be either mechanically stripped, or removed with a mild solvent rinse. We are currently conducting tests to verify the compatibility of the solvents with the graphite epoxy material.

Two leading vendors were chosen for tests of the gold coating process:

- Epner Technology, an electroplating company from Brooklyn, New York,
- Evaporated Metals Films (EMF), an evaporated metals films company from Ithaca, New York.

Both of these companies have significant experience in coating NIR optics with low emissivity films.

EMF indicated that $\geq 0.150 \mu\text{m}$ of gold would produce the low NIR emissivity surface that we needed. Epner routinely creates $0.500 \mu\text{m}$ thick gold coatings on materials for low NIR emissivity surfaces. Mask

blank samples have been sent to both vendors, with the intention of having 2 gold-coated mask blank substrates be coated by each vendor to allow laser cutting development tests at the SALT facility, along with test coupons for checking adhesion and abrasion resistance to MIL-PRF-13830.

We are currently asking both vendors to coat to 0.500 μm , which will be a more rigorous test of the laser cutting system. Due to the organic nature of the graphite epoxy composite mask blanks, both process need to create a seed layer that will adhere to the graphite epoxy, and then possibly a barrier material between the gold and the seed material. Since the overall thickness of the mask blanks is only 200 microns, we want to keep the metal thickness to a minimum so that CTE issues between the metal layers and the mask blank substrates do not become a problem.

5.4. Detector

5.4.1. Selection and Operating Parameters

A Teledyne Imaging Sensors HAWAII 2RG 2048 \times 2048 HgCdTe array has been selected as the detector for the RSS-NIR (**Figure 5-51**). The detector has a pixel size of 18 μm , a 1.7 μm cutoff wavelength, and it has had the CdZnTe substrate removed for improved performance. It is fully capable of meeting (or exceeding) the read noise, dark current, quantum efficiency, and other functional performance requirements for the RSS-NIR outlined at PDR. The array consists of 2040 \times 2040 sensitive pixels plus four rows and columns of reference pixels on each side. A block diagram is shown in (Loose et al. 2007) and (b). A guide mode capability is also available in which a sub-array can be used for telescope guiding while the full field collects science data. The operating parameters and characteristics for the HAWAII 2RG array are summarized in **Table 5-7**.

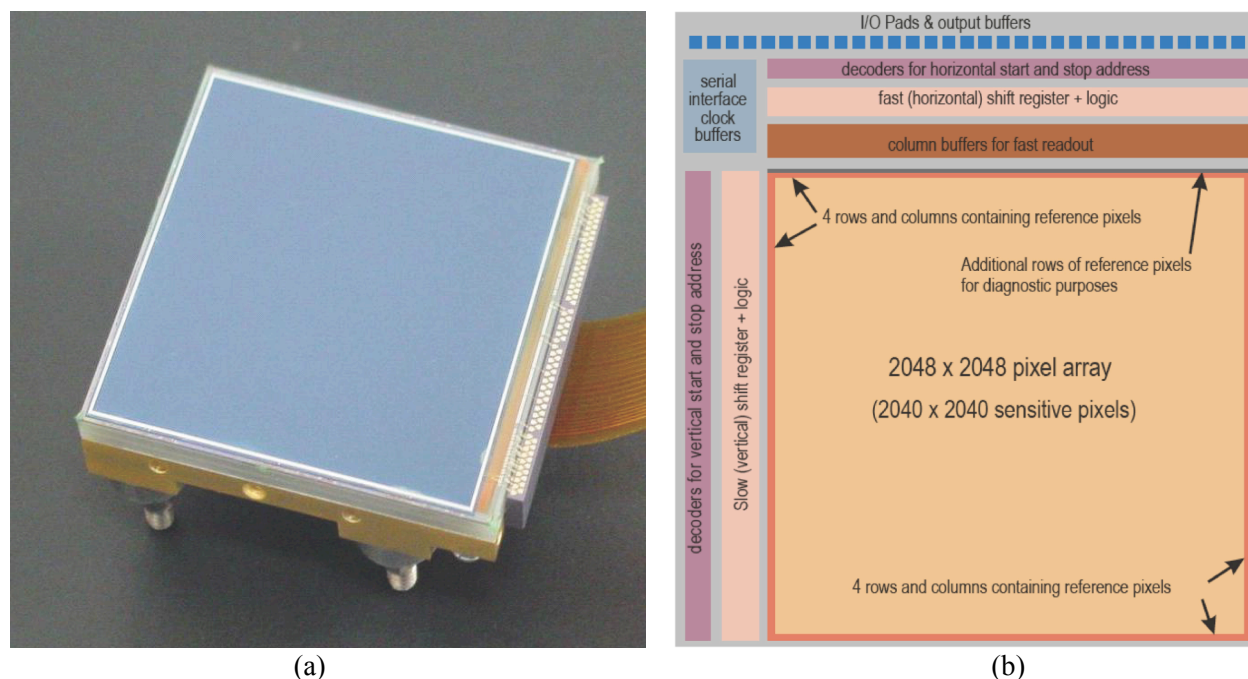


Figure 5-51. (a) Photograph of the HAWAII 2RG (Loose et al. 2007) and (b) Block diagram for the HAWAII 2RG (Loose et al. 2007).

Table 5-7. HAWAII 2RG Operating Parameters and Characteristics\

Parameter	Value
IR Material	HgCdTe
Substrate	CdZnTe (Removed)
Array Configuration	2048 × 2048 pixels
Pixel Pitch	18 μm
Output Ports	1, 4, 32 (Selectable)
Readout Mode	Ripple
Pixel Readout Rate	100 kHz to 5 MHz (Continuously adjustable)
Sampling	CDS, Fowler, Up-the-Ramp
Read Noise (Median)	< 15 e ⁻ CDS (100 kHz)
Dark Current (Median)	≤ 0.01 e ⁻ s ⁻¹ (140 K)
Mean Quantum Efficiency	≥ 80%
Well Capacity	> 100,000 e ⁻
Pixel Operability	> 95%
Fill Factor	> 98%
Power Dissipation	< 4 mW (100 kHz)

The Teledyne SIDECAR Application Specific Integrated Circuit (ASIC) will be used to control the detector clock and bias voltages and carry out the output digitization (**Figure 5-52**). The ASIC is packaged on a separate board, and is available as a Room-Temperature Development kit for testing and a performance-optimized Cryogenic Focal Plane Electronics kit. A JADE2 card provides the interface between the ASIC and a PC via USB 2.0.

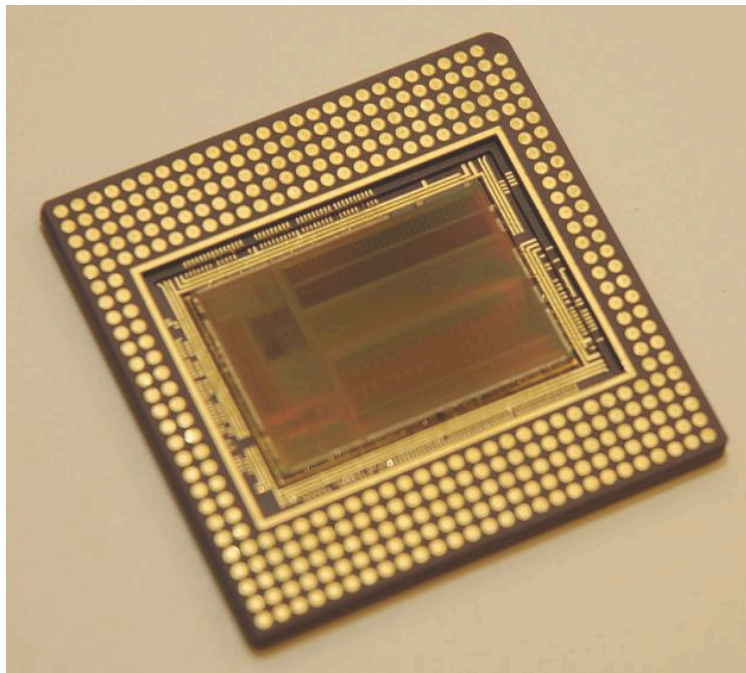


Figure 5-52. Photograph of the SIDECAR ASIC (Loose et al. 2007).

HAWAII 2RG arrays have been previously fielded in instruments at several ground-based telescopes (e.g., Gemini, CFHT, OClW, VLT, University of Hawaii), and will be used in the near-IR instruments on

the *James Webb Space Telescope (JWST)*. Therefore, this array has been extensively tested for astronomical applications, and support is readily available from the development community.

5.4.2. Detector Operating Temperature

The selection of the operating temperature of the detector is a complex set of compromises to get the optimum performance from the system. The RSS-NIR is a queue scheduled facility instrument that has multiple modes of operation and is used to observe objects that have large differences in brightness and spatial extent, thereby requiring vastly different detector integration times between successive exposures. The most challenging observations are those that have very faint signals, requiring long exposures resulting in signals that are very low compared to the known detector and system noise sources.

The operating temperature directly affects the following detector characteristics that have the most effect on the signal-to-noise characteristics of faint signals with long exposures are:

1. Dark Current
2. Quantum Efficiency
3. Read Noise
4. Interpixel Crosstalk
5. Intensity of Glow Centers
6. Persistence

The majority of these effects can be compensated for by careful calibration and characterization of the detector system and selection of the optimum read-out method for the total image integration, but the one effect that cannot be easily compensated for is persistence. Persistence is the "carry over" of signals from brighter sources in previous images that affect the current image. Persistence is not as significant an issue when looking at bright objects with short integration times, but it becomes particularly troublesome when a previous exposure integrated over a longer period of time had a bright object that is in the same location on the detector as a very weak source on the current exposure. Therefore, the two major factors in the selection of the detector operating temperature are dark current and persistence.

5.4.2.1. Dark Current

The RSS-NIR's detector dark current specification is ≤ 0.1 e/s, with a goal of ≤ 0.01 e/s. The goal would give a nominal dark current integration of ≤ 10 electrons for a 1000 second integration period, and ≤ 3 electrons for a 300 second integration period. The following 2 graphs show what the expected dark current is vs. temperature. In both cases, the goal of ≤ 0.01 e/s is expected to be met at temperatures ≤ 120 K.

Measured/scaled dark current values for $\lambda_c=1.7 \mu\text{m}$ by Gert Finger et al., are shown in **Figure 5-53**, with the dark current of the PICNIC array was scaled to the pixel size of 18 mm.

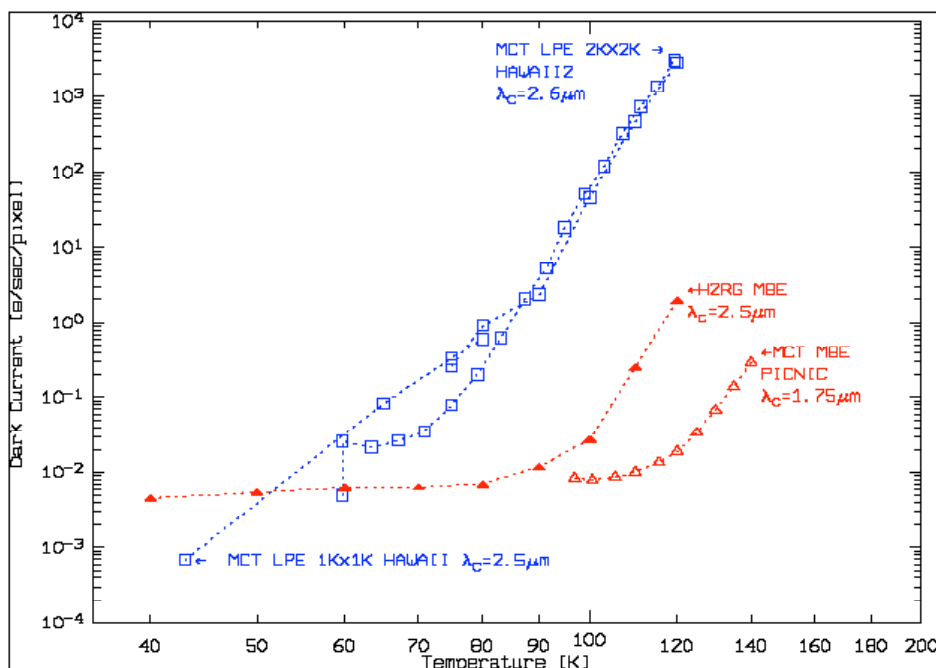


Figure 5-53. Dark current versus temperature for HgCdTe arrays. Squares: LPE material. (squares: Hawaii 1 1Kx1K, filled squares: Hawaii 2 2Kx2K). Triangles: MBE on CdZnTe substrate. (filled triangles: Hawaii 2RG engineering grade array, triangles: $\lambda_c=1.7 \mu\text{m}$ PICNIC).

Typical values for dark current values for $\lambda_c=1.7 \mu\text{m}$ by James W. Beletic et al. of Teledyne, are shown in **Figure 5-54**.

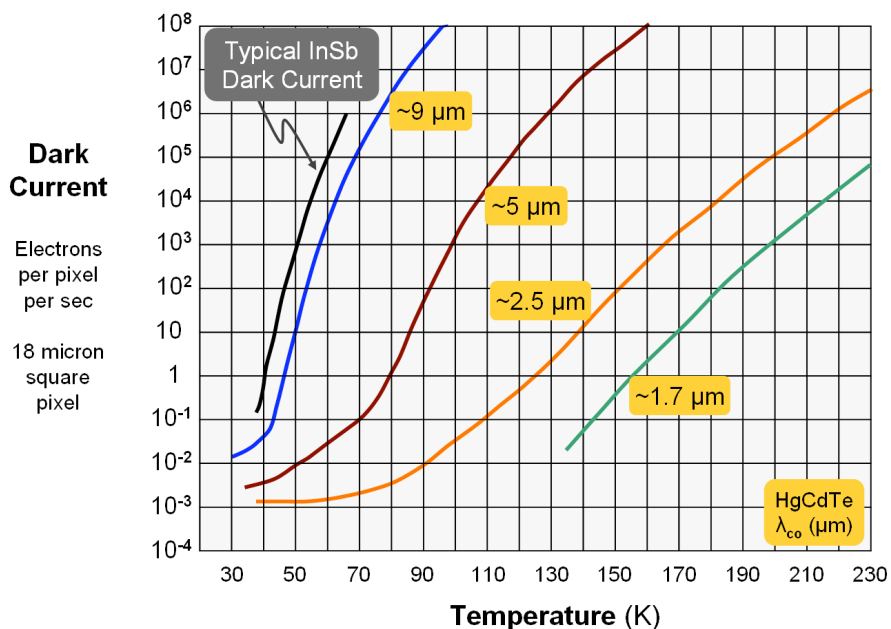


Figure 5-54. The dark current of MBE grown HgCdTe detector material. The dark current is shown for an 18 μm pixel and can be scaled for smaller or larger pixel pitch. The cutoff wavelength (λ_{co}) is shown with the approximation symbol, since λ_{co} is a function of temperature and there will be slight variation in cutoff wavelength of a HgCdTe detector as it cools.

5.4.2.2. Persistence

The effect of persistence at a particular pixel is the largest when the previous image had a long integration time, coupled with a signal that fills a large percentage of the full well capacity of that pixel. This generates a larger residual signal that will affect the pixel for a longer period of time before the persistence dies out. Current models of persistence (Smith et al. 2008) indicate that it is caused by impurities and dislocation trapping sites in the detector material. One of the problems is that the lattice matching between the HgCdTe detector material and the CdZnTe substrate is worse for $\lambda_c=1.7 \mu\text{m}$ as compared to $\lambda_c=2.5 \mu\text{m}$, which may be the reason that $\lambda_c=1.7 \mu\text{m}$ detectors appear to have more persistence than $\lambda_c=2.7 \mu\text{m}$ detectors. The cadmium fraction of $1.7 \mu\text{m}$ material is ≈ 0.6 per James W. Beletic et al. 2008, with a substrate of CdZnTe. The CdZnTe substrate crystals were shown to have a lattice constant of $6.442 \pm 0.003 \text{ \AA}$ per Guoqiang Li et al. 2008, whereas the lattice spacing of HgCdTe for $x=0.62$ ($\approx \lambda_c=1.7 \mu\text{m}$) is 6.472 \AA and for $x=0.44$ ($\approx \lambda_c=2.5 \mu\text{m}$) is 6.468 \AA per A Rogalski 2005.

Persistence measured for $\lambda_c=1.7 \mu\text{m}$ detectors by Roger M. Smith et al. 2008, are shown in **Figure 5-55**, and the persistence decay curve for 300 second integration periods is shown in **Figure 5-56**. Note that in **Figure 5-55**, $1 \text{ ADU} \approx 1 \text{ electron}$.

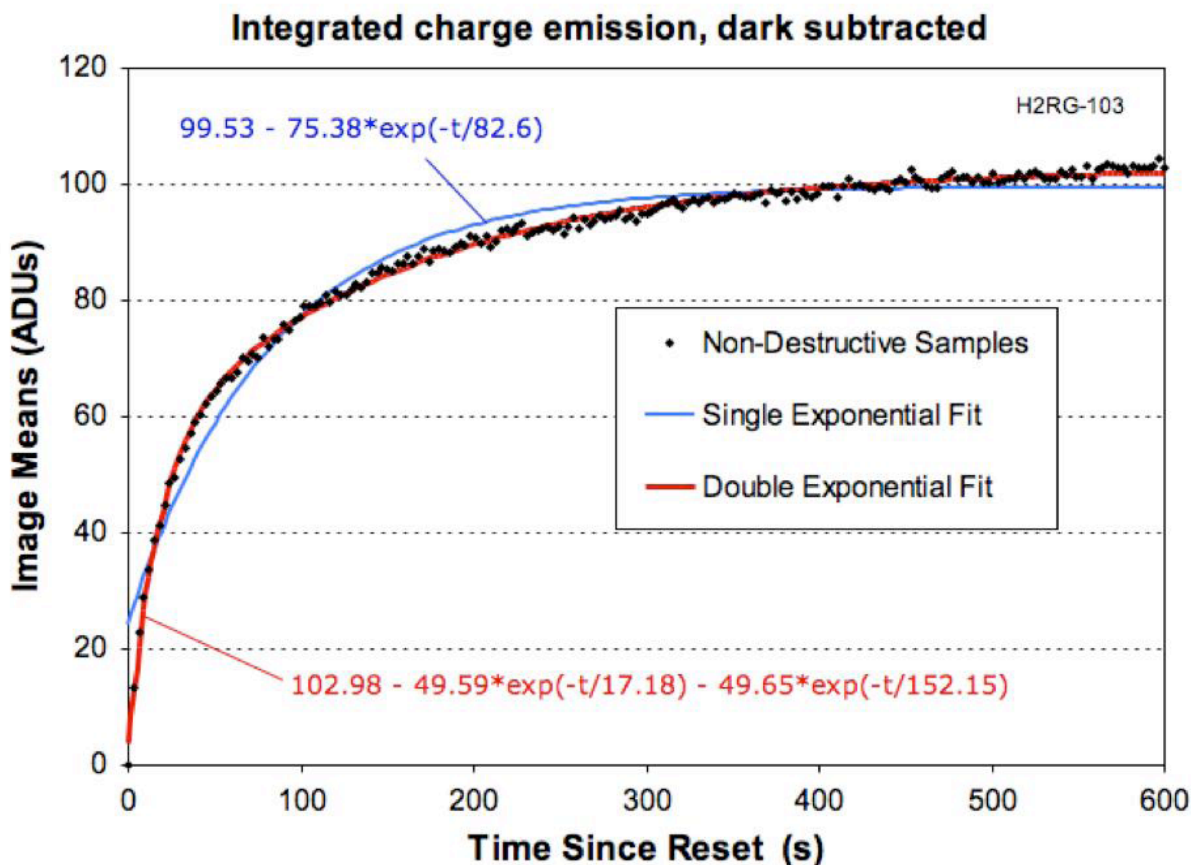


Figure 5-55. Non-destructive readout during several 600s dark exposures were averaged and subtracted from a similar sequence following a 300s bright exposure to generate this integrated persistence curve. Least squares fit of single and double exponentials with unconstrained offset are shown.

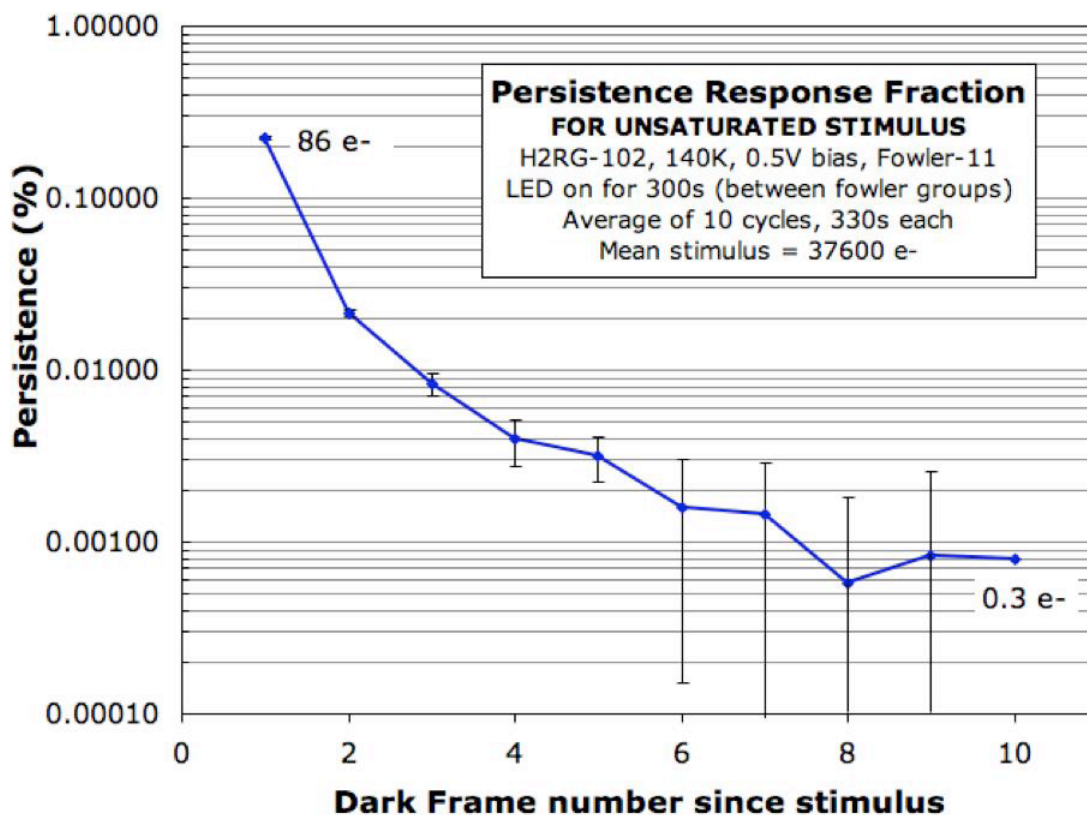


Figure 5-56. Decay of mean persistence during dark frames after an unsaturated stimulus. The mean persistence in the first 300s dark was 86e- and only 0.3e- in the last dark. Many pixels and ten cycles, taking 3630 seconds each, were averaged to obtain sufficient precision.

It is significant to note that it takes 3 integration periods of 300 seconds each before the persistence is ≤ 3 e, and 5 integration periods of 300 seconds each before the persistence is ≤ 1 e. At 3 e, the persistence signal is on the same order as the dark current, but to become relatively insignificant, it needs to be ≤ 1 e.

There is also some evidence that persistence has a shorter time constant at higher temperatures, when all of the other conditions on the detector are the same, so that higher temperatures should mean less persistence effect (personal communication between Don Thielman and Richard Blank).

For this reason, it is very important that we address the persistence with a combination of detector read-out mode selection, persistence modeling, and as high of a temperature as the system design can afford. Note, this is highly dependent upon the integration period, bias levels, exposure level, rate of exposure, and what sort of sampling is used and what wavelength cutoff the detector has, so that tests with the actual detector will be important.

The 120 K temperature was chosen for several reasons:

1. Teledyne, and other instruments that are working with $\lambda_c=1.7 \mu\text{m}$ material run at 140 K.
2. At 130 K the Teledyne specs show that we should be just barely able to meet our goal requirements for dark current.
3. At 120 K, we should have no problem meeting or exceeding our goals for dark current.

4. The warmer temperature, as compared to temperature colder than 120 K, should help reduce the persistence.
5. The lower end of the nominal temperature of 100 K gives us a better selection of cryocoolers as compared to a detector temperature of 77 K.

Given this, the nominal design operating point for the RSS-NIR detector was selected to be 120 K, with a design operating range between 100 K and 140 K, as a balance that should give us dark current specs that are at or below our goals, cold enough to suppress a fair number of "hot pixels", and yet warm enough to give us an advantage with regards to shorter persistence times.

5.4.3. Integration and Test Plan

The testing and integration of the HAWAII 2RG detector and associated systems will be carried out in our facilities at the University of Wisconsin-Madison. In addition to the science-grade detector, cryogenic ASIC, and JADE2 card, Teledyne will also deliver a multiplexor (MUX), an engineering-grade detector, and a room-temperature ASIC for testing purposes. These test devices will be used to gain experience operating the detector system components, verify signals (e.g., clocks, bias voltages, outputs) and functionality, and carry out preliminary detector characterization measurements prior to working with the science-grade array.

The detector testing will involve measuring characteristics such as gain, readout noise, dark current, linearity, persistence, inter-readout crosstalk, and quantum efficiency (QE) at the operating temperature of 120 K. The tests will mostly require collecting several dark frames and flat-fields, though an illuminating source will be required for QE, and possibly persistence, measurements. Appropriate detector regions (e.g., full field, sub-arrays, areas with few defects) will be used for each of these measurements. The Correlated Double Sampling (CDS), Fowler, and Up-the-Ramp readout methods will be experimented with through these tests as well. Many of these measurements will be repeated with the complete instrument as part of the commissioning activities at SALT. Brief descriptions of the detector tests are given below.

5.4.3.1. Gain

The gain will be measured using the photon transfer method. This technique involves producing a plot of signal variance as a function of mean signal. Assuming the only contributions to the noise are from photon statistics and detector readout, a linear fit to the data will yield a slope equal to the inverse of the gain. The gain will have units of $e^- \text{ADU}^{-1}$. The plot also allows one to inspect the linearity and saturation level. An example of a photon transfer curve is shown in **Figure 5-57**.

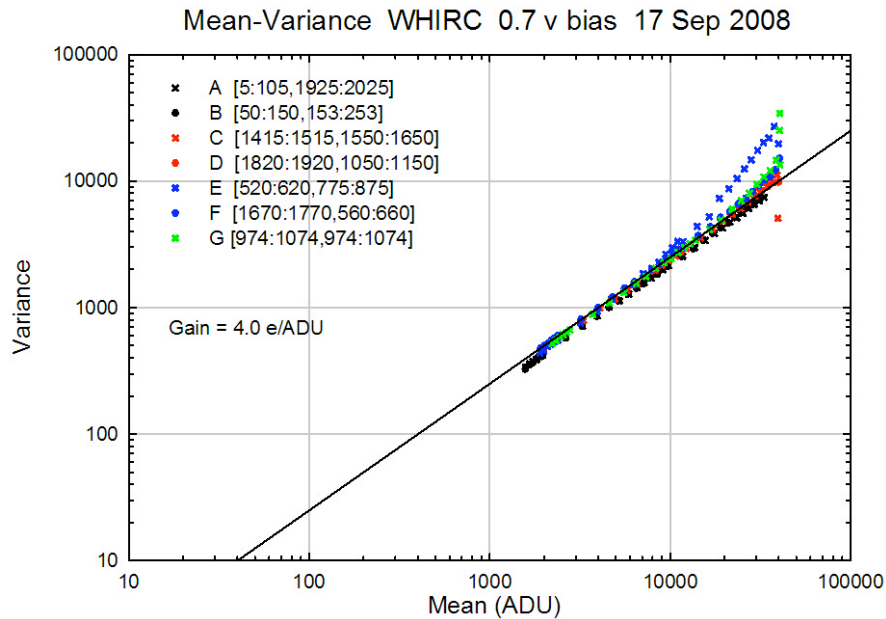


Figure 5-57. A photon transfer curve for the WIYN High-resolution InfraRed Camera (WHIRC)¹. The WHIRC detector is a Raytheon Vision Systems VIRGO 2K × 2K HgCdTe array. The symbols correspond to different pixel regions on the detector.

5.4.3.2. Readout Noise

The readout noise will be measured by obtaining a series of short dark frames (minimum exposure time). A frame containing the standard deviation of each pixel will be produced (**Figure 5-58**). A histogram of these data is produced and the mean of the standard deviation values gives the readout noise (**Figure 5-59**). In addition, the variance axis intercept on the photon transfer curve provides us with another way to measure the readout noise.

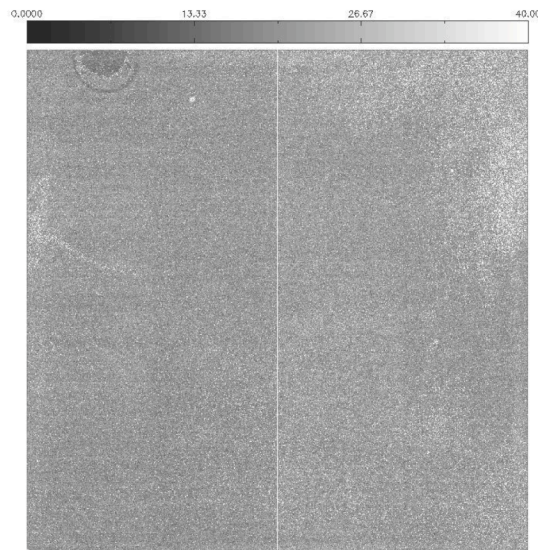


Figure 5-58. A readout noise map for a HAWAII 2RG detector (2.5 μm cutoff) with the SIDECAR ASIC². The CDS readout method was used.

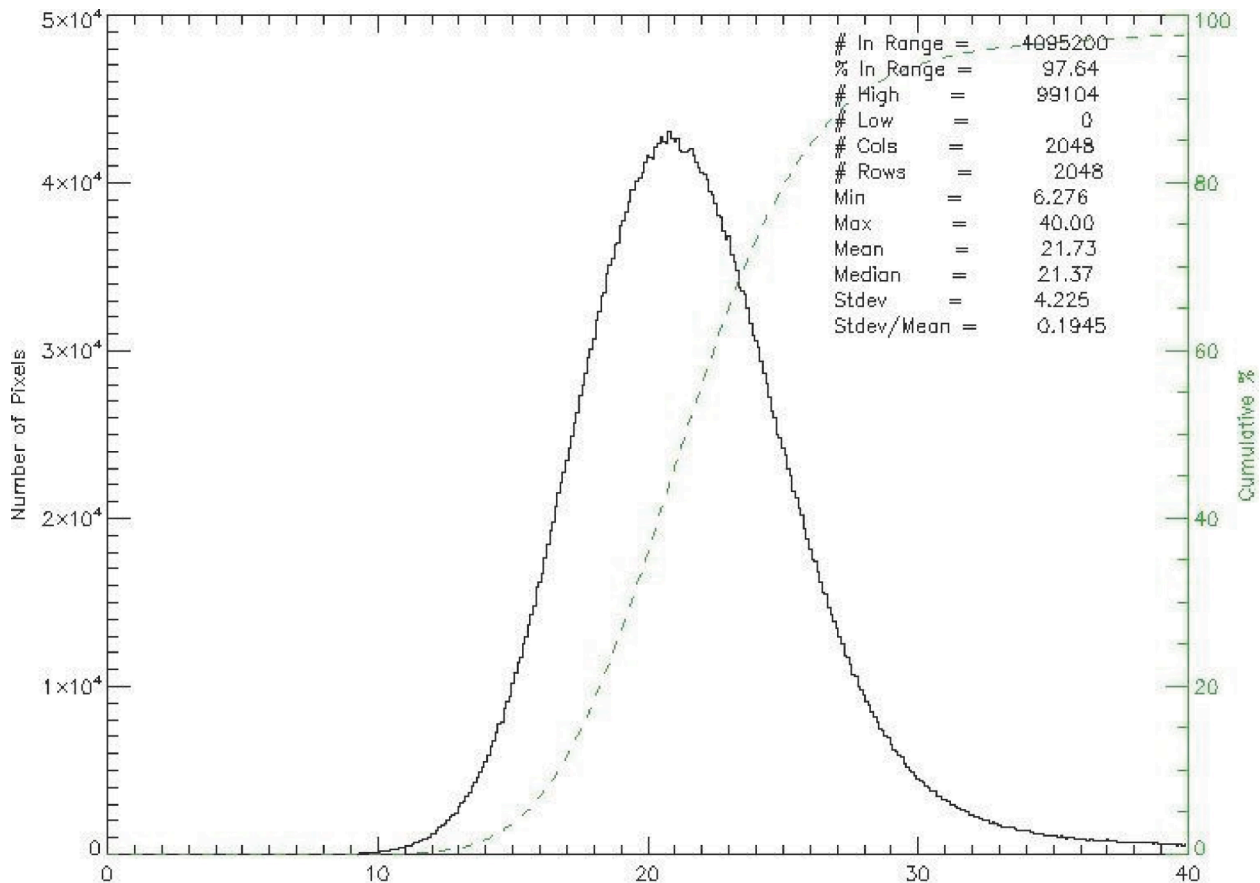


Figure 5-59. A readout noise histogram for a HAWAII 2RG detector (2.5 μm cutoff) with the SIDECAR ASIC². The CDS readout method was used.

5.4.3.3. Dark Current

The dark current will be measured by obtaining dark frames with long exposure times. These frames will be combined to give a mean dark frame and the signal rate will be determined. The gain value will be used to report a dark current in $e^- s^{-1}$. A dark defect map will be produced by identifying pixels with anomalously high and low dark current values.

5.4.3.4. Linearity

The linearity can be characterized by defining a function that is a signal rate normalized to the value at short exposure times (such as the minimum exposure time). A polynomial fit to the normalized signal rate versus mean signal data allows one to derive a linearity correction that can be applied as part of the data reduction procedure. An example of a linearity plot is shown in **Figure 5-60**.

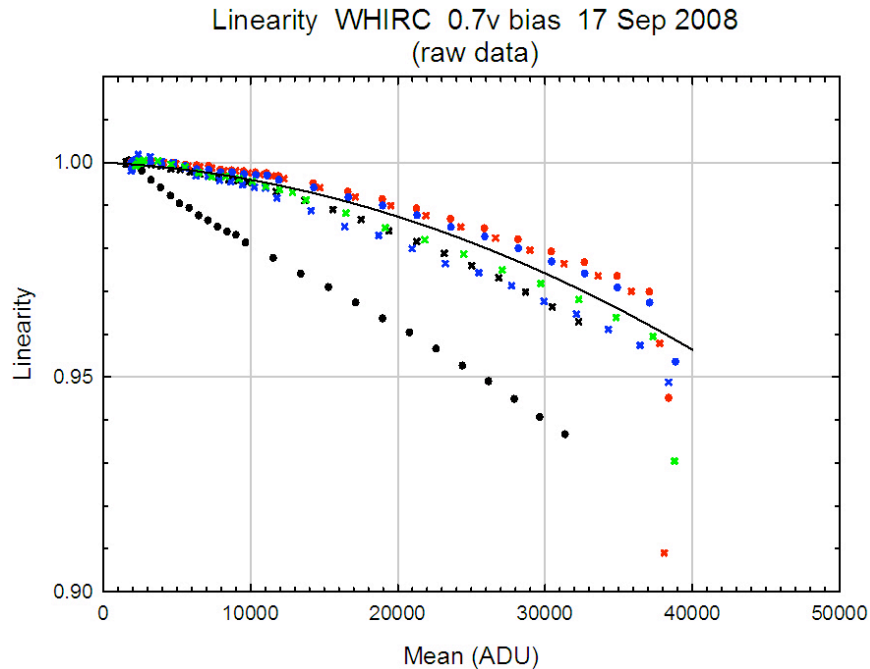


Figure 5-60. A linearity plot for WHIRC fit with a second-order polynomial^{1,3}. The linearity correction is derived from the best-fit parameters. The symbols correspond to different pixel regions on the detector.

5.4.3.5. Persistence

As discussed in Section 5.4.2, calibrating out the effects of persistence in an image is not easily done. Our strategy will be to develop a persistence model for our detector by measuring its dependence on such factors as readout method, exposure time, exposure rate, signal level, and detector bias. This will involve searching for, and analyzing, any remnant image in a series of dark frames, or possibly frames illuminated with a source. Based on the results of these tests, we will explore mitigation options and develop a calibration technique.

5.4.3.6. Inter-readout Crosstalk

A frame is produced in which pixels in a single channel are exposed to near saturation. The frame is then examined for ghost images of these pixels in the other channels.

5.4.3.7. Quantum Efficiency (QE)

The detector QE will be measured as a function of wavelength by blackbody radiometry. The experimental setup is under consideration. Filter and window transmission curves will be required for the calculation. Mean QE values will be reported, as well as the QE for each pixel with histograms and maps. A QE defect map will be produced by identifying pixels with anomalously low QE values.

5.4.3.8. Operability

By combining the dark and QE defect maps, one can produce a map that permits an estimation of the total operability.

5.4.4. Cryogenic Long Wavelength Blocking Filters

The semi-warm instrument design of RSS-NIR forces us to block long wavelengths with filters inside the cryogenic Dewar to decrease the thermal background. Different instrument modes will require different amounts of background filtering, so we need to have a variety of options available.

5.4.4.1. Cutoff Wavelengths

We have a 5 position filter wheel in the cryogenic Dewar. One position will be open (or contain a filter that begins blocking at a wavelength beyond our detector cutoff to allow narrow band Fabry-Perot observations to go out as far as possible), one position is blocked off for detector calibrations, and 3 positions are for long wavelength cutoff filters. Based on the instrument thermal backgrounds determined in Section 5.3 and the temperature statistics for the SALT site, we can pick long wavelength cutoffs that will allow sky-limited spectroscopy to be carried out in different ambient conditions. **Figure 5-48** in Section 5.3.1 gives the typical percentages of astronomically dark hours available for sky-limited spectroscopic observations over the course of a year. We are currently baselining no slit cooling, with it left as a future upgrade path. This means that the filters we choose now should assume no slit cooling.

We have initially chosen cutoff wavelengths of $\lambda_{\text{cutoff}} = 1.65\text{-}1.67$ mm, 1.6 mm, and 1.55 mm for our 3 blocking filters. The longest range is to allow observations of the Fe II 1.644 mm line, desired by many science programs. Thermal modeling to date has shown that with a cutoff at 1.65 mm, sky-limited spectroscopy could be done 29% of the time at $R=4000$ and 7% of the time at $R=7000$. Further modeling will determine just how far beyond 1.65 mm we can push so that observations of the 1.644 mm line will not be compromised and we will still have acceptable thermal background levels. The 1.6 and 1.55 mm cutoffs will be selectable based on nightly ambient temperatures and what observations are in the SALT queue. At 1.55 mm, sky-limited spectroscopy at $R=7000$ should be possible 86% of the time. Shortening this wavelength any would quickly get into the atmospheric absorption trough at 1.35-1.45 mm, making the extra ~ 0.5 mm hardly worth the incremental extra coverage. After further detailed thermal analyses and science case development, the exact wavelengths of these 3 cutoff filters can be modified before the critical design stage with no impact to the instrument design.

5.4.4.2. Detector QE Falloff

Little data exist on the falloff of detector quantum efficiency (QE) much beyond the cutoff wavelength. **Figure 5-61** shows a theoretical prediction from Teledyne (top). They claim that the detector sensitivity falls to a negligible level by 10% beyond the cutoff wavelength, which would be at $\lambda = 1.87$ mm for a $\lambda_c = 1.7$ mm cutoff detector. The two lower plots show a fit to the QE decrease of a HAWAII 2RG-1.7mm detector from the SNAP program (Schubnell et al. 2008, Ferlet 2008). When these data were measured, the SNAP test setup could only measure an absolute QE to 3-4% accuracy. Therefore, the data points only went to $\lambda = 1.76$ mm (Schubnell, private communication). This fit was extrapolated to longer wavelengths by Ferlet when analyzing thermal stray light for the FMOS fiber-fed NIR spectrographs on Subaru. The measured data show that the QE for this particular detector was down to 0.03 at $\lambda = 1.76$ mm. Assuming that the fit extrapolation holds, it predicts that the detector QE will be down to $2.46E-04$ by $\lambda = 1.87$ mm, the Teledyne theoretical prediction of the point where sensitivity should be negligible.

Once we find out our exact detector cutoff wavelength, based on the upcoming Teledyne manufacturing runs and their results, these existing detector QE data will be used to develop the final specifications for our long wavelength cutoff filter performance requirements.

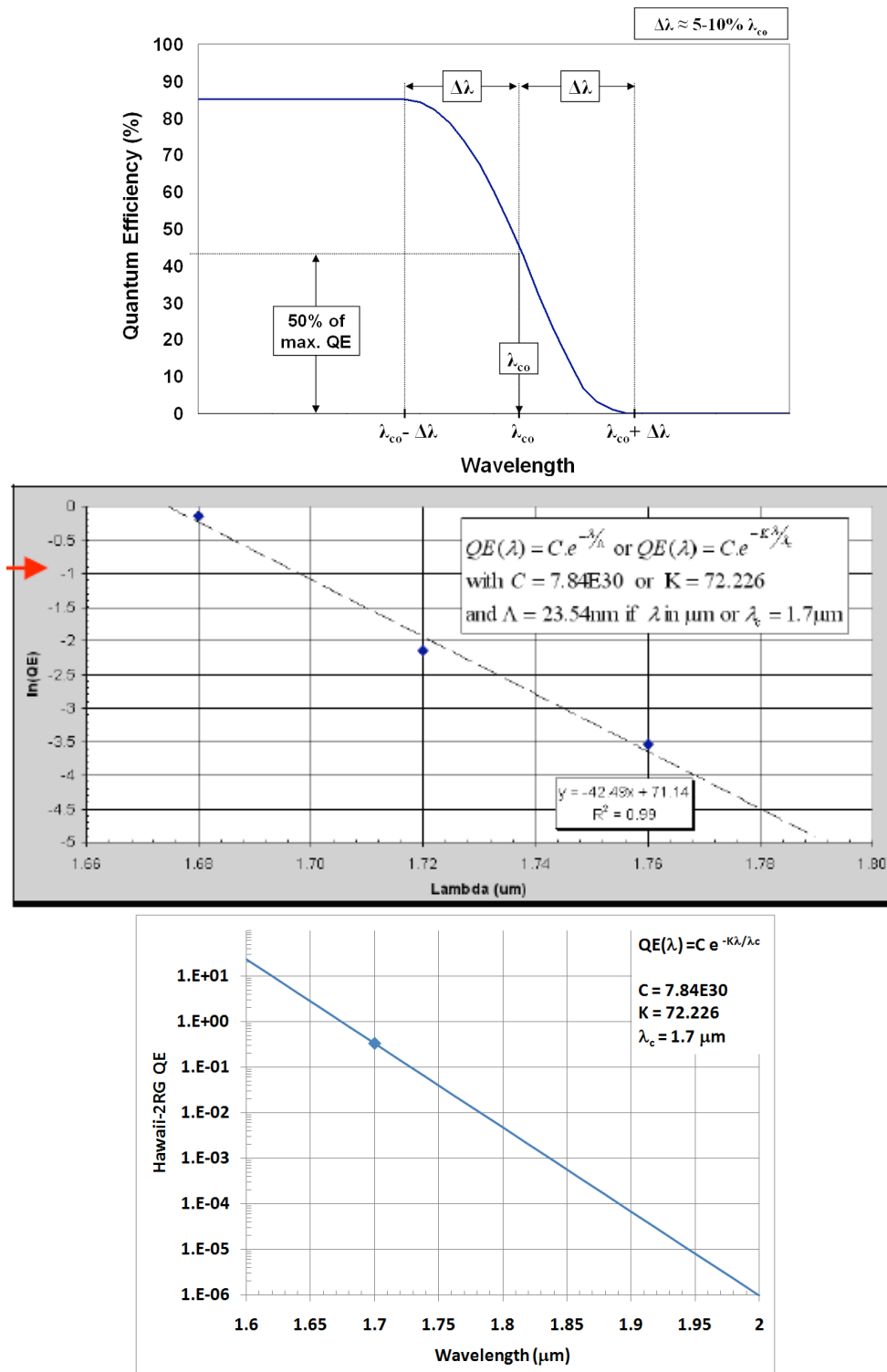


Figure 5-61. Falloff of HAWAII 2RG quantum efficiency as a function of wavelength. The top plot is a theoretical prediction from Teledyne. The center plot is measured QE data from a detector in the SNAP project (Schubnell et al. 2008). The bottom plot is a fit to this measured QE data extrapolated to longer wavelengths for analysis of FMOS (Ferlet 2008).

5.4.4.3. Similar Instruments

A number of NIR instruments have attempted designs that were not fully cryogenic and relied on long wavelength blocking filters. Some were successful and some were not, where the level of success seems to depend heavily on the correct implementation of blocking filters.

CIRPASS (Parry et al. 2004) was a very successful fiber-fed NIR spectrograph used as a visiting instrument on Gemini and on the William Herschel Telescope. It operates at a spectral resolution of $R \sim 3000$ out to wavelengths of 1.67 or 1.8 mm. The spectrograph resides inside a freezer operating at -40 °C. Long wavelength blocking filters are contained within the cryogenic Dewar. One with a cutoff at 1.85 mm stays permanently mounted in the beam, and additional filters with cutoffs at 1.4 and 1.67 mm are selectable via a filter wheel.

FMOS (Dalton et al. 2006) is a fiber-fed spectrograph currently being commissioned on Subaru. Its design is partly based on CIRPASS. The spectrograph resides in a -70 °C freezer. The detector is sensitive out to $\lambda = 2.5$ mm, but light beyond 1.8 mm is blocked with a single cutoff filter. Initial commissioning revealed that the cutoff filter had not been properly specified for blocking far enough beyond the 2.5 mm detector cutoff. A filter leak at ~ 2.7 mm led to a large thermal background reaching the detector. The cutoff filter was corrected, and now instrument thermal backgrounds match very closely the levels predicted by their thermal modeling using ASAP (Gavin Dalton, private communication).

LRS-J (Tufts et al. 2004) was an extension to the Low Resolution Spectrograph (LRS) on the Hobby-Eberly Telescope (HET). It suffered from similar thermal background problems as FMOS. It used a 2.5 mm sensitive detector with a cutoff filter blocking $\lambda > 1.35$ mm because no instrument cooling was implemented upstream of the cryogenic Dewar containing the blocking filter, camera optics, and detector. The thermal background difference at $\lambda = 1.35$ and 2.5 mm is 7 orders of magnitude – too much blocking to get from a single filter.

All of these instruments used a detector that was sensitive out to $\lambda = 2.5$ mm. We believe that our selection of a detector cutoff wavelength of 1.7 mm will be a large step in the right direction of making our implementation a success. Our required blocking level at 1.7 mm will be 5 orders of magnitude below the background at $\lambda = 2.5$ mm. This fact, coupled with our extensive thermal analysis and ray tracing, and the fact that we have planned a number of cutoff filters that can be used in different ambient operating conditions, should all work together to make RSS-NIR a success.

5.5. Electrical/Electronics Design

The electrical and electronics design retains the same basic architecture as in the early concepts for the RSS-NIR instrument. Changes in the architecture address issues that were raised in the PDR with regards to mass/size/volume issues, provisions to protect the instrument in emergency power loss conditions, and to provide an architecture that enables future changes or enhancements without the need for major architectural or hardware changes. While changes have been made, the impact to the control software and spares was also considered at the same time to minimize the impact to those areas. Some of the significant areas are:

Detector Controller

The use of the SIDECAR and JADE2 card with the Teledyne detector vastly simplifies the complexity of the detectors controller and reduces the volume, mass and power needed for this critical subsystem.

cRIO replacement of the PXI chassis and custom FPGA functions

The CompactRIO (cRIO) system by National Instruments was chosen over a PXI chassis. This change provides a much smaller chassis interface with the same basic functionality as the PXI chassis and with the advantage that the custom FPGA function that was used in the RSS-VIS can now be incorporated into the FPGA that is part of the cRIO chassis. The cRIO also has an embedded microcontroller that will allow us to put more functionality into the cRIO chassis if needed. Last, the interface from the cRIO by a local ethernet connection, along with the embedded microcontroller allows for the future implementation of a closed loop system on the fold mirror for flexure compensation that would not have been possible with the previous architecture.

Motor Controller/Drivers

Combined motor controller/driver modules for the majority of the actuators that are commanded by RS-485 connections allows a significant reduction in the NIR Control Chassis (NCC) and Control Interface Box (CIB) complexity. This change makes it much easier to change motor types or add or subtract motors without impacting the cRIO system.

Thermal Control and Protected Power

As the RSS-NIR is much more complex thermally, the thermal control is more extensive than for the RSS-VIS, and an uncontrolled rise in the Pre-Dewar temperature has the potential to damage the instrument. To mitigate this, a protected power distribution system with a thermal control system has been conceived that is capable of autonomously returning the RSS-NIR to a safe thermal state in the event of the loss of power.

1-Wire System

Interface of a large number of the low level housekeeping sensors will be done via a Dallas/Maxim electronics 1-Wire interface that allows for a large number of sensors and controls to interface using only four wires in our implementation. (Ground, Power, Signal, Shield).

Data Flow

Preliminary numbers and concepts have been developed for the handling of the large amounts of raw frame data that are generated by the sensitive scientific IR detector. The architecture of the system was designed to handle these data flows, and allows changes in the data reduction system without impacting the architecture or overall hardware connections.

Summary

The overall electrical and electronics design retains the same basic architecture, uses smaller and more efficient electronics, minimally impacts the software architecture, and provides for future changes and capabilities.

5.5.1. Detector Controller

Control of the detector is significantly simplified with the SIDECAR ASIC, the JADE2 card and the associated software from Teledyne. The SIDECAR ASIC, the JADE2 card, and the associated software significantly assist us in the development, characterization and operation of the detector system, and simplify the overall design of the detector controller subsystem.

With the incorporation of the SIDECAR ASIC and JADE2 card into the Detector subsystem, the major design drivers for the Detector Controller are the data flow, data handling and control software. The architecture of this subsystem allows us to use many of the same elements for the development,

characterization, integration and operation phases of the program and allows the use of advanced features in the future without changing the architecture or the hardware. In particular, we designed a system that would permit future implementation of the guide mode to enable real-time control of the NIR's fold mirror for image stabilization.

In the following we will first address the hardware considerations, followed by data flow considerations/architecture, and conclude with control and data reduction.

For the following discussions, see **Figure 5-62**, RSS-NIR Detector Data Flow Block Diagram. This is also in a larger 11 x 17 format in Appendix 9.1.

5.5.1.1. Hardware Considerations

The detector and the SIDECAR are both mounted within the Dewar to minimize the power dissipation by the detector drivers and also to minimize the noise pick-up by the analog signals between the detector and the SIDECAR. Running the SIDECAR at cryogenic temperatures also reduces the noise within the SIDECAR, making it negligible compared to noise from the detector.

The JADE2 card is mounted within the pre-dewar on the outside of the Dewar enclosed within its own climate controlled enclosure. This minimizes potential noise pick-up on the digital lines between the SIDECAR and the JADE2 card and reduces the power dissipated in the SIDECAR output drivers. An alternative location for the JADE2 card is outside of the pre-dewar on the RSS structure, if the drivers on the SIDECAR and the noise environment will permit the additional length in the cables between the SIDECAR and the JADE2 card.

The USB 2-to-Fiber Interfaces provide the SALT requested optically isolated data lines between the payload and the RSS-NIR's Detector Controller Computer (NDET) in the SALT computer room. This optical isolation provides an electrical isolation between the detector's electrical subsystem and the rest of the RSS-NIR's electrical systems.

Power for the JADE2 card and the USB 2-to-Fiber Interface on the RSS structure will each be provided with separate, isolated, low-noise power supplies. The JADE2 card power supply provides a low noise power source for the SIDECAR and ultimately the detector, and allows grounding to be selected for the lowest system noise for the detector. The separate power supply for the USB 2-to-Fiber Interface will isolate digital noise on the USB interface from the SIDECAR/detector and allows grounding for the lowest system noise for the detector.

Fiber optic connection between the USB 2-to-Fiber Interfaces is 110 meters, less than the maximum of 150 meters of fiber optics that are allowed by USB 2 hardware protocols. Optical isolation of the USB 2-to-Fiber Interface at NDET provides a common ground with NDET that electrically isolates it from the telescope, thereby reducing the potential for electrical noise in the system.

NDET computer resides in the SALT computer room and communicates via the local ethernet to the RSS Control computer (PCON), and SALT's control and interface computers (SAMMI and SOMMI). The ethernet interface of the NIR Instrument's NIR CompactRIO Chassis (NCC) to the local ethernet allows NDET to send data directly to the NCC for real-time control of the fold mirror if this feature is desired in the future.

The PCON is a LabView based, state machine driven control system that controls the sequencing of the RSS instrument's operation, but is not designed as a true real-time controller. As such, it expects state changes from its interfaces and controls the system in a sequence based manner.

Lastly, the NCC provides the interface and local control for the RSS-NIR's lower level control and housekeeping functions, and is connected to the local ethernet via its own pair of fiber optic isolators and 110 meters of fiber optics.

This architecture allows PCON to remain a state machine driven system, thereby significantly reducing the software design effort as the RSS-NIR software will be an addition to the existing software for the RSS-VIS. The architecture allows NDET and NCC to both interface directly with PCON, and provides

the ability for NDET to communicate directly to the NCC for real-time control of the fold mirror if this is desired in the future.

5.5.1.2. Data Flow Considerations

The RSS-NIR has multiple modes of operation, but the Fowler sampling mode of operation significantly drives the overall data flow rates and storage requirements. CDS like sampling and up-the-ramp do not stress the system as does Fowler sampling. Data flow speeds are primarily driven by the readout rate of the detector, which should be as short as practical, as long as the higher readout speed doesn't cause additional noise in the system¹. Data buffering is a function not only of the cadence of the integration period, but also a function of the number of Fowler reads that are used.

The highest data flow rates are between the detector and the SIDECAR, and the SIDECAR and the JADE2 card. The maximum sustained data flow is generated when the detector is readout to the SIDECAR in 32 parallel channels, with each channel digitizing at a speed of 500k samples per second, digitizing to 16 bits of resolution, which generates a rate of 32 MB/s. The JADE2 card provides a USB 2 interface that is capable of the maximum 32 MB/s rate, and USB 2 connections by definition have a fundamental rate of 60 MB/s, so neither of these will be a limit.

The nominal speed for the RSS_NIR detector is 32 channels at 200k samples per second with 16 bits of resolution, for a rate of 12.8 MB/s. The nominal rate was chosen to mitigate the potential for additional noise and heat generation at the maximum readout rate and yet drive the system at rate that makes it less sensitive to other external influences. The requirement for the data flow path must be selected above the nominal data flow rate to allow for overhead and data buffering synchronicity issues, so the minimum data rate is currently selected to be **16 MB/s**.

The SIDECAR data memory buffers slightly less than 1% of a single read of the full detector array and is capable of handling the 32 MB/s data flow from the detector to the ASIC through to the JADE2 card. The JADE2 card provide for buffering of 3 to 4 images of data long as the JADE2 buffers do not overflow. The instantaneous readout rate of the detector through the SIDECAR to the JADE2 card may exceed the Nominal rate of 16 MB/s. Readout clocking of data by the SIDECAR causes a slight overhead, so the effective transfer rate from the JADE2 card to the NDET computer is slightly slower than the instantaneous transfer rate from the SIDECAR to the JADE2 card.

NDET must be capable of accepting data at an average rate of ≥ 12.24 MB/s, for multiple frames in a row, as we may perform Fowler 256 sampling with 256 consecutive frames at the nominal readout rate.

Data buffering capability by NDET is driven by Fowler sampling, which requires NDET to buffer 256 Fowler reads in local memory or the ability to write the data to disk as fast as it is received. As a note, 256 frames of whole array data from a 2048 x 2048 detector with 2 bytes per pixel is ≈ 2.1 GB of data.

Given an average of 300 seconds per exposure plus an average of 120 seconds of overhead for instrument set-up and 12 hours total exposure time (in winter), then the total number of exposures could be as many as 102. If each exposure is a 4.2 GB Fowler 256 read, then 428 GB of data storage is required, which is within the capability of today's large disk drives. This assumes that all of the raw frames will be kept while post processing is taking place and then transferred to archival storage or dumped from the NDET computer before the subsequent night's exposures. All of a night's frames need to be stored until post-processing for persistence is done, as the persistence processing needs the data from 1 to 10 or more of the previous integration periods.

Given a reduced data set for a single image on the order of 25 MB/image, a winter night's worth of observing may result in 30 GB of data that would have to be transferred via the external network during a day. This is an effective rate of ≈ 250 kb/second, assuming 24 hours per day for data transfer. If all of the raw data was transferred in 24 hours, this would require a rate of ≈ 40 Mb/s via the external network.

Data transfers between PCON and NDET are minimal, with only high level message passing taking place to command NDET to set up the SIDECAR and detector for the next exposure and then synchronization commands to enable the integration of an image and the readout of the frames of data. The data flow between PCON and NDET and PCON and NCC are not expected to burden the local ethernet system.

5.5.1.3. Control and Data Reduction

The detector control system must support a set of functions to allow easy test, integration, characterization and operation of the detector in a lab environment and in the operation at the SALT site. The software must be also be structured to allow future upgrades without major changes to either the hardware or the software, and should be constructed in a modular fashion so that new modules can be separately tested and integrated with the total software system.

At a minimum the control requirements are:

1. High level message passing from/to command PCON for SIDECAR and detector set-up and synchronization commands
2. Integration periods from ≈ 0.7 seconds to > 1000 seconds.
3. Readout ports selectable: 1, 4 and 32.
4. Pixel readout rates from 100 kHz to 5 MHz
5. Sampling modes: CDS, Fowler, Up-the-Ramp
6. Selection of Fowler $N \geq 256$.
7. Selection of Up-the-Ramp cadence rates from 10 seconds to 300 seconds
8. Selection of Up-the-Ramp number of samples from 2 to 400
9. Control of all of the settable detector parameters, including bias voltages, timing, etc.
10. Control of all of the settable SIDECAR parameters, including preamp gains, timing, etc.
11. Selection of 16 bit or 12 bit digitization
12. Support the Teledyne provided software
13. Capable of setting or resetting individual pixels, or groups of pixels.
14. Capable of guide mode operation

The detector control system must provide data reduction that at a minimum allows the operators of the telescope and the RSS-NIR instrument to be able to determine the health of the instrument and to be able to do a quick-look at the image for alignment and image quality purposes.

The software needs to support data reduction that performs at a minimum:

1. Dark Current correction
2. Conversion gain correction
3. Read Noise statistics

Depending upon the external network capabilities from the SALT site to remote observers, and/or the availability of post processing at the SALT site, the detector control system may need to provide data reduction capabilities on-site at the SALT facilities to prevent overburdening the external network connections.

In addition to the above, the software may need to support the following data reduction elements (but is not limited to this list):

1. Quantum Efficiency correction
2. Interpixel crosstalk compensation
3. Compensation of Glow Centers
4. Persistence calculations / compensation
5. Calculation statistics

Summary

The detector controller hardware is greatly simplified by the SIDECAR and the associated Teledyne software, but still is a high-speed data handling system that allows sophisticated control of the detector and SIDECAR with an architecture that allows for future enhancements without the need to re-design the system.

5.5.2. Motion Control

The motion control for the RSS-NIR instrument needs to control many devices that perform a number of diverse functions for the control of the instrument. While we have tried to minimize the number of different actuators, this has been difficult due to the different requirements for the various actuators. Even with the various types of actuators, the goal was to use a minimum number of motion controller module types by finding highly configurable ones. The use of stand-alone motion controllers also allows us to add or subtract motion controllers with minimal impact to the rest of the control system. The interface to the control computer (PCON) will be implemented with a CompactRIO system that will communicate with the motor and actuator drivers via multi-drop serial communications. This approach reduces the number of spares that are needed, and implements a flexible architecture that allows for changes as the design progresses. Following are the major pieces of the system:

For the following discussions, see **Figure 5-63**, RSS-NIR Instrument Control System Functional Block Diagram . This is also in a larger 11 x 17 format in Appendix 9.1.

5.5.2.1. CompactRIO (cRIO) Controller

The main hub for the control system is the cRIO system from National Instruments. This system is smaller, lower power, more flexible than the previous PXI chassis, and allows for local real-time control. The cRIO system contains a programmable FPGA that allows incorporation of the hardware interlocks into the cRIO chassis that were handled separately in the RSS-VIS. The cRIO allows the controller inputs and outputs to be viewed as just an extension of the PCON control computer. This makes the software architecture with LabView as simple as the original RSS-VIS instrument.

The cRIO consists of a local embedded controller, a power supply, and an FPGA controlled expansion chassis with different plug-in modules depending on the function needed. The cRIO communicates with PCON via an Ethernet port connected by a fiber optic extension.

Digital I/O will be implemented with the NI 9403, which is 32-channel bidirectional digital port. The digital I/O is mainly used to detect the limit sensors used throughout the system.

Analog I/O will be implemented with the NI 9205, which is the 32-channel analog input module. The analog sensors are mainly used for environmental measurements such as temperature, pressure and humidity.

Communications from the cRIO to lower level controllers and interfaces is by either RS-485 or RS-232. The RS-485 is more advantageous since it allows numerous devices to be set up on the same bus resulting in a smaller amount of wiring. The only disadvantage is that the controller cannot run too many operations through a single port at the same time. This, in general, is not a problem since most operations are sequential. For the cRIO, the RS-485 module is the NI 9871. The RS-232 module is the NI 9870. Both of these modules are offered with four ports per module.

As the system gets finalized, more modules will be plugged into the expansion chassis as the needs arise. The expansion chassis has eight slots and if the system grows larger, another expansion chassis can be daisy-chained to the original.

5.5.2.2. Piezo Stage Drivers

The NIR requires very fine positioning control of the fold mirror, which will be implemented via piezo stages. The piezo stages require a special high voltage control system, which is made by Physik Instrumente (PI) of Germany. For the Z/Tip/Tilt, the P-541.TCD actuator will be used which contains three piezos in a single mechanism. For the piston movement (large travel), the P-290 actuator was base lined. All of the PI piezo electronics will fit into a standard 19" rack. The E-503, which is a triple piezo driver, will drive the P-541. The E-508 is the high voltage piezo driver compatible with the P-290. Since all the drivers need a servo feedback control, two of the E-509 servo control modules will be used in the rack. To finish out the rack, an E-517 provides a local digital display for diagnostics and communicates to the cRIO through an RS-232 link.

5.5.2.3. Motor Controllers

The motor controllers are made by Performance Motion Devices (PMD), which manufactures a line of configurable motor controllers. The most compact is the ION 500 Series drive controller, which can drive stepper motors up to 350 watts and communicates using RS-485. These units will run off 24 volts to improve performance and reduce wire sizes. Due to their compact size (110 mm x 80 mm x 38 mm) they

can be placed easily for mechanical packaging and thermal dissipation. The ION 500 will be configured for encoder feedback for precise positioning of the stages. All the motor control parameters including acceleration, deceleration, and jerk can be changed on the fly via the RS-485 communication lines. The ION 500 can control both stepper motors and DC brushless motors so this single unit can be made to work with the numerous kinds of motors in the system, allowing fewer kinds of interfaces to LabView and a smaller number of spares.

5.5.2.4. Motors

The motors for most of the mechanism movements are made by Ultramotion and are from the product line called "The Digit." The majority of the actuators are NEMA 17 sized motors and for the elements requiring larger forces, a NEMA 23 size actuators are used. Each motor/actuator is configured for its own load, amount of travel, backlash, mounting hardware, step size, and speed. Options for each motor include a power-off brake and an incremental optical encoder.

The Camera Articulation Mechanism requires a special motor due to its large loading. It is a NEMA 23 DC brushless motor from Dynetic Systems, model BL2330 with a 700:1 gear ratio.

5.5.2.5. Encoders

Most of the absolute encoders in the system are selected from Netzer Precision. A Rotary Electric Encoder Model DS-58-32 measures the rotational position of the grating mechanism. The linear encoder used is an LA-10. Netzer has many unique features that are well suited for this application. They are robust in harsh environments and are accurate absolute encoders. This is important, so when the power comes up after a power failure, the position of the stage will be known without requiring any movement of the particular actuator.

5.5.2.6. Pneumatics

Pneumatic actuators, brakes and locks will be controlled via pneumatic valves, the same as used in the RSS-VIS. They will be driven by discrete digital I/O lines from the cRIO chassis. At the current time, the only pneumatic actuator is on the beamsplitter. Other pneumatics include the etalon locks, camera articulation lock, air lock door lock, and air lock door seal. In addition to the motion control, the pneumatics also controls the purge air controls for the pre-dewar, air-lock, and NIR doublet.

5.5.2.7. Switches

The reliability of the limit switches is very important for the reliable operation of the instrument. Switches that will perform the best for this application are hall-effect. These switches work under a wide range of temperature and have no moving parts. A simple magnetic circuit must be designed for each individual application due to operational requirements and magnetic field strength at the sensing location. Some actuators will be designed with two hall-effect switches to determine if the locking pin is all the way up, down or somewhere in the middle. This will help prevent the load from being dropped under certain conditions. A typical hall-effect switch will work down to -40° C and can operate anywhere from 4.5 to 24 volts. The baseline hall switches are Optek Technology's Model OH090U.

5.5.3. Environmental Control

The environmental control of the RSS-NIR is important not only to the normal operation of the instrument, but it is also a critical element in preventing damage to the instrument from temperature and humidity excursions that are too large, or rates that are too fast. The critical components within the RSS-NIR are a number of crystalline optical elements that are fragile and can be damaged by rapid temperature changes or exposure to a high relative humidity.

A second important issue is the change-out of filters via the air lock. The filters need to be cycled in a controlled manner from the environment within the pre-dewar to the local environment and then from the local environment to the pre-dewar conditions. This needs to be done without disturbing the temperature or humidity stability within the pre-dewar and without condensing moisture on the filters when they are removed from the air lock to the outside environment. Under no circumstance should the local environmental air be allowed into the pre-dewar when the pre-dewar is at any temperature less than the local dew point.

Lastly, we must create a system that can handle a longer power failure of the main power feeding the SALT facility. The thermal control system must be designed to prevent damage to the instrument from an uncontrolled return to ambient temperature due to a loss of power. To accomplish this, select elements of the thermal control system need to have two special characteristics:

1. Designed to be capable of returning the pre-dewar to ambient temperature in a controlled fashion without any outside intervention, including commands from the control system using backup power.
2. Provide power from multiple power sources capable of running the thermal elements long enough to control the temperature rate of rise, until it could passively warm-up without exceeding the maximum $\Delta T/\Delta t$ for the pre-dewar.

For the following discussions, see **Figure 5-64**, RSS-NIR Instrument Control System Environmental Block Diagram. This is also in a larger 11 x 17 format in Appendix 9.1.

RSS-NIR Redbook
Mid-Term Review Design Document
May 2009

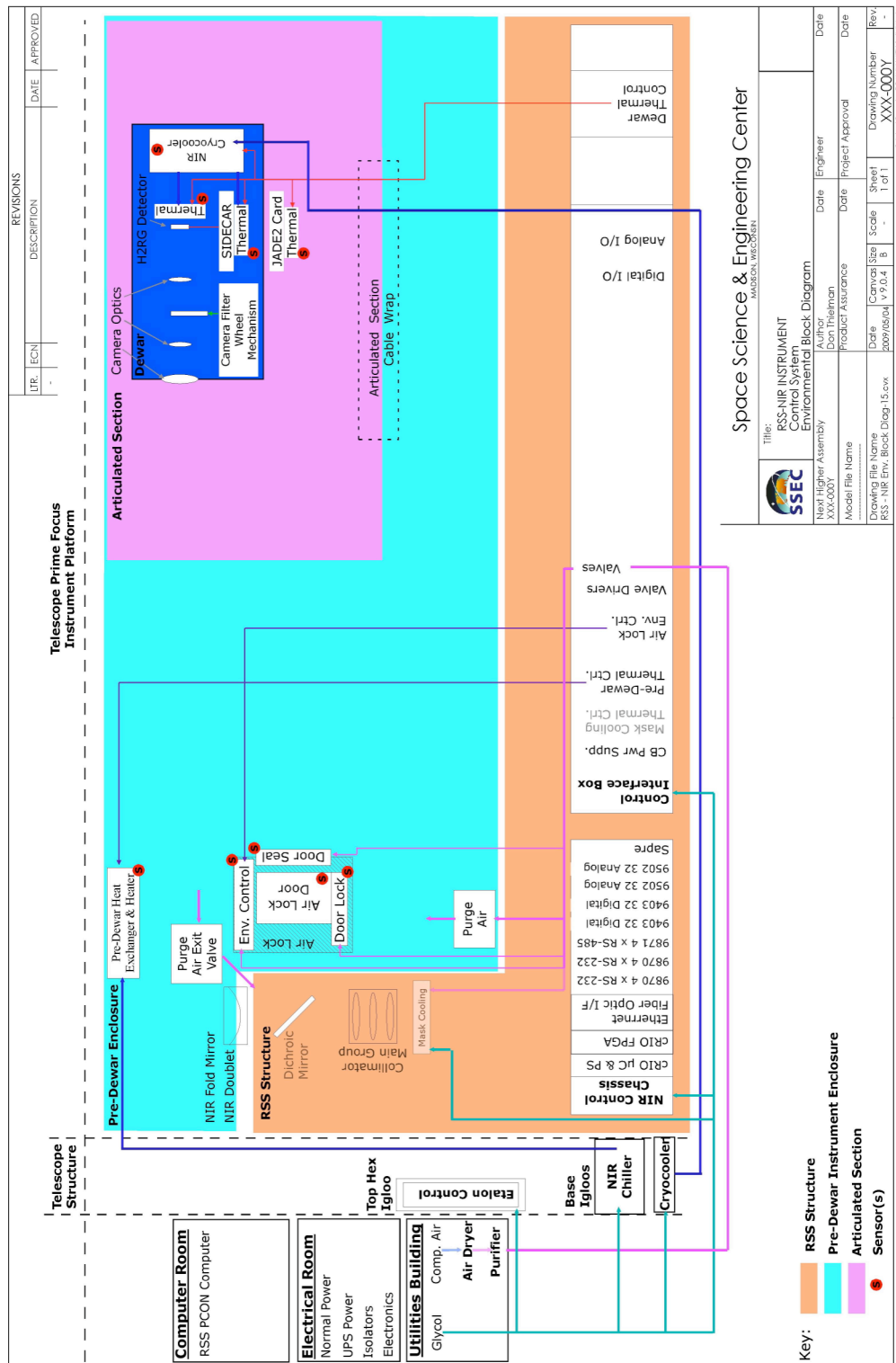


Figure 5-64. RSS-NIR Instrument Control System Environmental Block Diagram.

5.5.3.1. Pre-dewar

Cooling of the pre-dewar is effectively a multi loop control system. The primary cooling capacity is the NIR chiller in Igloo 6 with a local temperature control loop on the temperature of the return fluid. This fluid is set to a temperature that is a few degrees lower than the pre-dewar set point temperature minus the temperature delta across the fluid-air heat exchanger within the pre-dewar. This system is not expected to be fast or accurate enough to precisely control the temperature of the pre-dewar. The precise control loop of the pre-dewar temperature will be done by a controlled "buck" heater on the fluid-air heat exchanger within the pre-dewar, that will allow much faster response and more stable temperature control. The overall coordination of the NIR chiller and the heat exchanger heater will be accomplished by an outer loop that is controlled by PCON via serial links to the NIR chiller controller and the heat exchanger heater controller. PCON will also be responsible for also coordinating normal temperature ramps to cool down and warm-up the pre-dewar.

Humidity control of pre-dewar will be controlled via pneumatic valves that provide cooled purge air into the pre-dewar at a controlled purge gas flow rate to provide positive pressure within the pre-dewar and to keep the air within the pre-dewar below the dew point at all times. There will be a controlled outflow of air from the pre-dewar that will be slightly warmed, to provide the purge of the NIR Doublet within the Optical Tower, thereby allowing double usage of the purge gas. Purge rates would be elevated when cooling down to remove any residual moisture from within the pre-dewar. All of the normal purge gas control would be done from the PCON computer via the NCC and then the individual pneumatic valves. In the event of a power failure, the valves would be automatically configured for the emergency warm-up of the pre-dewar.

5.5.3.2. Dewar

A single cold head controls the cryogenic elements within the Dewar. The Dewar has two actively controlled zones, and the remaining elements are passively controlled by conduction and radiation coupling. The cryocooler compressor is in an igloo at the base of the telescope while the cold head is inside the Dewar. The temperature of the cold head is biased at a temperature 5 to 10 K below the set point for the detector, and as such, is also used to cool the getter colder than any other element within the Dewar. The two actively controlled zones are the detector and the SIDECAR, each of which are connected to the cold head by their respective cold straps. There is a thermal mass along with an associated heater on each cold strap that is used in conjunction with a Lake Shore 325 Temperature Controller to control the temperature of the Detector and the SIDECAR separately. This is done to prevent thermal transients in the SIDECAR from significantly affecting the temperature of the Detector. Overall control of the Lake Shore controller is by the PCON via an RS-485 interface to the NCC. All other elements are passively cooled within Dewar by either cold straps to the cold head, other cooled elements, or radiation coupling between elements. The Dewar cryogenic systems will be controlled by protected power only if the uncontrolled temperature rise of the Dewar would exceed the maximum $\Delta T/\Delta t$.

5.5.3.3. Air Lock

The air lock environmental control system controls the cycling of temperature and environment from the pre-dewar conditions to the ambient environment when extracting filters from the pre-dewar, and from an ambient environment to the pre-dewar conditions when inserting filters from the pre-dewar. This requires coordination between the humidity control system and the temperature control system, and differs upon filter extraction or insertion modes. For the extraction mode, the environment in the air lock will start out

cold and very dry, so that only temperature control will be needed. In the insertion mode, the temperature will remain at ambient until the purge of the air lock has lowered the dew point to be equal that of the pre-dewar, and then the temperature will ramp down. Temperature control will be by a heater on a heat exchanger that is a chiller fluid-air cooling loop with an on/off control valve on cooling loop. The rate of both heating and cooling can be easily controlled with a Supercool PR-59 Controller by the PCON via an RS-232 interface to the NCC.

To prevent inadvertent opening of the air lock when the inner door is not sealed, there will be multiple interlocks, both in software and in hardware, to prevent improper operation, and to sense the proper operating of the seals, doors, and locks. This is a non-critical element, and is not expected to be backed-up with critical power in the advent of a power failure.

5.5.3.4. Optical Tower

The optical tower contains the NIR doublet that acts as the window between the interior of the pre-dewar and the external environment between the NIR doublet and the RSS dichroic mirror. In this area, we need environmental control of the second optical element since it is CaF₂, which is susceptible to damage from rapid temperature changes. We are planning on passive thermal control with the active control of the purge gas between the lens elements and on the "outside" face of the NIR doublet element to prevent fogging. To reduce the total amount of purge gas needed, the outflow purge gas from the pre-dewar will be vented to the "outside" face of the NIR doublet. This venting will be via a pneumatic valve within the pre-dewar under the control of the PCON via a discrete digital interface to the NCC.

5.5.3.5. Electronics Boxes

Power dissipation for both of the RSS-NIR electronics boxes external to the pre-dewar (NCC and CIB) will be rejected to the SALT glycol cooling loops via cold plates and air mixing fans within the enclosures and by insulation on the outside of the electronics boxes. Some of the elements within the NCC and the CIB have minimum temperatures above the minimum temperature of the glycol loop, and will use a simple thermostatic-switch-controlled patch heaters to maintain a minimum temperature on the particular element.

Within the pre-dewar, on the side of the Dewar, the JADE2 card's minimum temperature will be controlled primarily via passive insulation, and a simple thermostatic-switch-controlled patch heater. A thermostatic-switch-controlled fan will control the JADE2 card's maximum temperature.

5.5.3.6. Igloo

The igloo that contains the NIR chiller, and possibly the NIR cryocooler, will need to operate even in the event of a grid power failure until the pre-dewar is in a safe thermal condition. There must be an automatic power handoff from grid power to back-up power and also automatic ventilation from inside the igloo to outside environment in case of the loss of glycol cooling flow within the igloo. This could be accomplished with fans that would automatically ventilate the igloo to the environment at the base of the telescope by a set of insulated, fan pressure opened louvers.

5.5.3.7. Mask Cooling

If mask cooling is implemented, the mask will be cooled by a thermoelectric cooler that rejects the heat to the SALT glycol cooling loop. Temperature control of the thermoelectric cooler will be by a Supercool

PR-59 Controller by the PCON via an RS-232 interface to the NCC. Purge air will be controlled by the PCON via an NCC digital interface driving a pneumatic valve.

5.5.4. Housekeeping

The housekeeping function of the RSS-NIR instrument is a diverse set of sensors and control subsystems that verify and control the operation of elements that are necessary for stable operation of the instrument. While we have tried to reduce the number of different sensors and controls, this has been difficult due to the different requirements for the various functions that are needed within the instrument. Even with the various types of sensors and controls, the goal was to use a minimum number of I/O module types and controls by finding highly configurable ones.

For reference, see **Figure 5-63**, RSS-NIR Instrument Control System Functional Block Diagram, in the 5.5.2 Motion Control section. This is also in a larger 11 x 17 format in Appendix 9.1

The decision to use the cRIO system, along with a 1-Wire system for slower and less precise sensors and controls, allows us to accommodate a large number of discrete digital and analog inputs and also allows multiple RS-232 and RS-485 connections for stand-alone sensor systems. This approach allows us to easily add or subtract additional inputs or communication interfaces with minimal impact to the rest of the control system. If more I/Os are needed than what the current 8 slot chassis provides, an extension chassis will be added. Note, room for the additional chassis will be reserved in the NCC for this possibility. The majority of the interfaces to the control system software that resides within PCON will be via the cRIO system, with a small number of connections directly from PCON's serial connections.

The requirement to provide as many housekeeping functions as possible with off-the-shelf equipment, is at odds with the need to keep the electronics small, with low mass and low power. Where possible commercial off the shelf (COTS) equipment has been selected, but where we have many devices of the same function, or ones of special needs, or the COTS solution is too large, massive or power hungry, we will design and create well documented custom interfaces. Thermal constraints also limit the number of wires that we have to run from inside the pre-dewar to the exterior environment. A large number of wires equates to a large heat leak into the pre-dewar, and a larger number of feed-through contacts that we need to provide.

An example of a custom interface is the hall sensor assemblies and read-outs for lock position verification of the filters, gratings, etalon, and beamsplitter. All of the sensor assemblies contain 2 sensors that can have 4 states that have a common mechanical, magnetic, and electrical design resulting in sensor/readout assemblies that are significantly smaller than commercially available devices. The read-out circuits use a single 1-Wire serial bus to read out all of the lock position sensors, which is based upon a design developed for another program within SSEC. The combination of the custom hall sensor assemblies along with the 1-Wire circuit results in a small, efficient position sensing system for 23 locations and 46 sensors, with only four wires needed for the interface to all of the sensors.

The following list summarizes the number of housekeeping element types for the RSS-NIR instrument:

Table 5-8. Housekeeping I/O Summary

Type	Qty.
Analog Input, cRIO	35
Digital Input, cRIO	35
1-Wire - Hall Sensors	18
1-Wire - Other devices	28
Digital Output - cRIO	17
RS-232, cRIO	9
RS-485, cRIO	9
PCON RS-232	2

Given the numbers for each of the sensor types, and the discrete number of inputs for each of the cRIO interface cards, we can optimize the number of cards by moving some of the analog and digital inputs from discrete cRIO interfaces to 1-Wire interfaces. Interfaces for the RS-232 and RS-485 can also be selected to optimize the number of modules needed. Note, the RS-485 is a multi-drop interface, so multiple controllers can be tied to a single RS-485.

This results in a cRIO chassis that has the following modules:

1. 9502: 32 input Analog module
2. 9502: 32 input Analog module
3. 9403: 32 input/output Digital module
4. 9403: 32 input/output Digital module (includes 8 I/Os for four 1-Wire networks)
5. 9870: 4 channel RS-232 module
6. 9870: 4 channel RS-232 module
7. 9871: 4 channel RS-485 module (one RS-232 interface and 3 RS-485 multi-drop networks.)
8. Spare

This approach minimizes size, mass and power for the control system interface, while providing the flexibility to choose the most efficient set of modules needed to do the interfacing functions, while still allowing for expansion as needed.

5.5.5. Communications

The communications architecture for the RSS-NIR instrument is designed to provide the functionality that is needed for the command and data handling of the instrument, while providing the ability for future enhancements to the system.

Command communication requirements for the state-machine driven architecture of the RSS-NIR instrument are not as stringent as if the system was based upon a real-time control system. Real-time commands are allowed between the NDET and the cRIO for future system enhancements, but the data flow in this case would be kept to a minimum to reduce the impact to other systems within the RSS-NIR and the SALT telescope as a whole.

Data handling requirements are most critical between the detector and the NDET computer that handles the frame data from the RSS-NIR instrument. Due to the large amount of raw data that can be generated by a near infrared detector operating in either Fowler or up-the-ramp sampling, the data flow from the NDET at the SALT facility to the outside world must be taken into consideration. This may affect the

amount of data reduction and data archiving that is done on-site at the SALT facility compared to what is done at remote facilities.

Communication within the RSS-NIR system can be broken down into several areas:

1. Discrete signals either interfacing directly to the cRIO or buffered and then to the cRIO.
2. cRIO discrete RS-232 and RS-485 communications to individual COTS subsystems.
3. cRIO RS-485 multi-drop communications to multiple COTS subsystems.
4. cRIO 1-wire communications to multiple sensors.
5. High speed, fiber optic buffered, ethernet connection between the cRIO and the local ethernet.
6. PCON discrete RS-232 communications to individual COTS subsystems.
7. PCON ethernet connection to the local ethernet.
8. High speed, fiber-optic buffered, USB 2 connection between the Detector subsystem and its associated NDET control computer.
9. NDET ethernet connection to the local ethernet.
10. NDET connection to facilities remote from the SALT site.

Of the above the general nature of the communications for the first 4 areas are covered in the Motion Control and Housekeeping sections of this document. As the system design progresses, the data flow and command requirements for these areas will be verified to ensure that no one area becomes a limiting factor to the system. Specifically, the state-machine approach to the control software allows for interruptions or delays in the communications that only delays the operations, and does not cause system faults or failures.

The data and command communications between the PCON and the cRIO are again based upon the state-machine control software, which allows for delays in the communications without causing system faults or failures. The data and command traffic between PCON and the cRIO chassis is not expected to be a very high rate, but will be measured and compared to the total local ethernet traffic to verify that we will not be bandwidth limited.

The data and command communications between the PCON and NDET are again based upon the state-machine control software, which allows for delays in the communications without causing system faults or failures. The data and command traffic between PCON and NDET is high level command and synchronization messages, and is expected to be a very low data rate, but will be measured and compared to the total local ethernet traffic to verify that we will not be bandwidth limited.

High Speed Data Flow Considerations

The detailed nature of the data flow considerations from the Detector to the NDET computer has been covered in the Detector Controller section of this document, but several important system areas need to be discussed.

The RSS-NIR Fowler and up-the-ramp sampling modes significantly drive overall data flow rates. Data buffering is a function not only of the cadence of the frame period, but also a function of the number of frame that are generated by each final image that is generated.

The highest nominal raw data flow rates are an average of **12.8 MB/s** based upon 32 channels in parallel at 200k samples/sec, with 2 bytes per sample. The requirement for the data flow path to allow for overhead and data buffering synchronicity issues was currently selected to be **16 MB/s**. Note, these are high values, but could be well within what could be seen for a single night of observation. A more

nominal expected rate, based upon an average mix of exposure requirements, would be 20% of the numbers above.

Data buffering capability by NDET is driven by Fowler 256 sampling that requires NDET to buffer a total of 512 frames in local memory or the ability to write the data to disk as fast as it is received. 512 frames of data from the 2048 x 2048 detector, with 2 bytes per pixel, is ≈ 4.2 GB of data. Fowler 256 is the maximum sampling expected to give an improvement to the data sets at the current time. This number may either go up or down depending upon the actual detector itself and the noise environment of the system as a whole.

Given an average of 420 seconds per each image and 12 hours total observing time, then there are 102 images x 4.2 GB per image = 428 GB of data. All of the raw frames need to be kept while initial processing is done and then transferred to archival storage before the subsequent night's images. All of a night's frames need to be stored as the persistence processing needs the data from 1 to 10 or more of the previous integration periods for each image. If all of the raw data from the highest nominal raw data was transferred to a site remote from the SALT facility in 24 hours, this would require an average rate of ≈ 40 Mb/s via the external network. Even the nominal expected rate would require an average rate of ≈ 8 Mb/sec via the external network.

A **reduced** data set for a single image should be on the order of 25 to 50 MB/image, resulting in 2.5 to 5.1 GB of data that gives a continuous average rate of ≈ 250 to 500 kb/s. If all of the **raw** data was sent this would require a highest nominal rate of ≈ 40 Mb/sec and a continuous nominal expected rate of 8 Mb/s via the external network.

Depending upon the external network capabilities from the SALT site to remote observers, data reduction capabilities on-site at the SALT facilities may need to be provided to prevent overburdening the external network connections from the SALT site to the outside world.

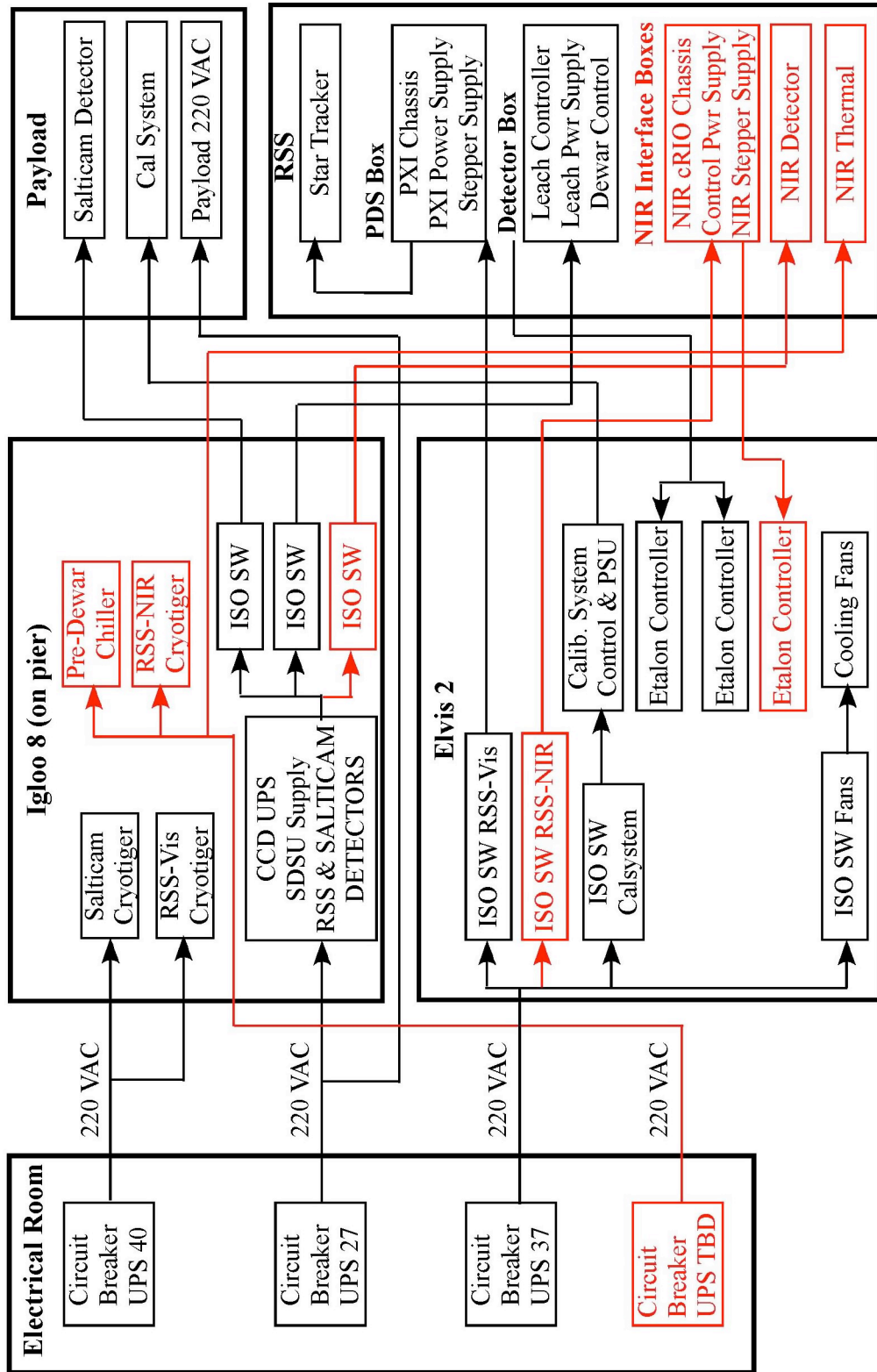
5.5.6. Power Distribution

Power distribution for the RSS-NIR instrument has evolved into a system that is driven by two primary functions:

1. Powering of all of the elements of the RSS-NIR instrument under normal operating conditions, including normal cool-down of the Dewar and the pre-dewar, normal observational operations, and warm-up of the Dewar and the pre-dewar for scheduled maintenance.
2. During emergency conditions, where the main grid power to the SALT facility has been interrupted, major portions the RSS-NIR instrument are without power or have been shut down, and what power is available from either UPS or generator sources is being provided to a "protected power" circuit within the RSS-NIR instrument to enable an emergency warm-up of the Dewar and the pre-dewar at the maximum rates allowed. This emergency condition would begin after a short delay (of 1 to 3 minutes after loss of main grid power) and would attempt to condition the Dewar and the pre-dewar temperatures, as rapidly as is allowed by the optics and mechanical designs, to temperatures that would prevent the damage to the optics and mechanics as a result of a total power loss from all sources.

For the following discussion, see **Figure 5-65**, RSS-NIR Power Distribution Block Diagram. This is also in a larger 11 x 17 format Appendix 9.1.

RSS Power Distribution Block Diagram



File: RSS Power Distribution-15.cvx 21009-05-04

Figure 5-65. RSS-NIR Power Distribution Block Diagram.

5.5.6.1. Normal Operations

Under normal operations, power for all of the systems is provided by the main grid power via the circuit breakers in the electrical room. The power distribution for the RSS-NIR is expected to come from two existing circuit breakers, UPS 27 and UPS 37, which also provide power for the RSS-VIS and a new circuit breaker UPS TBD.

While the final values need to be checked, the power numbers for the RSS-NIR control and housekeeping have been significantly reduced in some areas, particularly in the cRIO chassis and some of the other housekeeping subsystems. UPS 37 is expected to have reserve capacity to power the control and housekeeping systems.

The initial power estimates for the RSS-NIR detector subsystem were significantly higher than the ≤ 10 watts or less now expected. Even if the other Dewar related subsystems, such as the cryogenic temperature control and monitoring, ion pump, and pressure monitoring are added to this circuit, the total additional power to this circuit is ≤ 150 watts. UPS 27 is expected to have the capacity to power all of the detector and Dewar subsystems.

Under normal conditions, the power for the RSS-NIR cryocooler and Chiller in Igloo 6, and the pre-dewar thermal control subsystem, heat exchanger, buck heater, and fans will be powered by the UPS TBD circuit breaker.

5.5.6.2. Emergency Operations

Emergency conditions are defined as a loss of main grid power to the SALT facility for a period of time longer than 1 to 3 minutes, where there is no expectation that main power may return any time sooner than 15 minutes. It also assumes that there is the possibility that the back-up generator may not be able to provide power for a period of more than 6 to 12 hours, and that the UPS system cannot supply power for the protected systems for more than 12 hours by itself.

Under emergency conditions, power for all of the non-essential RSS-NIR systems will be either powered down or put into a standby mode by the computer to conserve the remaining UPS power for the critical loads. The power distribution circuit breakers UPS 27 and UPS 37 do not need to be on for the RSS-NIR in an emergency situation.

The critical components of the RSS-NIR that require emergency backup power are the cryocooler and chiller in igloo 6, and the pre-dewar thermal control subsystem including the heat exchanger, buck heater, and fans. These components will be powered by the UPS TBD circuit breaker for a period long enough to allow the thermal systems to bring the various elements up to a temperature from which they can passively rise up to room temperature without exceeding any of the maximum rates allowed by the optical and mechanical designs. As a loss of main grid power may also interrupt the flow of the facility glycol cooling loop, the cryocooler and chiller will need to be air-cooled units, and the igloo will need to have a fan that can exchange air from within the igloo to the environment under the telescope in case the glycol coolant flow stops.

There will need to be a monitor on all of the power sources that will determine if main grid power has been lost and what other power sources are now supplying power. The monitor needs to be a stand-alone system that needs no external control from computers, for the system to function properly under all conditions. This monitor would annunciate an emergency condition after a short delay of 1 to 3 minutes

by sending a dedicated hardware signal to all of the critical systems. This hardware signal would then cause all of the thermal control subsystems to begin a pre-programmed temperature ramps to put the RSS-NIR into a safe condition as rapidly as possible. If main power was restored before the temperature ramps were completed, the PCON computer could halt the temperature ramps and then begin a cool-down procedure from whatever thermal state the RSS-NIR system was in at the time of power restoration.

Depending upon the reliability of the back-up power sources at the SALT facility, it may be necessary to provide a redundant back-up to the normal back-up power sources.

Summary

This design provides a manageable power system for RSS-NIR instrument with low impact to the current SALT systems, and reduces the demand on the SALT back-up power systems to a minimum, while protecting the instrument itself from damage.

5.6. Control System Software

The approach to developing the RSS-NIR control system software is to

- Mimic the RSS-VIS implementation
- Use the same tools, strategies, and designs already delivered to SALT
- Enhance the User Interface and control system with NIR controls
- Add “NDET” in analogy to “PDET” to manage the detector and collect science data

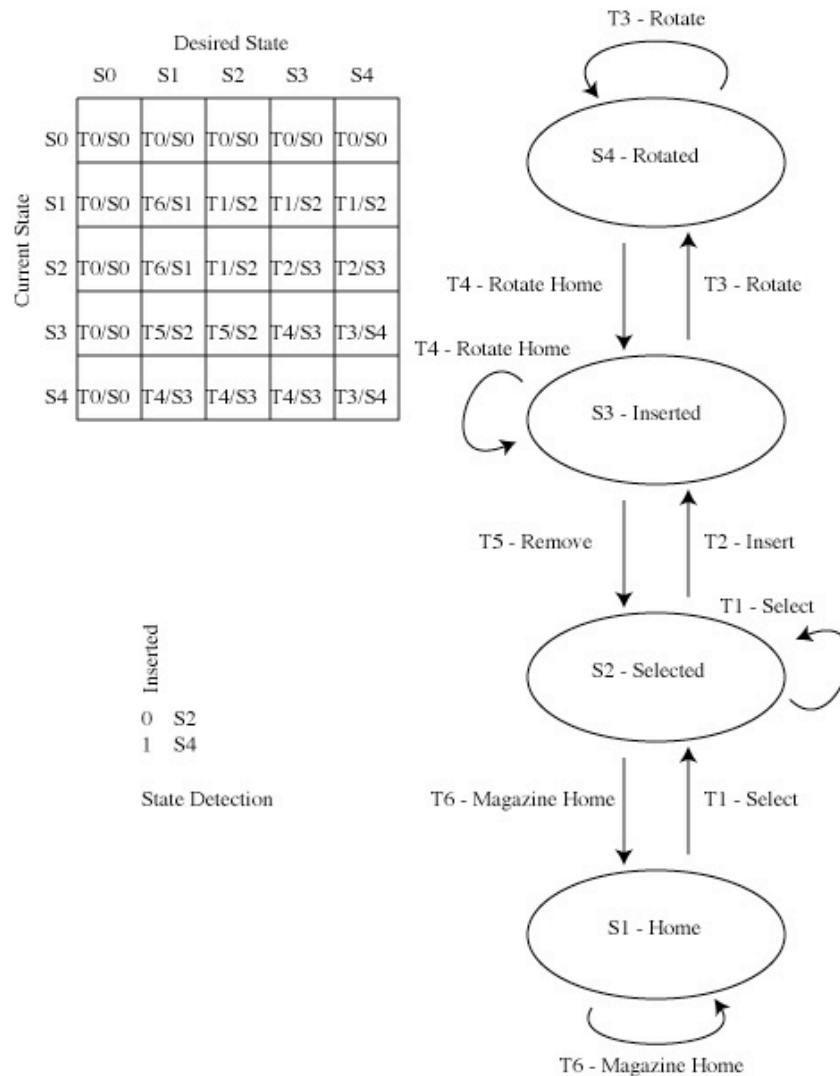
This is a low-risk, well-defined software effort, and will produce a product that the SALT staff will recognize and understand “out of the box”. The RSS-VIS control system, into which we will build the NIR control, can be viewed as the world’s most detailed Interface Control Document.

We are in frequent contact with Janus Brink and Anthony Koeslag, and will remain in close touch so that there are no “surprises” in approach, design, or implementation.

5.6.1. Architecture

5.6.1.1. Low Level State Machines

The architecture of the RSS-NIR control system software is completely defined by that of the RSS-VIS system. At the lowest level, the control system consists of small, highly specific modules that control individual mechanisms. These are implemented as table-driven state machines (see **Figure 5-66**). The bubbles represent the states a given mechanism goes through (in this case, the grating). The arrows are the transitions that move you between states.



PFIS Grating State Diagram

Figure 5-66. RSS-VIS Grating State Diagram

When using the mechanism, there is always a current state and the desired state. The state table is indexed by these two state values; the indexed cell provides two things: the next transition, and the state that leaves you in. The state machine loops over this table, and stops when it lands on the diagonal of the state table, where the current state is the same as the desired state.

This is a particularly compact and flexible way to implement a sequence of events. Each transition is implemented just once, in its own module, and the modules are sequenced entirely by the state table, not in a procedural flow.

These state machine modules are embedded in a higher-level layer, where individual mechanisms are integrated into an instrument-level treatment. This is the level where the instrument configuration is managed, mechanisms are synchronized, and parallel operations performed.

5.6.1.2. Instrument-level State Diagram

Figure 5-67 shows the instrument-level state diagram. This defines all the legal operational states, and the pathways between them.

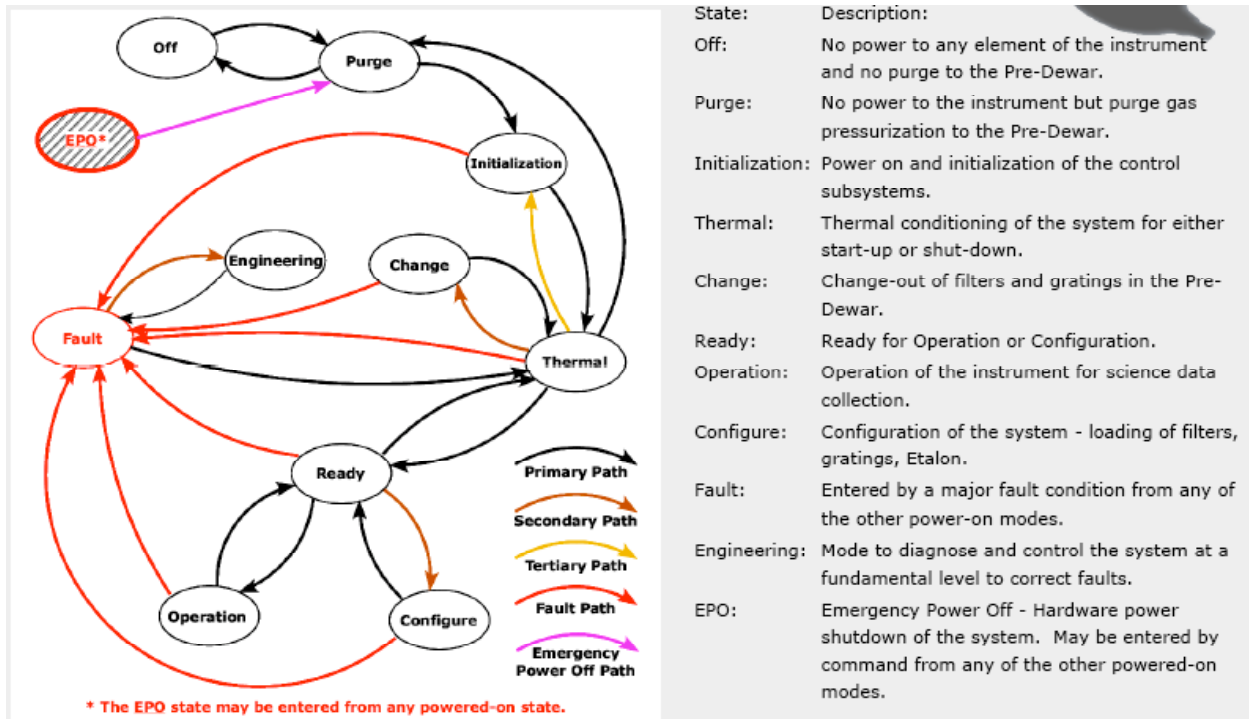


Figure 5-67. Instrument-level State Diagram (get original from Don?)

5.6.1.3. Instrument-level Control Software

This Execution Engine is embedded in the top-level layer, which maintains communications with the networked Graphical User Interface. Commands come in, and status (telemetry) goes out to other systems in the observatory. Figure 5-68 outlines the architecture of the Execution Engine.

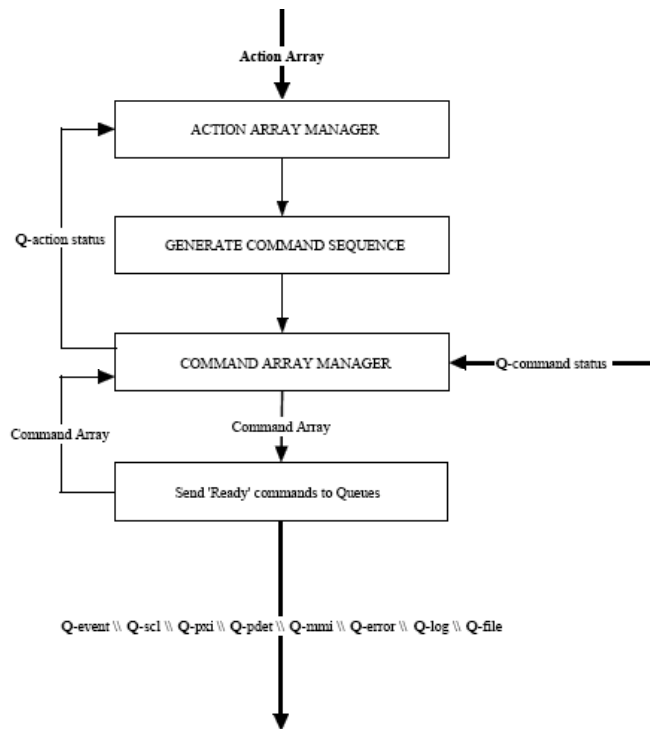


Figure 5-68. Execution Engine.

The low-level command queues implement the functionality of PCON. As the command queues are being processed, the modules report their status back up to the Execution Engine. **Figure 5-69** shows the Status Managers.

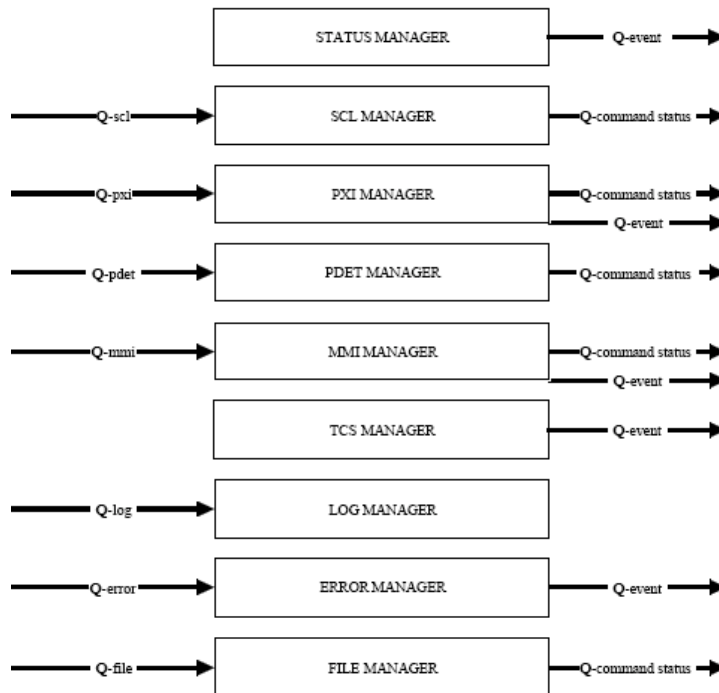


Figure 5-69. Status Managers.

The instrument-level RSS-VIS control system software modules were delivered to SALT, where Anthony Koeslag integrated them into a higher-level “observatory aware” system. We plan to enhance his PCON control program by developing NIR mechanism state machines, adding them to the existing PCON program (which we already have back in Madison), and extending the command and data layer to encompass the added controls and data.

5.6.1.4. Graphical User Interface

The GUI is a stand-alone LabView module that connects to PCON via ethernet. It can connect from PCON itself on a local host connection, or from another SALT control computer. **Figure 5-70** outlines what is called the “Remote MMI.”

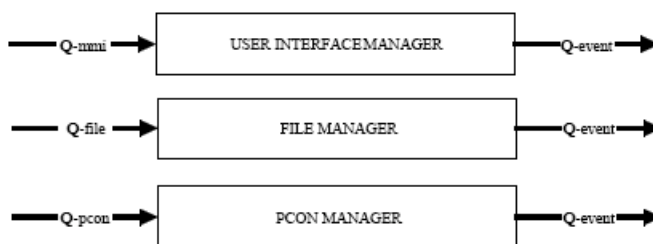


Figure 5-70. Remote MMI (Graphical User Interface)

We will enhance the GUI with new tabs for the RSS-NIR functionality, and embed the commands and procedures exactly as is done for the RSS-VIS. **Figure 5-71** shows one of the control panels on the existing “Remote MMI.”

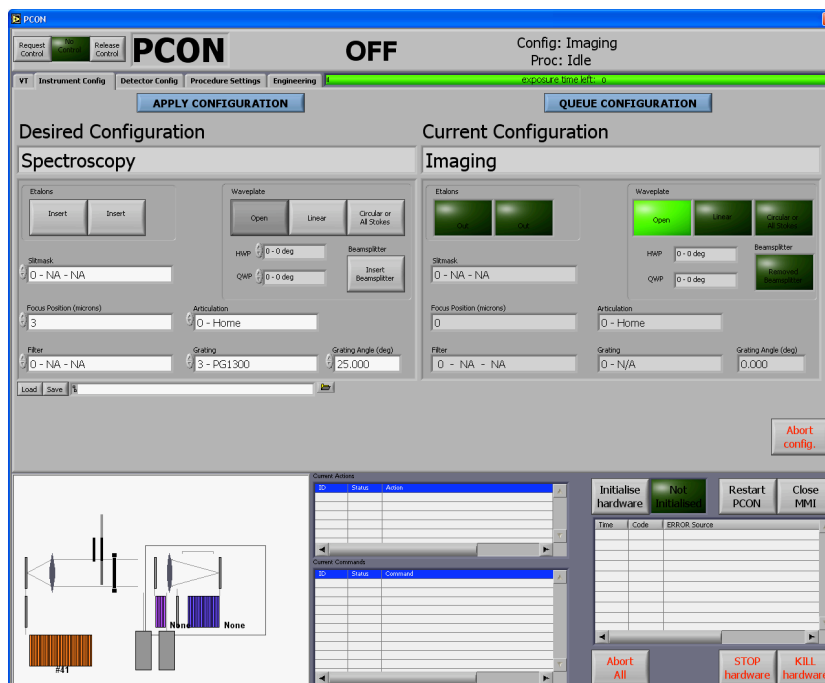


Figure 5-71. Remote MMI Configuration Panel

5.6.1.5. Mechanism Simulators

For the RSS-VIS development, we implemented simulator modules that could be “swapped in” in place of the LabView hardware drivers. After the swap, the state machines run exactly as designed, but without having to have any hardware attached. This worked very well for us; it allowed software development in advance of having the actual mechanism, and freed the developers from needing access to the instrument while implementing higher-level functions. We intend to repeat this amazing feat.

5.6.1.6. Development Plan

The development plan is to

- Specify the desired functionality of the mechanisms
- Create the state diagrams that produce the desired behavior
- Code the state machines and driver-level simulators
- Embed the state machines in the higher-level configuration management modules
- Specify the commands, procedures, and data clusters
- Extend the PCON program as needed
- Extend the GUI as needed

Note that all but the last two tasks can be done without awareness of the RSS-VIS side.

5.6.2. Implementation

We will implement the control system software in a way that leverages all of the work already invested for RSS-VIS. Some changes are necessary:

- Windows XP instead of 2000
- LabView 8 instead of 6.1
- Compact-RIO instead of PXI

The principal change is in moving from the PXI technology to Compact-RIO (see **Figure 5-72**). This is driven by our desire to reduce the wire harness by using a networked control architecture instead of the fan-out style based on the PXI chassis. Compact-RIO is a network-based small footprint technology that supports motion control, and digital and analog I/O. Each of the small-footprint 4- or 8-slot nodes features an embedded processor capable of running a stand-alone “LabView Real-Time” program.



Figure 5-72. Compact-RIO distributed control system.

We will use the embedded controllers to perform the hardware-based interlock protection and to manage the stand-alone thermal control system. On RSS-VIS, hardware interlock protection was performed by JTAG-loaded CPLDs on a custom circuit board, programmed using a commercial product from Xilinx; on RSS-NIR, this function will be self-hosted on PCON under the same LabView umbrella as the rest of the RSS control system.

LabView 8 is required by the Compact-RIO technology, and Windows 2000 is no longer a viable choice. The move to LabView 8 has been discussed with Janus Brink and Anthony Koeslag, and they see no issue with upgrading PCON to this version of LabView. NI assures us that the DataSocket technology used for network communications at SALT is compatible across versions.

5.6.3. Thermal Control

RSS-NIR will have an active thermal control system. Thermal control functions include

- Pre-dewar temperature monitoring
- Pre-dewar heaters control
- Pre-dewar skin temperature monitoring
- Pre-dewar skin heaters control

The control and monitoring functions will be implemented as firmware in a Compact-RIO FPGA.

5.6.4. Motion Control

RSS-VIS has 8 axes of motion control, 3 in the collimator and 5 in the camera. RSS-NIR will add 9 more. We have targeted National Instrument's Compact-RIO line of motor controllers. These will integrate well with the RSS-VIS PXI-7334 stepper motor controllers under the management tool "Measurement and Automation Explorer".

The motorized axes are

1. Optics Storage Assembly
2. Filter insertion
3. Grating insertion
4. Grating rotation
5. Etalon insertion
6. Insertion rotation
7. Camera focus
8. Camera filter wheel (in Dewar)
9. Camera articulation

5.6.5. Data Flow

Data flow will follow the design of RSS-VIS. A detector control computer, NDET, will operate along side of PDET, and provide the same services. These services include

- exposure setup (exposure time, fowler sampling)
- exposure control (start, stop)
- data readout and capture

- keyword collection and FITS file writing
- quick-look display and data reduction

We intend to acquire NDET in the same way that we used for PDET: as a turnkey system and delivered ready to go. We will use the PDET interface modules, modified as necessary for the Teledyne infrared sensor and JADE-2 control electronics, to specify the required functionality in the procurement of NDET.

There is no flow of image data from NDET to PCON.

5.7 Operating Modes

The main operational modes of RSS-NIR are 1) Imaging, 2) Long slit spectroscopy, 3) Multi-object spectroscopy (MOS), 4) Fabry-Perot imaging, and 5) Polarimetry, which can be added to any of the previous 4 modes. These duplicate the modes of the visible arm of RSS, except for the ones requiring special detector modes of operation. The HgCdTe detector used in RSS-NIR does not have charge shuffling capabilities like a CCD, so all modes utilizing those capabilities are not possible with RSS-NIR. **Figure 5-73** summarizes the operational modes available for RSS-NIR and also indicates the RSS modes that will not be available: the high-speed, shuffle, and drift scan detector configurations.

Optics configuration			Detector Configuration			
Config	Pol	Slit	Normal	Hi Spd	Shuffle	Drift
Imaging	No	No	X	x		x
	L,C,S	No	x			
		Multislit	X		x	
VPH Spectroscopy	No	No	x			x
		Longslit	X	X	x	
		Multislit	X		x	
	L,C,S	Longslit	X		x	
		Multislit	X			
Fabry-Perot	No	No	X		x	
	L,C,S	No	x			

Figure 5-73. Summary of the modes of operation for RSS-NIR, with an indication of RSS modes that are not available with the NIR detector.

Each of these modes uses a variety of the 4 types of mechanisms in the instrument: 1) the focal plane slits and masks; 2) the dispersive elements, consisting of either volume phase holographic gratings or the

Fabry-Perot etalon; 3) the polarizing optics, two waveplates and a polarizing beamsplitter, and 4) broadband and narrowband filters in the pre-dewar, and long wavelength cutoff filters in the cryogenic Dewar. Permutations of these mechanisms combine to give RSS-NIR the versatility to address a broad range of astrophysical research programs.

5.7.1 Imaging

The imaging mode of RSS-NIR is performed with the camera in the non-articulated position. Standard J and H broadband filters are provided inside the pre-dewar, though H will be H-short due to our detector cutoff at 1.7 microns. Narrowband filters for use as order blocking filters in the Fabry-Perot mode also reside in the cooled pre-dewar enclosure. The cryogenic Dewar contains 3 long wavelength blocking filters, primarily for use in spectroscopy mode, but available for imaging as well.

Science uses:

- Broadband imaging in J and H-short bands over entire 8 arcmin FOV
- Narrowband imaging using Fabry-Perot filters over entire 8 arcmin FOV
- Imaging for MOS setups

Involved mechanisms:

- Pre-dewar filter inserter
- Cryogenic Dewar filter inserter (if blocking filter required)

Target acquisition: Target acquisition is performed using either the SALTICAM or guide probes.

Tracking during exposure: Uses guide probes or SALTICAM w/dichroic).

5.7.2 Longslit Spectroscopy

Single slit spectroscopy is offered with the same suite of slits as the visible arm, 7 long slits available at the focal plane slit mask magazine. The only difference is that the back sides will be gold coated to lower the thermal emissivity for the NIR arm. Slits vary from 0.45" to 3.0" in width and are 8' long. A complement of 4 VPH gratings cover the operational wavelength range from 0.9 to 1.7 microns at resolutions of $R = 2000 - 7000$. An additional low resolution grating with $R \sim 800$ allows coverage of the entire spectral range in one observation for targets much brighter than the sky. This option will be useful for time variability studies of non sky-limited bright objects where simultaneous spectral coverage is important. This low resolution grating will not be a VPH because of their poor performance in this regime.

Science Uses:

- Conventional long slit spectroscopy over 7.5' fields at arbitrary position angles.

Involved Mechanisms:

- Slit magazine
- Grating inserter
- Grating rotation
- Camera articulation
- Cryogenic filter inserter for long wavelength blocking

Typical sequence of operation:

- Select grating and slit to be used; insert elements
- Rotate grating and camera to required positions
- Rotate rotator to desired position angle
- Image field with slit viewing camera (SALTICAM)
- Locate desired object and move tracker to place object in slit
- Begin tracking/guiding using either guide probes or slit viewer
- Begin exposure

Target acquisition: By guide probe, and using visual peak-up with SALTICAM as slit viewing camera.

Tracking during exposures: By guide probe, or by reflected light from slit viewed by SALTICAM.

5.7.3 Multi-Object Spectroscopy

Science Uses:

- Multi-object spectroscopy in fields up to 6' diameter. Redshift surveys. Spectral surveys of stars and galaxies.

Involved Mechanisms:

- Grating inserter
- Grating rotator
- Slitmask magazine for custom masks
- Camera articulation
- Cryogenic filter inserter for long wavelength blocking

Target acquisition: Multi-stage process, similar to that at other multi-object spectrographs.

- Afternoon flats to locate positions of slitmask guide star boxes on detector
- Image of science field with SALTICAM (or direct imaging with RSS-NIR)
- Movement of tracker to align science field with anticipated mask position
- Insertion of slitmask
- Image field with RSS-NIR to fine-tune pointing
- Final tweak of tracker position to center objects in slits
- Insert and rotate grating
- Articulate camera
- Begin guiding using guide probes
- Start science exposures

Anticipated acquisition time required: 15 minutes (this is increased from the 5 minutes stated in the PFIS documentation, based on experience at the HET)

Tracking during exposure: By guide probe

Limitations: No slit viewing system is available

5.7.4 Fabry-Perot Imaging

Science Uses:

- High resolution imaging spectroscopy of multiple or extended objects. Dynamical studies of HII regions, star clusters, galaxy clusters.

Involvement Mechanisms:

- Pre-dewar filter inserter
- Cryogenic filter inserter (if long wavelength blocking is required)
- Etalon inserter

Mode of operation:

- Acquire field using SALTICAM
- Begin tracking using guide probe
- Select and insert appropriate blocking filter
- Insert and tune etalon
- For each wavelength desired
 - Set etalon
 - Wavelength zero point calibration
 - Expose and readout detector
 - Obtain transmission measurement from guide system

Target acquisition: By guide probe, and using visual peak-up with SALTICAM

Tracking during exposures: By guide probe

5.7.5 Polarimetry

Polarimetry can be added to any of the main instrument modes of operation. A standard slitmask is inserted into the focal plane to block the top and lower quarters of the field of view. This is required to limit the size of the input image because the polarizing beamsplitter later in the optical path shears the two orthogonal polarizations in the science field onto the upper and lower halves of the detector for recording.

5.7.5.1 Imaging Linear Polarimetry

Sciences Uses:

- Broadband or narrowband polarimetric surveys of interstellar polarization; intrinsic stellar polarization

Involvement Mechanisms:

- Narrowband filter inserter (if required)
- Cryogenic broadband filter inserter (if required)
- 1/2-waveplate
- Polarizing beamsplitter
- Slitmask mechanism (standard slitmask #2)

Target acquisition: By guide probe and direct imaging with RSS-NIR or SALTICAM

Mode of operation:

- Point to field using guide probes or imaging on RSS-NIR or SALTICAM to acquire
- Begin guiding using guide probes
- For each of 8 1/2-waveplate positions
 - Rotate waveplate to desired angle
 - Expose

- Readout

Limitations: Spatial field of view is limited to 4' x 8'

5.7.5.2 Imaging Circular Polarimetry

Science Uses:

- Broadband or narrowband circular polarimetric surveys of interstellar polarization; intrinsic stellar polarization; low-resolution spectral polarimetry

Involved Mechanisms:

- Narrowband filter inserter (if required)
- Cryogenic broadband filter inserter (if required)
- 1/2-waveplate
- 1/4-waveplate
- Polarizing beamsplitter
- Slitmask magazine (standard slitmask #2)

Target acquisition: By guide probe and direct imaging with RSS-NIR or SALTICAM

Mode of operation:

- Point to field using guide probes or direct imaging on RSS-NIR or SALTICAM to acquire
- Begin guiding using guide probes
- For each of 8 1/2-waveplate positions
 - Rotate waveplate to desired angle
 - For each of 2 1/4-waveplate positions
 - Expose
 - Readout orthogonal polarizations (in separate locations on detector) in one image

5.7.5.3 Fabry-Perot Imaging Linear Spectral-Polarimetry

Science uses:

- R=2500 imaging spectropolarimetric studies of extended objects such as HII regions, reflection nebulae, star cluster, young stellar associations, nuclei of galaxies

Involved Mechanisms:

- Narrowband filter inserter
- Etalon slide
- 1/2-waveplate
- Polarizing beamsplitter
- Slitmask magazine (standard slitmask #2)

Target acquisition: By guide probe and direct imaging with RSS-NIR or SALTICAM

Tracking during exposures: By guide probe

Mode of operation:

- Point to field using guide probes or direct imaging on RSS-NIR or SALTICAM to acquire
- Begin guiding using guide probes

- For each wavelength desired
 - Select and insert order blocking filter
 - Set etalon
 - Wavelength zero point calibration
 - For each of 8 $\frac{1}{2}$ -waveplate positions
 - Rotate waveplate to desired angle
 - Expose
 - Readout orthogonal polarizations (in separate locations on detector) in one image
 - Wavelength zero point calibration

Limitations: Field of view limited to central 4' x 8'

5.7.5.4 Fabry-Perot Imaging Circular Spectral-Polarimetry

Science Uses:

- R=2500 imaging circular spectropolarimetric studies of extended objects such as HII regions, reflection nebulae, star clusters, young stellar associations, nuclei of galaxies

Involved Mechanisms:

- Narrowband filter inserter
- Etalon slide
- $\frac{1}{2}$ -waveplate
- $\frac{1}{4}$ -waveplate
- Polarizing beamsplitter
- Slitmask magazine (standard slitmask #2)

Target acquisition: By guide probe and direct imaging with RSS-NIR or SALTICAM

Tracking during exposures: By guide probe

Mode of operation:

- Point to field using guide probes or direct imaging on RSS-NIR or SALTICAM to acquire
- Begin guiding using guide probes
- For each wavelength desired
 - Select and insert order blocking filter
 - Set etalon
 - Wavelength zero point calibration
 - For each of 8 $\frac{1}{2}$ -waveplate positions
 - Rotate waveplate to desired angle
 - For each of 2 $\frac{1}{4}$ -waveplate positions
 - Expose
 - Readout orthogonal polarizations (in separate locations on detector) in one image
 - Wavelength zero point calibration

Limitations: Field of view limited to central 4' x 8'

5.7.5.5 Longslit Linear Spectral-Polarimetry

Science Uses:

- R=2000 to R=7000 slit spectral polarimetric studies of cataclysmic variables, young stellar objects, stars with disks, AGN, interstellar absorption features

Involved Mechanisms:

- Cryogenic filter inserter for long wavelength blocking filter
- Grating inserter
- Camera articulation
- $\frac{1}{2}$ -waveplate
- Polarizing beamsplitter
- Slitmask mechanism (long slit plate #7)

Target acquisition: By slit viewing SALTICAM

Tracking during exposures: Guide probe or reflected light from slit viewed by SALTICAM

Mode of operation:

- Point to field using guide probes or slit-viewing SALTICAM to acquire
- Place object on slit
- Begin guiding using guide probes or slit-viewing camera
- For each of 8 $\frac{1}{2}$ -waveplate positions
 - Rotate waveplate to desired angle
 - Expose
 - Readout orthogonal polarizations (in separate locations on detector) in one image

Limitations: Only central 4' x 8' of longslit spatial field is available. Slit plate #7 is designed for use as the main spectropolarimetric longslit.

5.7.5.6 Longslit Circular Spectral-Polarimetry

Science Uses:

- R=2000 to R=7000 slit spectral polarimetric studies of cataclysmic variables, young stellar objects, stars with disks, AGN, interstellar absorption features

Involved Mechanisms:

- Cryogenic filter inserter for long wavelength blocking filter
- Grating inserter
- Camera articulation
- $\frac{1}{2}$ -waveplate
- $\frac{1}{4}$ -waveplate
- Polarizing beamsplitter
- Slitmask mechanism (long slit plate #7)

Target acquisition: By slit viewing SALTICAM

Tracking during exposures: Guide probe or reflected light from slit viewed by SALTICAM

Mode of operation:

- Point to field using guide probes or slit-viewing SALTICAM to acquire
- Place object on slit
- Begin guiding using guide probes or slit-viewing camera
- For each of 8 1/2-waveplate positions
 - Rotate waveplate to desired angle
 - For each of 2 1/4-waveplate positions
 - Expose
 - Readout orthogonal polarizations (in separate locations on detector) in one image

Limitations: Only central 4' x 8' of longslit spatial field is available. Slit plate #7 is designed for use as the main spectropolarimetric longslit.

5.7.5.7 Multi-slit Linear Spectral-Polarimetry

Science Uses:

- Multi-object linear spectropolarimetry in fields up to 4' diameter. Polarimetric surveys.

Involved Mechanisms:

- Cryogenic filter inserter for long wavelength blocking filter
- Grating inserter
- Camera articulation
- 1/2-waveplate
- Polarizing beamsplitter
- Slitmask mechanism (custom slitmasks, upper 4' only)

Target acquisition: Multi-stage process, similar to that in use at other multi-object spectrographs

Mode of operation:

- Afternoon flat fields to locate positions of slitmask guide star boxes in detector
- Image of science field with SALTICAM (or direct image with RSS-NIR)
- Movement of tracker to align science field with anticipated mask position
- Insert slitmask
- Image of field to fine-tune pointing
- Final tweak of tracker position to center objects in slits
- Insert grating
- Begin guiding using guide probes
- Articulate camera
- For each of 8 1/2-waveplate positions
 - Rotate waveplate to desired angle
 - Expose
 - Readout orthogonal polarizations (in separate locations on detector) in one image

Tracking during exposures: By guide probe

Limitations: No slit-viewing system is available

5.7.5.8 Multi-slit Circular Spectral-Polarimetry

Science Uses:

- Multi-object circular spectropolarimetry in fields up to 4' diameter. Polarimetric surveys.

Involved Mechanisms:

- Cryogenic filter inserter for long wavelength blocking filter
- Grating inserter
- Camera articulation
- $\frac{1}{2}$ -waveplate
- $\frac{1}{4}$ -waveplate
- Polarizing beamsplitter
- Slitmask mechanism (custom slitmasks, upper 4' only)

Target acquisition: Multi-stage process, similar to that in use at other multi-object spectrographs

Mode of operation:

- Afternoon flat fields to locate positions of slitmask guide star boxes in detector
- Image of science field with SALTICAM (or direct image with RSS-NIR)
- Movement of tracker to align science field with anticipated mask position
- Insert slitmask
- Image of field to fine-tune pointing
- Final tweak of tracker position to center objects in slits
- Insert grating
- Begin guiding using guide probes
- Articulate camera
- For each of 8 $\frac{1}{2}$ -waveplate positions
 - Rotate waveplate to desired angle
 - For each of 2 $\frac{1}{4}$ -waveplate positions
 - Expose
 - Readout orthogonal polarizations (in separate locations on detector) in one image

Tracking during exposures: By guide probe

Limitations: No slit-viewing system is available

5.7.6 Simultaneous Visible-NIR Operation

Simultaneous operation of both the visible and NIR instruments has been envisioned from the beginning. After configuration and verification of the placement of common components that affect both spectrographs, such as the slitmasks and waveplates, further operation and data acquisition of each spectrograph will be set up as two separate threads to run each individually, but simultaneously. This will avoid the situation of either arm waiting on the other during the data acquisition phase.

One complication for simultaneous visible and NIR observations is the different observing style required in the near infrared. Because the night sky is so bright and variable in this part of the spectrum, observations are normally limited to relatively short exposures and the telescope is nodded to slightly different locations on the sky for each exposure. In the case of spectroscopy, this would mean nodding the science target along the slit, if its subtended angle on the sky is small. This technique improves the quality of the resulting sky subtraction in the presence of a highly variable background, while allowing each

exposure to still contain the science target. In the case of spectroscopy on extended objects that fill the slit, nods would be off to sky areas away from the science target.

In imaging mode on an 11-m telescope, exposure times in most cases should be short enough that sky variations will not be an issue. If, however, long exposures are desired, multiple visible and NIR images can be collected simultaneously, nodding the telescope on the sky between exposures. Then the visible images can be sky-subtracted and co-added in the same way as the NIR images.

Simultaneous visible and NIR observations will also occur in the case of spectroscopy on faint sky-limited objects for which very long total exposure time and broad spectral coverage is required. Multiplexing with both spectrographs at once will significantly decrease the total required observing time, even if simultaneity of the obtained spectra may not be a specific requirement of the science program. For cases where exposure times of individual frames on the NIR side need to be shorter than on the visible side and the objects subtend small angles on the sky, we have the capability to nod along the slit by 10's of arcsec using the NIR fold mirror.

For extended objects that fill the slit, nodding off the field by many arcminutes will have to be achieved using the telescope. In this case exposure times may have to be selected as a compromise between sky variations on the NIR side and read noise limits on the visible side.

5.8. SALT Facility Interface Control

The interface control between the SALT facility and the RSS-NIR instrument is managed by a number of elements that includes

1. Bi-weekly teleconferences between SALT and RSS-NIR personnel
2. The SALT RSS-NIR Questions document that is passed back and forth between SALT and RSS-NIR to document interface questions and the responses
3. The RSS Interface Control Document (ICD) formally documents the requirements and interfaces between the SALT facility and the RSS, including both the VIS and the NIR sides.

A number of issues that are currently under discussion are:

5.8.1. ADC Optical Performance

Optical performance requirements on the SALT - ADC. The requirements for the ADC should be such that the ADC cannot affect the NIR atmospheric dispersion when the VIS and NIR are operating in simultaneous operation.

5.8.2. Moving Baffle Gold Coating.

Gold coat back of the moving baffle to reduce thermal emissions from that surface that would affect the NIR instrument.

5.8.3. Calibration Source Change.

Replace the "red" light guide with a new calibration fiber that extends the spectral range into the NIR. Replacing one of the single-gas Pen-Ray lamps with a new mixed-gas lamp. The new Pen-Ray lamp should be able to use the existing Pen-Ray's supply.

5.8.4. ADC Stray Light.

Add a requirement to the ICD to have reflective foil be added to the backsides of M4 and M2 to reduce the thermal emissions from those surfaces that would affect the NIR instrument. Ockert Strydom indicated that the instrument can see the back side of M2, but coating the backside of M4 and M2 may cause other "stray light" problems that may require coating of other parts of the SAC assembly.

5.8.5. Data Path from SALT Facility to Cape Town.

We are working to define the data path from SALT facility to the outside world, and its capability. Ockert Strydom has indicated that there is a 384Kb/s link currently, and that they want to go to a 1Gb/s line in the future, but that depends upon a number of factors.

5.8.6. Data Archiving capability at SALT.

We need to determine data archiving capabilities at SALT. Currently, the data is pipelined to Cape Town, and data reduction is done there with some archiving of data at the SALT facility.

5.8.7. Labview Version Update and Compatibility.

SALT is currently using LabView version 6.0 and NIR wants to use 8.6. As indicated in section 5.6, SALT is open to RSS-NIR using version 8.6.

5.8.8. Critical Power Distribution.

To plan for emergency shut down of the RSS-NIR, we need to define:

- What is the power distribution system for "critical power" in case of a main grid failure?
- What is the UPS capability and how much is it loaded at the current time?
- Are there any signals that would be able to indicate to our control system what power source we are running on?
-

These questions relate to the ability to control the temperature rise of the Pre-dewar in case of a major power failure or our requirement for another UPS for our critical loads.

6. MANAGEMENT

6.1. Structure and Organization

The RSS-NIR project team consists of staff from the University of Wisconsin, Rutgers University, University of California – Santa Cruz, and John Hopkins University. The principal investigator is Prof. Andrew Sheinis and the project scientist is Dr. Marsha Wolf. The balance of the science team includes co-investigators Ken Nordsieck, Matthew Bershady, and Amy Barger at the University of Wisconsin and Theodore Williams at Rutgers University.

The project organization chart, shown in **Figure 6-1**, shows the structure of the project team. The role and experience of key staff members is described below.

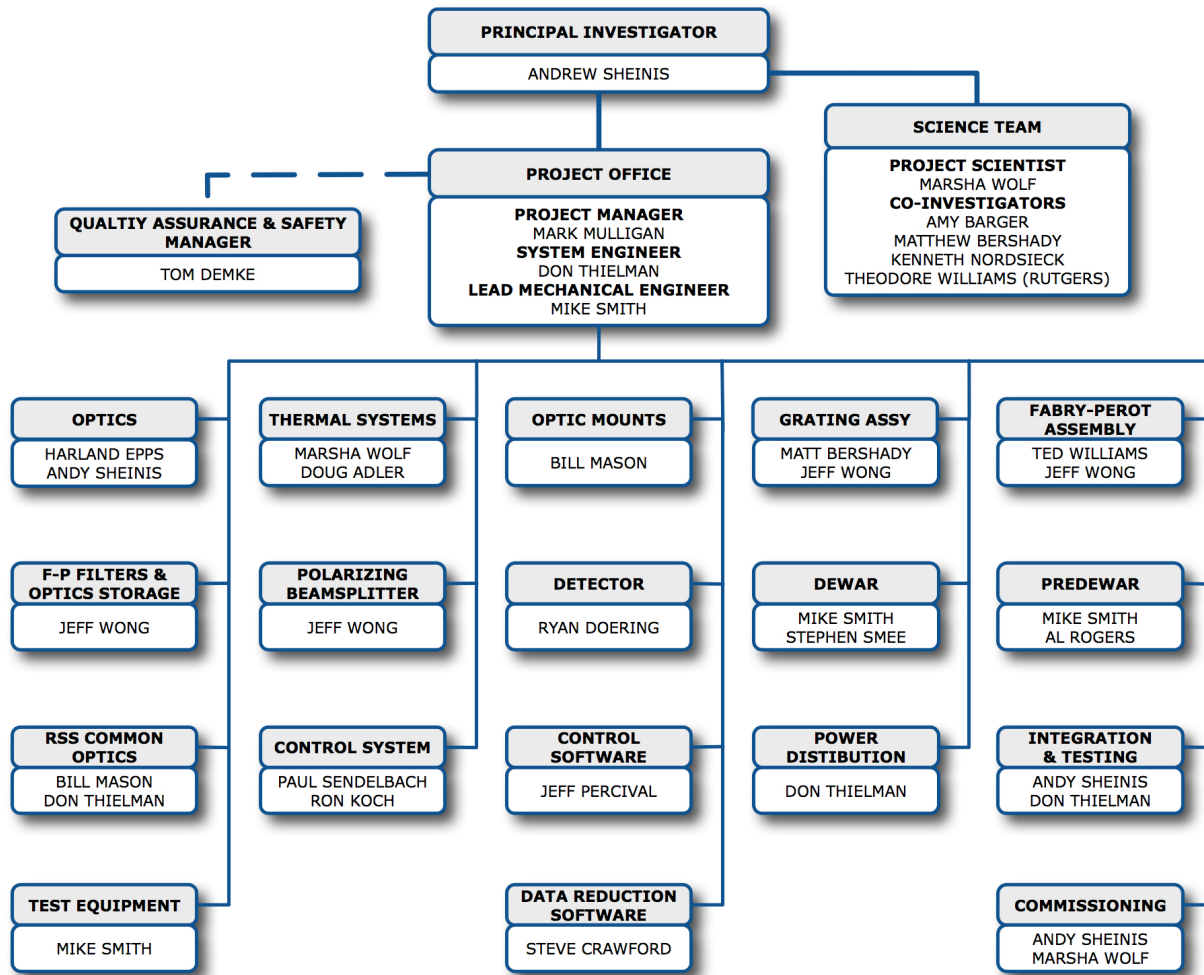


Figure 6-1. RSS-NIR Project Organization Chart.

6.1.1. Principal Investigator (PI)

Andrew Sheinis, University of Wisconsin, has the overall authority and responsibility for the delivery of the instrument to the SALT Foundation. He is responsible for defining the scientific objectives of the instrument to meet his and the science team’s research goals. The PI provides the programmatic guidelines to which he would like the project managed. Ultimately, the PI is responsible for all scientific, technical, financial, and programmatic decisions. For this project, Dr. Sheinis will also have an integral role in the design, fabrication, integration, and testing of the optical system. He has over 25 years of experience in the development of optical instrumentation and was the Project Engineer on the Echelle Spectrograph and Imager for the Keck Observatory before coming to the UW.

6.1.2. Project Scientist (PS)

Marsha Wolf, University of Wisconsin, is responsible for formally defining and documenting the instrument scientific objectives and ensuring they are met within the design and operation limits of the

instrument and facility. In addition, she provides guidance to the PI on instrument scientific and programmatic matters. Specific to his project, Dr. Wolf is responsible for modeling the optical and thermal performance of the instrument. She has over 20 years of experience in electrical engineering, electro-optics, and astronomy. For her graduate work, she supported the HET spectrograph development.

6.1.3. Co-Investigators (Co-I)

Kenneth Nordsieck, University of Wisconsin, advises on the overall instrument design relying on his lifetime of experience with the development of astronomical instruments. As the PI for the RSS-VIS, he functions as the advocate for the RSS-VIS to ensure that the RSS-NIR design does not have a negative impact on the RSS-VIS and Ken will support commissioning activities.

Matthew Bershad, University of Wisconsin, along with the PS, is formally defining and documenting the instrument scientific objectives. He and the PS are working with the systems engineer and lead mechanical engineer to ensure the science objectives are properly flowed into engineering requirements. Matt will support commissioning.

Amy Barger, University of Wisconsin, will be providing supporting for the commissioning of the instrument.

Theodore Williams, Rutgers University, is responsible for the specification, implementation, and testing of the Fabry-Perot etalon. Dr. Williams performed the same function for the RSS-VIS instrument and will support commissioning.

6.1.4. Project Manager (PM)

Mark Mulligan, University of Wisconsin, reports directly to the PI. The PM supports the PI in defining programmatic guidelines and is then responsible for their execution. He is responsible for managing the project on a day-to-day basis. The PM works together with the appropriate engineering disciplines to formulate plans and processes ensuring good communication across the project. The PM is responsible for executing the agreed upon project development plans while ensuring the project scope, schedule, and budget are met. Mark has 18 years of experience as an engineer and project manager working on instrument development projects for ground, air or space-based platforms. Recently, he was the project manager for drill system in support of the IceCube neutrino detector at the South Pole. Prior to that, he was the deputy project manager for IceCube.

6.1.5. Systems Engineer (SE)

Don Thielman, University of Wisconsin, provides oversight for the entire design. The SE is responsible for flowing the science requirements into engineering requirements to define the instrument design. He is responsible for assessing the current design against the functional performance requirements and the operational modes (as defined in the operational concepts definition document), developing and maintaining the required interface control documents to manage internal and external interfaces, ensuring acceptance testing (subsystem and instrument) verifies all performance requirements, supporting instrument commissioning, and developing an Operations and Maintenance Manual. In addition, the SE is tasked with identifying, tracking, and mitigating design, integration, and testing risks. Don has over 25 years of experience as an electrical and systems engineer. He was recently the systems engineer for the successful development of a deep ice sheet coring drill system that is capable of providing an unprecedented 122 mm diameter core to a depth of 3500 meters.

6.1.6. Quality Assurance and Safety Manager (QAS)

Tom Demke, University of Wisconsin, is responsible for assuring that all instrumentation meets its design and safety requirements. The QAS plays an integral role in instrument development as he is responsible for implementing the project safety program, ensuring design reviews are conducted, conducting safety reviews, checking design documentation, and examining all test procedures and results. The QAS works together with the PI and PM to integrate safety and quality into the instrument development. Tom has over 20 years of experience in quality assurance. He was the QAS on IceCube from the project start through the first drilling seasons and has been the QAS on multiple projects ranging in scope and size since.

6.1.7. Lead Mechanical Engineer

Michael Smith, University of Wisconsin, is responsible for leading the mechanical design effort. Michael is coordinating the work of two other engineers and a designer. He was the lead engineer on the RSS-VIS instrument, which provides him with an intimate knowledge of the existing RSS hardware to which the RSS-NIR must integrate. His knowledge of the RSS is an invaluable resource to the project.

6.1.8. Optical Designer

Harland Epps, University of California – Santa Cruz, working with the PI, is responsible for the optical design. Dr. Epps has a lifetime of experience in optical design of astronomical instruments and his list of work includes the HIRES, LRIS, ESI, and DEIMOS instruments at the W.M. Keck Observatory as well as other designs on almost all major telescope observatories.

6.1.9. Dewar Design Consultant

Stephen Smee, John Hopkins University, is responsible for the design and testing of the RSS-NIR Dewar. Dr. Smee, Manager of the Instrument Development Group, has recently been the Lead Engineer on two instruments that integrated infrared detectors into cryogenic Dewars. One is the WIYN High Resolution Infrared Camera (WHIRC), which just completed its successful commissioning in November 2008. The second system was for the 4STAR infrared survey camera for the Magellen telescope.

6.1.10. Detector Development

Ryan Doering, University of Wisconsin, is responsible for the checkout, characterization, integration, and testing of the detector. This is a significant role on the project and Dr. Doering held a similar role for successful the WHIRC instrument.

6.2. Project Management

Mark Mulligan is responsible for the overall project management. As described above, he is responsible for executing the agreed upon project development plans while ensuring the project scope, schedule, and budget are met. As indicated in Figure 6.1, technical leads have been assigned to each subsystem. They are responsible for ensuring that the subsystem design meets or exceeds its requirements, which are flowed down from the Functional Performance Requirements Document. The project work is coordinated through a weekly technical design meeting and the status, progress and issues are handled in a separate

weekly meeting. Communication among the leads has been well coordinated and is aided by the fact that most are on the UW campus.

6.3. Risk Assessment and Management

There are four areas of risk that are assessed, monitored, and mitigated throughout the life of the project: safety, technology, cost, and schedule.

6.3.1. Technology

The project identified a few technical risks early on that have been addressed to ensure the success of the instrument. They are described below.

1. **Thermal Stray Light.** Since the RSS-NIR is a semi-warm NIR spectrograph, thermal stray light noise is understandably identified as an issue. Results from previous semi-warm near-infrared spectrograph implementations have shown difficulties in achieving the predicted instrument sensitivities, due to higher than expected background levels. In many cases these background levels have been orders-of-magnitude above predictions. This can be due to unforeseen ray paths past baffles and through cutoff filters at high angles of incidence. This type of error has in some cases been a “show stopper” for past instruments and thus is what the RSS-NIR team has considered the greatest risk to the design.

In order to mitigate this risk, we have devoted very significant effort up front to developing the in-house capability to analyze and model these problems. Unlike previous systems, we are performing a detailed thermal stray light analysis *in advance of* and *in parallel with* the mechanical design. Dr. Wolf is performing a thermal stray light analysis of the instrument using Advanced Systems Analysis Program (ASAP). The objective is to fold into the design the results from the analysis to keep the instrument sky limited in spectroscopy and Fabry-Perot imaging modes. As the design further matures, the modeling will determine where to place baffling and the design of the cold pupil mask. The analysis has already had an impact.

- The retaining ring of the field lens is being redesigned to a three-point mount to dramatically reduce its thermal signature.
- Cooling the slit has been evaluated and would allow sky-limited spectroscopy out to a wavelength of 1.7 microns. This option is conceptually feasible and may be added as a later upgrade.
- The multi-slit masks will be gold coated to reduce thermal emission.

This level of detail is not typically done for astronomical instruments, but this is a clear case where it will make the difference in the success of the instrument. This analysis and the results are described in detail in section 5.3.

2. **Flexure.** The second most significant risk to RSS-NIR performance is flexure. We define flexure as any motion of the optical system producing image motion on the detector. This can be due to gravity which is entirely repeatable or other causes such as bearing induced strains, which are not repeatable.

The RSS is mounted at prime focus of the SALT telescope on an anti-image-rotation bearing, the rho stage. This in turn is mounted to a 6-axis tracker, which comprises a large two axis (X-Y)

stage and a hexapod (angle and piston). The tracker allows the instrument payload to move in declination and position angle on the sky, resulting in a change of gravity vector seen by a coordinate system located on the instrument of 37 ± 6 degrees in altitude and 230 degrees in azimuth.

In order to minimize passive flexure and thermal effects with a minimum of weight and materials, the RSS-VIS structure was designed as a heat-treated open truss weldment of hollow Invar tubes. Its envelope is a cylinder 1.5m long and 3 m in diameter, centered on the focal plane, with the instrument placed mostly above (beyond) the focal plane. *The RSS-NIR will mount to the same structure. It has all the mounting locations for the RSS-NIR optical/mechanical/electrical components.* The entire structure is mounted to 12 hard points on a 2 m diameter ring near the focal plane.



Figure 6-2. *RSS-VIS shown in its flexure test and integration platform. RSS-NIR will use a similar platform but will have the ability to vary the azimuth angle.*

Lab flexure tests were performed before installation in both Madison and Cape Town. These tests were done on the RSS dolly. The dolly has a single pivot axis, which allows the instrument to be tilted to $\pm 37^\circ$ around that axis, see **Figure 6**. For the RSS-VIS tests the instrument was mounted with the tilt axis along the camera axis in the unarticulated position.

For the imaging mode flexure tests, the instrument was configured with a pinhole mask in the slitmask and a calibration source. A series of images were taken as the instrument was tilted from side to side on the dolly. These spot positions on these images were then compared and the flexure quantified. The results showed a large amount of field rotation and some lateral shift.

For the spectroscopy mode flexure tests, the instrument was configured with a slitmask with a row of pinholes down the center, a line lamp in the calibration system and the camera and grating articulated to 90° and 45° , respectively. In the same manner as above, the instrument was tilted and images taken. The results showed a large amount of image motion perpendicular to the dispersion axis, which was shown to be due to grating rotation about the optical axis.

Further flexure testing was performed on the telescope. The instrument setup was much the same but the rho-stage was used to change the gravity vector on the instrument. Final flexure testing did not meet the spec of 0.15 arcsec/track perpendicular to dispersion by about 3x, but did meet the spec of 0.1 arcsec/track parallel to dispersion. These measurements were shown to be close enough to the specification to be of little scientific impact and hence was agreed to by SALT.

In order to minimize flexure in the RSS-NIR instrument 5 primary mitigation plans are in place:

1. Test the entire instrument at the full range of altitude and azimuth angles it will experience on the telescope. This will require modification of the flexure test stand to have its own rho stage or equivalent.
 2. Learn from and modify the mechanical design parameters that allowed for the RSS-VIS flexure. These areas primarily include the grating mount and the camera cradle.
 - a. Mount the filter, etalon, and grating magazines and mechanisms independent of the camera and Dewar assembly.
 - b. Provide a lightweight independent stiff truss structure to support the camera/Dewar articulation.
 3. Mechanically isolate the insertion optical mechanisms from their location and holding mechanisms for the filter, etalon, and gratings.
 4. Incorporate the design for a passive flexure compensation mechanism. This amounts to adding active tip/tilt capability to the NIR fold mirror.
 5. Provide a system architecture that allows for the future real-time active flexure compensation by implementation of software that uses the detector's guide mode capability, along with centroiding and motion compensation software within the NDET which can communicate directly to the cRIO chassis via the local ethernet, thereby commanding the fold mirror's motion controllers.
3. **Hardware Integration.** As noted in point 2, we are designing an instrument that must integrate on a platform with another instrument in South Africa. To mitigate the integration risk, a number of measures are being taken.
- The RSS-NIR design engineers will support and participate in a reassembly of the RSS-VIS in June 2009. This provides an opportunity to gain invaluable knowledge of the RSS-VIS, the support structure and the SALT facilities.
 - The RSS-NIR will perform end-to-end image quality and throughput testing of the system. RSS-NIR throughput measurements have been made of the collimator system at the Pilot Group, Monrovia CA in March prior to returning it to South Africa. The RSS-NIR camera and detector will be tested as a unit for image quality (using interferometry and a star test) and flexure in the lab at UW. We will evaluate the possibility of a null lens to test the RSS-NIR doublet at UW.
 - The RSS-NIR will undergo mechanical and flexure testing that better simulates the actual telescope mounting configurations. The RSS-NIR system will be assembled at UW and mounted to an optical table in the same way that it will be mounted to the spaceframe weldment of the RSS-VIS in Cape Town. This optical table will be tilted to the appropriate range of angle allowing flexure and stage operation to be performed under conditions similar to those experienced in operation.
 - The RSS-NIR team holds bi-weekly telecoms with South Africa to discuss interface control issues in order to develop an accurate Interface Control Document.

- The project was fortunate to hire back to the UW Michael Smith. In addition to being an extremely capable engineer, Mike was the lead engineer on the RSS-VIS. His intimate knowledge of the VIS instrument is invaluable to the project team.
4. **Software Integration.** Similar to the hardware integration, the RSS-NIR software control system must be integrated with the RSS-VIS and compatible with SALT Facility systems. The facility standard is LabView 6.1. To reduce risk, the RSS-NIR has taken the following steps.
- Evaluated and found control system hardware to ensure that it is compatible with LabView 6.1 (the current version is 8.6) if required to use it.
 - Discussed with SALT upgrading the control system hardware to LabView 8.6. SALT is open to this idea and the project team has been provided with the latest version of the RSS-VIS software to evaluate upgrading it.
 - Hired the RSS-VIS software developer, Jeff Percival, to develop the RSS-NIR system and its integration with the RSS-VIS.

6.3.2. Safety

The QAS is responsible for assessing the potential safety risks of the instrument and the mitigations to those risks. The safety of the project staff is the priority of the project.

Working with the project team engineers, the QAS is performing a safety assessment to identify all potential safety hazards. An analysis is done of each potential hazard to assess the severity of its impact, probability it will occur, and the ability to detect it. A score is assigned to each of those criteria. These scores are multiplied together to produce a Risk Priority Number (RPN). Hazards with a score above 36 must be mitigated. This may involve replacing a component, a design change, an operational requirement or other mitigation. With each change, the hazard is re-evaluated to produce a new RPN. If the RPN is below 13, no further action is required (the hazard is considered a minor risk and acceptable). If the score remains at 13 or higher, it needs to either be further mitigated or a justification written explaining why it is acceptable. Typically, the QAS determines the validity of the justification, but it may require a waiver to the SALT facility. The goal of the safety risk mitigation is to retire all hazards to a RPN of 12 or less. The process is integrated throughout the design phases to attempt to mitigate issues as early as possible.

6.3.3. Cost

The PM is responsible for managing the cost risk on the project. A ground-based instrument development project like RSS-NIR, may assign 15-20% of its budget to contingency at this stage. There is \$812,405 of contingency on the \$5.3M budget, or approximately 17%. (Contingency is not computed against the cost of the detector since it is known.) Since the project is now through the preliminary design phase and technical issues have been identified, this level of contingency is a reasonable amount.

6.3.4. Schedule

The PM is responsible for managing the schedule risk of the project. The primary means to mitigate schedule risk is to identify the critical path and manage it. For the RSS-NIR, the critical path is the design of the camera optical system: ordering of optical blanks, figuring, and coating, and the integration and testing with the detector/Dewar assembly. To manage the critical path, the project office must maintain good communication with the staff and vendors responsible for the optics, provide the appropriate resources as needed, and ensure that the design develops per the plan.

In addition to the critical path, long lead items present risks to the schedule. All long lead items need to be identified as early as possible and orders placed as soon as the technical maturity of the design and the project spending profile allows. Once placed on order, the project office must be in communication with the vendor to monitor progress.

Additions key to mitigating schedule risk include good communication between the project office and the staff to identify resource requirements and to apply them as required to maintain progress for both critical path and non-critical path tasks. This is primarily accomplished through weekly status and progress meetings. The project office is responsible for monitoring progress versus the plan, identifying deviations, and determining if resources need to be applied to keep the project on schedule.

As mentioned in Section 6.3.3 Cost, to help mitigate schedule risk, the baseline plan includes three months of schedule reserve for IV&T and one month for Commissioning, as these two activities often require more time than the baseline plan.

6.4. Quality

6.4.1. Quality Assurance

Quality is defined as meeting the needs and expectations of the customer. The quality goal for the project is to fulfill the requirements as defined by the SALT science community.

SSEC has developed a number of quality processes that may be used for the RSS-NIR project. These processes were all designed to be compliant with ISO 9001. Some of the processes that may be used in the development, testing, installation, commissioning, service and operation of the RSS-NIR are listed in **Table 6-1**.

Table 6-1. SSEC Quality Processes

Document Number	Topic
1008-0002	Document Control
1008-0004	Change Control
1008-0005	Training
1008-0006	Test Equipment Calibration
1008-0007	Project Life Cycle Process (Design Control)
1008-0012	Complaint Handling
1008-0014	Project Safety
1008-0017	Quality Records
1008-0021	Software Development
1008-0024	Project Management Plan

6.4.2. Configuration Management

RSS-NIR configuration management is managed through SSEC processes for document, change, software and design control. Project documentation will be created, reviewed, approved and maintained through SSEC Document Control Procedure, 1008-0002, with the exception that the document numbering format has been modified from standard SSEC practices to comply with the SALT document numbering format. Project changes will be managed through SSEC Change Control Procedure, 1008-0004. The

SSEC Project Life Cycle Process, 1008-0007, and Software Development Process, 1008-0021, describe the processes for designing and managing the configuration of project hardware and software. These documents describe processes consistent with SSEC and SALT facility practices and guidelines. Additional detail is described in the RSS-NIR Project Management Plan, document number 3501BP0001.

6.4.3. Safety

The health and safety of individuals involved in the development and use of the RSS-NIR is the requirement of highest importance. Safety of the system and its components are of secondary importance. While safety is an aspect of quality, the project office believes that safety should be emphasized in the planning process in order to ensure the RSS-NIR system is designed, assembled, tested, serviced and operated in a safe manner. The protection of personnel and equipment is approached by: (1) Eliminating or reducing the likelihood that a hazardous condition can occur by design, and (2) Minimizing the severity of the adverse consequences if an incident occurs by controls, training, and design to reduce propagation of problems. The entire project team is responsible for the safety of those using the instrument and the instrument itself. Additional detail is described in the RSS-NIR Project Management Plan, document number 3501BP0001.

6.4.4. Design Control

Project development follows the process as outlined in SSEC Project Life Cycle Process, 1008-0007. The document describes a process in which the project progresses through a series of phases or stages. At the end of each phase, a review, by an internal or external panel, is held to determine if the project is ready to proceed to the next phase. The reviews serve to determine if the project has produced deliverables or met milestones before it can proceed. As appropriate to the particular review, they ensure that:

- Science goals have been defined and agreed upon
- Engineering requirements are sufficient to meet the scientific goals
- Project planning and monitoring is in place
- Interfaces are established, defined, and documented
- Design is compliant with applicable standards
- Safety hazards are identified and mitigated
- Design meets the engineering requirements
- Components are adequately specified
- Subsystems are tested and integration ready
- Instrument performance is verified
- Instrument is operationally ready

The project team is responsible for producing a set of deliverables or a review package for each review that provides the verification to the review panel that the instrument development is mature enough to progress to the next phase. Details of the deliverables can be found in the RSS-NIR Project Management Plan, document number 3501BP0001.

6.5. Systems Engineering

The RSS-NIR relies on its Systems Engineer, Don Thielman, to ensure the overall design and testing of the instrument is coordinated between subsystems, engineering disciplines, the NIR and VIS instruments, and the RSS and the SALT facility. To ensure this, Don attends the weekly technical design meetings, leads the bi-weekly NIR call to the SALT facility, and conducts or assigns design trades to optimize the

design in a cost-effective manner considering performance, cost, schedule, and risk. Further, Don, along with the Lead Mechanical Engineer Mike Smith, reviews the Functional Performance Requirements Document to ensure that the science drivers have been properly flowed into engineering requirements and test plans to assess whether or not they can be reasonably achieved within the cost and schedule constraints of the project. Ultimately, Don will ensure that the system design is tested and verified for its performance against the design requirements.

6.6. Work Breakdown Structure

The RSS-NIR WBS is predominately organized by subsystem. The exceptions are Project Administration (science, project management, quality assurance and safety, and systems engineering); Integration, Verification, and Testing; and Commissioning. The last two reflect phases of the development while Project Administration is the oversight.

The budget was developed at subsystem level with the exception of the Optics, which were developed at one level lower. Spending is tracked and compared to the budget at the subsystem level. **Figure 6-3** presents the WBS.

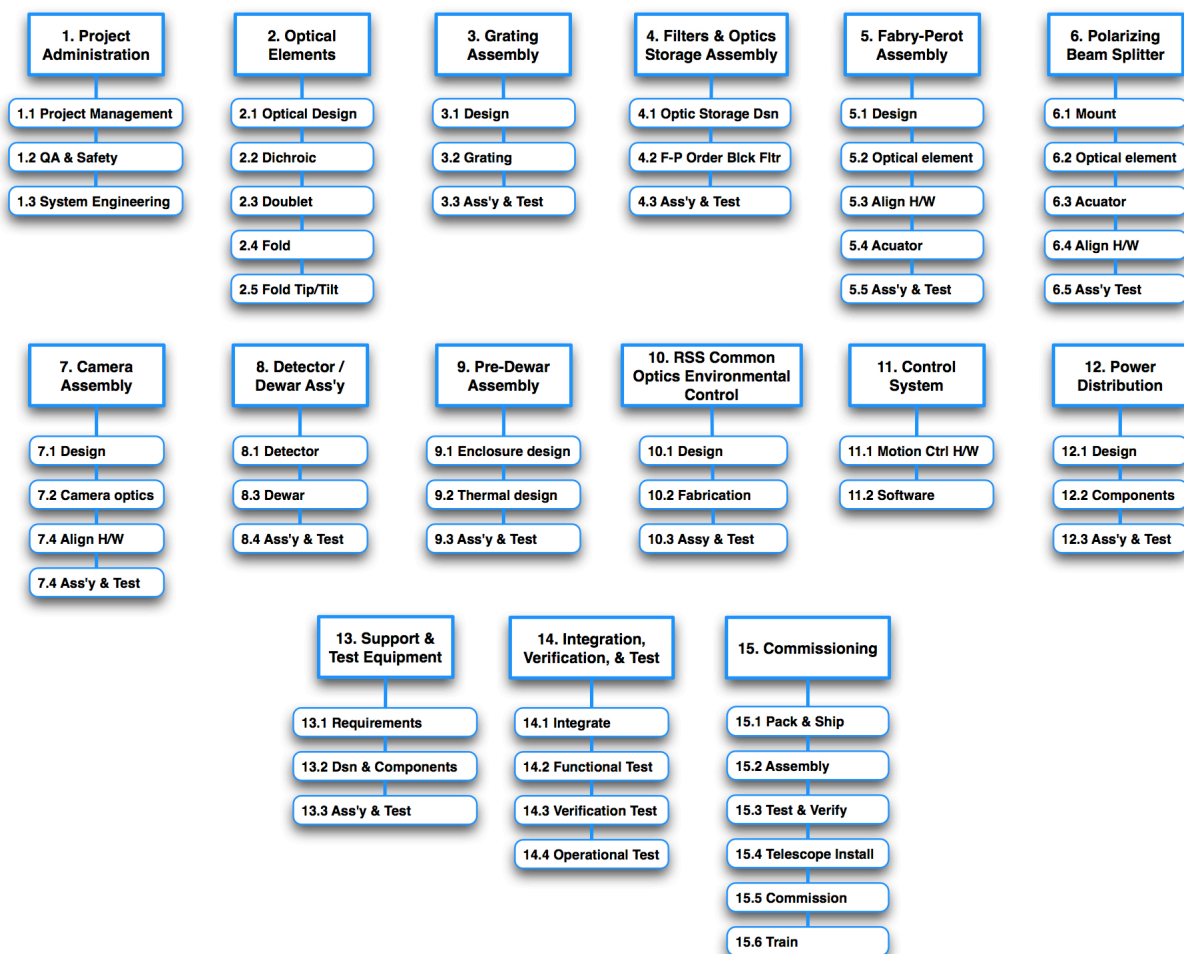


Figure 6-3. RSS-NIR Work Breakdown Structure.

6.7. Schedule

A subsystem level schedule is provided in **Figure 6-4** with an additional level of detail for key (critical path) subsystems. A flow diagram is provided in **Figure 6-5**, which better illustrates the dependent flows. The project started in May 2006 with a Conceptual Design Review. At that time, the project team was primarily the PI, PS, an engineer and a designer. A PDR was held in Jul 2008 with the addition of a project manager, systems engineer, opto-mechanical engineer, and mechanical engineer. While the project did not ramp up as quickly as it would have preferred, it has now reached complement of the necessary disciplines to complete the project as illustrated in **Figure 6-1**.

The project has been in an extended preliminary design phase since the PDR while additional resources were added and the team prepared for the Mid-Term Review. The detailed design phase will last 9 months until the Critical Design Review in late February / early March 2010. This will be followed by a 7-month subsystem development phase; a 7-month integration, verification, and testing phase; and finally a 5-month integration and commissioning phase at the SALT facility. The schedule includes 3 months of reserve for IV&T and another month for the commissioning phase at SALT. With schedule contingency, the RSS-NIR will be fully commissioning in March 2012.

Key activities during the upcoming detailed design phase include:

- Developing detailed designs of all subsystems
- Develop engineering model mechanism(s) test beds to verify operation, accuracy, and environmental compatibility
- Placing optical blank orders and proceeding with figuring and coatings
- Proceeding with other long lead item purchases which include the gratings, filters, and Fabry-Perot etalon (assuming funding is available)
- Commence detector familiarization, characterization, and testing with the engineering model detector and lab electronics
- Develop Dewar design and pursue long lead item, which may include the cryocooler, cooling control system hardware, and the filter mechanism actuator to ensure the Dewar is available to integrate with the detector and camera optics.

RSS-NIR Redbook
Mid-Term Review Design Document
May 2009

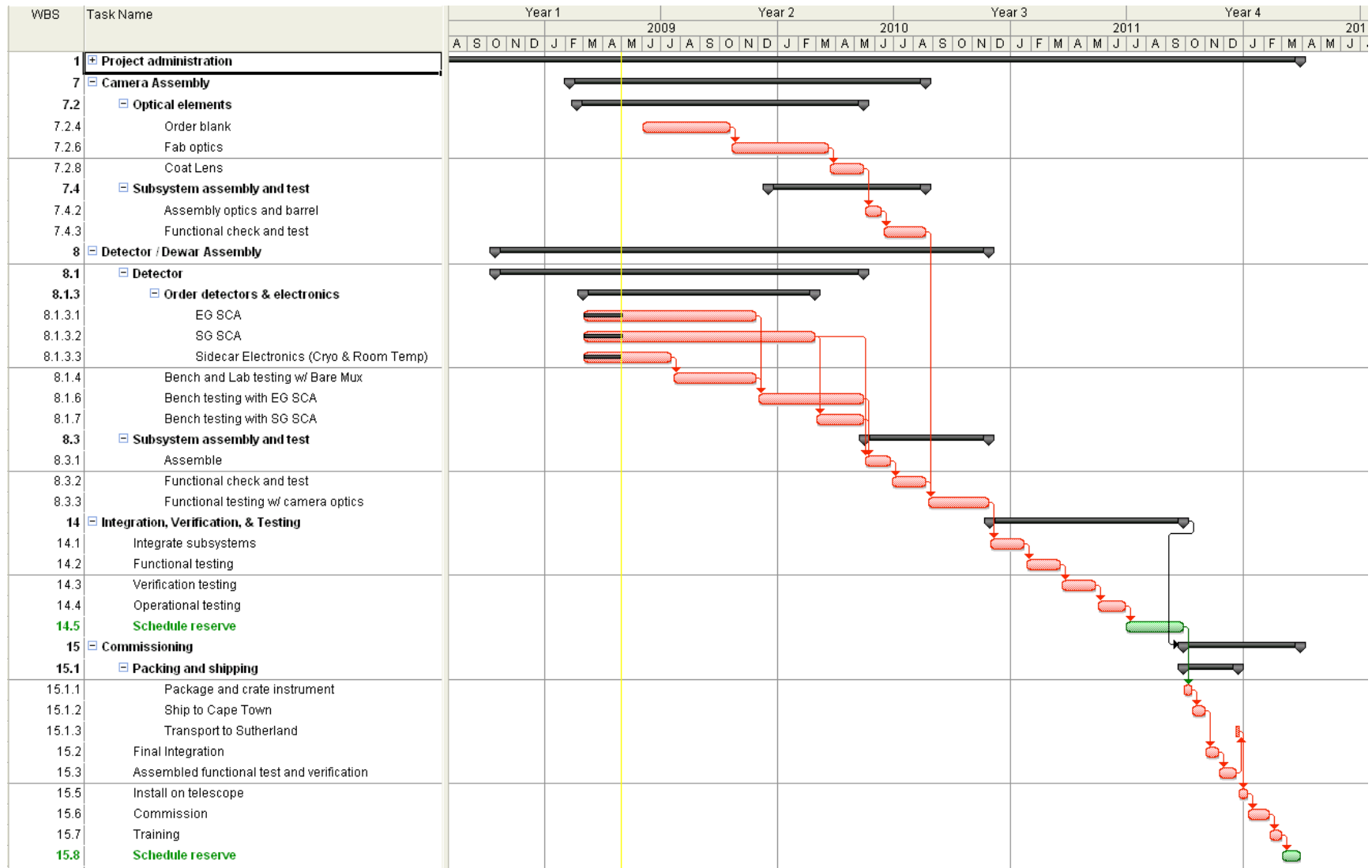


Figure 6-4. RSS-NIR Critical Path

RSS-NIR Redbook
 Mid-Term Review Design Document
 May 2009

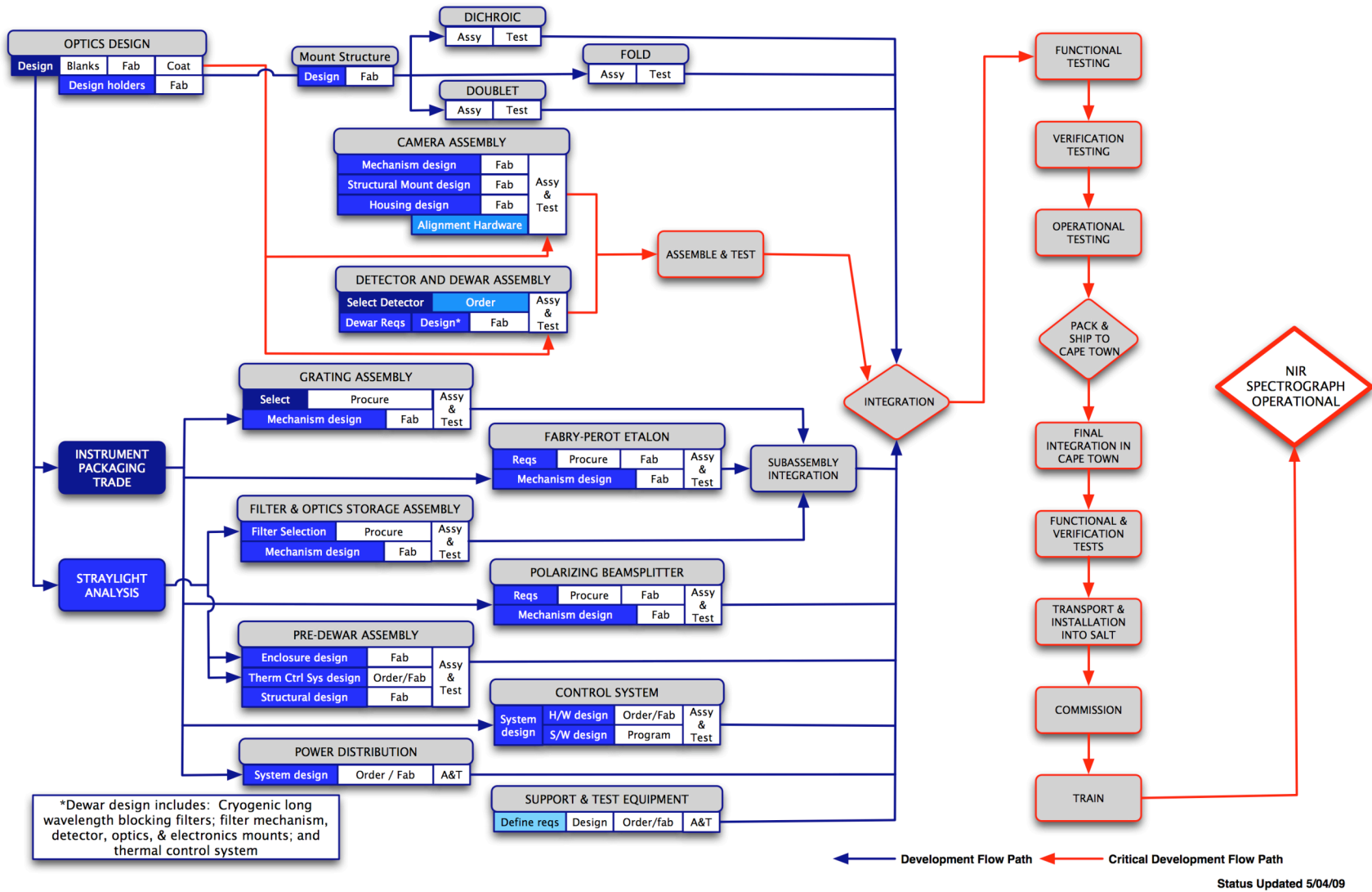


Figure 6-5. RSS-NIR development flow diagram. Progress is indicated by shading. Tasks are complete when the fill color matches the outline.

6.8. Deliverables

The project deliverables to SALT include:

- NIR instrument integrated on the RSS spaceframe
- Specialized test and calibration equipment
- Documentation including engineering drawings, ICD, and requirements and specification documents
- Operation, calibration, preventive maintenance and service procedures (manuals)
- Analyses reports, such as, stray light and thermal
- Acceptance test procedures and reports
- Operational software with source code.
- Shipping containers
- Quarterly status and financial reports

6.9. Milestones and Reviews

The RSS-NIR Project will conduct internal and external reviews throughout the duration of the project. Two have been completed. David Buckley, SALT Project Scientists, organizes the external reviews. Review results are provided to the SALT Board. The results of internal reviews are shared with the David Buckley.

Table 6-2. Milestones and Reviews

Review	Review Panel	Date
Conceptual Design Review	External Review Panel	May 2006
Preliminary Design Review	External Review Panel	July 2008
Mid-Term Review	External Review Panel	May 2009
Critical Design Review	External Review Panel	Feb 2010
Safety Review	RSS-NIR Project Team	Aug 2010
Test Readiness Review	RSS-NIR Project Team	Nov 2010
Hazard Analysis Review	RSS-NIR Project Team	Apr 2011
Pre-Ship Review	RSS-NIR Project Team	Jun 2011
Pre-Installation Review	RSS-NIR Project Team & SALT Facility Staff	Oct 2011
Commissioning Review	SALT & RSS-NIR Project Team	Feb 2012
Project Complete	-	Mar 2012

6.10. Funding, Spending, and Budget

Funding. The RSS-NIR has received \$3.3M from the Wisconsin Alumni Research Foundation and just under \$2.0M from the National Science Foundation. The SALT consortium has provided \$145k and is committed to providing an additional \$155k. Another \$925k was formally requested at a SSWG in 2008. The total RSS-NIR funding is just over \$6.5M as shown in **Table 6-3**.

Table 6-3. RSS-NIR Funding Summary

WARF		\$3,300,000
NSF		\$1,996,775
SALT		
Initial Rec'd	\$145,000	
Committed	\$155,000	
Requested	\$925,000	
		\$1,225,000
TOTAL FUNDING		\$6,521,775

Spending. Through March 2009, \$446,216 has been spent leaving a balance of \$6,075,559. The Department of Astronomy/Space Astronomy Lab tracked project spending prior to July 1, 2008. Spending through then was \$59,773. Since then, the Space Science and Engineering Center has been responsible for the project accounting. **Table 6-4** summarizes the spending and balance remaining.

Table 6-4. RSS-NIR Spending Summary

Funding		\$6,521,775
Spending prior to 7/1/08		\$59,733
Spending post to 6/30/08		\$386,483
BALANCE		\$6,075,559

Budget. The budget estimate to complete the project is \$5,364,831. This leaves \$710,728 for contingency, which represents 15.2% of the budget. Please note, the cost of the detector (on order, \$520,000) and the camera and doublet optic blanks (formal bids received, \$155,495) are not included in the percent contingency calculations since their costs are known. The budget and contingency are summarized in **Table 6-5**.

Table 6-5. RSS-NIR Budget and Contingency Summary. Please note, the cost of the detector (on order, \$520,000) and the camera and doublet optic blanks (formal bids received, \$155,495) are not included in the percent contingency calculations since their costs are known.

Balance of Funding		\$6,075,559
Budget (04/09-03/12)		\$5,364,831
Contingency	15.2%	\$710,728
TOTAL BUDGET		\$6,075,559

This does not include the purchase of the Fabry-Perot etalon and controller. In April, a ROM estimate was received from ICOS for an etalon with water free silica (Infrasil 302) glass and a controller in the amount of \$271,920. A request has been submitted to the NSF for a 10% increase in their funding support through

the MRI program. The project hopes to have an answer by July 2009. An informal agreement has been made with Ted Williams at Rutgers University to fund the purchase of the controller. Combined, this will provide for the purchase. The Rutgers funding is contingent upon receiving the NSF funding. The purchase of the etalon brings the total cost of the RSS-NIR is \$6,793,695.

Table 6-6. RSS-NIR Total Cost with Fabry-Perot

Spending to date (3/31/09)		\$446,216
Budget to complete		\$5,364,831
Contingency	15.2%	\$710,728
Fabry-Perot w/ controller ROM		\$271,920
		\$6,793,695

The project duration is 45 months, including 4 month of schedule reserve, which started in July 2008 (for budget purposes) and ends March 2012. Project years run July 1 to June 30. We are in the 4th quarter of Project Year 1. Financial status and progress reports are submitted quarterly David Buckley, SALT Project Scientist.

The budget was developed per the Work Breakdown System described in section 6.6. Each WBS elements represents a subsystem with a deliverable. The exceptions are project administration; integration, verification, and testing; and commissioning, which represent project management and phases of the project.

6.10.1. Budget Detail

A detailed project budget is provided in

Table 6-7. Labor detail is provided for each individual. Please note, 1800 hours per year is considered full-time. A 15.2% contingency is computed across all cost categories (labor, materials, capital equipment, subcontracts/services, and indirect expenses).

Additional budget detail concerning funding, spending, labor, and WBS subsystems is provided in the Budget Summary detail book.

RSS-NIR Redbook
Mid-Term Review Design Document
May 2009

Table 6-7. NIR Budget Detail.

**NEAR INFRARED SPECTROGRAPH FOR SALT
 BUDGET ESTIMATE**

BUDGET SUMMARY	PY01	PY02	PY03	PY04	O/H RATE: 45.0%	
	2008-2009 APR - JUN	2009-2010 JUL - JUN	2010-2011 JUL - JUN	2011 - 2012 JUL - MAR	TOTAL	Ave FTE Project Life
LABOR						
Principal Investigator, Andrew Sheinis	150	300	300	150	900	0.19
Project Scientist, Marsha Wolf	450	1,800	1,800	750	4,800	1.00
Co-Investigator, Matt Bershady	150	150	150	0	450	0.09
Co-Investigator, Amy Barger	0	0	150	0	150	0.03
Sr. Scientist Advisor, Ken Nordsieck	75	75	75	0	225	0.05
Project Manager, Mark Mulligan	255	1,020	1,020	250	2,545	0.53
Quality Assurance & Safety Manager, Tom Demke	75	300	300	25	700	0.15
Systems Engineer, Don Thielman	225	900	900	450	2,475	0.52
Electrical Engineer, Paul Sendelbach	60	440	200	0	700	0.15
Lead Mechanical Engineer, Mike Smith	450	1,800	1,800	450	4,500	0.94
Electronics Technician	0	725	1,280	0	2,005	0.42
Opto-mechanical Engineer, Jeff Wong*	225	900	655	0	1,780	0.37
Software Programmer, Jeff Percival	225	900	1,145	375	2,645	0.55
Postdoc, Ryan Doering	450	1,800	1,800	225	4,275	0.89
Mechanical Engineer, Bill Mason	435	1,740	1,250	450	3,875	0.81
Designers*	105	2,245	225	0	2,575	0.54
Machinist	0	2,175	1,325	0	3,500	0.73
Instructor	0	600	600	600	1,800	0.38
Co-Investigator, Ted Williams	75	75	75	0	225	0.05
Controls Engineer, Ron Koch*	225	900	725	0	1,850	0.39
Graduate Students	225	1,650	1,800	750	4,425	0.92
Undergraduate Students	360	2,090	1,330	250	4,030	0.84

*Labor costs for these resources are presented in Subcontracts/Services.

TOTAL HOURS:	4,215	22,585	18,905	4,725	50,430	10.51
TOTAL FTEs:	9.37	50.19	42.01	10.50	10.51	
SALARY	\$164,574	\$719,547	\$686,818	\$204,082	\$1,775,021	
FRINGE	\$57,464	\$252,198	\$247,698	\$74,811	\$632,171	
TOTAL LABOR	\$222,038	\$971,745	\$934,516	\$278,893	\$2,407,192	
MATERIAL	\$40,740	\$187,020	\$58,100	\$19,000	\$304,860	
CAPITAL EQUIPMENT	\$244,974	\$884,330	\$296,550	\$10,000	\$1,435,854	
TRAVEL	\$18,621	\$21,729	\$4,439	\$95,303	\$140,092	
SUBCONTRACTS / SERVICES	\$57,043	\$395,408	\$157,693	\$8,900	\$619,043	
TOTAL DIRECT	\$523,492	\$2,101,371	\$1,351,188	\$412,096	\$4,388,147	
TOTAL INDIRECT	\$78,453	\$456,117	\$304,372	\$137,741	\$976,684	
TOTAL	\$601,946	\$2,557,488	\$1,655,560	\$549,837	\$5,364,831	
**TOTAL BUDGET RESERVE:				15.2%	\$710,728	
TOTAL INSTRUMENT COST WITH CONTINGENCY:					\$6,075,559	

**DOES NOT INCLUDE THE DETECTOR (ORDER PLACED) NOR CAMERA AND DOUBLET BLANKS (BIDS RECEIVED) IN THE PERCENT CONTINGENCY

6.10.2. Material Costs

A detailed list of material purchases is provided in **Table 6-8**, which represents \$304,860. Material expenses represent purchases of less than \$5,000. The estimates are based on vendor pricing or quotes, RSS-VIS experience, or purchases on other projects.

Table 6-8. RSS-NIR Material Detail

MATERIAL SUMMARY LIST		
1.0 PROJECT ADMINISTRATION		
Publications (SPIE,...)	\$	4,000
Conference Fees (4 attendees @ \$1250/ea)	\$	10,000
Computer (desktop or laptop)	\$	9,000
Solidworks Lic (AIS), PDM (TAD)	\$	3,350
Solidworks PDM Enterprise Training	\$	8,000
Miscellaneous	\$	6,400
MTR	\$	7,500
CDR	\$	7,500
	\$	<u>55,750</u>
2.0 OPTICAL ELEMENTS		
2.1 Optical Design		
SolidWorks Maintenance (MJW)	\$	750
Computer (PS)	\$	3,000
Software (PS)	\$	1,000
Computer (Grad)	\$	6,000
Software (Grad)	\$	2,000
	\$	-
	\$	-
	\$	-
	\$	-
	\$	-
	\$	<u>12,750</u>
2.2 Dichroic		
Lens holder	\$	750
Material	\$	250
Miscellaneous	\$	500
SolidWorks Annual Fee (WPM)	\$	1,000
SolidWorks PDM (WPM)	\$	2,800
	\$	-
	\$	-
	\$	-
	\$	-
	\$	<u>5,300</u>
2.3 Doublet		
Lens holder	\$	750
Material	\$	250
Miscellaneous	\$	1,000
	\$	-
	\$	-
	\$	-
	\$	-
	\$	-
	\$	-
	\$	<u>2,000</u>
2.4 Fold Mirror		
Lens holder	\$	750
Material	\$	250
Miscellaneous	\$	1,000
	\$	-
	\$	-
	\$	-
	\$	-
	\$	-
	\$	<u>2,000</u>
2.5 Fold Mirror Mechanism		
Linear Encoder (1)	\$	1,000
Limit Sensors (11)	\$	500
Material	\$	150
Misc	\$	300
	\$	-
	\$	-
	\$	<u>1,950</u>
3.0 GRATING ASSEMBLY		
Material	\$	500
Holder	\$	500
Bearings	\$	500
Drive Screw	\$	500
Drive Gear, coupling, or other device	\$	300
Hall Sensors (6)	\$	120
Miscellaneous	\$	500
	\$	<u>2,920</u>
4.0 FILTER & OPTICS STORAGE ASSEMBLY		
Material	\$	750
Storage optics drive screw	\$	250
Storage optics bearing blocks	\$	750
Filter insertion drive screw	\$	250
Filter insertion bearings	\$	250
Miscellaneous hardware	\$	1,500
SolidWorks PDM (JPW)	\$	2,800
Hall Sensor (60)	\$	900
	\$	<u>7,450</u>
5.0 FABRY-PEROT ETALON		
Material	\$	750
Bearings & precision guides	\$	1,000
Drive shaft	\$	500
Miscellaneous	\$	1,000
Hall Sensors (6)	\$	90
Pneumatic Lock (3)	\$	900
	\$	<u>4,240</u>
6.0 POLARIZING BEAM SPLITTER		
Material	\$	750
Frame	\$	500
Insertion mechanism, pneumatic (2)	\$	1,000
Hall Sensors (3)	\$	45
Miscellaneous	\$	1,250
Guide rails and bearings	\$	1,200
	\$	-
	\$	-
	\$	<u>4,745</u>
7.0 CAMERA SUBASSEMBLY		
Material & Misc H/W	\$	3,000
Gearbox, drive gear, precision bearings/rollers	\$	4,000
Pneumatic Lock, Articulation	\$	500
Camera Focus Linear Encoder (2)	\$	1,500
Limit Switches (5)	\$	375
Hall Sensors (6)	\$	90
Articulation Actuator (2) [Dynatec Sys BL2330]	\$	2,200
Articulation Position Encoder, Absolute (2)	\$	2,500
Solidworks & S/W PDM (WPS)	\$	3,800
	\$	<u>17,965</u>
8.0 DETECTOR / DEWAR ASSEMBLY		
CPU Workstation	\$	3,000
Software and IDL licensing	\$	2,000
Material	\$	1,000
Filter wheel actuator [Phytron]	\$	1,500
Filter wheel encoder, absolute	\$	1,250
Cryocooler Compressor & Fittings	\$	11,500
Hall Sensors & Misc	\$	3,810
Temperature sensors & controller	\$	8,000
Cabling	\$	4,500
	\$	<u>36,560</u>
9.0 PREDEWAR SUBASSEMBLY		
Materials - thermal insulating	\$	3,000
Materials - structural	\$	1,000
Enclosure thermal control (heaters, controller, wiring)	\$	3,000
Baffling coatings - paint	\$	1,000
Pneumatics (3) & Misc. H/W	\$	6,500
Thermocouples & Hall Sensors (6)	\$	1,090
SolidWorks Licenses - Renewals (DPA/ARR)	\$	1,290
PDM Licenses - Renewals (ARR)	\$	2,800
CAD CPU & Monitor	\$	6,000
	\$	<u>25,680</u>
11.0 CONTROL SYSTEM		
Enclosure material	\$	500
Additional sensors	\$	1,200
Cabling	\$	6,000
Labview Software Licensing	\$	2,400
PC Boards	\$	7,500
Miscellaneous	\$	14,000
Computer Hardware	\$	6,000
	\$	<u>37,600</u>
12.0 POWER DISTRIBUTION		
Power Supplies	\$	7,500
PC Boards	\$	7,500
Cabling	\$	5,000
Material	\$	500
Heat sinks	\$	500
Miscellaneous Hardware	\$	8,000
	\$	<u>29,000</u>
13.0 SUPPORT AND TEST EQUIPMENT		
Material	\$	5,000
Testing Computer support hardware	\$	5,000
Software and licensing	\$	3,000
	\$	-
	\$	-
	\$	-
	\$	-
	\$	<u>13,000</u>
14.0 INTEGRATION, VERIFICATION, AND TESTING		
Miscellaneous Expenses	\$	10,000
Labview Software License	\$	1,200
SolidWorks Licenses - Renewals	\$	4,500
PDM Licenses - Renewals	\$	2,000
	\$	-
	\$	-
	\$	-
	\$	-
	\$	<u>17,700</u>
15.0 COMMISSIONING		
Miscellaneous equipment / expenses	\$	10,500
Shipping container and packing materials	\$	2,500
SolidWorks Licenses - Renewals	\$	4,500
PDM Licenses - Renewals	\$	-
LabView Renewal	\$	500
	\$	-
	\$	-
	\$	<u>18,000</u>

6.10.3. Capital Equipment

A detailed list of capital equipment purchases (>\$5,000) is provided in **Table 6-9**, which represents \$1,435,854. Some of the purchases listed below are for less than \$5,000. They have been listed they will be part of a larger order that is greater than \$5,000. Indirect charges are not applied to any capital equipment purchase regardless of the funding source. The estimates are based on vendor pricing or quotes, RSS-VIS experience, or purchases on other projects.

Table 6-9. RSS-NIR Capital Equipment Detail

<u>CAPITAL EQUIPMENT SUMMARY LIST</u>		
1.0 PROJECT ADMINISTRATION	\$ -	6.0 POLARIZING BEAM SPLITTER
	\$ -	Polarizing beam splitter
	\$ -	Coating
	\$ -	\$ 55,000
		\$ 5,000
		\$ 60,000
2.0 OPTICAL ELEMENTS		7.0 CAMERA SUBASSEMBLY
2.1 Optical Design	\$ -	Optical blanks & Witness Samples(7)
	\$ -	Lens fabrication
	\$ -	Lens coating
	\$ -	Camera Focus Actuator (1) [Physic M-235]
	\$ -	\$ 127,567
	\$ -	\$ 77,000
		\$ 28,000
		\$ 3,373
		\$ 235,940
2.2 Dichroic		8.0 DETECTOR / DEWAR ASSEMBLY
Mirror blank	\$ 10,000	SG H2RG FPA
Mirror figuring	\$ 10,000	EG H2RG FPA
Mirror coating	\$ 15,000	Sidecar - Bare Mux, Cryo & Room Temp
	\$ -	Bare Mux
	\$ -	Filters
	\$ 35,000	\$ 350,000
		\$ 50,000
		\$ 67,000
		\$ 25,000
		\$ 20,000
		\$ 512,000
2.3 Doublet		9.0 PREDEWAR SUBASSEMBLY
Optic Blank	\$ 27,928	Baffling coating - plating
Lens grinding, surfacing, and figuring	\$ 22,000	Chiller - FTS ULT Series RC210
Coating	\$ 8,000	Chiller plumbing
	\$ 57,928	\$ 5,000
		\$ 32,000
		\$ 7,500
		\$ 44,500
2.4 Fold Mirror		11.0 CONTROL SYSTEM
Purchase Lens	\$ 7,500	Motor Controller & Motion Control Boards
	\$ -	DAQ and I/O hardware
	\$ 7,500	\$ 19,500
		\$ 7,500
		\$ 27,000
2.5 Fold Mirror Mechanism		12.0 POWER DISTRIBUTION
Tip/Tilt Stage+Piston Piezo [Physik P-541.Z	\$ 11,743	
Controller, Power Supply [Physik E-500.0]	\$ 2,490	\$ -
Servo Modules [Physik E-509.S3 & E-509.C	\$ 6,865	\$ -
Amplifier Modules [Physik E-503.0 & E-508.0	\$ 4,772	\$ -
I/F Modules [Physik E516.i1 & E-516.i3]	\$ 7,135	\$ -
	\$ 33,005	\$ -
		\$ -
3.0 GRATING ASSEMBLY		13.0 SUPPORT AND TEST EQUIPMENT
Grating Insertion Actuator (1) [Ultramotion	\$ 750	Test setup optics & lamps
Grating Absolute Encoder (1)	\$ 1,075	Throughput test equipment
Grating Rotation Stage Actuator (2) [Physik	\$ 8,356	Other test equipment
Grating Absolute Rotary Encoder (2)	\$ 2,150	\$ 10,000
Gratings	\$ 80,000	\$ 10,000
	\$ 92,331	\$ 30,000
		\$ -
		\$ -
		\$ 50,000
4.0 FILTER & OPTICS STORAGE ASSEMBLY		14.0 INTEGRATION, VERIFICATION, AND TESTING
F-P Order Blocking Filters	\$ 234,000	
OSA Drive Actuator (2) [Ultramotion HT23]	\$ 1,900	\$ -
OSA Absolute Position Encoder (2)	\$ 2,150	\$ -
Filter Insertion & Lock Actuators (2) [Ultramot	\$ 1,500	\$ -
Filter Absolute Position Encoder (1)	\$ 1,075	\$ -
	\$ 240,625	\$ -
		\$ -
5.0 FABRY-PEROT ETALON		15.0 COMMISSIONING
F-P Insertion Actuator (1) [Ultramotion HT23]	\$ 950	Instrument Shipping
F-P Absolute Encoder (1)	\$ 1,075	\$ 10,000
	\$ 2,025	\$ -
		\$ 10,000

6.10.4. Travel Plans

The table shown in **Table 6-10** is used to plan and budget all travel plans for the project. Data is entered for every trip, which includes purpose, origin, destination, number of travelers, duration, number of cars, and the number and timing of the trip(s). A travel cost is auto-computed and entered into the budget.

7. REFERENCES

1. Becker, G.D., Rauch, M., Sargent, W.L.W., 2008, arXiv: 0812.2856.
2. Beletic, et al., 2008, Proc. SPIE, 7021, 70210H.
3. Bershady, et al., 2004, astro-ph/0403478.
4. Buckley, D. A. H., Brink, J., Loaring, N. S., Swat, A., Worters, H. L., 2008, Proc. SPIE, 7014, 70146H-1.
5. Dalton, G.B., Lewis, I.J., Bonfield, D.G., Holmes, A.R., Brooks, C.B., Lee, H., Tosh, I.A.J., Froud, T.R., Patel, M., Dipper, N.A., Blackburn, C., 2006, Proc. SPIE, 6269, 62694A-1.
6. Dasyra, K. M., Ho, L. C., Armus, L., Ogle, P., Helou, G., Peterson, B. M., Lutz, D., Netzer, H., Sturm, E. 2008, ApJ, 674, L9.
7. de Grijs, et al., 2004, MNRAS, 352, 263.
8. Elmegreen, D.M., Elmegreen, B.G., Rubin, D.S., Schaffer, M.A., 2005, ApJ, 631, 85.
9. Epps, H.W., and Elston, R., 2002, SPIE Vol. 4841, pp. 1280-1294.
10. Ferlet, M.J., 2008, Proc. SPIE, 7014, 701436.
11. Finger, G., SPIE-2004 Vol5499 issue1.
12. Gallagher, J.S., et al., 2008, A&A, 486, 165.
13. Glickman, E., Helfand, D. J., & White, R. L. 2006, ApJ, 640, 579.
14. Lancon, et al., 2007, A&A, 468, 205.
15. Guoqiang Li, Shao-Ju Shih, Yizhong Huang, Tao Wang and Wanqi Jie
Journal of Crystal Growth, Volume 311, Issue 1, 15 December 2008, Pages 85-89.
16. D. Joyce, 2008, private communication.
17. Loose, M., Beletic, J., Garnett, J., & Xu, M. 2007, Proc. SPIE, 6690, 66900C.
18. Meixner, M., Smee, S., Doering, R. L., et al. 2008, *Proc. SPIE*, 7014, 70142W.
19. Nestor, D.B., Turnshek, D.A., Rao, S.M., Quider, A.M., 2007, ApJ, 658, 185.
20. Nordsieck, et al., 2003, Proc. SPIE 4843, 170.
21. Parry, I., Bunker, A., Dean, A, Doherty, M., Horton, A., King, D., Lemoine-Busserole, M., Mackay, C., McMahan, R., edlen, S., harp, R., Smith, J., 2004, Proc. SPIE, 5492, 1135.

22. Portilla, J. G., Rodriguez-Ardila, A., Tejeiro, J. M. 2008, RevMexAA, 32, 80.
23. Ramos Almeida, C., Perez Garcia, A. M., Acosta-Pulido, J. A. 2009, ApJ, 694, 1379.
24. Rogalski, A., 2005, Rep. Prog. Phys. 68, 2267–2336.
25. Ryan-Weber, E.V., Pettini, M., Madau, P., 2006, MNRAS, 371, L78.
26. Schubnell, M., Brown, M. G., Karabina, A., Lorenzon, W, Mostek, N., Mufson, S.,. Tarlé, G, Weaverdyck, C., 2008, Proc. SPIE 7021, 70210L.
27. Smail, I., Ivison, R.J., Blain, A.W., 1997, ApJL, 490, L5.
28. Smith, Roger M., Maximilian Zavodny, Gustavo Rahmer, Marco Bonati, 2008, Proc. of SPIE Vol. 7021, 70210K.
29. Steidel, C.C., Sargent, W.L.W., 1992, ApJS, 80, 1.
30. Thielman, Don and Richard Blank (Teledyne Imaging Sensors), private communication.
31. Tufts, J.R., Hill, G.J., MacQueen, P.J., Wolf, M.J., 2004, Proc. SPIE, 5492, 1150.
32. Wolf, M.J., 2005, PhD Dissertation, University of Texas at Austin.

8. DEFINITIONS, NOMENCLATURE, ACRONYMS AND ASSUMPTIONS

This purpose of this section is to provide definitions, nomenclature, acronyms and assumptions for the RSS-NIR MTR to present consistency between the various sections of the document.

This document may include existing elements from the RSS Visible side.

This first section will be Assumptions for the NIR.

This second section will be the nomenclature, definitions and acronyms in alphabetical order with the following format:

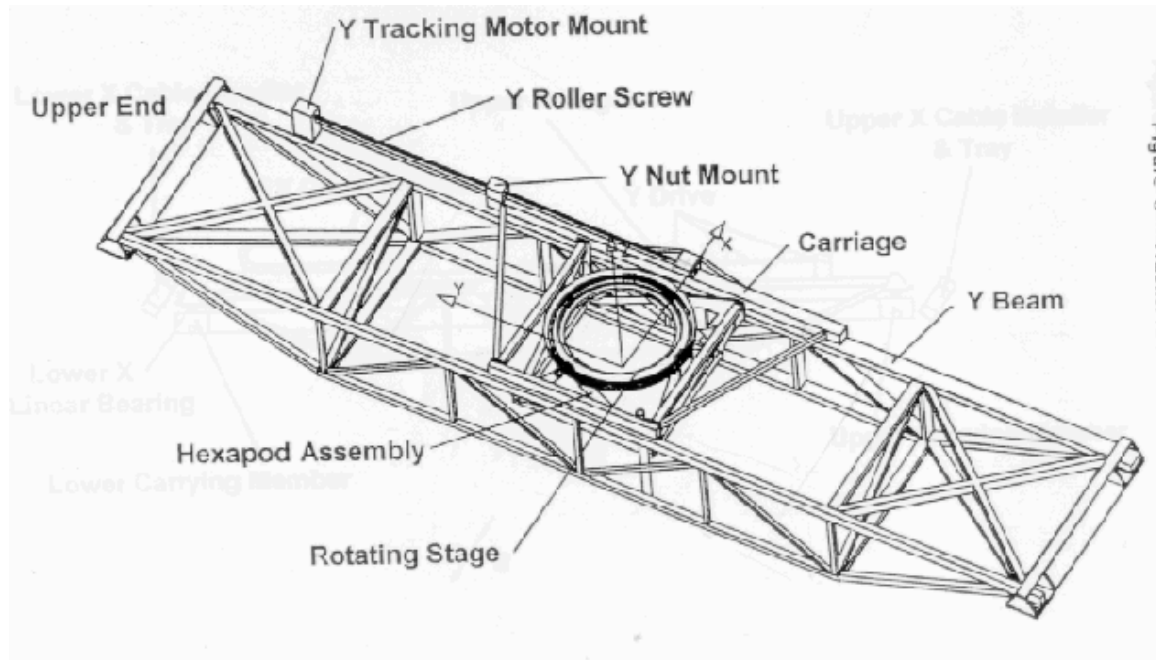
Name

Subsystem, **Aka:** (aliases)

Definition / Description

8.1. Assumptions

1. ISO standards will be used for all drawings.
2. Metric fasteners should be used; Hex cap, SS or Zinc plated, Use Helicoil inserts for any threaded locations in Aluminum.
3. Captive fasteners should be used on all skins and elements that are routinely opened when the instrument is on the telescope.
4. Captive fasteners should be used on all skins and elements that are routinely opened when the instrument is on the telescope. No tool should be required to open these fasteners. (This prevents tools from falling onto the mirror when the instrument is being serviced.)
5. Co-ordinate systems:
The phi, theta and rho are the respective rotations about the X, Y and Z axes when the RSS and NIR are in their respective 0° positions as stated in section 0.12 of the NIR System Mechanism Specification. This definition using the zero position is used to reduce ambiguity about what the axes and rotations are if the payload has been rotated on the rho ring and if the Camera Articulation stage has been moved from the 0° position.
Where this comes from is from the SALT 1510AS0001 Issue 1, Section 6.2.2.
This is the SALT Tracker System Specification, but beware the positive Z axis should be pointing **down towards the mirror**, not up as show in this diagram and **the positive X axis is to the left**, not to the right as shown in this diagram:
SALT Technical Report 1000AS0031 Issue A, Section 2 defines the rotations:
All coordinate systems are right handed. The orientation of coordinate systems with respect to each other is described by the classical Euler method, using successive rotations. For SALT the rotations will consistently be :
 - 1st rotation: about x – axis, through angle (Φ or as defined)
 - 2nd rotation: about y' – axis, through angle (θ or as defined)
 - 3rd rotation : about z'' – axis, through angle (ρ or as defined)
6. There is a position on the camera filter wheel that blocks all direct external light to the detector, and minimizes the stray light reaching the detector.
7. The camera is focused by adjusting elements L4 and L5 external to the Dewar.



8.2. Nomenclature, Acronyms, Definitions and Aliases

Active Lock Mechanism

Optics Storage Subsystem and Camera Articulation Subsystem: **AKA:** -
 A Mechanism that provides the Optics Storage Subsystem and Camera Articulation Subsystem with active locking functions that lock upon the removal of power or pneumatics to the actuator.

Actuator

Definition: **AKA:** -
 The portion of a mechanism that provides the force to move an element. Examples are gas piston, linear actuator, stepper motor and associated lead screw.

A/D

Definition: **AKA:** -
Analog to Digital converter.

ADC

Definition: **AKA:** -
Atmospheric Dispersion Corrector.

Air Lock

Optical Storage Subsystem: **AKA:** Air Lock

This is the air lock for exchanging filters without the need to warm-up and open the entire pre-dewar.

Air Lock Mechanism

Optical Storage Subsystem: **AKA:** Air Lock
 This is the air lock door mechanism and includes the door lock mechanism, and the associated locks and sensors.

AKA

Definition: **AKA:** -
Also Known As

ASIC

Definition: **AKA:** -
Application Specific Integrated Circuit

ASAP

Optics: **AKA:** -
 Advanced Systems Analysis Program, a program capable of executing a user driven thermal stray light analysis

Assembly

Definition: **AKA:** -
 A combination of mechanisms and elements that provides a major subsystem element such as the Optics Storage Assembly.

b

Definition: **AKA:**
Bit or bits

B

Definition: **AKA:**
Byte or bytes

Beamsplitter

Camera Subsystem: **AKA:** Wollaston Prism
This is the Wollaston prism that can be inserted into the optical path immediately in front of the NIR camera.

Beamsplitter Insertion Mechanism

Camera Subsystem: **AKA:** -
This is the mechanism that inserts and retracts the polarizing beamsplitter to/from the optical path for the camera. The frame and insertion mechanism is attached to the camera mount and rides with the rotating camera assembly.

C

Definition: **AKA:** -
Celsius.

Cable Wrap

Definition: **AKA:** -
A cable wrap is defined as any portion of the SALT system that provides for flexure in the cabling (and pipe connections) between moving elements of the telescope, its payload, and the instruments.

Camera Articulation Mechanism

Camera Subsystem: **AKA:** -
This moves the camera barrel and associated mount that will pivot around the same axis as the grating rotation movement. The polarizing beamsplitter mechanism will also be on this mechanism. The camera mount rotation is approximately twice the angular displacement of the grating rotation.

Camera Filter Wheel Mechanism

Camera Subsystem: **AKA:** -
This moves the IR wavelength blocking camera filters within the camera Dewar. This includes a

completely opaque screen/shutter for calibration. One of the filter positions is an optically clear aperture. Only 1 filter position needs to be placed in the optical beam at any one time.

Camera Focus Mechanism, Camera Subsystem

Camera Subsystem: **AKA:** -
This moves the optical elements that perform the camera focus.

CDS

Definition: **AKA:** -
Correlated Double Sampling.

CMOS

Definition: **AKA:** -
Complementary metal-oxide-semiconductor.

Control Interface Box, CIB

Control Subsystem: **AKA:** -
Control Interface Box for the NIR. This is the box that contains the lower level and discrete interfaces between the NCC and the NIR instrument itself.

Cutoff Wavelength

Definition: **AKA:** -
The long wavelength end of a detector where the QE falls to < 50% of the peak QE.

dB

Definition: **AKA:** -
Decibels.

Detector Electronics

Detector Subsystem: **AKA:** -
This is the electronics for the detector, including temperature read-out and control for the Dewar, controller and digitizer for the detector, detector subsystem interface to the NDET, and the Dewar's ion pump controller.

Dewar

Dewar Subsystem: **AKA:** -
This is Dewar for the RSS-NIR instrument.

DNL

Definition: **AKA:** -

Differential nonlinearity

ESD

Definition: **AKA:** -
Electrostatic discharge

Etalon

Fabry-Perot Subsystem: **AKA:** FP,
Fabry-Perot, FP Etalon
This is the Fabry-Perot etalon for the NIR.

Etalon Insertion Mechanism

Optics Storage Subsystem: **AKA:** -
This is the insertion/retraction mechanism for the Fabry-Perot etalon that moves the etalon to/from the Optics Storage Assembly and the Etalon Holder.

Filter Insertion Mechanism

Optics Storage Subsystem: **AKA:** -
This is the insertion/retraction mechanism for the NIR filters (that are in the pre-dewar immediately following the fold mirror) that moves the filters to/from the Optics Storage Assembly and the Filter Holder.

Fixed Filter Cassette Holder

Optics Storage Subsystem: **AKA:** -
This is the fixed filter cassette holder in the Optics Storage Assembly. It includes the lock mechanism sensors for each filter position in the holder.

Fixed Grating Cassette Holder

Optics Storage Subsystem: **AKA:** -
This is the fixed Grating cassette holder in the Optics Storage Assembly. It includes the lock mechanism sensors for each grating position in the holder.

Fold Mirror Mechanism

Optical Subsystem: **AKA:** -
These are the movement mechanisms for tilting the fold mirror in 2 orthogonal directions. This motion will have the capability to move the collimated beam outside of the field of view of the camera and then back in again. Note, this may require a piston motion actuator that allows

the location of the center of the mirror to remain fixed while being tipped and tilted.

Fowler N Sampling

Definition **AKA:** -
Fowler sampling is defined as N samples before and N samples after the integration of an image.

FOV

Optics: **AKA:** -
Field-of-view

Frame

Definition **AKA:** -
A single read of the array, without corrections to the data.

FPA

Definition: **AKA:** -
Focal Plane Array.

Frame

Definition: **AKA:** -
A single read of the array or a portion of the array, without corrections or with only minimal corrections to the data.

FTIR

Definition: **AKA:** -
Fourier Transform InfraRed

Grating Insertion Mechanism

Optics Storage Subsystem: **AKA:** -
This is the insertion/retraction mechanism for the NIR gratings that moves the gratings to/from the Optics Storage Assembly and the Grating Holder. It is also used to move the filters to/from the Optics Storage Assembly and the Grating Holder.

Grating Rotation Mechanism

Grating Subsystem: **AKA:** -
This is the rotation mechanism for the NIR grating Holder.

Holder

Definition: **AKA:** -

These are the devices for the filters, gratings, etalon and beamsplitter that hold the respective elements in the optical path.

HW

Definition: **AKA:** H/W
Hardware

ICD

Definition: **AKA:**
InInterface Control Document

IDC

Definition: **AKA:** H/W
Integrated Detector Control

Igloo

Definition: **AKA:** -
An insulated structure on the SALT telescope who's outside is climate controlled to within $\pm 2^{\circ}\text{C}$ of the ambient temperature. There are igloos on the rotating base of the telescope and on the top Hex structure of the telescope.

Image

Definition: **AKA:** -
A reduced data set from a subsystem that will be an image of the data taking into account corrections to the data from items such as dark current, gains, persistence, etc.

INL

Definition: **AKA:** -
Integral nonlinearity.

Inserters Rotation Mechanism

Optics Storage Subsystem: **AKA:** -
Mechanism that rotates the filter, grating and etalon insertion mechanisms.

Instrument Air

SALT Support Subsystem: **AKA:** -
Clean, dry air for instrument use with requirements of very low dew point and very clean air.

Integration (time)

Definition: **AKA:** -

The time between resets of the entire array, a subset of the array, or an individual pixel.

IR

Definition: **AKA:** -
InfraRed

K

Definition: **AKA:** -
Kelvin.

kHz

Definition: **AKA:** -
kilohertz.

Lock Mechanism

Optics Storage Subsystem: **AKA:** -
Mechanism that provides the passive filter, grating and etalon locking functions.

LSB

Definition: **AKA:** -
Least Significant Byte or bit depending upon context.

LVDS

Definition: **AKA:** -
Low voltage differential signal.

M

Definition: **AKA:** -
Mega = 1×10^6 .

Mechanism

Definition: **AKA:** -
This is a combination of elements such as brackets, end effectors, and actuators that together combine to perform an action such as the Filter Insertion Mechanism.

mm

Definition: **AKA:** -
millimeter .

MTR

Definition: **AKA:** -
NIR Mid Term Revew

Mux.

Definition: **AKA:** -
Multiplexer.

mW.

Definition: **AKA:** -
milliwatt.

NDET

NIR Detector subsystem: **AKA:** -
The detector control and data handling computer
for the NIR instrument.

NIR

RSS System: **AKA:** RSS-NIR
Near InfraRed, but also used to indicate the Near
InfraRed subsystem portion of the RSS
instrument depending upon content.

NIR Chiller

Pre-Dewar Subsystem: **AKA:** -
The subsystem that provides the fundamental
cooling capability for the NIR pre-dewar.

NCC

Control Subsystem: **AKA:** -
NIR Control Chassis. This contains the primary
interface between the PCON computer and the
NIR instrument.

NIR Cryocooler

Dewar Subsystem: **AKA:** Cryotiger
The subsystem that provides the fundamental
cooling capability for the NIR Dewar.

NSF

Definition: **AKA:** -
National Science Foundation

Optical Path

Definition: **AKA:** Optical Beam
This is the optical path through the NIR
instrument, including deviation from gratings
and other elements.

Optics Storage Assembly

Optical Storage Subsystem: **AKA:** All-In-
One, Storage Optics Assembly
This is the assembly that holds the filters,
gratings and etalon when they are not in the

optical path, and properly positions the various
elements to be inserted into their respective
holders in the optical path. It also contains
significant elements of the filter exchange
mechanism and portions of the Air Lock.

p/p

Definition: **AKA:** -
Pusher/puller

Payload

SALT Tracker System: **AKA:** -
This is the portion of the SALT system that
resides on the top of the Hexapod, and includes
both the rotating and no-rotating portions of the
payload system.

PCON

RSS system: **AKA:** -
This is the computer that is controlled by a state
machine driven LabView program that controls
both the RSS-VIS and RSS-NIR portions of the
RSS instrument.

PDET

RSS-VIS subsystem: **AKA:** -
The detector control and data handling computer
for the RSS-VIS instrument.

PDR

Definition: **AKA:** -
Preliminary Design Review

PI

Title: **AKA:** Andrew Sheinis
Principal Investigator

PM

Title: **AKA:** Mark Mulligan
Project Manager

Pre-Dewar

NIR Subsystem: **AKA:** -
The cooled enclosure of the NIR that is outside
of the Dewar, and encloses the majority of the
optical elements at a -40°C temperature.

PS

Title: **AKA:** Marsha Wolf

Project Scientist

PXI

Control Subsystem: **AKA:** PXI chassis
This is a National Instrument's PXI chassis proposed for the NIR in the PDR and is now superseded by the compact RIO chassis in the MTR.

QAS

Title: **AKA:** Tom Demke
Quality Assurance and Safety Manager

QE

Definition: **AKA:** -
Quantum Efficiency.

Removable Filter Cassette Holder

Optics Storage Subsystem: **AKA:** -
This is the removable filter cassette holder in the Optics Storage Assembly. It includes the lock mechanism sensors for each filter position in the holder.

R

Definition: **AKA:** -
Resolution, with respect to spectrometry.

Rho stage

SALT Tracker System: **AKA:** -
This is the rho angular stage of the payload interface of the tracker that accommodates $\pm 115^\circ$ of rotation.

RPN

Title: **AKA:** Andrew Sheinis
Risk Priority Number: Scored figure applied to identified hazards as a means to track and mitigate.

RMS

Definition: **AKA:** -
Root Mean Square.

RSS

SALT System: **AKA:** -
Robert Stobie Spectrograph, which encompasses the Visible instrument and NIR side of the instrument.

RSS-NIR

RSS System: **AKA:** NIR, RSS/NIR
Robert Stobie Spectrograph - Near InfraRed side of the RSS instrument.

RSS-VIS

RSS System: **AKA:** PFIS, RSS/Vis, Vis
Robert Stobie Spectrograph - Visible instrument, formerly known as PFIS.

SAAO

Definition: **AKA:** -
South African Astronomical Observatory.

SAC

Definition: **AKA:** -
Spherical Aberration Corrector.

SALT

SAAO Telescope: **AKA:** -
Southern African Large Telescope.

SE

Title: **AKA:** Don Thielman
Systems Engineer

SW

Definition: **AKA:** S/W
Software

TEC

RSS Common Optics or pre-dewar: **AKA:** -
Thermo-electric Cooler

VPH

Definition: **AKA:** -
Volume Phase Holographic (grating)

UW

Definition: **AKA:** -
University of Wisconsin-Madison

WARF

Definition: **AKA:** -
Wisconsin Alumni Research Foundation

WBS

Definition: **AKA:** -

RSS-NIR Redbook
Mid-Term Review Design Document
May 2009

Work Breakdown Structure: a means to organize a project, typically done by deliverable subsystems.

μ
Definition: **AKA:** -
microns, referring to wavelengths or distance measurements. $1 \mu = 1E-6$ meters.

μV
Definition: **AKA:** -
Microvolts

9. APPENDICES

9.1. 11 x 17 Diagrams